

---

# **Development of New Materials for Solar Cells Application**



**Mohammed Sulaiman Almeataq**

A thesis submitted to  
The University of Sheffield  
as partial fulfilment for the degree of Doctor of Philosophy

Department of Chemistry

**December 2013**

---

---

To my family

---

**Declaration**

This thesis is submitted for the degree of doctorate of philosophy (PhD) at the University of Sheffield, having been submitted for no other degree. It records the research carried out at the University of Sheffield from January 2010 to December 2013. It is entirely my original work, unless where referenced.

Signed:.....

December 2013

## Abstract

Conjugated polymers have attracted much attention and academic research as a result of their potential use in the area of organic photovoltaic. In this project, series of copolymers have been synthesised successfully via Suzuki cross-coupling. Furthermore, these copolymers are designed according to the concept weak donor and strong acceptor system to have high open circuit voltage and low band gap energy.

This project reports the synthesis of three low band gap copolymers (**P1**), (**P2**) and (**P3**) which have similar chemical structure to PCDTBT where thiophene repeat units are replaced with N-methylpyrrole repeat units. In **P2**, the carbazole repeat units have been substituted with fluorine group in the positions 3 and 6 in order to lower the band gap energy due to fluorene-hydrogen electrostatic interaction. Also, the carbazole repeat units have been replaced with fluorene in **P3**. The results indicate wider band gap energy compared to the thiophene analogous polymers.

This thesis also covers the synthesis of a series of low band gap 2,6- and 2,7-based anthracene copolymers (**P6-P12**). These copolymers consist of 2,6- or 2,7- linked anthracene and thiophene or selenophene as donor units, and benzothiadiazole used as acceptor units. In addition, octyloxy substituents were introduced to the benzothiadiazole repeat units. The results indicate that 2,6-anthracene based copolymers have slightly higher conjugation properties compared to 2,7-anthracene copolymers. Introduction of alkyloxy substituents on the benzothiadiazole repeat units improve the solubility but reduce the conjugation properties of the resulting polymers.

DPP-based donor/acceptor low band gap copolymers (**P16-P20**) are also reported in this project. These copolymers show very low optical band gap energy in the range (1.72-1.36 eV) as a result of the strong accepting ability of DPP with its low LUMO level. The physical and electrochemical properties of these copolymers illustrate promising results for use in bulk heterojunction devices.

### Acknowledgments

First of all I would like to express my heartfelt gratitude to my parents for raising me up with their endless love, guidance, support and encouragement. Besides my parents, I would like to thank my brothers and sisters for their help and support. Also, I am deeply grateful to my wife for her patience. This thesis would not have been possible without her encouragement and support.

I would like to express the deepest appreciation to my supervisor Dr. Ahmed Iraqi, for his guidance, support and advice during my PhD. Also, I would like to thank all members of Iraqi group in the past and present for their invaluable help and all members of the F-floor.

I would like to thank Professor David Lidzey and the Lidzey group from the department of Physics and Astronomy at The University of Sheffield for studying photovoltaic properties of the polymers.

I would like to thank Rob Hanson, Simon Thorpe, Sue Bradshaw, Mel Hannah for their help with various measurements. In addition, I would like to thank Nick Smith and Peter Farran in the chemistry store and everyone in the department of Chemistry who has helped me.

Last but not least I would like to thank the Royal Embassy of Saudi Arabian, Culture Bureau in London for their services and help, and King Abdulaziz City for Science and Technologies for their financial support.

---

**Table of Contents**

<b>DECLARATION</b> .....	<b>I</b>
<b>ABSTRACT</b> .....	<b>II</b>
<b>ACKNOWLEDGMENTS</b> .....	<b>III</b>
<b>TABLE OF CONTENTS</b> .....	<b>IV</b>
<b>TABLE OF FIGURES</b> .....	<b>X</b>
<b>TABLE OF SCHEMES</b> .....	<b>XIII</b>
<b>TABLE OF TABLES</b> .....	<b>XVI</b>
<b>ABBREVIATIONS</b> .....	<b>XVII</b>
<b>CHAPTER ONE: INTRODUCTION</b> .....	<b>1</b>
<b>1.1. Background to conjugated polymers</b> .....	<b>1</b>
<b>1.2. Chemical structure of conjugated polymers</b> .....	<b>3</b>
<b>1.3. The properties of conjugated polymers</b> .....	<b>4</b>
1.3.1. Conjugated polymer's conductivity .....	4
1.3.2. Solubility of conjugated polymers .....	6
<b>1.4. Synthesis of conjugated polymers</b> .....	<b>6</b>
1.4.1. Suzuki Cross Coupling .....	7
1.4.1. Stille Coupling Reaction.....	7
<b>1.5. Introduction to Solar Cells</b> .....	<b>9</b>
1.5.1. Brief History of Organic Solar Cells .....	9
1.5.2. Operating Mechanism for Organic Solar Cells .....	10
1.5.2.1. Operating Mechanism For Homojunction Devices .....	10
1.5.2.2. Operating Mechanism For Heterojunction Devices .....	11
1.5.3. Inorganic and Organic Solar Cells .....	12
1.5.4. The Concept of Heterojunction .....	13
1.5.5. Organic Solar Cell Device Structure .....	14
1.5.5.1. Single Layer Devices .....	15
1.5.5.2. Bilayer Heterojunction Devices .....	15
1.5.5.3. Bulk heterojunction devices.....	16
1.5.5.4. Ordered bulk heterojunction devices .....	17

---

1.5.6. Donor – acceptor system .....	17
1.5.7. General requirements for the active layer in organic solar cell .....	19
1.5.7.1. Short Circuit Current.....	19
1.5.7.2. The Open Circuit Voltage .....	20
1.5.7.3. Film morphology .....	21
1.5.8. Organic Solar Cell Materials .....	21
1.5.8.1. Fluorene-based Conjugated Polymers. ....	22
1.5.8.2. Carbazole-based Conjugated Polymers.....	23
1.5.8.3. Benzothiazole Derivatives-based Conjugated Polymers. ....	25
1.5.8.4. Thiophene, selenophene and pyrrole based conjugated polymers.....	26
1.5.8.5. Diketopyrrolopyrrole based conjugated polymers.....	28
1.5.8.6. Anthracene based conjugated polymers.....	29
1.5.8.7. Fullerene and Non fullerene Acceptor Materials.....	30
<b>CHAPTER TWO: AIMS AND OBJECTIVES.....</b>	<b>31</b>
<b>2.1. Carbazole and fluorene – Pyrrole based copolymers (P1, P2, P3) .....</b>	<b>31</b>
<b>2.2. Carbazole and fluorene – Pyrrole and bisoctyloxy substituted benzothiadiazole based copolymers (P4, P5, P6).....</b>	<b>32</b>
<b>2.3. 2,6 - Linked anthracene based copolymers (P7 – P9) .....</b>	<b>33</b>
<b>2.3. 2,7 - Linked anthracene based copolymers (P10 – P12) .....</b>	<b>35</b>
<b>2.4. Anthracene based homopolymers (P13, P14, P15).....</b>	<b>36</b>
<b>2.5. Diketopyrrolopyrrole (DPP) based copolymers (P16, P17, P18, P19, P20).....</b>	<b>36</b>
<b>CHAPTER THREE: EXPERIMENTAL .....</b>	<b>39</b>
<b>3.1. Materials .....</b>	<b>39</b>
<b>3.2. Measurements.....</b>	<b>39</b>
3.2.1. Melting Point .....	39
3.2.2. Mass Spectrometry .....	40
3.2.3. Nuclear Magnetic Resonance Spectroscopy (NMR).....	40
3.2.4. Infra Red Absorption Spectra (IR) .....	40
3.2.5. Gel Permeation Chromatography analysis (GPC).....	40
3.2.6. UV-visible absorption spectroscopy.....	41
3.2.7. Cyclic Voltammetry (CV) .....	41
3.2.8. Thermo-gravimetric analysis .....	42
3.2.9. Elemental analysis .....	42
<b>3.3. Synthesis of Monomers .....</b>	<b>43</b>
3.3.1. 4,4'-Dibromo-2,2'-dinitrobiphenyl (1) .....	43
3.3.2. 4,4'-Dibromobiphenyl-2,2'-diamine (2).....	44
3.3.3. 2,7-Dibromo-9H-carbazole (3).....	45

---

---

3.3.4. Heptadecan-9-ol (4).....	45
3.3.5. Heptadecan-9-yl 4-methylbenzenesulfonate (5).....	46
3.3.6. 2,7-Dibromo-9-(heptadecan-9-yl)-9H-carbazole (6).....	47
3.3.7. 9-(Heptadecan-9-yl)-2,7-bis(4,4,5,5-tetramethyl-1,3,2-dioxaborolan-2-yl)-9H-carbazole (7).....	48
3.3.8. 4,7-Dibromobenzo[c][1,2,5]thiadiazole (8).....	49
3.3.9. 1-Methyl-2-(tributylstannyl)-1H-pyrrole (9).....	50
3.3.10. 4,7-Bis(1-methyl-1H-pyrrol-2-yl)benzo[c][1,2,5]thiadiazole (10).....	50
3.3.11. 4,7-Bis(5-bromo-1-methyl-1H-pyrrol-2-yl)benzo[c][1,2,5]thiadiazole (11).....	51
3.3.12. 1,2-Bis(octyloxy)benzene (12).....	52
3.3.13. 1,2-Dinitro-4,5-bis(octyloxy)benzene (13).....	53
3.3.14. 4,5-Bis(octyloxy)benzene-1,2-diamonium chloride (14).....	54
3.3.15. 5,6-Bis(octyloxy)benzo[c][1,2,5]thiadiazole (15).....	54
3.3.16. 4,7-Dibromo-5,6-bis(octyloxy)benzo[c][1,2,5]thiadiazole (16).....	55
3.3.17. Attempted synthesis of 4,7-bis(1-methyl-1H-pyrrol-2-yl)-5,6-bis(octyloxy)benzo[c][1,2,5]thiadiazole (17).....	56
3.3.18. 2,6-Dibromoanthracene-9,10-dione (19).....	56
3.3.19. 1-Bromo-4-(dodecyloxy)benzene (20).....	57
3.3.20. 2,6-Dibromo-9,10-bis(4-(dodecyloxy)phenyl)-9,10-dihydroanthracene-9,10-diol (21).....	58
3.3.21. 2,6-Dibromo-9,10-bis(4-(dodecyloxy)phenyl)anthracene (22).....	59
3.3.22. 2,2'-(9,10-Bis(4-(dodecyloxy)phenyl)anthracene-2,6-diyl)bis(4,4,5,5-tetramethyl-1,3,2-dioxaborolane) (23).....	60
3.3.23. 4,7-Di(thiophen-2-yl)benzo[c][1,2,5]thiadiazole (24).....	61
3.3.24. 4,7-Bis(5-bromothiophen-2-yl)benzo[c][1,2,5]thiadiazole (25).....	62
3.3.25. 2,7-Dinitro-9,10-anthraquinone (26).....	62
3.3.26. 2,7-Diaminoanthracene-9,10-dione (27).....	63
3.3.27. 2,7-Dibromoanthracene-9,10-dione (28).....	64
3.3.28. 2,7-Dibromo-9,10-bis(4-(dodecyloxy)phenyl)-9,10-dihydroanthracene-9,10-diol (29).....	65
3.3.29. 2,7-Dibromo-9,10-bis(4-(dodecyloxy)phenyl)anthracene (30).....	66
3.3.30. 2,2'-(9,10-Bis(4-(dodecyloxy)phenyl)anthracene-2,7-diyl)bis(4,4,5,5-tetramethyl-1,3,2-dioxaborolane) (31).....	67
3.3.31. 3,6-Di(thiophen-2-yl)pyrrolo[3,4-c]pyrrole-1,4(2H,5H)-dione (32).....	68
3.3.32. 2,5-Bis(2-ethylhexyl)-3,6-di(thiophen-2-yl)pyrrolo[3,4-c]pyrrole-1,4(2H,5H)-dione (33).....	69
3.3.33. 3,6-Bis(5-bromothiophen-2-yl)-2,5-bis(2-ethylhexyl)pyrrolo[3,4-c]pyrrole-1,4(2H,5H)-dione (34).....	70
<b>3.4. Synthesis of Polymers .....</b>	<b>72</b>
3.4.1. Poly [9-(heptadecan-9-yl)-9H-carbazole-2,7-diyl-alt-(4',7'-bis(1-methyl-1H-pyrrol-2'-yl)-2',1',3'-benzothiadiazole)-5,5-diyl] (P1).....	72
3.4.2. Poly[3,6-difluoro-9-(heptadecan-9-yl)-9H-carbazole-2,7-diyl-alt-(4',7'-bis(1-methyl-1H-pyrrol-2'-yl)-2',1',3'-benzothiadiazole)-5,5-diyl].....	74
3.4.3. Poly [9,6-dioctyl-9H-fluornene-2,7-diyl-alt-(2',7'-bis(1-methyl-1H-pyrrol-2-yl)-2',1',3'-benzothiadiazole)-5,5-diyl].....	75

---

3.4.4. Poly(9,10-bis(4-(dodecyloxy)phenyl)-anthracene-2,6-diyl-alt-(4,7-dithiophen-2-yl)- 2',1',3'-benzothiadiazole-5,5-diyl] .....	76
3.4.5. Poly(9,10-bis(4-(dodecyloxy)phenyl)-anthracene-2,6-diyl-alt-(5,6-bis(octyloxy)-4,7-di(thiophen-2-yl)benzo[1,2,5]thiadiazole-5,5-diyl] .....	78
3.4.6. Poly(9,10-bis(4-(dodecyloxy)phenyl)-anthracene-2,6-diyl-alt-(5,6-bis(octyloxy)-4,7-di(selenophen-2-yl)benzo[1,2,5]thiadiazole-5,5-diyl] .....	79
3.4.7. Poly(9,10-bis(4-(dodecyloxy)phenyl)-anthracene-2,7-diyl-alt-(4,7-dithiophen-2-yl)- 2',1',3'-benzothiadiazole-5,5-diyl] .....	80
3.4.8. Poly(9,10-bis(4-(dodecyloxy)phenyl)-anthracene-2,7-diyl-alt-(5,6-bis(octyloxy)-4,7-di(thiophen-2-yl)benzo[1,2,5]thiadiazole-5,5-diyl] .....	82
3.4.9. Poly(9,10-bis(4-(dodecyloxy)phenyl)-anthracene-2,7-diyl-alt-(5,6-bis(octyloxy)-4,7-di(selenophen-2-yl)benzo[1,2,5]thiadiazole-5,5-diyl] .....	83
3.4.10. Poly[9,10-bis(4-(dodecyloxy)phenyl)-anthracene-2,6-diyl] .....	85
3.4.11. Poly[9,10-bis(4-(dodecyloxy)phenyl)-anthracene-2,7-diyl] .....	86
3.4.12. Poly [9,10-bis(4-(dodecyloxy)phenyl)-anthracene-2,6-diyl-alt-9,10-bis(4-(dodecyloxy)phenyl)-anthracene-2,7-diyl] .....	88
3.4.13. Poly [9-(heptadecan-9-yl)-9H-carbazole-2,7-diyl-alt-3,6-bis(thiophen-5-yl)-2,5-di(2-ethylhexyl)-pyrrolo[3,4-c]pyrrole-1,4-dione-5',5'-diyl] .....	89
3.4.14. Poly [3,6-difluoro-9-(heptadecan-9-yl)-9H-carbazole-2,7-diyl-alt-3,6-bis(thiophen-5-yl)-2,5-di(2-ethylhexyl)-pyrrolo[3,4-c]pyrrole-1,4-dione-5',5'-diyl] .....	91
3.4.15. Poly [9,6-dioctyl-9H-fluornene-2,7-diyl-alt-3,6-bis(thiophen-5-yl)-2,5-di(2-ethylhexyl)-pyrrolo[3,4-c]pyrrole-1,4-dione-5',5'-diyl] .....	92
3.4.16. Poly [9,10-bis(4-(dodecyloxy)phenyl)-anthracene-2,6-diyl-alt-3,6-bis(thiophen-5-yl)-2,5-di(2-ethylhexyl)-pyrrolo[3,4-c]pyrrole-1,4-dione-5',5'-diyl] .....	94
3.4.17. Poly [9,10-bis(4-(dodecyloxy)phenyl)-anthracene-2,7-diyl-alt-3,6-bis(thiophen-5-yl)-2,5-di(2-ethylhexyl)-pyrrolo[3,4-c]pyrrole-1,4-dione-5',5'-diyl] .....	95
<b>CHAPTER FOUR: RESULTS AND DISCUSSION – MONOMERS.....</b>	<b>97</b>
<b>4.1. Synthesis of monomers for polymers P1, P2 and P3 .....</b>	<b>97</b>
4.1.1. 4,4'-Dibromo-2,2'-dinitrobiphenyl (1) .....	99
4.1.2. 4,4'-dibromobiphenyl-2,2'-diamine (2) .....	101
4.1.3. 2,7-Dibromo-9H-carbazole (3) .....	103
4.1.4. Heptadecan-9-ol (4) .....	104
4.1.5. Heptadecan-9-yl 4-methylbenzenesulfonate (5) .....	106
4.1.6. 2,7-Dibromo-9-(heptadecan-9-yl)-9H-carbazole (6) .....	107
4.1.7. 9-(Heptadecan-9-yl)-2,7-bis(4,4,5,5-tetramethyl-1,3,2-dioxaborolan-2-yl)-9H-carbazole (7) .....	109
4.1.8. 4,7-Dibromobenzo[c][1,2,5]thiadiazole (8) .....	112
4.1.9. 1-Methyl-2-(tributylstannyl)-1H-pyrrole (9) .....	113
4.1.10. 4,7-Bis(1-methyl-1H-pyrrol-2-yl)benzo[c][1,2,5]thiadiazole (10) .....	114
4.1.11. 4,7-Bis(5-bromo-1-methyl-1H-pyrrol-2-yl)benzo[c][1,2,5]thiadiazole (11) .....	116
<b>4.2. Synthesis of monomers of polymers (P4, P5 and P6) .....</b>	<b>119</b>

4.2.1. 1,2-Bis(octyloxy)benzene (12) .....	120
4.2.2. 1,2-Dinitro-4,5-bis(octyloxy)benzene (13) .....	121
4.2.3. 4,5-Bis(octyloxy)benzene-1,2-diaminium chloride (14) .....	123
4.2.4. 5,6-Bis(octyloxy)benzo[c][1,2,5]thiadiazole (15) .....	123
4.2.5. 4,7-Dibromo-5,6-bis(octyloxy)benzo[c][1,2,5]thiadiazole (16).....	125
4.2.6. 4,7-Bis(1-methyl-1H-pyrrol-2-yl)-5,6-bis(octyloxy)benzo[c][1,2,5] thiadiazole (17) .....	126
<b>4.3. Synthesis of monomers for copolymers (P7, P8 and P9) .....</b>	<b>127</b>
4.3.1. 2,6-Dibromoanthracene-9,10-dione (19) .....	129
4.3.2. 1-Bromo-4-(dodecyloxy)benzene (20) .....	130
4.3.3. 2,6-Dibromo-9,10-bis(4-(dodecyloxy)phenyl)-9,10-dihydroanthracene 9,10-diol (21) .....	131
4.3.4. 2,6-Dibromo-9,10-bis(4-(dodecyloxy)phenyl)anthracene (22) .....	132
4.3.5. 2,2'-(9,10-Bis(4-(dodecyloxy)phenyl)anthracene-2,6-diyl)bis(4,4,5,5- tetramethyl-1,3,2-dioxaborolane) (23) .....	133
4.3.6. 4,7-Di(thiophen-2-yl)benzo[c][1,2,5]thiadiazole (24).....	135
4.3.7. 4,7-Bis(5-bromothiophen-2-yl)benzo[c][1,2,5]thiadiazole (25) .....	136
<b>4.4. Synthesis of monomers for copolymers (P10, P11 and P12) .....</b>	<b>138</b>
4.4.1. 2,7-Dinitro-9,10-anthraquinone (26) .....	139
4.4.2. 2,7-Diaminoanthracene-9,10-dione (27) .....	140
4.4.3. 2,7-Dibromoanthracene-9,10-dione (28).....	141
4.4.4. 2,7-Dibromo-9,10-bis(4-(dodecyloxy)phenyl)-9,10-dihydroanthracene- 9,10-diol (29) .....	142
4.4.5. 2,7-Dibromo-9,10-bis(4-(dodecyloxy)phenyl)anthracene (30).....	143
4.4.6. 2,2'-(9,10-Bis(4-(dodecyloxy)phenyl)anthracene-2,7-diyl)bis(4,4,5,5- tetramethyl-1,3,2-dioxaborolane) (31) .....	144
<b>4.5. Synthesis of monomers for polymers (P16, P17, P18, P19 and P20) .....</b>	<b>146</b>
4.5.1. 3,6-Di(thiophen-2-yl)pyrrolo[3,4-c]pyrrole-1,4(2H,5H)-dione (32).....	147
4.5.2. 2,5-Bis(2-ethylhexyl)-3,6-di(thiophen-2-yl)pyrrolo[3,4-c]pyrrole-1,4 (2H,5H)-dione (33).....	149
4.5.3. 3,6-Bis(5-bromothiophen-2-yl)-2,5-bis(2-ethylhexyl)pyrrolo[3,4-c]pyrrole- 1,4(2H,5H)-dione (34).....	151
<b>CHAPTER FIVE: RESULTS AND DISCUSSION – POLYMERS .....</b>	<b>153</b>
<b>5.1. Carbazole – Pyrrole based copolymers (P1, P2, P3) .....</b>	<b>153</b>
5.1.1. Preparation of P1, P2, P3.....	153
5.1.2. Characterization of P1, P2, P3.....	156
5.1.2.1. Gel Permeation Chromatography studies of P1, P2 and P3.....	156
5.1.2.2. <sup>1</sup> HNMR analysis of P1, P2 and P3 .....	157
5.1.2.3. UV-visible absorption spectroscopy analysis of P1, P2 and P3 .....	160
5.1.2.4. Cyclic Voltammetry (CV) analysis of P1, P2 and P3 .....	163
5.1.3. Thermal analysis of P1, P2, P3.....	165
<b>5.2. 2,6- Linked anthracene based copolymer (P7, P8, P9) .....</b>	<b>167</b>

---

5.2.1. Preparation of P7, P8, P9.....	167
5.2.2. Characterization of P7 , P8 , P9.....	169
5.2.2.1. Gel Permeation Chromatography studies of P7, P8 and P9.....	169
5.2.2.2. <sup>1</sup> HNMR analysis of P7, P8 and P9 .....	169
5.2.2.3. The UV-visible absorption spectroscopy analysis of P7, P8 and P9 .	173
5.2.2.4. Cyclic Voltammetry (CV) analysis of P7, P8 and P9.....	176
5.2.3. Thermal analysis of P7, P8, P9.....	178
<b>5.3. 2,7- Linked anthracene based copolymers (P10, P11, P12).....</b>	<b>180</b>
5.3.1. Preparation of P10 , P11 , P12.....	181
5.3.2. Characterization of P10, P11, P12.....	182
5.3.2.1. Gel Permeation Chromatography studies of P10, P11 and P12.....	182
5.3.2.2. <sup>1</sup> HNMR analysis of P10, P11 and P12 .....	183
5.3.2.3. UV-visible absorption spectroscopy analysis of P10, P11 and P12 ..	187
5.3.2.4. Cyclic Voltammetry (CV) analysis of P10, P11 and P12.....	191
5.3.3. Thermal analysis of P10, P11, P12.....	193
<b>5.4. Anthracene based polymers (P13, P14, P15) .....</b>	<b>195</b>
5.4.1. Preparation of P13 , P14 , P15.....	195
5.4.2. Characterization of P13 , P14 , P15.....	197
5.4.2.1. Gel Permeation Chromatography studies of P13, P14 and P15.....	197
5.4.2.2. <sup>1</sup> HNMR analysis of P13, P14 and P15 .....	197
5.4.2.3. UV-visible absorption spectroscopy analysis of P13, P14 and P15 ..	200
5.4.2.4. Cyclic Voltammetry (CV) analysis of P13, P14 and P15.....	202
5.4.3. Thermal analysis of P13, P14, P15.....	203
<b>5.5. Diketopyrrolopyrrole (DPP) based copolymers (P16, P17, P18, P19, P20)</b>	<b>205</b>
.....	.....
5.5.1. Preparation of P16, P17, P18, P19, P20 .....	206
5.5.2. Characterization of P16, P17, P18, P19, P20 .....	208
5.5.2.1. Gel Permeation Chromatography studies of P16, P17, P18, P19 and P20 .....	208
5.5.2.2. <sup>1</sup> HNMR analysis of P16, P17, P18, P19 and P20 .....	209
5.5.2.3. UV-visible absorption spectroscopy analysis of P16, P17, P18, P19 and P20.....	213
5.5.2.4. Cyclic Voltammetry (CV) analysis of P16, P17, P18, P19 and P20 .	219
5.5.3. Thermal analysis of P16, P17, P18, P19 and P20 .....	223
<b>5.6.1. Photovoltaic studies.....</b>	<b>225</b>
<b>CHAPTER SIX: CONCLUSION AND FUTURE WORK.....</b>	<b>228</b>
<b>REFERENCES.....</b>	<b>232</b>

---

---

**Table of Figures**

Figure 1. The chemical structures of some conjugated polymers. ....	2
Figure 3. Increase of conjugation leads to bands. N =number of conjugated double bonds. ....	5
Figure 4. Alkyl chains are attached to conjugated polymers in order to increase their solubility.....	6
Figure 5. Suzuki cross coupling. ....	7
Figure 6. Stille cross coupling.....	8
Figure 7. Operating Mechanism for homojunction organic solar cells.....	11
Figure 8. Operating Mechanism for heterojunction organic solar cells. ....	12
Figure 9. The difference between organic and inorganic solar cells.....	13
Figure 10. Structure of organic solar cell. ....	15
Figure 11. The structure of bilayer heterojunction devices.....	16
Figure 12. The structure of bulk heterojunction devices.....	16
Figure 13. The structure of ordered bulk heterojunction devices. ....	17
Figure 14. Molecular orbital diagram for donor-acceptor polymers.....	18
Figure 15. Example of donor and acceptor units. ....	19
Figure 16. The energy levels for donor-acceptor system. ....	20
Figure 18. The chemical structure of fluorene. ....	22
Figure 19. The chemical structure of PF10TBT. ....	23
Figure 20. The chemical structure of carbazole. ....	23
Figure 21. The chemical structure of poly(3,6-carbazole) and poly( 2,7-carbazole) and the starting materials for their preparation. ....	24
Figure 23. Some benzothiazole polymers for use in bulk heterojunction solar cells. ....	26
Figure 24. Some thiophene and selenophene derivatives. ....	27
Figure 25. Low band gap polymer containing N-substituted pyrrole. ....	28
Figure 26. The chemical structure of diketopyrrolopyrrole (DPP) and some of DPP containing polymers and recorded power conversion efficiencies. ....	29
Figure 27. The chemical structure of anthracene. ....	30
Figure 28. Molecular structure of some fullerene derivatives. ....	30
Figure 29. The chemical structures of P1, P2 and P3. ....	32
Figure 30. The chemical structures of P4, P5 and P6. ....	33
Figure 31. The chemical structures of P7, P8 and P9. ....	34
Figure 32. The chemical structures of P10, P11 and 12.....	35
Figure 33. The chemical structures of P13, P14, P15. ....	36
Figure 34. The chemical structures of P16 , P17 , P18, P19 and P20.....	38
Figure 35. Monomers required for the preparation of polymers P1, P2 and P3. ....	97
Figure 36. The <sup>1</sup> HNMR spectrum of 9-(heptadecan-9-yl)-2,7-bis(4,4,5,5-tetramethyl-1,3,2-dioxaborolan-2-yl)-9H-carbazole (7). ....	111
Figure 37. The <sup>1</sup> HNMR spectrum for 4,7-bis(5-bromo-1-methyl-1H-pyrrol-2-yl)benzo[c][1,2,5] thiadiazole (11).....	118
Figure 38. Monomers required for preparing P4, P5 and P6. ....	119
Figure 39. Monomers required for preparing P7, P8 and P9. ....	127

---

---

Figure 40. The $^1\text{H}$ NMR spectrum of 2,2'-(9,10-bis(4-(dodecyloxy)phenyl)anthracene-2,6-diyl)bis(4,4,5,5-tetramethyl-1,3,2-dioxaborolane) (23).....	135
Figure 41. The $^1\text{H}$ NMR spectrum for 4,7-bis(5-bromothiophen-2-yl)benzo[c][1,2,5]thiadiazole (25).....	137
Figure 42. Monomers required for preparing P10, P11 and P12. ....	138
Figure 43. The $^1\text{H}$ NMR spectrum for 2,2'-(9,10-bis(4-(dodecyloxy)phenyl)anthracene-2,7-diyl)bis(4,4,5,5-tetramethyl-1,3,2-dioxaborolane) (31).....	145
Figure 44. Monomers required for preparing P16, P17 ,P18, P19 and P20.....	146
Figure 45. The $^1\text{H}$ NMR spectrum for 3,6-bis(5-bromothiophen-2-yl)-2,5-bis(2-ethylhexyl) pyrrolo[3,4-c]pyrrole-1,4(2H,5H)-dione (34).....	152
Figure 46. The chemical structure of P1 , P2 , P3.....	153
Figure 47. The mechanism of Suzuki Cross Coupling.....	154
Figure 48. $^1\text{H}$ NMR spectrum of P1 in $\text{C}_2\text{D}_2\text{Cl}_4$ at 80 °C.....	158
Figure 49. $^1\text{H}$ NMR spectrum of P2 in $\text{C}_2\text{D}_2\text{Cl}_4$ at 80 °C.....	159
Figure 50. $^1\text{H}$ NMR spectrum of P3 in $\text{C}_2\text{D}_2\text{Cl}_4$ at 80 °C.....	160
Figure 51. Absorption spectra of P1(2), P2 and P3 in chloroform solutions. ....	161
Figure 52. Absorption spectra of P1(2), P2 and P3 as a thin films. ....	162
Figure 53. The H-F electrostatic interaction of P2.....	162
Figure 54. The chemical structure of PCDTBT, PFCDTBT and APFO 3. ....	163
Figure 55. Cyclic voltammetry curves of P1(2), P2 and P3 .....	164
Figure 56. TGA curves of P1, P2 and P3.....	166
Figure 57. The chemical structure of P7 , P8 , P9.....	167
Figure 58. $^1\text{H}$ NMR spectrum of P7 in $\text{C}_2\text{D}_2\text{Cl}_4$ at 80 °C.....	170
Figure 59. $^1\text{H}$ NMR spectrum of P8 in $\text{C}_2\text{D}_2\text{Cl}_4$ at 80 °C.....	171
Figure 60. $^1\text{H}$ NMR spectrum of P9 in $\text{C}_2\text{D}_2\text{Cl}_4$ at 80 °C.....	172
Figure 61. Absorption spectra of P7, P8 and P9 in chloroform solutions.....	173
Figure 62. Absorption spectra of P7, P8 and P9 as thin films.....	175
Figure 63. The chemical structure of PCDTBT, PCDTOBT and PCDSOBT. ....	176
Figure 64. Cyclic voltammetry curves of P7, P8 and P9. ....	177
Figure 65. TGA curves of P7, P8 and P9.....	179
Figure 66. Chemical structures of P10, P11 and P12.....	180
Figure 67. $^1\text{H}$ NMR spectrum of P10 in $\text{C}_2\text{D}_2\text{Cl}_4$ at 100 °C .....	184
Figure 68. $^1\text{H}$ NMR spectrum of P11 in $\text{C}_2\text{D}_2\text{Cl}_4$ at 100 °C.....	185
Figure 69. The $^1\text{H}$ NMR for the P12 in $\text{C}_2\text{D}_2\text{Cl}_4$ at 100 °C.....	186
Figure 70. Absorption spectra of P10, P11 and P12 in Chloroform solution. ....	187
Figure 71. Absorption spectra of P10, P11 and P12 as thin films.....	188
Figure 72. Absorption spectra of P7 and P10 as thin films.....	189
Figure 73. Absorption spectra of P8 and P11 as thin films.....	190
Figure 74. Absorption spectra of P9 and P12 as thin films.....	191
Figure 75. Cyclic voltammetry curves of P10, P11 and P12. ....	192
Figure 76. TGA curves of P10, P11 and P12.....	194
Figure 77. The chemical structure of P13 , P14 , P15.....	195
Figure 78. $^1\text{H}$ NMR spectrum of P13 in $\text{C}_2\text{D}_2\text{Cl}_4$ at 100 °C.....	198
Figure 79. $^1\text{H}$ NMR spectrum of P14 was carried out in $\text{C}_2\text{D}_2\text{Cl}_4$ at 100 °C.....	199
Figure 80. $^1\text{H}$ NMR spectrum of P15 in $\text{C}_2\text{D}_2\text{Cl}_4$ at 100 °C.....	200
Figure 81. Absorption spectra of P13, P14 and P15 in chloroform solutions.....	201

---

---

Figure 82. Absorption spectra of P13, P14 and P15 as a thin films.....	202
Figure 83. Cyclic voltammetry curves of P13, P14 and P15. ....	203
Figure 84. TGA curves of P13, P14 and P15. ....	204
Figure 85. The chemical structures of P16, P17, P18, P19 and P20.....	205
Figure 86. <sup>1</sup> HNMR spectrum of P16 in C <sub>2</sub> D <sub>2</sub> Cl <sub>4</sub> at 100 °C.....	209
Figure 87. <sup>1</sup> HNMR spectrum of P17 in C <sub>2</sub> D <sub>2</sub> Cl <sub>4</sub> at 100 °C.....	210
Figure 88. <sup>1</sup> HNMR of P18 in C <sub>2</sub> D <sub>2</sub> Cl <sub>4</sub> at 100 °C. ....	211
Figure 89. <sup>1</sup> HNMR spectrum of P19 in C <sub>2</sub> D <sub>2</sub> Cl <sub>4</sub> at 100 °C. ....	212
Figure 90. <sup>1</sup> HNMR spectrum of P20 in C <sub>2</sub> D <sub>2</sub> Cl <sub>4</sub> at 100 °C.....	213
Figure 91. Absorption spectra of P16, P17 and P18 in Chloroform solutions.....	214
Figure 92. . Absorption spectra of P19 and P20 in Chloroform solutions. ....	214
Figure 93. Absorption spectra of P16, P17 and P18 as thin films.....	215
Figure 94. The H-F electrostatic interaction of P17.....	216
Figure 95. Absorption spectra of P19 and P20 as thin films.....	216
Figure 96. Absorption spectra of P7 and P19 as thin films.....	218
Figure 97. Absorption spectra of P10 and P20 as thin films.....	219
Figure 98. Cyclic voltammetry curves of P16, P17 and P18. ....	220
Figure 99. Cyclic voltammetry curves of P19 and P20. ....	221
Figure 100. TGA curves of P16, P17 and P18. ....	223
Figure 101. TGA curves of P19 and P20. ....	224

---

---

**Table of Schemes**

Scheme 1. The preparation route for 9-(heptadecan-9-yl)-2,7-bis(4,4,5,5-tetramethyl-1,3,2-dioxaborolan-2-yl)-9H-carbazole (7). .....	98
Scheme 2. The preparation route for 4,7-bis(5-bromo-1-methyl-1H-pyrrol-2-yl)benzo[c][1,2,5]thiadiazole (11).....	99
Scheme 3. Synthesis of 4,4'-dibromo-2,2'-dinitrophenyl (1). .....	99
Scheme 4. The mechanism of preparation of 4,4'-dibromo-2,2'-dinitrophenyl (1). .....	100
Scheme 5. Preparation of 4,4'-dibromobiphenyl-2,2'-diamine (2).....	101
Scheme 6. The mechanism of preparation of 4,4'-dibromobiphenyl-2,2'-diamine (2). .....	102
Scheme 7. The preparation of 2,7-dibromo-9H-carbazole (3). .....	103
Scheme 8. The mechanism of preparation of 2,7-dibromo-9H-carbazole (3). .....	103
Scheme 9. The preparation of heptadecan-9-ol (4). .....	104
Scheme 10. The mechanism of preparation of heptadecan-9-ol (4). .....	105
Scheme 11. The preparation of heptadecan-9-yl 4-methylbenzenesulfonate (5)...	106
Scheme 12. The mechanism of preparation of heptadecan-9-yl 4-methylbenzenesulfonate (5). .....	106
Scheme 13. The preparation of 2,7-dibromo-9-(heptadecan-9-yl)-9H-carbazole (6) .....	107
Scheme 14. The mechanism for the preparation of 2,7-dibromo-9-(heptadecan-9-yl)-9H-carbazole (6).....	108
Scheme 15. The preparation of 9-(heptadecan-9-yl)-2,7-bis(4,4,5,5-tetramethyl-1,3,2-dioxaborolan-2-yl)-9H-carbazole (7).....	109
Scheme 16. The mechanism of preparation of 9-(heptadecan-9-yl)-2,7-bis(4,4,5,5-tetramethyl-1,3,2-dioxaborolan-2-yl)-9H-carbazole (7). .....	110
Scheme 17. The preparation of 4,7-dibromobenzo[c][1,2,5]thiadiazole (8).....	112
Scheme 18. The mechanism of the preparation of 4,7-dibromobenzo[c][1,2,5]thiadiazole (8).....	112
Scheme 19. The preparation of 1-methyl-2-(tributylstannyl)-1H-pyrrole (9).....	113
Scheme 20. The mechanism of preparation of 1-methyl-2-(tributylstannyl)-1H-pyrrole (9).....	114
Scheme 21. The preparation of 4,7-bis(1-methyl-1H-pyrrol-2-yl)benzo[c][1,2,5]thiadiazole (10).....	114
Scheme 22. The mechanism of preparation of 4,7-bis(1-methyl-1H-pyrrol-2-yl)benzo[c][1,2,5]thiadiazole according to stille (10).....	115
Scheme 23. The preparation of 4,7-bis(5-bromo-1-methyl-1H-pyrrol-2-yl)benzo[c][1,2,5]thiadiazole (11).....	116
Scheme 24. The mechanism of the formation of 4,7-bis(5-bromo-1-methyl-1H-pyrrol-2-yl)benzo[c][1,2,5]thiadiazole (11). .....	117
Scheme 25. The preparation route of 4,7-bis(5-bromo-1-methyl-1H-pyrrol-2-yl)-5,6-bis(octyloxy)benzo[c][1,2,5]thiadiazole. ....	119
Scheme 26. The preparation of 1,2-bis(octyloxy)benzene (12). .....	120

---

---

Scheme 27. The mechanism of the preparation of 1,2-bis(octyloxy)benzene (12).	120
Scheme 28. The preparation of 1,2-dinitro-4,5-bis(octyloxy)benzene (13).	121
Scheme 29. The mechanism of the preparation of 1,2-dinitro-4,5-bis(octyloxy)benzene (13).	122
Scheme 30. The preparation of 4,5-bis(tetradecyloxy)benzene-1,2-diaminium chloride (14).	123
Scheme 31. The preparation of 5,6-bis(octyloxy)benzo[c][1,2,5]thiadiazole (15).	124
Scheme 32. The mechanism for the preparation of (15).	124
Scheme 33. The preparation of 4,7-dibromo-5,6-bis(octyloxy)benzo[c][1,2,5]thiadiazole (16).	125
Scheme 34. The preparation of 4,7-bis(1-methyl-1H-pyrrol-2-yl)-5,6-bis(octyloxy)benzo[c][1,2,5]thiadiazole (17).	126
Scheme 35. The preparation route of 2,2'-(9,10-bis(4-(dodecyloxy)phenyl)anthracene-2,6-diyl)bis(4,4,5,5-tetramethyl-1,3,2-dioxaborolane) (23).	128
Scheme 36. The preparation route of 4,7-bis(5-bromothiophen-2-yl)benzo[c][1,2,5]thiadiazole (25).	128
Scheme 37. The preparation of 2,6-dibromoanthracene-9,10-dione (19).	129
Scheme 38. The mechanism of the preparation of 2,6-dibromoanthracene-9,10-dione.	129
Scheme 39. The preparation of 1-bromo-4-(dodecyloxy)benzene (20).	130
Scheme 40. The mechanism of the preparation of 1-bromo-4-(dodecyloxy)benzene.	131
Scheme 41. The preparation of 2,6-dibromo-9,10-bis(4-(dodecyloxy)phenyl)-9,10-dihydroanthracene-9,10-diol (21).	131
Scheme 42. The mechanism of the preparation of 2,6-dibromo-9,10-bis(4-(dodecyloxy)phenyl)-9,10-dihydroanthracene-9,10-diol (21).	132
Scheme 43. The preparation of 2,6-dibromo-9,10-bis(4-(dodecyloxy)phenyl)anthracene (22).	133
Scheme 44. The preparation of 2,2'-(9,10-bis(4-(dodecyloxy)phenyl)anthracene-2,6-diyl)bis(4,4,5,5-tetramethyl-1,3,2-dioxaborolane) (23).	134
Scheme 45. The preparation of 4,7-di(thiophen-2-yl)benzo[c][1,2,5]thiadiazole (24).	136
Scheme 46. The preparation of 4,7-bis(5-bromothiophen-2-yl)benzo[c][1,2,5]thiadiazole (25).	136
Scheme 47. The preparation route of 2,2'-(9,10-bis(4-(dodecyloxy)phenyl)anthracene-2,7-diyl)bis(4,4,5,5-tetramethyl-1,3,2-dioxaborolane) (31).	139
Scheme 48. The preparation of 2,7-dinitro-9,10-anthraquinone (26).	139
Scheme 49. The preparation of 2,7-diaminoanthracene-9,10-dione (27).	140
Scheme 50. The preparation of 2,7-dibromoanthracene-9,10-dione (28).	141
Scheme 51. The preparation of 2,7-dibromo-9,10-bis(4-(dodecyloxy)phenyl)-9,10-dihydroanthracene-9,10-diol (29).	142
Scheme 52. The preparation of 2,7-dibromo-9,10-bis(4-(dodecyloxy)phenyl)anthracene (30).	143

---

---

Scheme 53. The preparation of 2,2'-(9,10-bis(4-(dodecyloxy)phenyl)anthracene-2,7-diyl)bis(4,4,5,5-tetramethyl-1,3,2-dioxaborolane) (31).....	144
Scheme 54. Preparation route to 3,6-bis(5-bromothiophen-2-yl)-2,5-bis(2-ethylhexyl) pyrrolo[3,4-c]pyrrole-1,4(2H,5H)-dione (34).....	147
Scheme 55. The preparation of 3,6-di(thiophen-2-yl)pyrrolo[3,4-c]pyrrole-1,4(2H,5H)-dione (32).....	148
Scheme 56. Proposed mechanism for the preparation of 3,6-di(thiophen-2-yl)pyrrolo [3,4-c]pyrrole-1,4(2H,5H)-dione (32) (adapted from Wallquist et al <sup>102</sup> ) .....	149
Scheme 57. The preparation of 3,6-di(thiophen-2-yl)pyrrolo[3,4-c]pyrrole-1,4(2H,5H)-dione (33).....	149
Scheme 58. The mechanism of the preparation of 3,6-di(thiophen-2-yl)pyrrolo[3,4-c]pyrrole-1,4(2H,5H)-dione (33).....	150
Scheme 59. The preparation of 3,6-bis(5-bromothiophen-2-yl)-2,5-bis(2-ethylhexyl)pyrrolo[3,4-c]pyrrole-1,4(2H,5H)-dione (34).....	151
Scheme 60. Preparation of P1.....	155
Scheme 61. Preparation of P2.....	156
Scheme 62. Preparation of P3.....	156
Scheme 63. Preparation of P7.....	168
Scheme 64. Preparation of P8.....	168
Scheme 65. Preparation of P9.....	169
Scheme 66. Preparation of P10.....	181
Scheme 67. Preparation of P11.....	182
Scheme 68. Preparation of P12.....	182
Scheme 69. Preparation of P13.....	196
Scheme 70. Preparation of P14.....	196
Scheme 71. Preparation of P15.....	197
Scheme 72. Preparation of P16.....	206
Scheme 73. Preparation of P17.....	206
Scheme 74. Preparation of P18.....	207
Scheme 75. Preparation of P19.....	207
Scheme 76. Preparation of P20.....	208

---

**Table of Tables**

Table 1. Yields and GPC results for P1, P2 and P3. ....	157
Table 2. Summary of photo-physical and electrochemical properties of P1, P2 and P3.....	165
Table 3. Yields and GPC results for P7 , P8 and P9. ....	169
Table 4. Summary of the photophysical and the electrochemical properties of P7, P8 and P9.....	178
Table 5. Yields and GPC results for P10 , P11 and P12. ....	183
Table 6. The UV-Vis and CV results of P6 – P12. ....	193
Table 7. Yields and GPC results for P13 , P14 and P15. ....	197
Table 8. Summary of the UV-Vis and CV results of P13-P15 .....	203
Table 9. Yields and GPC results for P16, P17, P18, P19 and P20.....	208
Table 10. UV-Vis and the CV results for P16 – P20. ....	221
Table 11. Photovoltaic properties of polymers. ....	225

**Abbreviations****A**

A Electron Acceptor

AcOH Acetic Acid

Al Aluminium

**B**

bs Broad singlet (NMR)

t-BuLi *tert*-Butyl lithium**C**

Ca Calcium

CB Conducting Band

CHCl<sub>3</sub> ChloroformCDCl<sub>3</sub>-d<sub>1</sub> Deuterated ChloroformC<sub>2</sub>D<sub>2</sub>Cl<sub>4</sub>-d<sub>2</sub> Deuterated 1,1,2,2-Tetrachloroethane

CT Photoinduced Charge Transfer

CV Cyclic Voltammetry

18-crown-6 1,4,7,10,13,16-Hexaoxacyclooctadecane

**D**

D Electron Donor

d Doublet (NMR)

DCM Dichloromethane

DMF N,N-dimethylformamide

DMSO Dimethyl sulfoxide

DP Degree of Polymerization

---

DPP	Diketopyrrolopyrrole
<b>E</b>	
$E_g$	Band gap energy
EtOAc	Ethyl Acetate
EtOH	Ethanol
Et <sub>2</sub> O	Diethyl ether
eV	Electron Volt
EQE	External Quantum Efficiency
<b>F</b>	
Fc	Ferrocene
FET	Field-Effect Transistor
FF	Fill Factor
FT-IR	Fourier Transform Infra-Red Spectroscopy
<b>G</b>	
GPC	Gel Permeation Chromatography
<b>H</b>	
HOMO	Highest Occupied Molecular Orbital
HPLC	High Performance Liquid Chromatography
Hz	Hertz
<b>I</b>	
IGS	Indium Gallium Selenium
IR	Infra-Red Spectroscopy
ITO	Indium Tin Oxide

IQE	Internal Quantum Efficiency
$I_{sc}$	Short Circuit Voltage
<b>L</b>	
LED	Light Emitting Diode
LUMO	Lowest Unoccupied Molecular Orbital
$\lambda$	Wavelength (nm)
<b>M</b>	
m	Multiplet
MEH-PPV	Poly(2-methoxy-5-(2-ethylhexyloxy)-1,4-Phenylene vinylene)
$M_n$	Number average molecular weight
$M_w$	Weight average molecular weight
M.p.	Melting point
MW	Megawatts
<b>N</b>	
NBS	N-Bromosuccinide
NMR	Nuclear Magnetic Resonance
nm	nanometer
<b>O</b>	
OFET	Organic field-effect transistor
OLED	Organic light emitting diode
OLET	Organic light emitting transistor
OSC	Organic Solar Cell
OPV	Organic Photovoltaic

### P

PA	Polyacetylene
PCBM	Phenyl-C <sub>61</sub> -butyric acid methyl ester (Phenyl-C <sub>71</sub> -butyric acid methyl ester)
PD	Polydispersity
PET	Poly(ethylene terephthalate)
P3AT	Poly(3-alkylthiophene)
P3HT	Poly(3-hexylthiophene)
PLED	Polymer light emitting diodes
PPh <sub>3</sub>	Triphenylphosphine
PPV	Poly( <i>para</i> -phenylenevinylene)
P3HS	Poly(3-hexylselenophene)
P3DPT	Poly(3-dodecylthiophene)
P3OPT	Poly(3-octylthiophene)
PPy	Polypyrrole
PT	Poly(thiophene)
PV	Photovoltaic

### R

R <sub>s</sub>	Small series resistance
R <sub>sh</sub>	Large shunt resistance

### S

S	Singlet (NMR)
---	---------------

### T

t	Triplet (NMR)
---	---------------

TGA	Thermo-gravimetric analysis
THF	Tetrahydrofuran
TLC	Thin Layer Chromatography
TW	Terawatts
<b>U</b>	
UV-vis	Ultra Violet-visible spectroscopy
<b>V</b>	
$V_{oc}$	Open Circuit Voltage
V	Volt

## Chapter One: Introduction

As the world's population increases and the standard of living improves, the demands for energy rises. This is a major concern since we currently depend upon a finite amount of traditional fossil fuel to meet most of our energy needs, and this source is depleting rapidly as well as getting hard to extract from the earth. It is expected that the global oil production will decrease within the next 10-20 years<sup>1</sup>, whilst, conversely, oil consumption is expected to increase within the same time period. In 2008, global consumption was approximately 15 TW<sup>2</sup>, and if current trends continue, this is expected to double by 2025 due to an increased demand from emerging economies, for example China and India<sup>3</sup>. Furthermore, global consumption is expected to more than double (to about 30-35 TW) by 2050<sup>4</sup>. In 2012, the natural resources such as petroleum, coal and natural gas provided 83% of U.S energy consumption. The natural resources are inexpensive and relatively easily to access, but they present a crucial problem to the world. Fossil fuel extraction and combustion processes produce various gases, such as carbon dioxide, carbon monoxide and sulphur dioxide, which cause increased pollution and global warming<sup>2,5</sup>. Consequently, new types of renewable and clean energy, such as biomass, wind and solar, are becoming essential. In the last few years, solar cells have become one of the most promising renewable sources reaching 560MW in 2002, and it is expected that global energy production from solar cells will reach 140 GW in 2030<sup>6</sup>.

### 1.1. Background to conjugated polymers

Since the discovery of the conductivity of semiconducting organic materials in 1961 by Okamoto and co-workers, conjugated polymers have attracted much interest and shown a great promise. These researchers reported that polyacetylene, the simplest linear conjugated system, has a conductivity of  $10^{-5}$  S/cm<sup>7</sup>. In 1958, polyacetylene was discovered by Natta but it was black, air sensitive and insoluble material, so for a long time it was of little interest<sup>8</sup>. In 1977, Heeger, Shirakawa

MacDiarmid and co-workers discovered the metallic conductivity of doped conjugated polyacetylene. It is reported that the conductivity of polyacetylene increased by up to ten orders of magnitude upon exposure to halogen vapours<sup>9</sup>. For their invaluable research and discovery Heeger, Shirakawa, and Macdiarmid were awarded the Nobel Prize in Chemistry in 2000<sup>10</sup>.

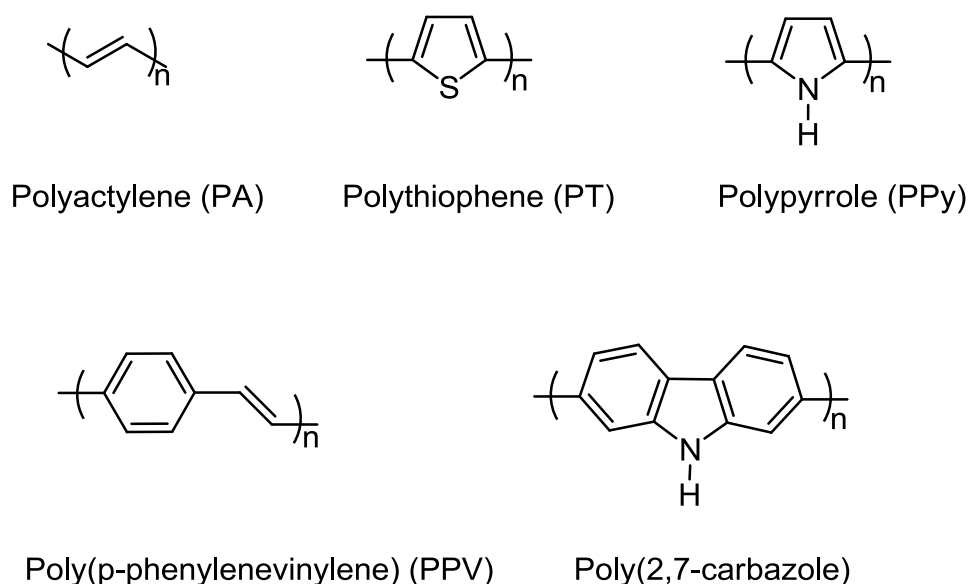


**Figure 1. The chemical structures of some conjugated polymers.**

Nowadays, semiconducting polymers have been developed for many uses. The first generation of conjugated polymers involved early work on polyacetylene, polypyrrole, polythiophene and polyaniline. Whilst the second generation of conjugated polymers involved the work on soluble conjugated materials, such as poly(3-alkylthiophene). The third generation focused on more complicated molecular structures with more atoms in the repeat unit for example donor – acceptor copolymer systems, such as the polycarbazole copolymer structure which was reported by Lelerc and bithiophene-acceptor copolymer reported by Konarks<sup>11</sup>. The conductivity of conjugated polymers means they have various potential applications, such as Organic Photovoltaic (OPV)<sup>12</sup>, Organic Light Emitting Diodes (OLED)<sup>13</sup>, Organic Thin Film Transistors (OTFT)<sup>14</sup>, sensors<sup>15</sup> and batteries<sup>16</sup>. Despite the fact that organic materials offer a lower level of electrochemical performance when compared with inorganic materials, they have many advantages over inorganic semiconductors. Inorganic materials demand a

very high degree of crystallinity and purity, increasing the cost of materials and manufacture <sup>17</sup>. On the other hand, organic materials can be fabricated into devices using cheap techniques, for example spin coating technique <sup>18</sup>, model-inkjet printing technique <sup>19</sup>, screen printing technique <sup>20</sup>, roll-to-roll printing technique <sup>21</sup>, spray coating technique <sup>22</sup> and even paint brush application <sup>23</sup>. Moreover, the structure of organic materials can be modified to provide the material properties necessary for specific applications, while inorganic materials have intrinsic properties <sup>24</sup>.

### 1.2. Chemical structure of conjugated polymers

Conjugated polymers are carbon-based macromolecules which possess an extended  $\pi$ -binding system with interchanging single and double bonds along the backbone of the conjugated polymer chain <sup>25</sup>. In the saturated plastic polymer, the four electrons around the carbon atom are in  $sp^3$  hybridized orbitals and each of forms a covalent bond (with an angle  $109.5^\circ$ ). In this case, all four electrons are employed to create  $\sigma$  bonds lacking  $\pi$  electrons. Hence, charge movement does not occur and a large band gap exists between  $\sigma$  bonding and  $\sigma^*$  anti-bonding, resulting in insulating materials. On the other hand, the chemical structure of conjugated polymer constructs of three  $sp^2$  and  $p_z$  orbitals. The single bond comprises of only the  $\sigma$ -bond (strong chemical bond), whilst the double bond contains  $\sigma$ -bond and  $\pi$ -bond. The three  $sp^2$  orbitals form an  $\sigma$ -bond, which lies in the plane with an angle of  $120^\circ$ . In addition, the  $p_z$  orbitals form a  $\pi$ -bond due to mutual overlapping with a neighbouring  $p_z$ , and this is perpendicular to the plane of the  $\sigma$ -bond. The  $\sigma$  bond are strong and form the shape of polymer backbone, whereas the  $\pi$  bonds are loosely bound due to less overlapping of the two  $p_z$  orbitals compared to the three  $sp^2$ . Thus, delocalization of electrons occur along the conjugation polymer system, and electrons belong to the whole chain instead of belonging to one atom <sup>11a,26</sup>.

The chemical properties of conjugated polymers are provided by the localized electrons in the  $\sigma$ -bond. However, the electrochemical and optical properties of conjugated polymers are provided by the localized electrons in the  $\pi$ -bonds. These

electrons can be moved easily along the chain. The two  $\pi$ -bands in the conjugated polymers are called molecular orbitals. The first one is called the Highest Occupied Molecular Orbital (HOMO), which is the filled  $\pi$ -band, whilst the second one is called the Lowest Occupied Molecular Orbital (LUMO), which is the empty  $\pi$ -band. Moreover, moving electrons from HOMO to LUMO provides optical and electrical properties. The chemical structure and electronic configuration result in the conjugated polymer having various properties, which can be utilized in a wide range of applications<sup>11a,27</sup>.

### 1.3. The properties of conjugated polymers

The unique structure of conjugated polymers leads to them having both optical and electronic properties<sup>28</sup>. In plastic polymers, such as polyethylene, the electron is excited from  $\sigma$ -bonded into  $\sigma^*$ -antibonded orbital, which leads to structural instability because  $\sigma$ -bond orbitals hold the chain of the polymer together, which makes these kind of materials photoresistor. However, in semiconducting polymers, excitation occurs within a  $\pi$ -band and it does not lead to bond breaking because the structure is held by  $\sigma$  – bonds, which makes these material conductors<sup>26b</sup>.

#### 1.3.1. Conjugated polymer's conductivity

The electronic properties of semiconducting polymers arise from their unique chemical structure and their number of the highest occupied molecular orbital (HOMO) level and the lowest unoccupied molecular orbital (LUMO) level. The band theory illustrates that the highest occupied band, which result from the HOMO of each monomer unit, is caused by the valence band ( $\pi$ ), whilst the lowest unoccupied band, which results from LUMO of each monomer unit, is caused by the conducting band ( $\pi^*$ ) as shown in Figure 2.<sup>29</sup>

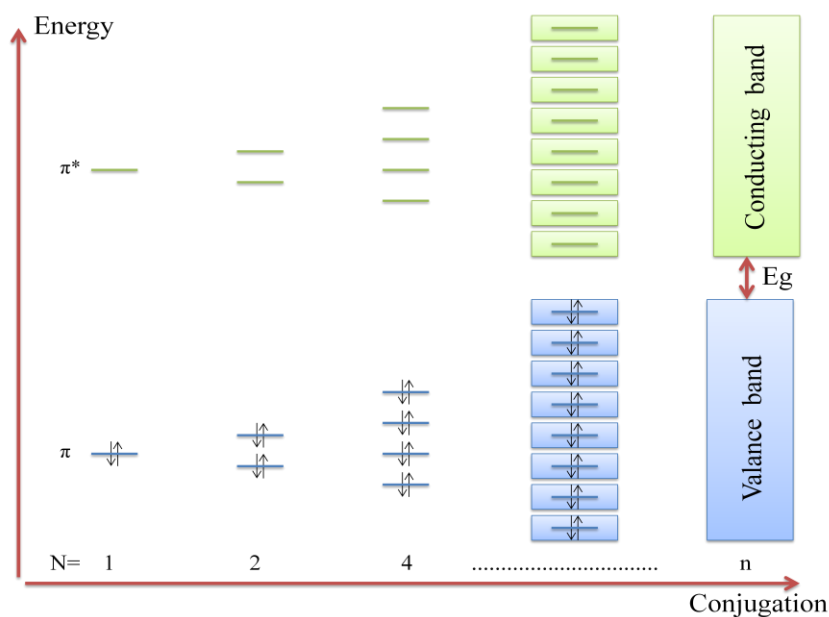


**Figure 2. Increase of conjugation leads to bands. N = number of conjugated double bonds.**

The alternation of single and double bonds along the polymer chain leads to there being a gap in the electron density states. For a single molecule, the difference in energy between the HOMO ( $\pi$ ) and LUMO ( $\pi^*$ ) is called the band gap energy ( $E_g$ ). The electronic properties and the conductivity of polymers are determined by band gap energy. The band gap can be managed by structure modification of the polymer. Furthermore, increasing the chain length leads to more conjugation and an increase in the number of molecular orbitals, as shown in Figure 2, and increasing conjugation results in increasing the energy level of the HOMO and decreasing the energy level of the LUMO. The large number of filled  $\pi$ -bonding orbitals that have energy close to each other and the large number of unfilled  $\pi$ -anti-bonding orbitals that have energy close to each other create a valance band and a conducting band with a small energy band gap separating them, which is the band gap energy. The effect of conjugation length might be reduced due to steric hindrance in the polymer backbone, which leads to twisting of the backbone of the polymer and reduction of the overlap between  $\pi$ -orbitals<sup>30</sup>. The band gap energy ( $E_g$ ) of semiconducting polymers is between 1 and 4 eV. On the other hand, the band gap energy of conducting materials is 0 eV and the band gap energy of insulating materials is larger than 4 eV.<sup>31</sup>

### 1.3.2. Solubility of conjugated polymers

An additional significant property of conjugated polymers is their solubility in common organic solvents when appropriate functional side groups are added. In addition, the deposition of conjugated polymer films can be achieved using spin-coating and spray coating techniques in air from solution. The fabrication of conjugated polymer based thin film devices are becoming less difficult and cheaper when compared with devices produced by vacuum deposition techniques. The formation and the morphology of the film are affected by the interaction of the solubilised polymer and substrate surface at the interface.

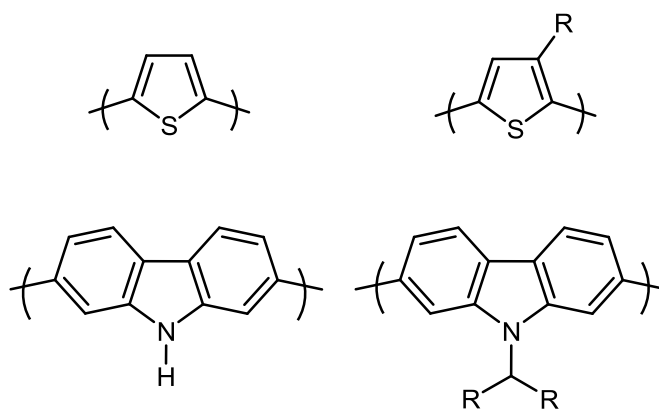


**Figure 3. Alkyl chains are attached to conjugated polymers in order to increase their solubility.**

### 1.4. Synthesis of conjugated polymers

There are many ways to prepare conjugated polymers. First of all, conjugated polymers can be prepared using electrochemical polymerization, either anodic, which is most commonly used, or cathodic. In addition, conjugated polymers can be prepared using metal catalysed reaction such as Kumada, Yamamoto, Suzuki and Stille cross coupling<sup>32</sup>. In this project, only Still cross coupling and Suzuki cross coupling polymerizations were used.

### 1.4.1. Suzuki Cross Coupling

In 1979, Suzuki et al. reported that a carbon-carbon bond can be formed between organoboron compounds and vinyl and aryl halide compounds by using a palladium catalyst in the presence of base<sup>33</sup>. The idea of palladium catalysed coupling is that two compounds are foregathered on the palladium due to the formation of metal-carbon bonds. In the next step, the two compounds are coupled to each other, and this leads to the creation of a new carbon-carbon single bond<sup>34</sup>. For his valuable work in the field of carbon-carbon bond formation using catalysed cross coupling reactions, Akira Suzuki was awarded the Nobel prize in Chemistry in 2010. He shared this with Professor Richard F. Heck and Ei-ichi Negishi<sup>35</sup>.

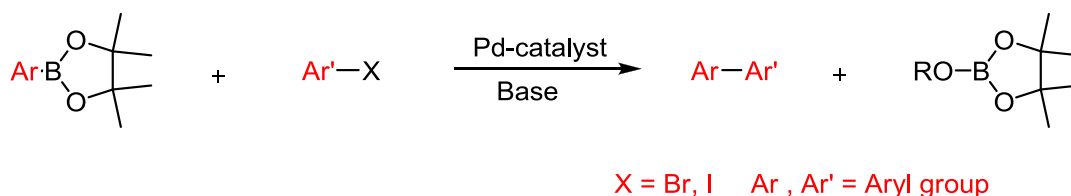


**Figure 4. Suzuki cross coupling.**

The high stability and low toxicity of organoboron compounds has made this cross coupling reaction very practical and of widespread interest due to its potential use in various applications. The most commonly used catalyst is Pd(PPh<sub>3</sub>)<sub>4</sub>. Some reactions need a more specialised combination of catalyst and ligand, such as palladium acetate Pd(OAc)<sub>2</sub> and tri-*o*-tolyl phosphine; the ligands are used to activate the catalyst<sup>36</sup>.

### 1.4.1. Stille Coupling Reaction

In 1978, Stille and Milstein reported that carbon – carbon bonds can be formed between an organotin compound and an organohalide compound using a palladium catalyst<sup>37</sup>. Stille cross coupling has been widely used for the coupling of aromatic and vinyl compounds. Furthermore, organotin compounds have many advantages, as they tolerate a wide range of functional groups and are air and moisture stable<sup>38</sup>.

In addition, conjugated polymers can be prepared using Stille cross coupling with a high yield.

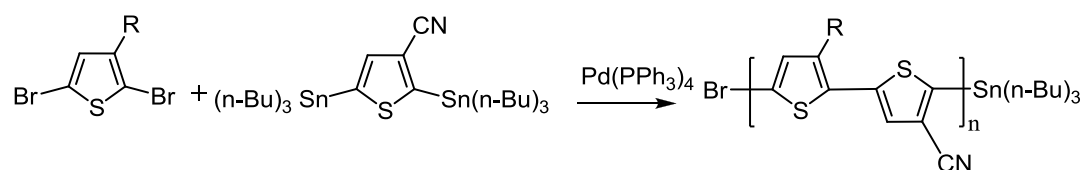


**Figure 5. Stille cross coupling.**

The yield in Suzuki cross-coupling and Stille cross-coupling are comparable. Some highly sensitive compounds do not tolerate the basic conditions of a Suzuki reaction. Nevertheless, the higher cost and toxicity of organotin compounds makes Suzuki cross-coupling the preferred choice<sup>39</sup>.

## 1.5. Introduction to Solar Cells

Solar cells or photovoltaic devices are solid or non-solid state devices which convert the energy of the solar radiation (photon) directly into electrical charges using photovoltaic effects<sup>40</sup>. Solar energy has attracted much attention of late. It is reported that earth's surface received  $1.78 \times 10^{14}$  KWh. So, if 0.16 % of the earth was covered with solar cells with a power conversion efficiency of 10%, then all electricity needs could be met<sup>41</sup>. Due to the high cost of ultrahigh crystalline silicon solar cells, a number of solar cell technologies have emerged in an attempt to reduce the cost of the technology, and these have shown promise. Nowadays, there are many types of solar cell, such as thin film inorganic technologies, for instance amorphous silicon, copper indium gallium selenium (IGS) and cadmium telluride (CdTe). In addition, emerging photovoltaic technologies, such as Dye-sensitized cells and organic solar cells have shown promising laboratory results combined with low manufacturing costs.

### 1.5.1. Brief History of Organic Solar Cells

Since the discovery of conjugated polymers by Heeger, Shirakawa, and MacDiarmid, they have been the subject of much academic research regarding their potential application. In 1979, the first organic solar cell based on two layers donor acceptor, and it was created from copper phthalocyanine and a perylene tetracarboxylic derivative. In addition, the study by Tang was not published until 1986, when he reported 1% efficiency<sup>42</sup>. In 1991, O'Regan and Gratzel built a non-solid state solar cell which is called a dye sensitized solar cell<sup>43</sup>. Power conversion efficiency of 11.4% has been recorded using these cells.<sup>44</sup> However, the non-solid state cells have disadvantages and need to be encapsulated to prevent the liquid electrolyte from leaking and drying up.<sup>45</sup> The technical difficulties associated with this type of solar cell render it unsuitable for practical use. In 1993, Heeger built the first polymer /C<sub>60</sub> heterojunction solar cell from a soluble derivative of poly(phenylene-vinylene) as the donor and buckminsterfullerene C<sub>60</sub> as the acceptor, but a low power conversion efficiency was reported.<sup>46</sup> Then in 1994, Yu

built the first bulk polymer / C<sub>60</sub> heterojunction using poly(3-octyl thiophene), poly[2-methoxy-5-(2'-ethyl-hexyloxy)-1,4-phenylene vinylene] and C<sub>60</sub><sup>47</sup>. The bulk polymer / polymer heterojunction solar cell was then built by Yu et al. and Halls et al. in 1995. They prepared devices using poly(3-octyl thiophene) as the acceptor and poly[2-methoxy-5-(2'-ethyl-hexyloxy)-1,4-phenylene vinylene] as the donor, and a spincoating technique was used to blend the two polymers<sup>48</sup>. The power conversion efficiency of organic solar cells had been very low, and it was difficult to pass the 1% efficiency barrier. The fundamental nature of charge photogeneration and transport in conjugated polymers lead to the low efficiency of organic solar cell devices. In inorganic material, light absorption generates free electron and hole charges directly due to intergap transition, but in organic materials, light absorption results in the production of bound electron-hole pairs called excitons<sup>49</sup>. In 2007 Heeger et al. built a new type of organic solar cell, a tandem solar cell, and power conversion efficiency of more than 6% were reported. In tandem solar cell, two solar cells with various absorption characteristics are connected in order that a wide range of the solar spectrum can be harvested<sup>50</sup>. Finally, the highest power conversion efficiency for organic solar cell has been recorded so far is 10%<sup>44</sup>.

### 1.5.2. Operating Mechanism for Organic Solar Cells

The conversion of photons into electricity by organic solar cells depends on three main processes:

- 1- Absorption of photon (light) and creation of excitons.
- 2- Diffusion and dissociation of excitons and holes and electrons creation.
- 3- Charge transport to the electrodes<sup>51</sup>.

#### 1.5.2.1. Operating Mechanism For Homojunction Devices

The first step is generation of excitons. The active layer of organic photovoltaic cells absorbs incidental light, which leads to the promotion of an electron from the

---

HOMO energy level to the LUMO energy level, creating an exciton. The second step involves diffusion and dissociation of the exciton at the interface between the active layer and the cathode. The last step is charge transport and collection by electrodes, meaning the electron is moved to the photocathode and the hole is moved to the photoanode, as shown in Figure 6<sup>52</sup>.

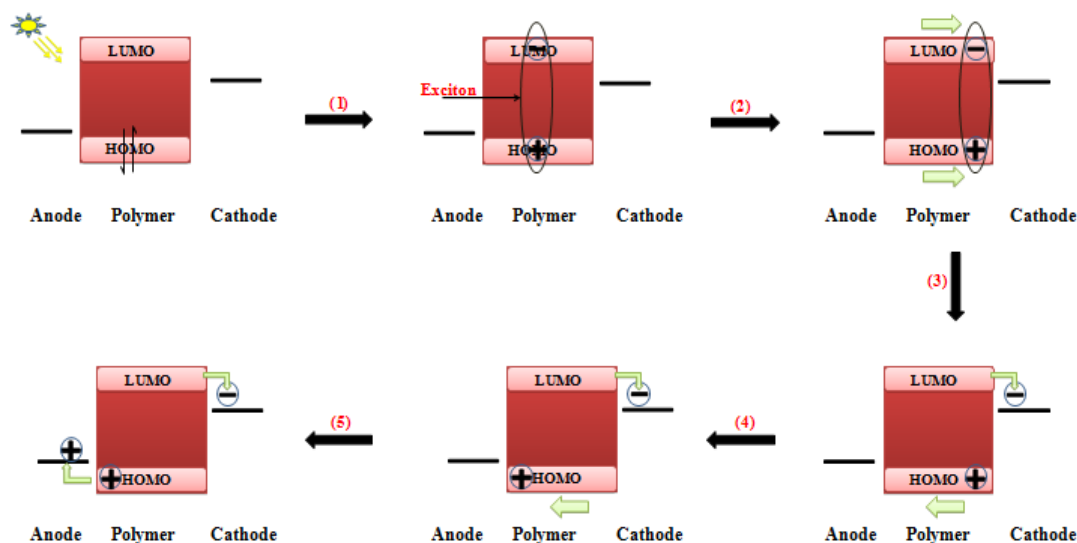


**Figure 6. Operating Mechanism for homojunction organic solar cells.**

### 1.5.2.2. Operating Mechanism For Heterojunction Devices

The conversion of sunlight into electrical energy process in organic heterojunction photovoltaic cells is more complicated than monojunction photovoltaics, as explained below.

The first step is generation of excitons. The active layer of organic photovoltaic cells absorbs incidental light, which leads to an electron from the HOMO energy level being promoted to the LUMO energy level. Thus, electron-hole pairs form a tightly bound state which is called an exciton.<sup>53</sup> When the excitons are created, they can diffuse randomly in the active layer. The average diffusion length of an exciton in a conjugated polymer is in the order of 5-20 nm<sup>54</sup>. For most conjugated polymers used in organic solar cells, the life time of excitons is approximately 300

picosecond<sup>55</sup>. When the excitons reach the donor-acceptor heterojunction interface, the electric field facilitates the dissociation of the excitons, and free charges (hole and electron) are generated. It has been illustrated that using two electrodes with different work functions leads to a built up electric field in the device, which is crucial for exciton dissociation and charge generation at the interface<sup>56</sup>. After the dissociation of excitons and the generation of free charge carriers, the hole stays in the HOMO of the donor, while the electron is transferred to the LUMO of the acceptor. This is the last step in charge transport and collection by the cathode and the anode<sup>53,57</sup>.

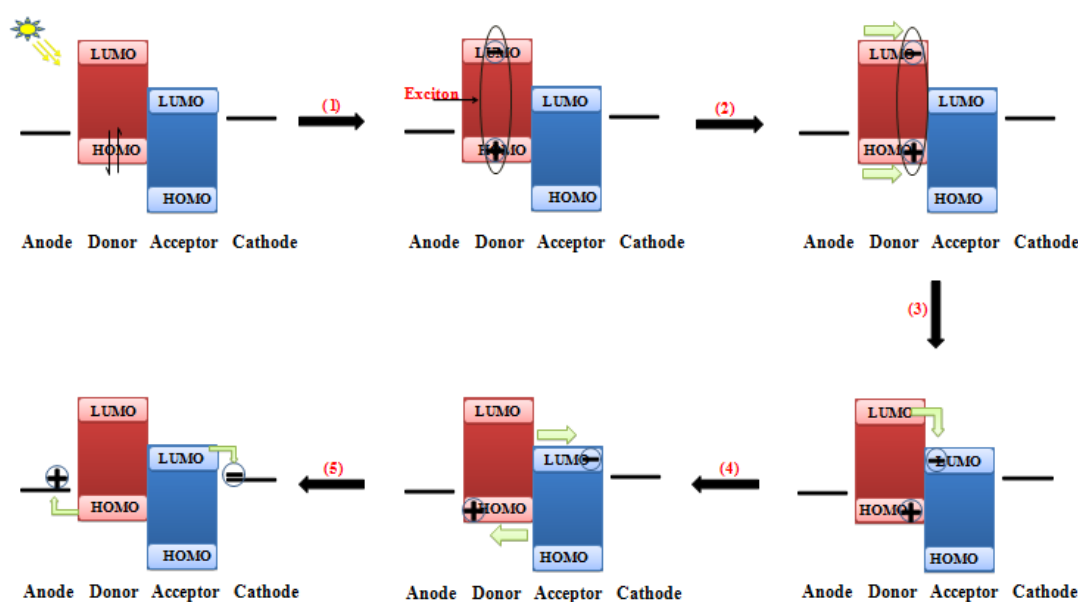


Figure 7. Operating Mechanism for heterojunction organic solar cells.

### 1.5.3. Inorganic and Organic Solar Cells

The main difference between inorganic solar cells and organic solar cells is in relation to charge generation. In the case of inorganic solar cells, absorption of photons leads to the formation of free electron and hole. For organic solar cells, photon absorption leads to the generation of excitons with the hole and the electron being bound to each other<sup>57b,58</sup>. Moreover, it has been reported that the hole mobility in conjugated polymers is in the range of  $10^{-1}$  to  $10^{-7}$   $\text{cm}^2/(\text{Vs})$  and the mobility of electrons in conjugated polymers is in the range of  $10^{-4}$ - $10^{-9}$   $\text{cm}^2/(\text{Vs})$ .

However, the mobility of holes and electrons in crystalline silicon are 475 and 1500  $\text{cm}^2/(\text{Vs})$  respectively<sup>59</sup>. On the other hand, the organic active layer in organic solar cells can be chemically modified by incorporating different functional groups in order to provide the material with specific properties.<sup>24</sup>

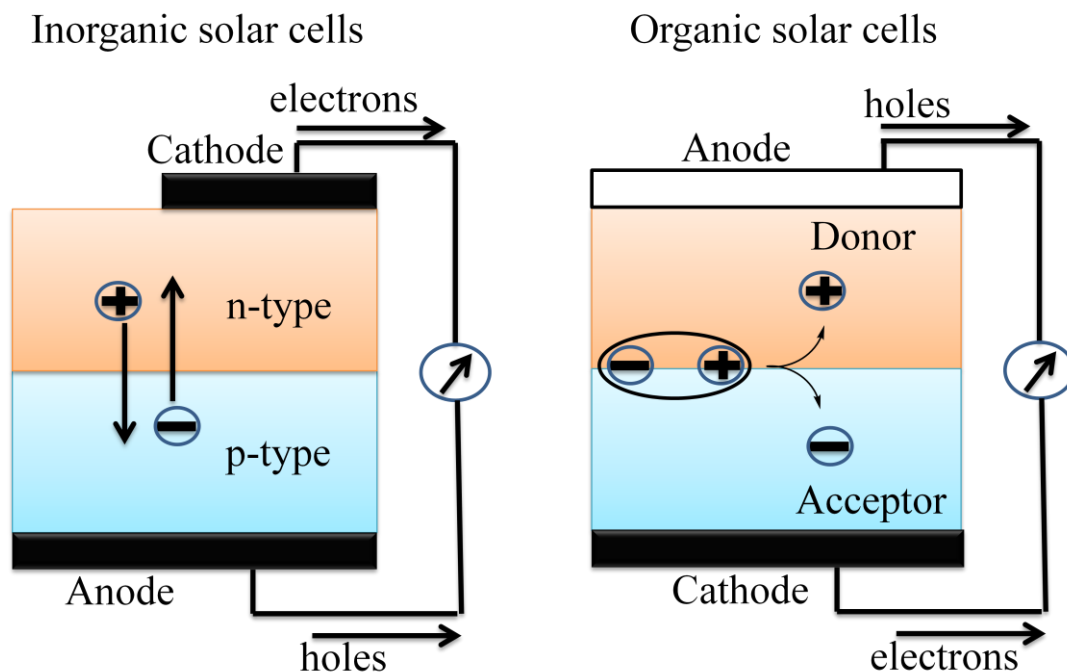


Figure 8. The difference between organic and inorganic solar cells.

#### 1.5.4. The Concept of Heterojunction

The idea of a heterojunction is to use two semiconducting materials with various electron affinities and ionisation potentials that support exciton dissociation. Using a donor-acceptor interface makes exciton dissociation easier, the interface allows the electrons to go through to the materials with the high electron affinity, and so holes stay in the materials with the lower ionisation potential. Thus, the bound of electron and hole pairs are separated by a barrier<sup>58a,60</sup>. The act of the photo-excited electron hopping from donating material to the accepting material (exciton dissociation process) is called photoinduced charge transfer (CT). The photoinduced CT from conjugated polymer to the fullerene ( $\text{C}_{60}$ ) takes place in sub-picoseconds ( $< 10^{-12}$  s). This ultrafast process was discovered by Heeger et al. and

Yoshina et al. in 1992<sup>53c,61</sup>. The photoinduced CT is followed by a charge being transferred to the electrodes (mobile carrier sweep out by internal voltage)<sup>62</sup>.

### 1.5.5. Organic Solar Cell Device Structure

Organic solar cell devices are manufactured in a sandwich structure, consisting of four layers, as show in Figure 9. The first layer is a transparent glass, the purpose of which is to protect the device. Other materials, such as polyethylene terephthalate (PET), can be used instead of glass to make the device more flexible. The second layer is a conductive anode made from Indium Tin Oxide (ITO), which has a large optical band gap (3.7eV) that does not allow wavelength longer than approximately 350 nm to be absorbed. The first and second layers are made of transparent materials that allow light to go through to the third layer, which is a photo active layer. This can be made from single or heterojunction materials. The final layer is aluminium, which acts as cathode. The cathode and anode are made from materials with different work functions; the anode being made from a high work function material, such as ITO, and the cathode being made from a low function work materials, such as Al. This structure provides built in potential, which leads to the generation of an electric field to facilitate CT<sup>63</sup>. In addition, the ITO surface is fabricated with a thin layer of poly(ethylenedioxythiophene) doped with a poly(styrene sulfonate) (PEDOT:PSS) coated from solution. The PEDOT:PSS layer acts as an electron-block layer, which improves hole injection into the anode by improving the electrical contact between the active layer and the ITO and adjusting energy levels between the HOMO energy level of the donor in the active layer and the work function of the ITO<sup>64</sup>. Moreover, Marks et al. investigated whether NiO can perform the same role of PEDOT:PSS in order to improve hole injection to the electrode, leading to the power conversion efficiency of the organic solar cell improving<sup>65</sup>. Graphene has been used as an anode instead of the ITO. However, lower power conversion efficiency was reported, possibly as a result of graphene being semi-transparentl<sup>66</sup>. Finally, it is reported that LiF or Ca can be used at the interface of the active layer and cathode in order to facilitate the electron injection

into cathode by adjusting the energy level between the LUMO of acceptor in the active layer and the work function of cathode <sup>67</sup>.

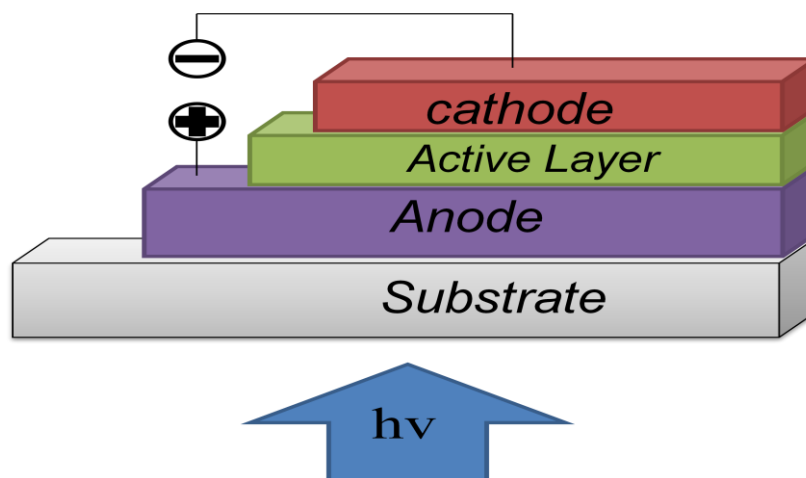


**Figure 9. Structure of organic solar cell.**

The structure of organic solar cell varies, depending on the nature of the active layer. The four types are described in the next section:

#### 1.5.5.1. Single Layer Devices

A single layer device is the simplest organic solar cell structurally. It consists of a single conjugated polymer sandwiched between two electrodes with different work functions. The thickness of the active layer is between 40-200nm. The power conversion efficiency is limited and so heterojunction donor / acceptor devices have been built <sup>59c,63b,68</sup>.

#### 1.5.5.2. Bilayer Heterojunction Devices

In a bilayer heterojunction, the active layer consists of two layers stacked together with a planar interface. One layer acts as a donor, while the other layer acts as an acceptor, and they are sequentially sandwiched between two electrodes with different work functions, as shown in Figure 10. The donor is made from a p-type organic material, while the acceptor is made from an n-type organic material. The

first conjugated polymer bilayer device was built by Sariciftici et al. by evaporating  $C_{60}$  on the top of a spin-cast MEH-PPV layer<sup>59c,63b,68</sup>.

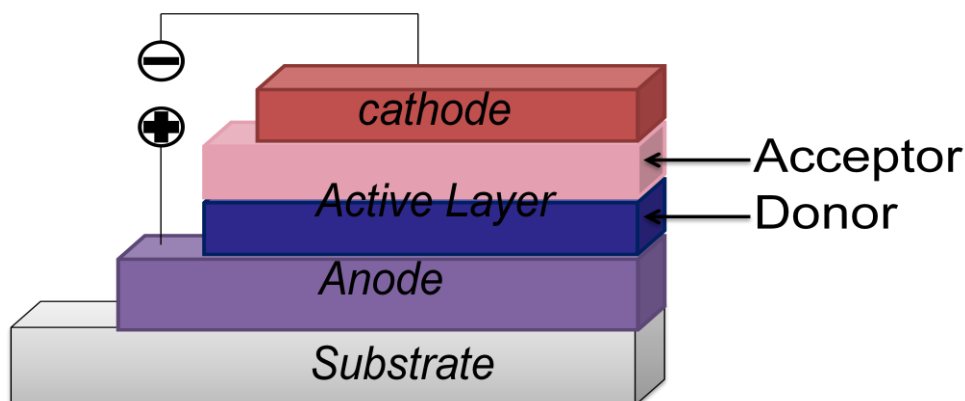


**Figure 10.** The structure of bilayer heterojunction devices.

### 1.5.5.3. Bulk heterojunction devices

In bulk heterojunction devices, the active layer consists of a donor and an acceptor, which are blended together in one layer between two electrodes with different work function, as shown in Figure 11. The interfacial area of the bulk heterojunction devices is significantly larger than that of bilayer structure, and this improves exciton dissociation efficiency. In bulk heterojunction devices, there is no specific direction for electron and hole, and so selecting different electrodes as cathode and anode is very critical with regard to charge carrier harvesting<sup>59c,63b,68</sup>.

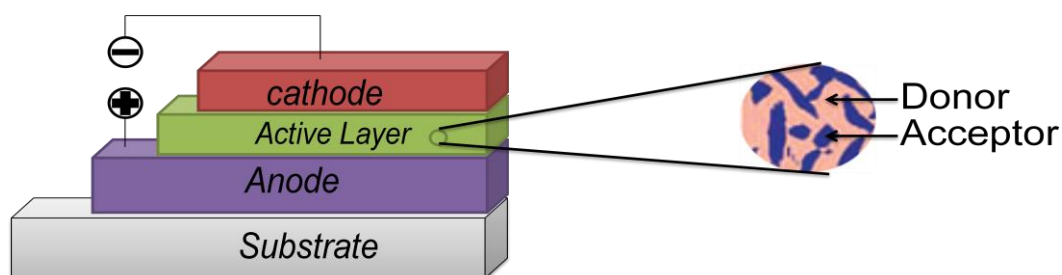


**Figure 11.** The structure of bulk heterojunction devices.

#### 1.5.5.4. Ordered bulk heterojunction devices

In ordered bulk heterojunction devices, the active layer is in between the bilayer and bulk heterojunction devices. This structure has many advantages over bulk heterojunction devices, for instance in bulk heterojunction devices, there are dead ends and the way path to the electrodes might be interrupted, which prevent holes and electrons from reaching the cathode or anode. On the other hand, there is no dead end in ordered devices due to optimizing the structure. However, despite their advantages, it is more difficult to make order bulk heterojunction devices than bulk heterojunction devices <sup>68-69</sup>.

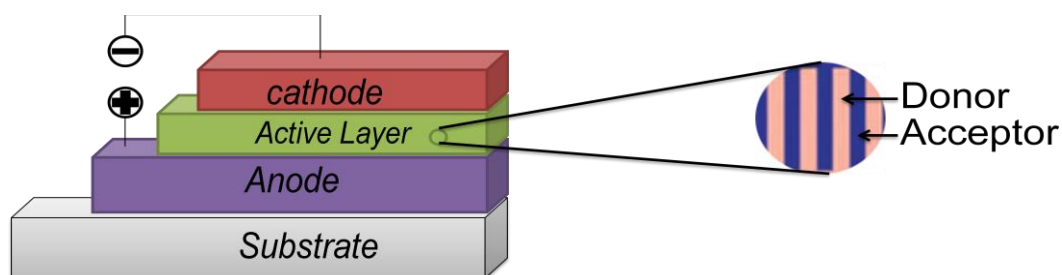


Figure 12. The structure of ordered bulk heterojunction devices.

#### 1.5.6. Donor – acceptor system

In order to increase the power conversion efficiency of organic solar cells, various conjugated polymers with differences in the constitution of the repeat units (such as homo-polymers, donor-acceptor systems, quinoid polymers and double cable polymers) have been investigated. A high power conversion efficiency was recorded with these systems, but a donor acceptor system is the most common used due to its advantages and the versatility of its design <sup>70</sup>.

Donor-acceptor system is a polymer with alternating electron rich and electron deficient monomers. Thus, the molecular orbital of the donor interacts with the molecular orbital of the acceptor to obtain a polymer molecular orbital in which the HOMO energy level of the polymer is close to the HOMO energy level of the donor and the LUMO energy level of the polymer is close to the LUMO energy level of

the acceptor, as shown in Figure 13. In a donor-acceptor system, orbital mixing of the donor and the acceptor results in reduced band gap energy and increased conjugation <sup>71</sup>.

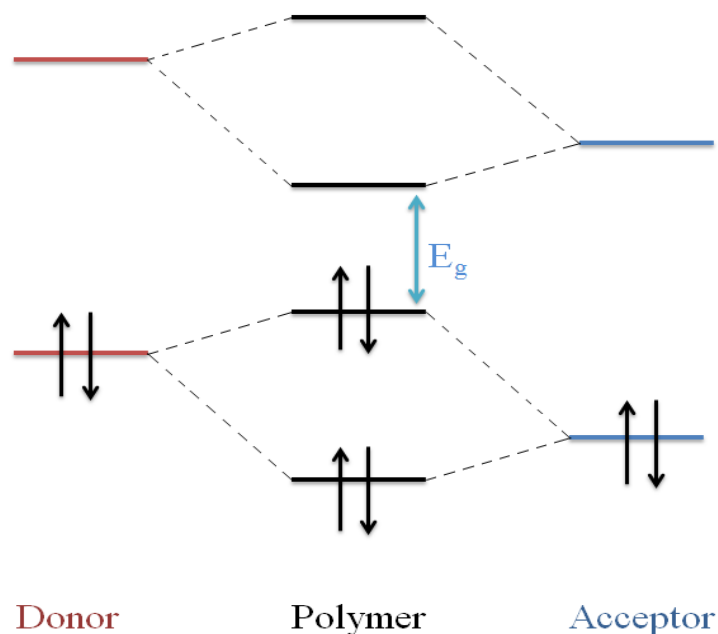


**Figure 13. Molecular orbital diagram for donor-acceptor polymers.**

The HOMO and LUMO energy levels of the polymer can be controlled by the donor and the acceptor, respectively. Adding electron donating groups such as amines and alkoxy groups to the donor decreases the ionization potential and increases the HOMO energy level, while adding electron withdrawing groups, such as ketones and nitro groups, to the acceptor increases electron affinity and lowers the LUMO energy level, as shown in Figure 14. The HOMO of the donor is responsible for the energy level of the polymer's HOMO while the LUMO level of the acceptor is responsible for the energy level of the polymer's LUMO <sup>72</sup>.

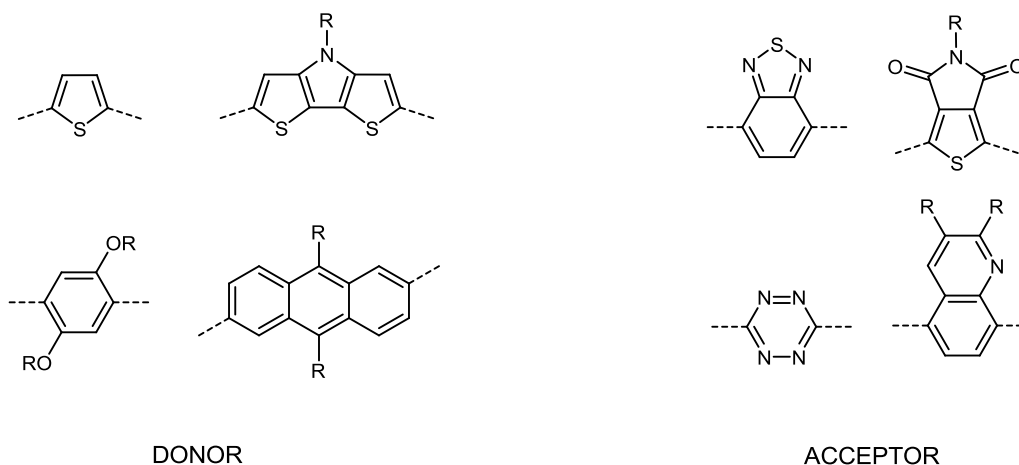


**Figure 14. Example of donor and acceptor units.**

### 1.5.7. General requirements for the active layer in organic solar cell

As mentioned before, over the past twenty years, a large number of structures, blends and materials have been studied in order to obtain the ideal organic solar cell with high power conversion efficiency. It is easier to prepare devices using inorganic solar cells because free charge migration is very fast and the collection is easier. On the other hand, the generation of electricity is three to five times more expensive using high crystalline inorganic solar cells than fossil fuel<sup>73</sup>. However, the efficiency of organic solar cells has improved over the last ten years. Power conversion efficiency over 10% and ten years lifetime are required<sup>59c</sup>. According to the literature, the theoretical power conversion efficiency for a bulk heterojunction organic solar cell is 23%<sup>74</sup>. To prepare an ideal polymer for use in an organic solar cell with high power conversion efficiency, the following requirements need to be met.

#### 1.5.7.1. Short Circuit Current

Short circuit current ( $I_{sc}$ ) is related to the number of excitons generated in solar illumination. The active layer should have a broad absorption in the solar spectrum in order to maximize exciton generation. The solar spectrum range is from 280nm to more than 3200nm. On the other hand, conjugated polymers can efficiently absorb photons with energy equivalent to their band gap energy. Due to the very low photon absorption of PCBM in visible and near IR region, the conjugated

polymer donor must act as the main photon absorber. As mentioned before, lowering the band gap energy leads to increased photon absorption, where the ideal polymer should have a band gap in the range of 1.4-1.5 eV<sup>70,75</sup>.

### 1.5.7.2. The Open Circuit Voltage

Open circuit voltage is related to the energy difference between the HOMO energy level of the polymer and the LUMO energy level of the acceptor. In theory, lowering the HOMO energy level of the polymer donor would increase the open circuit voltage. On the other hand, this would increase the band gap energy and so decrease short circuit current. In addition, the LUMO energy level of the polymer donor cannot be low because it is necessary to have at least 0.3 eV energy difference between the LUMO energy level of the polymer donor and the LUMO energy level of the acceptor in order to facilitate the charge dissociation process and avoid recombination. Also, the LUMO energy level of the acceptor and the HOMO energy level of the donor need to be with respect to the work function of cathode and anode in order to facilitate charge collection, as shown in Figure 15<sup>76</sup>.

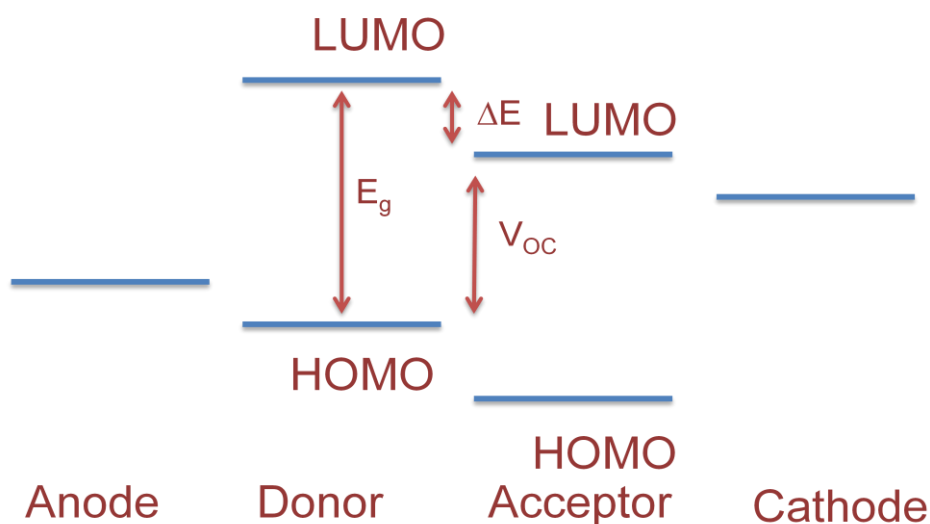


Figure 15. The energy levels for donor-acceptor system.

In order to increase the power conversion efficiency, an electron rich donor unit is polymerized with an electron deficient acceptor unit. Also, the HOMO and LUMO energy levels of the polymer can be controlled by the HOMO energy level of the

donor and the LUMO energy level of the acceptor, respectively. Thus, in order to achieve high open circuit voltage and low band gap energy, a weak donor –strong acceptor theory has been suggested<sup>70,77</sup>.

Thus, in the preparation of the polymer, a donor and acceptor repeated units with the appropriate HOMO and LUMO energy levels as well as suitable electrodes need to be used. A compromise has to be reached in order to make the ideal device. According to the literature, the HOMO energy level should be in the range 5.2 – 5.8 eV while the LUMO energy level should in the range 3.7 – 4.0 eV when the polymer blended with phenyl-C<sub>61</sub>-butyric acid methyl ester PCBM in order to obtain low band gap energy and high open circuit voltage<sup>78</sup>.

### 1.5.7.3. Film morphology

Identifying the ideal HOMO and LUMO energy levels for the donor and the acceptor is not the only issue when making ideal devices. The active layer needs to have uniform film forming properties in order to have good film morphology<sup>79</sup>. In addition, the active layer requires high hole mobility for the polymer donor and high electron mobility for the acceptor<sup>80</sup>. Finally, the active layer should be highly stable both thermally and electrochemically with a long term lifetime. Three year lifetime stability was reported by Knoarka in their organic solar cells<sup>70</sup>. In theory, when a polymer donor with a band gap energy of 1.5 eV, a HOMO energy level of approximately -5.4 eV and a LUMO energy level of -3.9 eV is blended with PC<sub>61</sub>BM, with a fill factor of 0.65, external quantum efficiency of 65 % and optimised morphology, 10% power conversion efficiency would be obtained<sup>70</sup>.

### 1.5.8. Organic Solar Cell Materials

Recently, organic solar cells have attracted much research attention due to their advantages over inorganic solar cell. As a consequence, understanding the mechanism, challenges and requirements of these devices has improved, which has lead to the power conversion efficiency increasing dramatically, reaching almost 10%. In this section, the organic materials that have been studied the most for use in organic solar cells are discussed.

---

### 1.5.8.1. Fluorene-based Conjugated Polymers.

Polyfluorene derivatives are a very important class of polycyclic hydrocarbon system; they have been of much research interest due to their attractive properties. They promise to be useful as active materials in electric devices, such as light emitting diodes, organic thin film transistors and organic solar cells <sup>81</sup>.

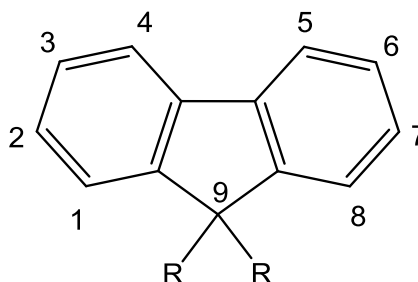


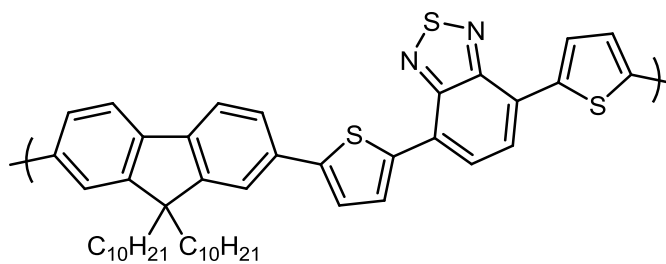
**Figure 16. The chemical structure of fluorene.**

The chemical structure of fluorene is shown in Figure 16. Fluorene consists of two phenyl rings, which are joined by a methylene bridge and a carbon-carbon bond. The methylene bridge provides the structure with more planarity and so rise the orbital overlap and the conjugation in the conjugated system. In addition, the methylene bridge in 9-position can be easily functionalised to improve both the solubility and processability of polymer <sup>82</sup>.

Polyfluorene derivatives have a wide band gap energy due to the low energy level of the HOMO, which is in the range of -5.5 to -5.8 eV, providing these derivatives with high thermal and chemical stability. In addition, these derivatives have high good hole and electron mobility, good processibility and great forming film morphology, which lead to them being widely investigated in electronic devices, especially organic light emitting diodes (OLED).

The high charge mobility and open circuit voltage of these derivatives makes them suitable for organic solar cells. However, the wide band gap energy and low HOMO energy level of these derivatives means they harvest less photons from sunlight. Nevertheless, due to the moderately electron rich nature of fluorene derivatives they are suitable as donor in the donor- acceptor system, which leads to narrowing of the band gap energy and harvesting more photons from sun light <sup>81b,83</sup>. Sweelssen et al. blended poly[ 9,9'-didecafluorene-alt-(bis-thiophene)

benzothiadiazole] (PF10TBT) with PCBM, and 4.2% power conversion efficiency was obtained, as shown in Figure 17<sup>84</sup>.



PF<sub>10</sub>TBT , PCE= 4.2%

**Figure 17. The chemical structure of PF10TBT.**

### 1.5.8.2. Carbazole-based Conjugated Polymers.

For more than three decades, carbazole, which is a cyclic aromatic hydrocarbon system, has been investigated extensively. The chemical structure of carbazole is similar to that of fluorene. It is a two phenyl group connected by a carbon – carbon bond. However, instead of the methylene bridge in fluorene, a nitrogen atom links the phenyl groups in carbazole. The unique structure of carbazole gives it many advantages, such as aromaticity, which provides high chemical and environmental stability. In addition, the nitrogen atom can be substituted with a different functional group to increase solubility and processibility. Furthermore, a different functional groups can be introduced to the carbazole ring. Carbazole derivatives have high hole migrating properties due to their high electron nature provided by the carbazole ring. Finally, carbazole is of interest since it can be prepared from cheap basic materials<sup>85</sup>.

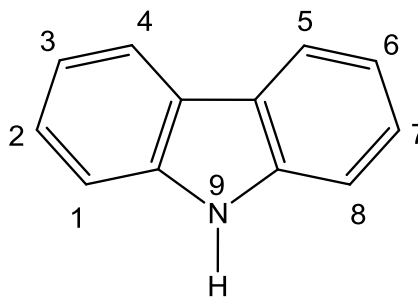


**Figure 18. The chemical structure of carbazole.**

Due to there being many carbazole derivatives, they have become very strong candidates for use in organic solar cells, organic light emitting diodes and organic thin film transistors. There are two common carbazole structures: 3,6-linked carbazole and 2,7-linked carbazole<sup>86</sup>. The poly(3,6-carbazole)s have been widely studied in relation to their use in OLED and electrochromic devices<sup>87</sup>. They can be prepared directly by using Yamamoto cross coupling in the presence of a Ni catalyst. However, they show a large amount of twisting<sup>85a,b</sup>.

In 2001, Morin and Leclerc synthesised the first 2,7 carbazole based polymer<sup>88</sup>. Many subsequent years of research on the use of poly(2,7-carbazole)s in OLED and OFET applications have revealed a great potential for their use in bulk heterojunction solar cell devices because 2,7-carbazole derivatives exhibit a low HOMO energy level which leads to them having good air stability and high open circuit voltage ( $V_{OC}$ ). In addition, the HOMO and LUMO energy levels of carbazole polymers can be modified easily by changing the side chain. The HOMO energy level (the ionisation potential) of carbazole derivatives is lower than that of fluorene derivatives because a nitrogen lone pair in carbazole participates in the aromatic system, which leads to an increase in delocalised electrons<sup>81b,85a,86</sup>.

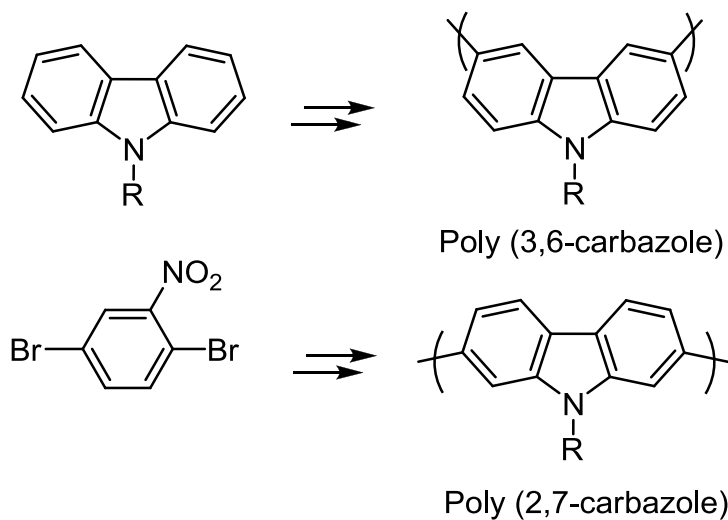


**Figure 19. The chemical structure of poly(3,6-carbazole) and poly(2,7-carbazole) and the starting materials for their preparation.**

The 2,7-carbazole homopolymer has been widely used as a donor in bulk heterojunction devices. The first poly(2,7-carbazole) based device was studied by Mullen et al. They blended poly(2,7-carbazole), as the donor, with

tetracarboxydiimide, as the acceptor. However, they obtained low power conversion efficiency (PCE=0.6%)<sup>89</sup>. The highest power conversion efficiency that has been recorded for poly(2,7-carbazole) is 6.1%, as reported by Heeger et al., as shown in **Error! Reference source not found.** They blended poly[N-9''-hepta-decanyl-2,7-carbazole-alt-5,5-(4',7'-di-2-thienyl-2',1',3'-benzothiadiazole)] (PCDTBT), as the donor, with the fullerene derivatives [6,6]-phenyl C<sub>70</sub>-butyric acid methyl ester (PC<sub>70</sub>BM), as the acceptor, in a bulk heterojunction device<sup>90</sup>.

### 1.5.8.3. Benzothiazole Derivatives-based Conjugated Polymers.

Benzothiazole derivatives have been widely used as acceptors in donor-acceptor systems in electronic devices due to the high electron deficiency of these materials. Low band gap energy can be obtained when these derivatives are polymerized with electron rich materials, such as carbazole and thiophene. There has been a great deal of research into the application of these derivatives polymerized with carbazole in solar cells such as PCDTPT, as shown in **Error! Reference source not found.**<sup>88,91</sup>. The highest power conversion efficiency recorded for 2,1,3-benzothiadiazole copolymer is 7.2%. This was achieved by blending PBDTDTffBT as shown Figure 20 with PCBM<sup>91a,92</sup>. In addition, Iraqi et al. and Zhang et al. demonstrated that adding alkoxy group to the PCDTBT on the 5- and 6- positions of benzothiadiazole increases the solubility of polymer but lowers power conversion efficiency, as shown in Figure 20<sup>93</sup>.

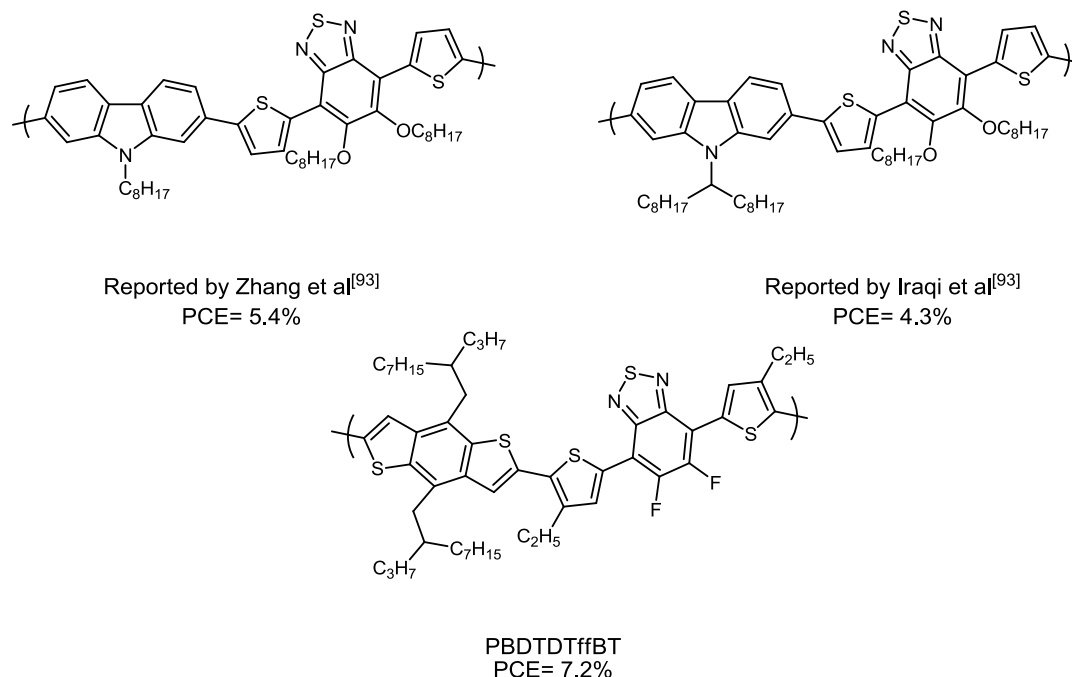


**Figure 20. Some benzothiazole polymers for use in bulk heterojunction solar cells.**

#### 1.5.8.4. Thiophene, selenophene and pyrrole based conjugated polymers

Thiophene is the most important and popular heterocyclic conjugated polymer used in electronic devices. Polythiophene derivatives, such as poly(3-hexylthiophene) (P3HT), poly(3-octylthiophene) (P3OT) and poly(3-dodecylthiophene) (P3DPT), have been widely used as the donor material in bulk heterojunction solar cells<sup>94</sup>. The discovery by McCullough et al. of the direct polymerization of 2-bromo-5-bromomagnesium-3-alkylthiophene, which is polymerised by Kumada cross coupling to obtain poly(3-alkylthiophene), makes these derivatives a popular choice in electronic devices<sup>95</sup>. In 1984, the first organic solar cells based on polythiophene and poly(3-methylthiophene) film were reported by Glenis et al., but poor power conversion efficiency was reported (PCE= 0.007 %) <sup>96</sup>. Much research has subsequently been performed in the area of polythiophene derivatives, revealing that poly(3-hexylthiophene) has higher and better photovoltaic performance when compared to the other thiophene derivatives. In 2005, Heeger and co-workers blended poly(3-hexylthiophene) with PCBM, resulting in 5.2% power conversion efficiency and 1.9 eV band gap energy<sup>97</sup>. In contrast to the band gap energy of

poly(3-hexylthiophene), poly(3-hexylselenophene) (P3HS) has a lower band gap energy of 1.6 eV. P3HT and P3HS have the same HOMO level, which means they would have comparable open circuit voltage, but P3HS has a lower LUMO energy level. Thus, P3HS has a large red shifted absorption maximum of 630nm, while P3HT has blue shifted absorption maximum at 550nm for thin film. In addition, P3HT has high power conversion efficiency of 5.2%, but P3SH has a power conversion efficiency of only 2.7% due to the internal quantum efficiency in P3SH being lower than P3TH, which results in a high probability of geminate recombination and low charge photo-generation yield. The poly(3-hexylselenophene) was investigated by Heeney et al., who reported that having low band gap is not enough to achieve high power conversion efficiency. Many criteria need to be fulfilled, as discussed previously, to obtain high power conversion efficiency<sup>94a,98</sup>. Recently, Zhang et al. blended thiophene-BDT polymer (thiophene acts as the donor and benzodithiophene acts as the acceptor) with PCBM and 7.7% power conversion efficiency was obtained, as shown in Figure 21<sup>99</sup>.

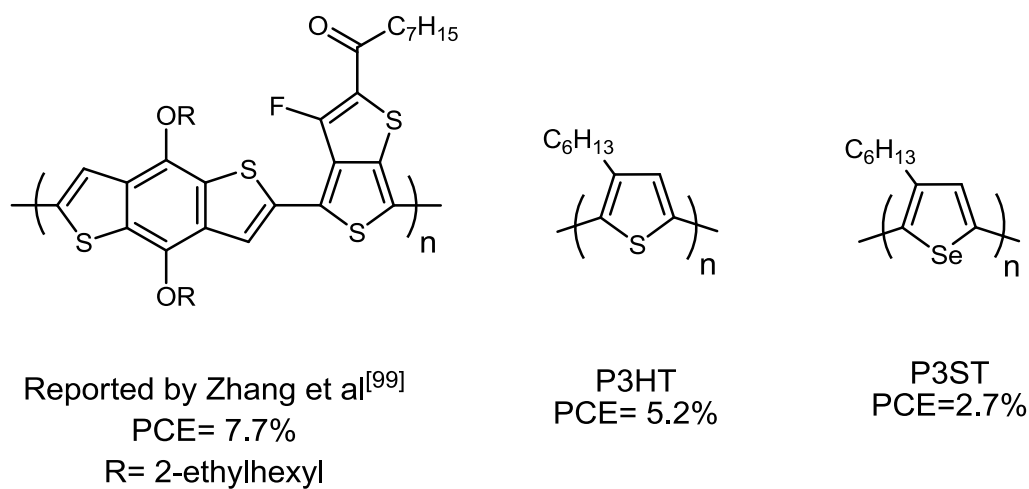


**Figure 21. Some thiophene and selenophene derivatives.**

Pyrrole has not received as much attention as thiophene despite it having many beneficial properties, such as an aromatic structure, which provides high stability. In addition, the nitrogen atom can be substituted with various functional groups to increase solubility and processibility. Zhang et al. have reported a low band gap polymer pyrrole- fluorene based copolymer, as shown in Figure 22. An absorption band maximum of 504nm was reported for the pyrrole based copolymer<sup>100</sup>.

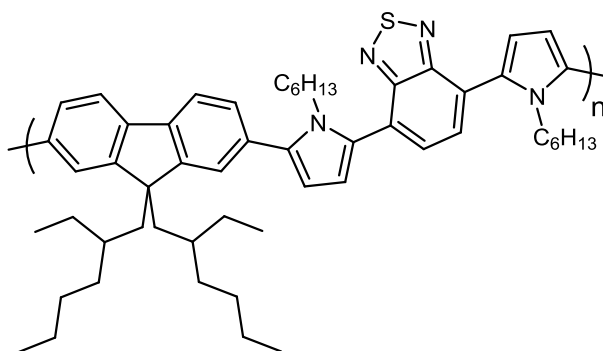
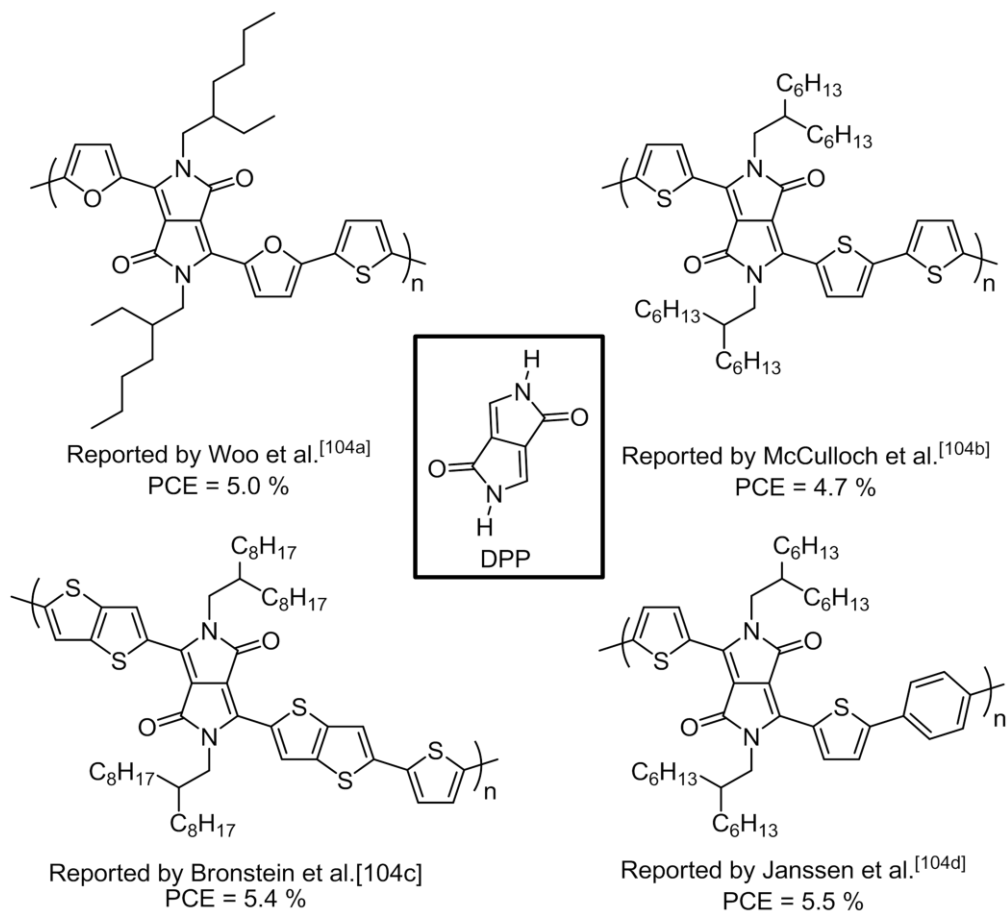


Figure 22. Low band gap polymer containing N-substituted pyrrole.

#### 1.5.8.5. Diketopyrrolopyrrole based conjugated polymers.

In 1979, Farnum et al. discovered diketopyrrolopyrrole. They aimed to prepare azetidiones via a Reformatsky – type reaction, but they obtained a red crystal, which has been widely used in various applications<sup>101</sup>. Some diketopyrrolopyrrole derivatives have been used in paints and plastic ink due to their high thermal and environmental stability<sup>102</sup>. Recently, very important progress has been made using DPP containing polymers for organic solar cells and organic field transistors. The high conjugation structure of DPP derivatives, which is due to high  $\pi$ - $\pi$  interaction, makes them suitable for use in electronic devices. In addition, the lactam parts, shown in Figure 23, gives the DPP derivatives a very high electron withdrawing effect, which leads to have high electron affinity. The two nitrogen atoms can be substituted with an alkyl group to increase the solubility of the polymer. Moreover, the process for preparing DPP derivatives is straightforward, involving only three steps<sup>94a,101b,103</sup>.

A number of DPP derivatives have been reported in the literature and power conversion efficiency in the range 4 - 6% has been obtained. Figure 23 shows some DPP derivatives with their recorded power conversion efficiencies.<sup>104</sup>.



**Figure 23. The chemical structure of diketopyrrolopyrrole (DPP) and some of DPP containing polymers and recorded power conversion efficiencies.**

#### 1.5.8.6. Anthracene based conjugated polymers.

Anthracene is a cyclic aromatic hydrocarbon system, consisting of three fused benzene rings. The chemical structure of anthracene leads to many advantages, such as aromaticity, which provides a high chemical and environmental stability. In addition, anthracene ring can be substituted with different functional groups in various positions to increase solubility and processibility. Anthracene has been used as a donor for dye-sensitized solar cells, and power conversion efficiency of 7% has been recorded. Furthermore, it has been used in small molecule organic solar cell, and power conversion efficiency of 4.84% has been obtained<sup>105</sup>.

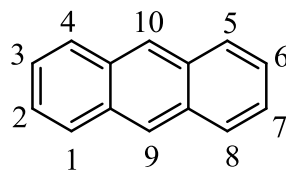


**Figure 24. The chemical structure of anthracene.**

### 1.5.8.7. Fullerene and Non fullerene Acceptor Materials

Fullerene derivatives are the best candidates for organic solar cell acceptor materials. The original fullerene chemical structure suffers from poor solubility, and so fullerene derivatives with solubilizing groups are widely used. Introducing solubilizing groups enhances the miscibility of fullerene derivatives with the donor material, but this does have a small effect on the electronic properties of the fullerene derivatives<sup>106</sup>. N-type non-fullerene polymer materials have been used as acceptors for organic solar cells. The power conversion efficiency recorded so far for these polymer acceptors is low compared to that of the fullerene derivatives<sup>107</sup>.

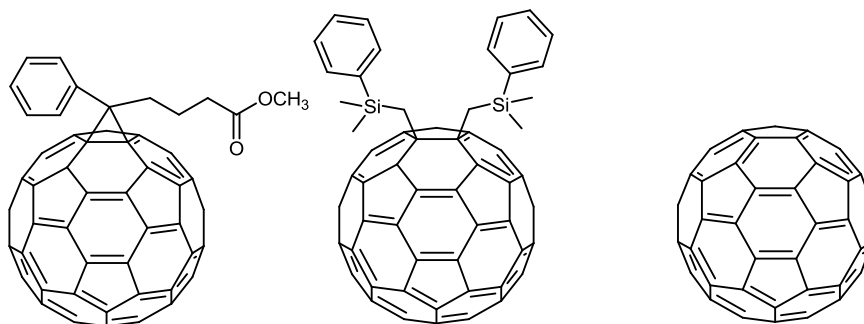


**Figure 25. Molecular structure of some fullerene derivatives.**

Furthermore, N-type inorganic semiconductor materials, such as Cds and ZnO nanocrystals, have been used as acceptors in bulk heterojunction solar cells<sup>59c</sup>. Moreover, carbon-nanotube<sup>108</sup> and graphene base<sup>109</sup> systems have been studied as acceptor materials, but so far only results using fullerene derivatives have been reported.

## Chapter Two: Aims and Objectives

In recent years, there has been an enormous amount of interest in the development of new sources of renewable energy. Organic solar cells have a bright future as a result of their advantages which makes this field very promising. The aim of this work is to develop and prepare new donor – acceptor organic materials for use as active layers in the bulk heterojunction organic solar cells. As mentioned before, there are many requirements that need to be fulfilled in order to have efficient materials. The target copolymers are analysed and blended with fullere derivatives in order to study their physical properties in solar cells.

### 2.1. Carbazole and fluorene – Pyrrole based copolymers (P1, P2, P3)

Thiophene based copolymers are the most common materials investigated as electron donating units in bulk heterojunction organic solar cells such as poly[N-9'-heptadecanyl-2,7-carbazole-alt-5,5-(4',7'-di-2-thienyl-2',1',3'- benzothiadiazole)] PCDTBT which is a donor acceptor system as a result of alternation of donor and acceptor repeat units along its polymer backbone. Previous studies in the Department of Chemistry of the University of Sheffield have shown that a copolymer comprising 2,7- linked 3,6-difluoro-9-alkyl-carbazole and 4,7-dithiophen-2-yl-benzo[1,2,3]thiadiazole gave promising results in solar cell devices. There was some evidence of the presence of hydrogen-fluorine or fluorine-sulfur interactions between the fluorine substituents at the 3- and 6-positions of carbazole repeat units and hydrogens or sulfur atoms on the adjacent thiophene rings along the polymer chains. Also, polyfluorene based copolymers have been widely studied in the literature and they have shown promise for use in organic solar cell applications. The aim of this work is to investigate analogous polymers where the thiophene repeat units are replaced with N-methylpyrrole repeat units in order to investigate the influence of replacing thiophene with N-methylpyrrole on the electronic and photophysical properties of the resulting materials. In addition, this work investigates analogous polymers where the thiophene repeat units are

replaced with N-methylpyrrole units in order to investigate if similar hydrogen-fluorine interactions are evident. As shown in Figure 26, the carbazole does not have substituents in the positions 3- and 6- in the first polymer **P1** poly [9-(heptadecan-9-yl)-9H-carbazole-2,7-diyl-alt-(4',7'-bis(1-methyl-1H-pyrrol-2'-yl)-2',1',3'-bezothiadiazole)-5,5-diyl] whereas these positions are protected with fluorine substituents in **P2** poly[3,6-difluoro-9-(heptadecan-9-yl)-9H-carbazole-2,7-diyl-alt-(4',7'-bis(1-methyl-1H-pyrrol-2'-yl)-2',1',3'-bezothiadiazole)-5,5-diyl] which provide more conjugation and stability to the polymer backbone. In the third copolymer, fluorene and methyl-pyrrole repeat units are going to act as donors and benzothiadiazole repeat units as acceptors in **P3** poly [9,6-dioctyl-9H-fluorene-2,7-diyl-alt-(2',7'-bis(1-methyl-1H-pyrrol-2-yl)-2',1',3'-bezothiadiazole)-5,5-diyl]. The photophysical and electrochemical properties of these copolymers will be investigated and the physical properties of these copolymers and their blends with fullerene derivatives will be studied.

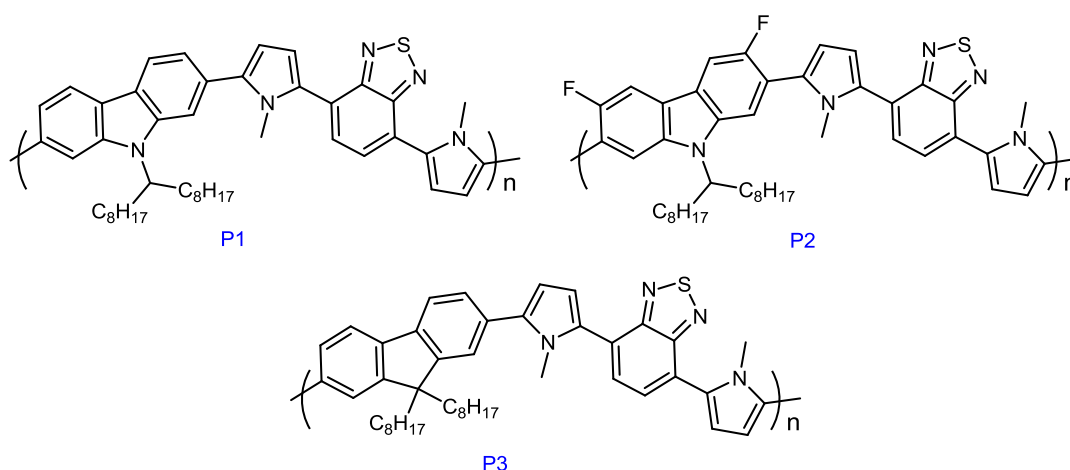
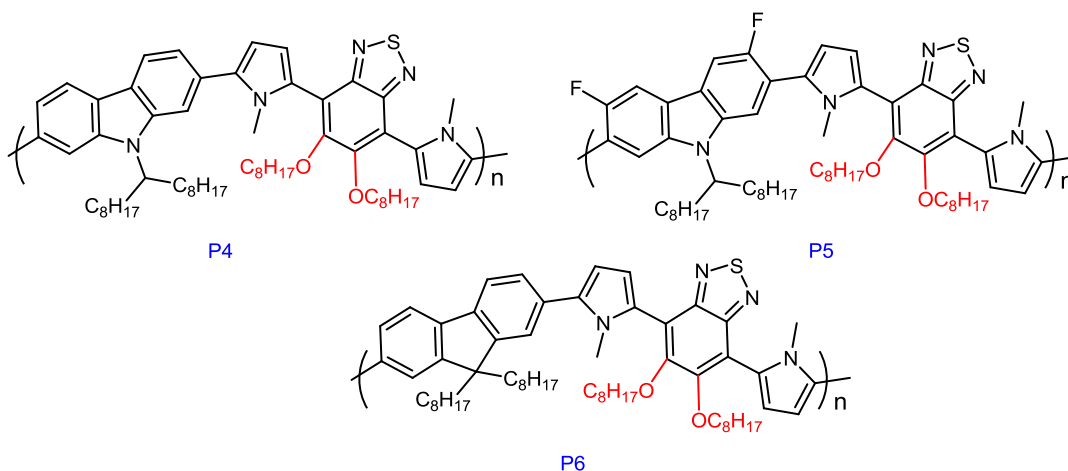


Figure 26. The chemical structures of P1, P2 and P3.

## 2.2. Carbazole and fluorene – Pyrrole and bisoctyloxy substituted benzothiadiazole based copolymers (P4, P5, P6)

Analogues to copolymers **P1**, **P2** and **P3** which have octyloxy substituents on benzothiadiazole repeat units are also to be made in order to provide materials with

higher molecular weights and processabilities. Recent work in the Iraqi group indicates that the solubility of these types of copolymers can be improved by attaching of solubilising groups on the benzothiadiazole repeat units without affecting the linearity of the copolymers. So, the aim is to prepare the three novel copolymers **P4**, **P5** and **P6**. In addition, the influence of adding alkyloxy substituents to the benzothiadiazole in poly[9-(heptadecan-9-yl)-9H-carbazole-2,7-diyl-alt-(5,6-bis(octyloxy)-4,7-di(1-methyl-1H-pyrrol-2-yl)benzo[c][1,2,5]thiadiazole)-5,5-diyl] **P4**, poly[3,6-difluoro-9-(heptadecan-9-yl)-9H-carbazole-2,7-diyl-alt-(5,6-bis(octyloxy)-4,7-di(1-methyl-1H-pyrrol-2-yl)benzo[c][1,2,5]thiadiazole)-5,5-diyl] **P5** and poly[9,9-dioctyl-9H-yl)-9H-fluorene-2,7-diyl-alt-(5,6-bis(octyloxy)-4,7-di(1-methyl-1H-pyrrol-2-yl)benzo[c][1,2,5]thiadiazole)-5,5-diyl] **P6** will be studied and compared to the previous copolymers **P1**, **P2** and **P3**. Again, the photophysical and electrochemical properties for these copolymers will be investigated and their physical properties along with their blends with fullerene derivatives will be studied.



**Figure 27. The chemical structures of P4, P5 and P6.**

### 2.3. 2,6 - Linked anthracene based copolymers (P7 – P9)

In recent years, conjugated polymers have received much effort in order to develop new donor – acceptor systems to be used as efficient electron donor materials to fullerene derivatives in organic solar cells. The electron rich repeat units are

required to maintain the HOMO energy level and provide a good intermolecular interaction between units which can be obtained using anthracene. The aim here is to prepare three novel copolymers where anthracene, thiophene and benzothiadiazole systems are used to prepare low band gap polymers. A first copolymer poly(9,10-bis(4-(dodecyloxy)phenyl)-anthracene-2,6-diyl-alt-(4,7-dithiophen-2-yl)-2',1',3'-benzothiadiazole-5,5-diyl) **P7** will be prepared. In addition, octyloxy substituents are to be attached to the benzothiadiazole repeat units in order to improve the solubility and processability in poly(9,10-bis(4-(dodecyloxy)phenyl)-anthracene-2,6-diyl-alt-(5,6-bis(octyloxy)-4,7-di(thiophen-2-yl)benzo[c][1,2,5]thiadiazole-5,5-diyl) **P8**. In the third polymer thiophene repeat units are to be replaced with selenophene repeat unit which should provide materials with better intermolecular Se–Se interactions and facilitate intermolecular charge transfer between polymer chains in poly(9,10-bis(4-(dodecyloxy)phenyl)-anthracene-2,6-diyl-alt-(5,6-bis(octyloxy)-4,7-di(selenophen-2-yl)benzo[c][1,2,5]thiadiazole-5,5-diyl) **P9** in films. Again, the photophysical and electrochemical properties for these copolymers will be investigated and the physical properties along with their blends with fullerene derivatives will be studied.

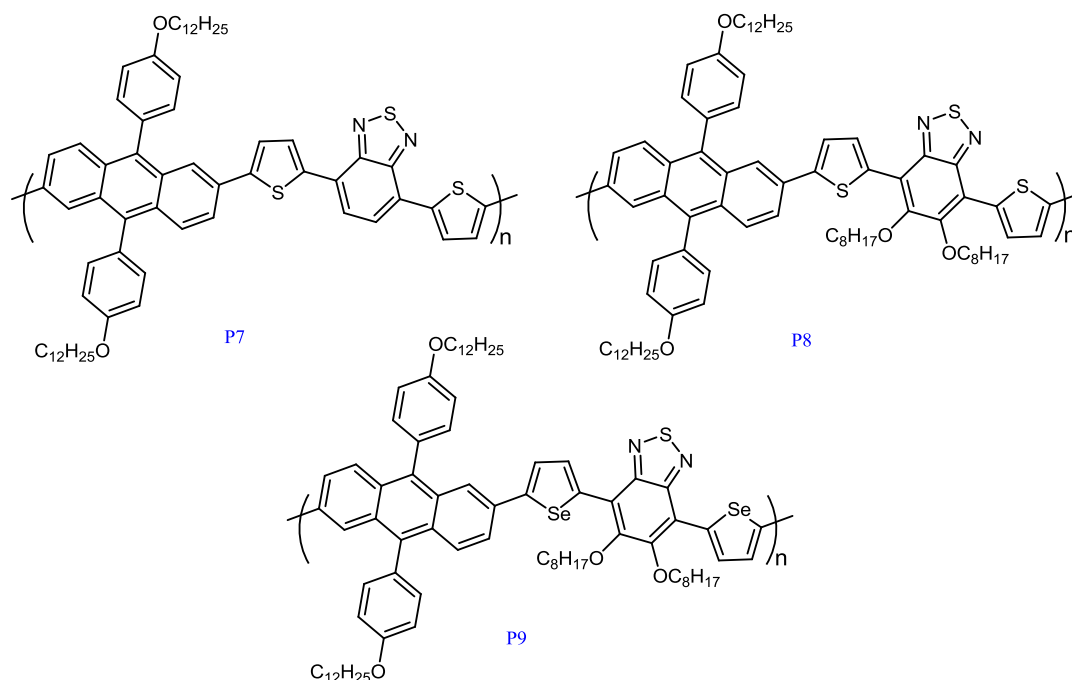


Figure 28. The chemical structures of P7, P8 and P9.

### 2.3. 2,7 - Linked anthracene based copolymers (P10 – P12)

The planarity of the chemical structure of a conjugated polymer has very important impact on its electronic and photophysical properties. Some conjugated polymers suffer from steric hindrance along the polymer backbone which leads to chain twisting and reduction of their electronic conjugation. So, the aim here is to prepare a new version of anthracene copolymers similar to the previous copolymers (**P7**, **P8** and **P9**) where the anthracene repeat units are linked through the 2- and 7- positions instead of 2- and 6- positions. Figure 29 shows the chemical structure of the new target copolymers poly(9,10-bis(4-(dodecyloxy)phenyl)-anthracene-2,7-diyl-alt-(4,7-dithiophen-2-yl)-2',1',3'-benzothiadiazole-5,5-diyl) **P10**, poly(9,10-bis(4-(dodecyloxy)phenyl)-anthracene-2,7-diyl-alt-(5,6-bis(octyloxy)-4,7-di(thiophen-2-yl)benzo[c][1,2,5]thiadiazole-5,5-diyl) **P11** and poly(9,10-bis(4-(dodecyloxy)phenyl)-anthracene-2,7-diyl-alt-(5,6-bis(octyloxy)-4,7-di(selenophen-2-yl)benzo[c][1,2,5]thiadiazole-5,5-diyl) **P12** are to be prepared. Their photophysical and electrochemical properties will be investigated and compared to those of the analogous copolymers **P7**, **P8** and **P9**. The physical properties of these copolymers and their blends with fullerene derivatives will be also studied.

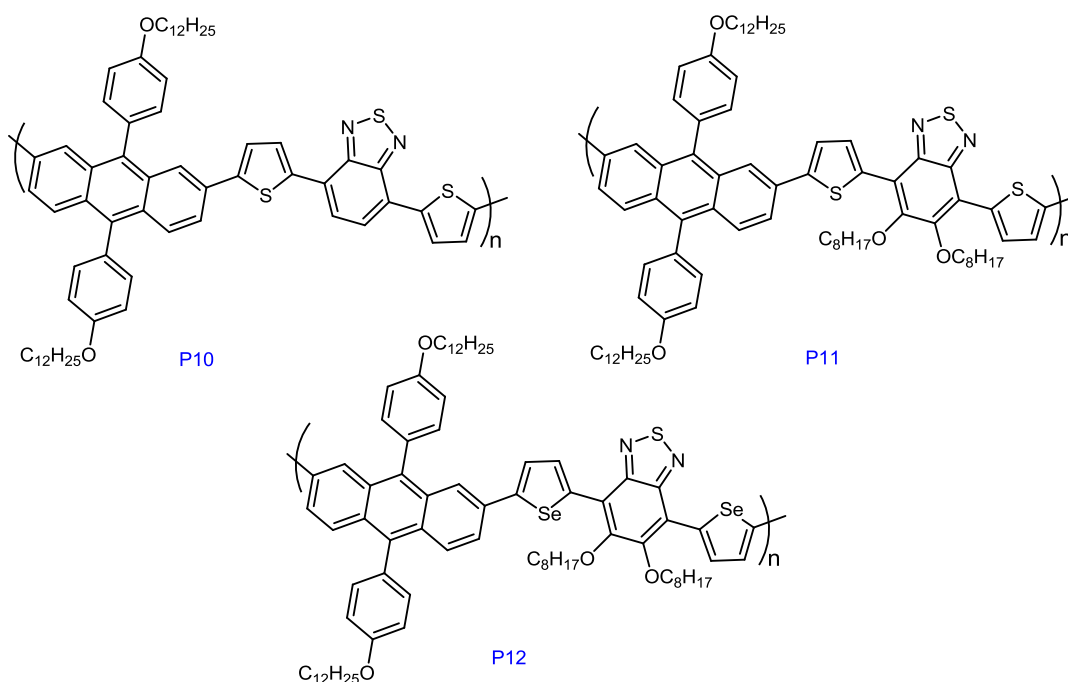
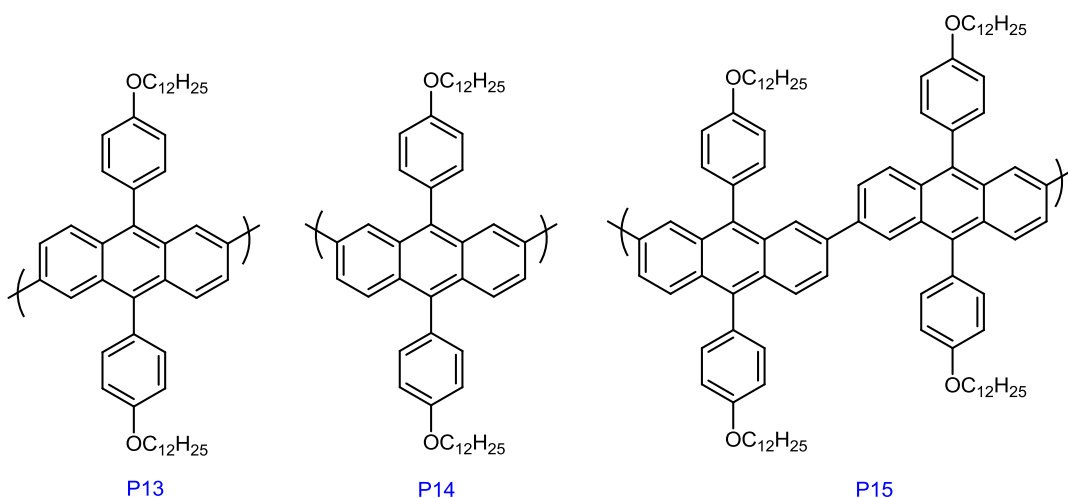


Figure 29. The chemical structures of P10, P11 and 12.

### 2.4. Anthracene based homopolymers (P13, P14, P15)

The effect of varying the linkage positions of anthracene repeat units from 2,6- to 2,7- positions will also be investigated in this project in order to provide further support to the findings from the two series of donor acceptor copolymers **P7**, **P8**, **P9**, **P10**, **P11** and **P12**. The target here is to prepare three novel polymers, in order to support the comparison of the previous versions of anthracene copolymers. Figure 30 shows the chemical structure of the target polymers poly[9,10-bis(4-(dodecyloxy)phenyl)-anthracene-2,6-diyl] **P13**, poly[9,10-bis(4-(dodecyloxy)phenyl)-anthracene-2,7-diyl] **P14** and poly[9,10-bis(4-(dodecyloxy)phenyl)-anthracene-2,6-diyl-alt-9,10-bis(4-(dodecyloxy)phenyl)-anthracene-2,7-diyl] **P15**. The properties of these polymers will be investigated and studied on order to find out the best structure option for electronic devices which has higher extended conjugation along polymer backbone.



**Figure 30. The chemical structures of P13, P14, P15.**

### 2.5. Diketopyrrolopyrrole (DPP) based copolymers (P16, P17, P18, P19, P20)

The ideal donor – acceptor copolymer for use in organic solar cells requires strong accepting units in order to lower the energy level of its LUMO and a weak electron donating unit in order to maintain its HOMO energy level around -5.4 eV.

Diketopyrrolopyrrole (DPP) units have been suggested due to their strong accepting properties and high electron affinity. In addition, the solubilising group can be attached to improve the solubility and processability of the resulting copolymer. Thus, the target in this part of the project is to prepare the low band gap copolymers; poly [9-(heptadecan-9-yl)-9H-carbazole-2,7-diyl-alt-3,6-bis(thiophen-5-yl)-2,5-di(2-ethylhexyl)-pyrrolo[3,4-c]pyrrole-1,4-dione-5',5'-diyl] **P16**, poly [3,6-difluoro-9-(heptadecan-9-yl)-9H-carbazole-2,7-diyl-alt-3,6-bis(thiophen-5-yl)-2,5-di(2-ethylhexyl)-pyrrolo[3,4-c]pyrrole-1,4-dione-5',5'-diyl] **P17**, poly [9,6-dioctyl-9H-fluornene-2,7-diyl-alt-3,6-bis(thiophen-5-yl)-2,5-di(2-ethylhexyl)-pyrrolo[3,4-c]pyrrole-1,4-dione-5',5'-diyl] **P18**, poly [9,10-bis(4-(dodecyloxy)phenyl)-anthracene-2,6-diyl-alt-3,6-bis(thiophen-5-yl)-2,5-di(2-ethylhexyl)-pyrrolo[3,4-c]pyrrole-1,4-dione-5',5'-diyl] **P19** and poly [9,10-bis(4-(dodecyloxy)phenyl)-anthracene-2,7-diyl-alt-3,6-bis(thiophen-5-yl)-2,5-di(2-ethylhexyl)-pyrrolo[3,4-c]pyrrole-1,4-dione-5',5'-diyl] **P20** as show in Figure 31. The photophysical and electrochemical properties for these copolymers will be investigated and the physical properties of these copolymers and their blends with fullerene derivatives will be studied.

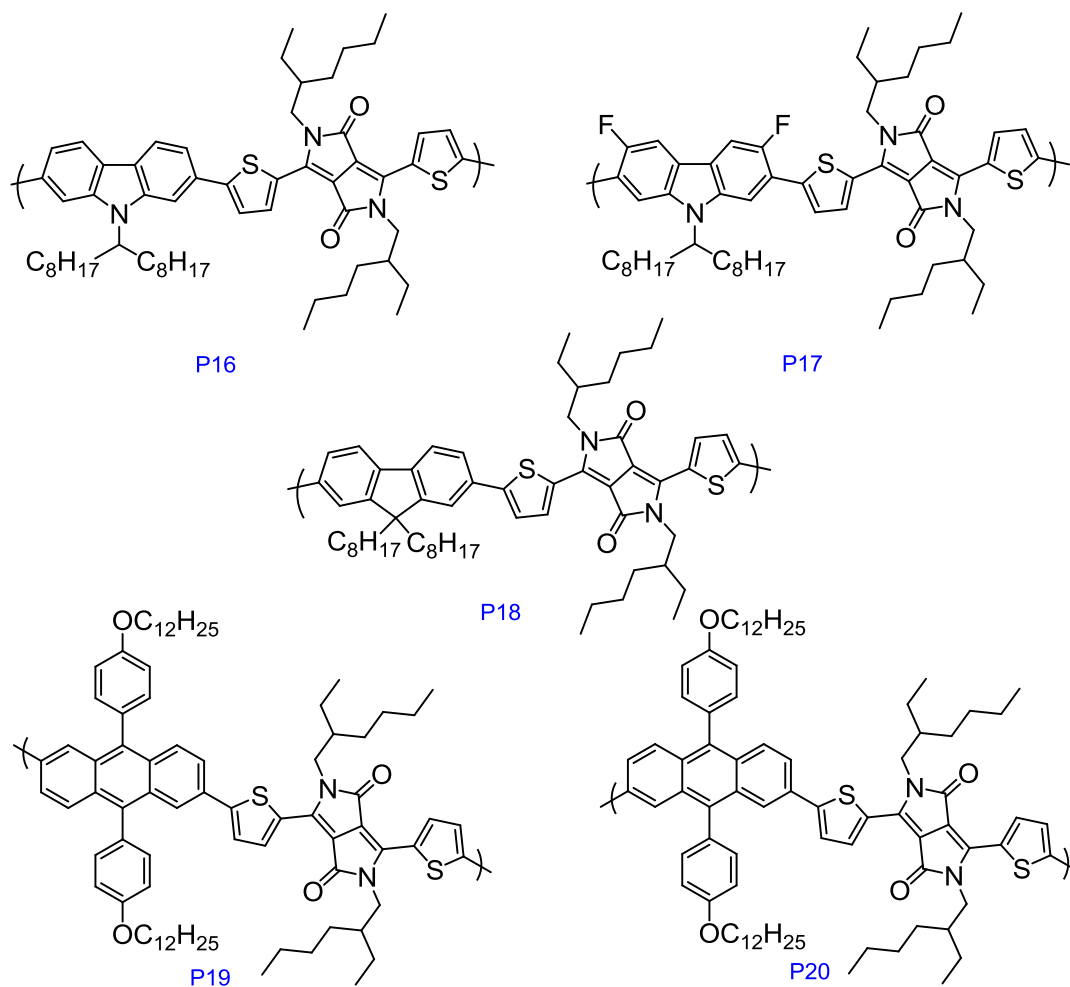


Figure 31. The chemical structures of P16 , P17 , P18, P19 and P20.

## Chapter Three: Experimental

### 3.1. Materials

All chemicals were purchased from commercial suppliers (Sigma Aldrich, Fisher Scientific, Alfa Aesa and Acros Organic) and were used directly without any treatment. Dry solvents such as hexane, DMF, chloroform, THF, toluene and acetonitrile were used for reaction unless mentioned and they obtained from the Grubbs solvent purification system. Solvents used for purifications and extractions, were obtained commercial supplier. Other chemicals such as acids, bases and reagents were also obtained comerically. All the reactions and polymerizations were performed under an inert atmosphere of argon or nitrogen.

3,6-Difluoro-9-(heptadecan-9-yl)-2,7-bis(4,4,5,5-tetramethyl-1,3,2-dioxaborolan-2-yl)-9H-carbazole (**35**) was prepared by A. Alghamdi and S. Alfifi of the Iraqi group using the same preparation route for monomer (**7**). 4,7-Bis(5-bromothiophen-2-yl)-5,6-bis(octyloxy)benzo[c][1,2,5]thiadiazole (**37**) was prepared by S. Alfifi of the Iraqi group using the same preparation route for monomer (**18**). 4,7-Bis(5-bromoselenophen-2-yl)-5,6-bis(octyloxy)benzo[c][1,2,5]thiadiazole (**38**) was prepared by A. Alghamdi and Dr. Hunnan Yi of the Iraqi group using the same preparation route for monomer (**18**). 9,9-Dioctylfluorene-2,7-diboronic acid bis(1,3-propanediol) ester (**36**) was bought from Sigma Aldrich.

### 3.2. Measurements

#### 3.2.1. Melting Point

Melting points were determined using Gallenkamp Melting Point Apparatus with a mercury thermometer.

### 3.2.2. Mass Spectrometry

Mass spectroscopy analysis was performed on Perkin Elmer Turbomass Mass Spectrometer equipped with autosystem XL GC and autosampler. Mass spectroscopy was recorded via chemical ionisation (CI) or electron impact (EI) methods.

### 3.2.3. Nuclear Magnetic Resonance Spectroscopy (NMR)

NMR spectroscopy was performed on Bruker Avance 250 (250 MHz) and Avance 400 (400 MHz) NMR spectrometer at 22 °C in chloroform-d<sub>1</sub> or DMSO-d<sub>6</sub> for monomers and intermediate products. The NMR spectroscopy of the copolymers were reported on Bruker 500 (500 MHz) NMR spectrometer at 80 °C and 100 °C in 1,1,2,2-tetrachloroethane-d<sub>2</sub>. Chemical shifts are recorded in part per million (ppm) and the coupling constant are measured in Hertz (Hz). The NMR multiplicities are characterised using the following abbreviations: singlet (s), broad singlet (bs), doublet (d), doublet-doublet (dd), triplet (t) and multiplet (m). Spectrums were investigated using TopSpin 3.0 and MestReC programs.

### 3.2.4. Infra Red Absorption Spectra (IR)

IR absorption spectra were recorded on the PerkinElmer Spectrum 100 FT-IR Spectrometer.

### 3.2.5. Gel Permeation Chromatography analysis (GPC)

The molecular weight of the polymers were measured using a GPC system which consists of Viscotek GPC max Model, Water 410 differential Refractometer detector and two polymer labs PLgel 5 µm Mixed-C (300 mm × 7.5 mm) column and a guard (50 mm × 7.5 mm). 1,2,4-Trichlorobenzene has been used as eluent and the flow rate is of 1 cm<sup>3</sup>/min were used. The measurements were carried at 140 °C and the polymers samples were prepared as solution in 1,2,4-trichlorobenzene (5 mg in 2 cm<sup>3</sup>). The GPC was calibrated with a series of polystyrene narrow standards. The separation of polymer molecules depends on the hydrodynamic volume that small polymer molecules entre the pore of the polystyrene (stationary

phase) and increasing the retention time while bigger polymer molecule travel faster in the pores and lower retention time obtained. However, the target polymers in this project have a rigid structure which makes the GPC measurements inaccurate. According to the literature, molecular weight of this type of polymers might be three times higher than reported molecular weight because the rigid structure of this type of polymers would increase their retention time.

### 3.2.6. UV-visible absorption spectroscopy

UV-visible absorption spectra were performed using Specord S 600 UV-Vis diode array spectrometer. The absorbance of copolymers were carried out in chloroform solution at ambient temperature via rectangular quartz cuvettes (light path length = 10 mm). In addition, thin films of copolymers for UV-visible absorption spectra analysis were performed by dip coating quartz plates in to around 1 mg cm<sup>-3</sup> solution of chloroform. They were then left to dry in the air at ambient temperature.

### 3.2.7. Cyclic Voltammetry (CV)

Cyclic voltammograms were measured via a Princeton Applied Research Model 263A Potentiostat/Galvanostat. The measurements were performed under an inert argon atmosphere at about 25 ± 2 °C. Approximately 10 ml of tetrabutylammonium perchlorate in dry acetonitrile solution (0.1 M) was employed as electrolyte solution. The system comprises of three electrodes, the first one is Ag/Ag<sup>+</sup> reference electrode which is a silver wire immersed in solution of silver nitrate in the electrolyte (0.01 mol L<sup>-1</sup>). The second electrode is a platinum working electrode which has 2 mm smooth platinum diameter and 3.14 × 10<sup>-2</sup> cm<sup>2</sup>. The last electrode is a platinum wire counter electrode. Polymer solid thin film were formed by drop casting around 1.0 mm<sup>3</sup> of polymer solution of chloroform, then they were left to dry in the air at ambient temperature. According to the IUPAC's recommendation, Ferrocene was used as reference redox system<sup>110</sup>.

### 3.2.8. Thermo-gravimetric analysis

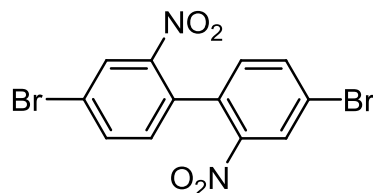
TGA curves were collected by Perkin Elmer TGA-7 Thermogravimetric Analyser at a scan rate of 10 °C per minutes under an inert nitrogen atmosphere. The sample weights were in the range 8 – 10 mg.

### 3.2.9. Elemental analysis

Elemental analyses of CHN were performed by using the Perkin Elmer 2400 CHN elemental analyser while elemental analyses of anion such as sulphur and halides were carried out by using the Schoniger oxygen flask combustion method. All intermediates products, monomers and polymers were analysed by elemental analysis. Although the elemental analysis of the target polymers indicates that there are difference between calculated values and found values because sample is not fully broken down to simple components when it is burnt in an excess of oxygen that is some of sample is converted into char.

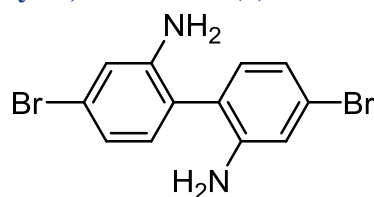
### 3.3. Synthesis of Monomers

#### 3.3.1. 4,4'-Dibromo-2,2'-dinitrobiphenyl (1)



4,4'-Dibromo-2,2'-dinitrobiphenyl (**1**) was synthesized according to the procedure by Yamato et al <sup>111</sup> .

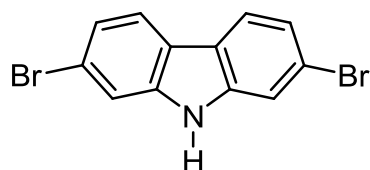
A mixture of 1,4-dibromo-2-nitrobenzene (100 g, 356.2 mmol) and copper powder (49.8 g, 783.6 mmol) in dry DMF 600 ml was heated at 120 °C for three hours. The reaction mixture was cooled to room temperature and toluene (750 ml) was added then the reaction mixture was stirred for a further 1 hour. The un-reacted copper powder and insoluble materials were filtered off and the filtrate was washed with a saturated NaCl solution (3 × 300 ml) then water (3 × 300 ml). The organic layer was dried over MgSO<sub>4</sub> and the solvent was removed in vacuo. The crude product was crystallized from ethanol and dried under high vacuum to obtain 4,4'-dibromo-2,2'-dinitrobiphenyl as yellow crystals (68.21g , 95% yield). The product gave a single spot on TLC (R<sub>f</sub>= 0.61) (silica-gel plates - ethyl acetate/hexane (1/1) (v/v)). M.p. 146-148 °C (literature <sup>112</sup> m.p. 148 °C). Mass (EI); (m/z): 400, 402, 404 (M<sup>+</sup>). <sup>1</sup>HNMR (400 MHz, CDCl<sub>3</sub>) δ<sub>H</sub>/ppm: 8.40 (d, *J* = 1.99 Hz, 2H), 7.85 (dd, *J* = 8.16, 2.01 Hz, 2H), 7.19 (d, *J* = 8.18 Hz, 2H). <sup>13</sup>CNMR (400 MHz, CDCl<sub>3</sub>); δ<sub>C</sub>/ppm: 147.3; 136.6; 132.0; 132.0; 128.0; 122.9. FT-IT (ATR): (cm<sup>-1</sup>) 3100, 1977, 1526, 1336, 1274, 1154 1097, 1002, 897, 867, 833, 776, 764, 728, 703. Elemental Analysis (%) calculated for C<sub>12</sub>H<sub>6</sub>Br<sub>2</sub>N<sub>2</sub>O<sub>4</sub>: C, 35.85; H, 1.50; N, 6.97; Br, 39.75. Found: C, 34.23; H, 1.33; N, 6.35; Br, 42.23.

**3.3.2. 4,4'-Dibromobiphenyl-2,2'-diamine (2)**

The 4,4'-dibromobiphenyl-2,2'-diamine (**2**) was synthesised according to a modified procedure by Yamoto et al<sup>111</sup>.

4,4'-Dibromo-2,2'-dinitrobiphenyl (**1**) (68.21 g, 169.7 mmol), ethanol (HPLC grade) (850 ml), 35% wt% hydrochloric acid (338 ml) and tin powder (-100 mesh) (80.6 g, 678.8 mmol) were added in flask. The reaction mixture was refluxed for 90 minutes. Then, a further portion of tin powder (-100 mesh) (80.6 g, 678.8 mmol) was added and the reaction mixture was refluxed for a further period of 1 hour. The reaction mixture was cooled to the room temperature and un-reacted tin powder was filtered off. The filtrate was added into a large amount of ice and 10% wt NaOH aqueous solution (1600 ml). The product was extracted by using diethyl ether (800 ml  $\times$  3) then dried over MgSO<sub>4</sub>. The solvent was removed in vacuo then recrystallization from ethanol was carried out to obtain 4,4'-dibromobiphenyl-2,2'-diamine as yellow powder (53 g, 89.6 % yield). The product gave a single spot on TLC ( $R_f = 0.17$ ) (silica-gel plates - ethyl acetate/hexane (1/1) (v/v)). M.p. 192-194 °C (literature<sup>112</sup> m.p. 192 °C). Mass (EI); (m/z): 340, 342, 345 ( $M^+$ ). <sup>1</sup>HNMR (400 MHz, CDCl<sub>3</sub>)  $\delta_H$ /ppm: 6.95 (s, 6H), 3.76 (s, 4H). <sup>13</sup>CNMR (400 MHz, CDCl<sub>3</sub>);  $\delta_C$ /ppm: 145.4; 132.2; 122.7; 122.0; 121.7, 118.1. FT-IT (ATR): (cm<sup>-1</sup>) 3419, 3390, 3282, 3173, 1629, 1576, 1551, 1529, 1494, 1475, 1407, 1340, 1276, 1254, 1136, 1079, 998, 938, 891, 859, 816, 797765, 744. Elemental Analysis (%) calculated for C<sub>12</sub>H<sub>10</sub>Br<sub>2</sub>N<sub>2</sub>: C, 42.14; H, 2.95; N, 8.19; Br, 46.72. Found: C, 42.13; H, 2.90; N, 7.94; Br, 46.85.

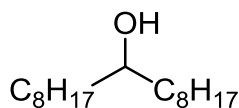
### 3.3.3. 2,7-Dibromo-9H-carbazole (3)



The 2,7-dibromo-9H-carbazole (**3**) was synthesised according to a modified procedure by Sonntag et al.<sup>113</sup>

To 4,4-dibromobiphenyl-2,2-diamine (**2**) (52 g, 152 mmol) was added concentrated phosphoric acid (85%) (1145 ml) and the mixture heated at 190 °C for 24 hours. The product was filtered and washed with water. The crude product was then solubilised in toluene and the solution filtered through a silica gel plug and dried over MgSO<sub>4</sub>. The solvent was removed using vacuum. Recrystallization was carried out from toluene / hexane (10 / 1) and dried under high vacuum. The product was obtained as white crystal (29.6 g, 60 % yield). The product gave a single spot on TLC ( $R_f = 0.43$ ) (silica-gel plates - toluene / hexane (1/1) (v/v)). M.p. 229-230 °C (literature<sup>114</sup> m.p. 230-232 °C). Mass (EI); (m/z): 323, 325, 327 ( $M^+$ ). <sup>1</sup>HNMR (250 MHz, CDCl<sub>3</sub>)  $\delta_H$ /ppm 8.06 (bs, 1H(N-H)), 7.89 (d,  $J = 8.29$  Hz, 2H), 7.58 (d,  $J = 1.62$  Hz, 2H), 7.38 (dd,  $J = 8.34, 1.67$  Hz, 2H). <sup>13</sup>CNMR (400 MHz, CDCl<sub>3</sub>);  $\delta_C$ /ppm: 140.2; 123.2; 121.7; 121.4; 119.7; 113.8. FT-IT (ATR): (cm<sup>-1</sup>) 3396.12, 1977, 1619, 1596, 1475, 1457, 1441, 1421, 1324, 1311, 1254, 1239, 1203, 1134, 1050, 997, 942, 87, 856, 802, 754, 727. Elemental Analysis (%) calculated for C<sub>12</sub>H<sub>7</sub>Br<sub>2</sub>N: C, 44.35; H, 2.17; N, 4.31; Br, 49.17. Found: C, 44.57; H, 2.10; N, 4.20; Br, 49.28.

### 3.3.4. Heptadecan-9-ol (4)

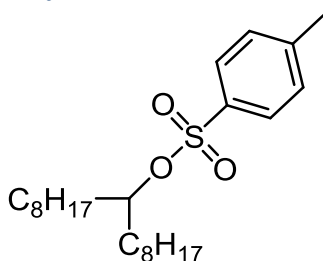


The heptadecan-9-ol (**4**) was synthesised according to a modified procedure by Leclerc et al.<sup>11b</sup>

Octylmagnesium bromide was firstly prepared by the drop-wise addition of 1-bromooctane (96.57 g, 0.50 mol) in THF (155 ml) to a suspension of Mg (13.37 g, 0.55 mol) in THF (260 ml). Ethyl formate (12.35 g, 166.7 mmol) was dissolved in

THF (278 cm<sup>3</sup>) and cooled to -78 °C. Octylmagnesium bromide (0.3 mol, 500 cm<sup>3</sup> of a 1 M solution in THF) was then added dropwise to the ethyl formate in THF solution and stirred overnight at room temperature. Methanol and then a saturated NH<sub>4</sub>Cl solution was added to quench the reaction, then extracted with diethyl ether (3 x 300 cm<sup>3</sup>) and washed with a saturated NaCl solution. The organic layer was dried over MgSO<sub>4</sub> and solvent removed in vacuo to give the product as colourless oil which turns into solid at room temperature (58.1 g, 90.6 % yield). The product gave a single spot on TLC (R<sub>f</sub> = 0.51), 10:1 40-60 petroleum ether/ethyl acetate. M.p: 29-30 °C (literature<sup>11b</sup> m.p. 28-31 °C). Mass (EI); (m/z): 256 (M<sup>+</sup>). <sup>1</sup>HNMR (400 MHz, CDCl<sub>3</sub>) δ<sub>H</sub>/ppm: 3.59 (m, 1H); 1.40 (m, 29H); 0.90 (t, J= 6.87 Hz, 6H). <sup>13</sup>CNMR (400 MHz, CDCl<sub>3</sub>); δ<sub>C</sub>/ppm : 72.0; 37.4; 31.9; 29.6; 29.6; 29.3; 25.6; 22.6; 14.1. FT-IT (ATR): (cm<sup>-1</sup>) 3315, 2996, 2916, 2872, 2848, 2502, 2159, 2030, 1977, 1465, 1375, 1352, 1241, 1135, 1124, 1089, 1065, 1054, 1026, 1008, 986, 894, 846, 796, 720. Elemental Analysis (%) calculated for C<sub>17</sub>H<sub>36</sub>O: C, 79.61; H, 14.15; Found: C, 79.73; H, 14.88.

### 3.3.5. Heptadecan-9-yl 4-methylbenzenesulfonate (5)

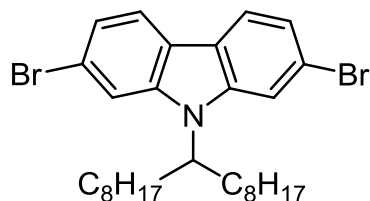


The Heptadecan-9-yl 4-methylbenzenesulfonate (**5**) was synthesised according to a modified procedure by Leclerc et al.<sup>11b</sup>

p-Toluenesulfonyl chloride (74.4 g, 0.39 mol) in DCM (270 ml) was added to heptadecan-9-ol (**4**) (55 g, 0.214 mol), Et<sub>3</sub>N (91.6 cm<sup>3</sup>, 0.66 mol) and Me<sub>3</sub>N.HCl (11.7 g, 0.26 mol) in DCM (270 ml) at 0 °C. The solution was stirred for 90 mins after which H<sub>2</sub>O was added and the product extracted with DCM (3 × 300 cm<sup>3</sup>). The organic phase was then washed with H<sub>2</sub>O and brine and then dried over MgSO<sub>4</sub> the solvent was removed in vacuo to give the product as a melting white solid. The product was purified via silica gel column chromatography, eluting with (89 %

petroleum ether (40:60), 9 % ethyl acetate, 2 % Et<sub>3</sub>N) to obtain the target product as a white solid (58.5 g, 66.5 % yield). The product gave a single spot on TLC ( $R_f = 0.52$ ), silica-gel plates 9:1 petroleum ether (40:60)/ethyl acetate. M.p.: 32 °C (literature<sup>11b</sup> m.p. 31-32 °C). Mass (EI); (m/z): 410 (M<sup>•+</sup>). <sup>1</sup>HNMR (250 MHz, CDCl<sub>3</sub>)  $\delta_H$ /ppm: 7.80 (d,  $J = 8.31$  Hz, 2H), 7.33 (d,  $J = 8.04$  Hz, 2H), 4.55 (m, 1H), 2.45 (s, 1H), 1.57 (m, 4H), 1.24 (m, 24H), 0.89 (t,  $J = 6.74$  Hz, 6H). <sup>13</sup>CNMR (400 MHz, CDCl<sub>3</sub>);  $\delta_C$ /ppm: 144.2; 134.8; 129.6; 127.7; 84.6; 34.1; 31.8; 29.7; 29.6; 29.1; 24.6; 22.6; 21.5, 14.0. FT-IT (ATR): (cm<sup>-1</sup>) 2954, 2921, 2852, 1597, 1495, 1466, 1354, 1305, 1294, 1185, 1172, 1150, 1096, 1063, 1020, 946, 895, 881, 841, 816, 766, 741, 720, 707. Elemental Analysis (%) calculated for C<sub>24</sub>H<sub>42</sub>O<sub>3</sub>S: C, 70.19; H, 10.31; S, 7.81. Found: C, 70.39; H, 11.05; S, 7.94.

### 3.3.6. 2,7-Dibromo-9-(heptadecan-9-yl)-9H-carbazole (6)

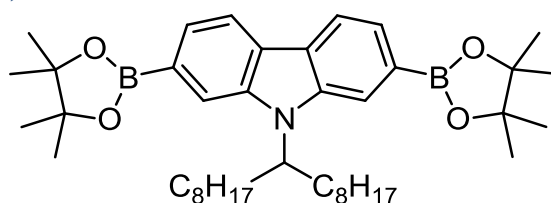


The 2,7-dibromo-9-(heptadecan-9-yl)-9H-carbazole (**6**) was synthesised according to a modified procedure by Leclerc et al.<sup>11b</sup>

2,7-Dibromo-9H-carbazole (**3**) (13 g, 40 mmol) and KOH (11.28 g, 200 mol) were dissolved in dried DMSO (110 cm<sup>3</sup>). 9-Heptadecane p-toluenesulfonate (**5**) (29.57 g, 72 mmol) dissolved in dried DMSO (62 cm<sup>3</sup>) was added dropwise over 2 hours at room temperature and the reaction was allowed to stir for 6 hours. After which the reaction was poured onto distilled H<sub>2</sub>O (300 cm<sup>3</sup>), and the product extracted with hexane (3 × 300 cm<sup>3</sup>). The combined organic fractions were dried over MgSO<sub>4</sub> and the solvent removed in vacuo. The product was purified via silica gel column chromatography pre-absorbed onto silica gel dissolved in DCM and eluted with petroleum ether (40:60) to give the product as a white crystal (13.01 g, 57.7 % yield). The product gave a single spot on TLC ( $R_f = 0.50$ ), silica-gel plates - petroleum ether (40:60). M.p. 59-60 °C (literature<sup>11b</sup> m.p. 59-61 °C). Mass (EI); (m/z): 563, 565, 567 (M<sup>+</sup>). <sup>1</sup>HNMR (250 MHz, CDCl<sub>3</sub>)  $\delta_H$ /ppm: 7.92 (t,  $J = 7.27$

Hz, 2H), 7.71 (s, 1H), 7.56 (s, 1H), 7.35 (d,  $J = 8.05$  Hz, 2H), 4.43 (m, 1H), 2.22 (m, 2H), 1.93 (m, 2H), 1.21 (m, 22H), 0.92 (m, 2H), 0.85 (t,  $J = 6.74$  Hz, 6H).  $^{13}\text{C}$ NMR (400 MHz,  $\text{CDCl}_3$ );  $\delta_{\text{C}}/\text{ppm}$ : 141.1; 138.0; 122.3; 121.7; 121.2; 114.5; 112.1; 57.9; 33.4; 31.7; 29.2; 29.2; 29.1; 26.7; 22.6; 14.0. FT-IT (ATR): ( $\text{cm}^{-1}$ ) 2951, 2918, 2850, 2160, 2030, 1977, 1622, 1585, 1479, 1465, 1450, 1421, 1376, 1331, 1271, 1236, 1218, 1130, 1088, 1058, 999, 943, 922, 844, 833, 790, 752, 721. Elemental Analysis (%) calculated for  $\text{C}_{29}\text{H}_{41}\text{Br}_2\text{N}$ : C, 61.82; H, 7.33; N, 2.49; Br, 28.36. Found: C, 61.63; H, 7.26; N, 2.44; Br, 28.31.

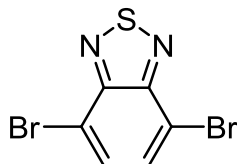
### 3.3.7. 9-(Heptadecan-9-yl)-2,7-bis(4,4,5,5-tetramethyl-1,3,2-dioxaborolan-2-yl)-9H-carbazole (7)



The 9-(heptadecan-9-yl)-2,7-bis(4,4,5,5-tetramethyl-1,3,2-dioxaborolan-2-yl)-9H-carbazole (**7**) was synthesised according to a modified procedure by Jo et al.<sup>115</sup> 2,7-Dibromo-9-(heptadecan-9-yl)-9H-carbazole (**6**) (5 g, 8.91 mmol), bis(pinacolato)diboron (7.92 g, 31.2 mmol), potassium acetate (5.3 g, 53.46 mmol) and  $\text{Pd}(\text{dppf})\text{Cl}_2$  (0.5 g, 0.53 mmol) in DMF ( $107 \text{ cm}^3$ ) was heated to  $100 \text{ }^\circ\text{C}$  for 36 hours. The reaction mixture was cooled to room temperature, then poured into  $\text{H}_2\text{O}$  ( $100 \text{ cm}^3$ ) and extracted with diethyl ether ( $3 \times 100 \text{ cm}^3$ ). The organic phases were combined, then washed with  $\text{H}_2\text{O}$  ( $3 \times 100 \text{ cm}^3$ ) and dried over  $\text{MgSO}_4$ . The crude product was purified *via* recrystallisation, the crude product was dissolved in the minimum amount of acetone and then precipitated in hot methanol which had been ran through a basic alumina column. The product was a white solid (3.51 g, 60 % yield). M.p.  $127\text{-}128 \text{ }^\circ\text{C}$  (literature<sup>115</sup> m.p.  $128\text{-}130 \text{ }^\circ\text{C}$ ). Mass (EI); ( $m/z$ ): 657.5( $\text{M}^+$ ).  $^1\text{H}$ NMR (400 MHz,  $\text{CDCl}_3$ )  $\delta_{\text{H}}/\text{ppm}$ : 8.15 (bs,  $J = 9.05$  Hz, 2H), 8.05 (bs, 1H), 7.91 (bs, 1H), 7.69 (d,  $J = 5.24$  Hz, 2H), 4.72 (m, 1H), 2.36 (m, 2H), 1.97 (m, 2H), 1.42 (s, 24H), 1.22 (m, 24H), 0.84 (t,  $J = 6.93$  Hz, 6H).  $^{13}\text{C}$ NMR (400 MHz,  $\text{CDCl}_3$ );  $\delta_{\text{C}}/\text{ppm}$ : 143.0; 139.5; 126.9; 124.9; 120.9; 119.9; 118.3; 115.6; 83.7; 56.3; 33.8; 31.7; 29.4; 26.7; 24.9; 22.5; 14.0. FT-IT (ATR): ( $\text{cm}^{-1}$ ) 2923,

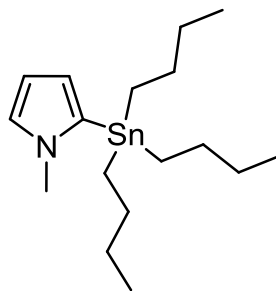
2852, 2160, 2030, 1975, 1559, 1480, 1451, 1430, 1379, 1347, 1335, 1263, 1211, 1141, 1078, 999, 967, 865, 824, 799, 735, 705. Elemental Analysis (%) calculated for  $C_{41}H_{65}B_2NO_4$ : C, 74.89; H, 9.96; N, 2.13. Found: C, 75.29; H, 9.85; N, 1.39.

### 3.3.8. 4,7-Dibromobenzo[c][1,2,5]thiadiazole (8)



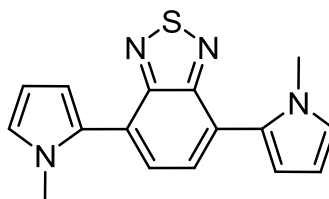
4,7-Dibromobenzo[c][1,2,5]thiadiazole (**8**) was synthesised according to a modified procedure by Zoombelt et al.<sup>116</sup>

1,2,5-Benzothiadiazole (20 g, 147 mmol) in HBr (48%, 60 ml, 1.49 g/ml) was refluxed (110 °C) with stirring. Bromine (22.6 cm<sup>3</sup>, 440cm<sup>3</sup>) was added slowly over 1.5 hour. HBr (48%, 40ml, 1.49 g/ml) was added to the reaction to facilitate stirring towards the end of the reaction, and then the reaction mixture was refluxed for 2 hours. The reaction mixture was filtered while hot and the solid washed well with H<sub>2</sub>O. The solid was dissolved in chloroform and the washed with Na<sub>2</sub>S<sub>2</sub>O<sub>3</sub> (200 ml × 4) NaHCO<sub>3</sub> (200 ml × 4) and water (200 ml × 4). The solution was dried using MgSO<sub>4</sub> then it was evaporated. Recrystallization was carried out from (1:1 THF:CH<sub>3</sub>OH) to obtain 4,7-dibromo-1,2,5-benzothiadiazole (35.3 g, 81.4 % yield) as white needles. M.p. 189-191 °C (literature<sup>117</sup> m.p. 189-190 °C). Mass (EI); (m/z): 292, 294, 296 (M<sup>+</sup>). <sup>1</sup>HNMR (250 MHz, CDCl<sub>3</sub>) δ<sub>H</sub>/ppm: 7.73 (s, 2H). <sup>13</sup>CNMR (400 MHz, CDCl<sub>3</sub>); δ<sub>C</sub>/ppm: 152.9, 132.3, 113.9. FT-IR (ATR): (cm<sup>-1</sup>) 2161, 2033, 1979, 1475, 1309, 1183, 935, 873, 842, 823. Elemental Analysis (%) calculated for C<sub>6</sub>H<sub>2</sub>Br<sub>2</sub>N<sub>2</sub>S: C, 24.51; H, 0.69; Br, 54.36; N, 9.53. Found: C, 24.90; H, 0.42; Br, 54.36; N, 8.72.

**3.3.9. 1-Methyl-2-(tributylstannyl)-1H-pyrrole (9)**

1-Methyl-2-(tributylstannyl)-1H-pyrrole (**9**) was synthesised according to a modified procedure by Torum et al.<sup>118</sup>

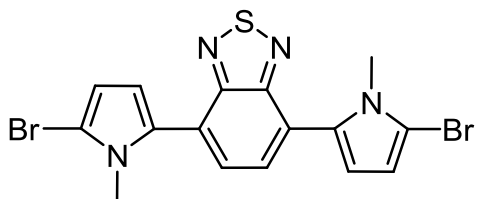
*t*-Butyl lithium (112.67 mmol , 66.3 ml) was added dropwise to *N*-methyl-pyrrole (112.67 mmol , 10 ml ) in THF (184 ml) at -78 °C. The reaction mixture was stirred for 30 min, and a yellow solution formed. The reaction mixture was stored at -15 °C for 16 hours. Bu<sub>3</sub>SnCl (112.67 mmol, 30.4 ml) was then added via syringe and the resulting solution was stirred at room temperature for two hours. Diethyl ether (150 ml) was added and the solution was washed with brine (4 × 100 ml). The organic layer was dried over MgSO<sub>4</sub> and filtered. The solvent was removed in vacuo to obtain the product as yellow oil (37.3 g, 89.4% yield). Mass (EI); (*m/z*): 371 (*M*<sup>+</sup>). <sup>1</sup>HNMR (250 MHz, CDCl<sub>3</sub>) δ<sub>H</sub>/ppm: 6.88 (dd, *J* = 2.13, 1.65 Hz, 1H), 6.30 (dd, *J* = 3.34, 1.47 Hz, 1H), 6.26 (t, *J* = 3.26, 2.46 Hz, 1H), 3.71 (s, 1H), 1.61-1.50 (m, 1H), 1.48-1.26 (m, 1H), 1.19-1.02 (m, 1H), 0.93 (t, *J* = 7.27 Hz, 1H). <sup>13</sup>CNMR (250 MHz, CDCl<sub>3</sub>); δ<sub>C</sub>/ppm: 132.5, 125.5, 119.3, 108.8, 108.5, 38.0, 29.3, 26.8, 17.5. FT-IT (ATR): (cm<sup>-1</sup>) 2955, 2923, 2870, 2851, 2155, 2031, 1512, 1463, 1405, 1376, 1339, 1289, 1180, 1072, 1001, 960, 873, 775, 711, 505. Elemental Analysis (%) calculated for C<sub>17</sub>H<sub>33</sub>NSn: C, 55.16; H, 8.99; N, 3.78. Found: C, 54.24; H, 9.49; N, 2.81.

**3.3.10. 4,7-Bis(1-methyl-1H-pyrrol-2-yl)benzo[*c*][1,2,5]thiadiazole (10)**

4,7-Bis(1-methyl-1H-pyrrol-2-yl)benzo[c][1,2,5]thiadiazole (**10**) was synthesised according to a modified procedure by Kim et al.<sup>119</sup>

4,7-Dibromo-1,2,5-benzothiadiazole (**8**) (10 g, 34.02 mmol) and 2-(tri-n-butylstannyl) 1-methyl-1H-pyrrole (**9**) (31.5 g, 85.04 mmol) were added to 250 ml of THF. PdCl<sub>2</sub>(PPh<sub>3</sub>)<sub>2</sub> (485 mg, 0.70 mmol) was added. The mixture was refluxed (85 °C) under argon atmosphere for 24 hours. Then, the residue was purified by column chromatography on silica gel (petroleum ether (40:60): ethyl acetate (9:1)). Recrystallization was carried out from ethanol, which gave the target product as red crystal (7.5g, 74.9% yield). The product gave a single spot on TLC (R<sub>f</sub>=0.6), silica-gel plates - petroleum ether (40:60): ethyl acetate (9:1). M.p. 110-112 °C. Mass (EI); (m/z): 294. (M<sup>+</sup>). <sup>1</sup>HNMR (250 MHz, CDCl<sub>3</sub>) δ<sub>H</sub>/ppm: 7.62 (s, 2H), 6.91 (t, 2H), 6.61 (dd, *J* = 3.64, 1.79 Hz, 2H), 6.37 (dd, *J* = 3.59, 2.76 Hz, 2H), 3.75 (s, 6H). <sup>13</sup>CNMR (250 MHz, CDCl<sub>3</sub>); δ<sub>C</sub>/ppm: 154.3, 130.1, 128.7, 125.3, 125.0, 111.95, 108.4, 35.7. FT-IT (ATR): (cm<sup>-1</sup>) 2161, 2031, 1975, 1582, 1525, 1480, 1464, 1424, 1409, 1317, 1292, 1252, 1227, 1097, 1063, 914, 891, 875, 858, 844, 797, 741, 720. Elemental Analysis (%) calculated for C<sub>6</sub>H<sub>2</sub>N<sub>4</sub>S: C, 65.28; H, 4.79; N, 19.03. Found: C, 64.89; H, 4.59; N, 19.74.

### 3.3.11. 4,7-Bis(5-bromo-1-methyl-1H-pyrrol-2-yl)benzo[c][1,2,5]thiadiazole (**11**)

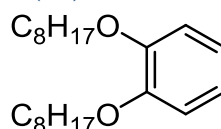


4,7-Bis(5-bromo-1-methyl-1H-pyrrol-2-yl)benzo[c][1,2,5]thiadiazole (**11**) was synthesised according to a modified procedure by Zhang et al.<sup>120</sup>

4,7-Bis(1-methyl-1H-pyrrole)-1,2,5-benzothiadiazole (**10**) (2.0 g, 6.79 mmol) in chlorobenzene (80 ml) was placed in a 250 ml flask. The reaction mixture was heated to 50 °C and N-bromosuccinimide (NBS) (2.357 g, 13.248 mmol) was added in two portions (the second portion was added after one hour) for three hours. The reaction mixture was allowed to cool to room temperature. The solvent was

removed by rotary evaporator. The residue was purified by column chromatography on silica gel (petroleum ether (40:60): ethyl acetate (5:1)) to obtain the target product as an orange powder (0.8 g 26.6% yield). The product gave a single spot on TLC ( $R_f = 0.3$ ), silica-gel plates - petroleum ether (40:60): ethyl acetate (5:1). M.p. 165-167 °C. Mass (EI); (m/z) 450, 452, 454 ( $M^+$ ).  $^1\text{H}$ NMR (250 MHz,  $\text{CDCl}_3$ )  $\delta_{\text{H}}$ /ppm: 7.58 (s, 2H), 6.88 (d,  $J = 1.90$  Hz, 2H), 6.56 (d,  $J = 1.89$  Hz, 2H), 3.67 (s, 6H).  $^{13}\text{C}$ NMR (250 MHz,  $\text{CDCl}_3$ );  $\delta_{\text{C}}$ /ppm: 153.8, 130.5, 129.1, 124.7, 124.3, 113.9, 95.7. FT-IT (ATR): ( $\text{cm}^{-1}$ ) 3125, 2943, 2524, 2160, 2029, 1974, 1584, 1496, 1468, 1420, 1408, 1355, 1339, 1304, 1266, 1242, 1186, 1082, 1058, 940, 922, 883, 850, 801, 792, 779, 759, 727, 716. Elemental Analysis (%) calculated for  $\text{C}_6\text{H}_2\text{N}_4\text{S}$ : C, 42.50; H, 2.67; N, 12.39; Br, 35.34. Found: C, 42.36; H, 2.26; N, 12.00; Br, 35.69.

### 3.3.12. 1,2-Bis(octyloxy)benzene (**12**)

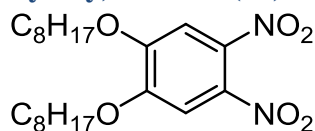


1,2-Bis(octyloxy)benzene (**12**) was synthesised according to a modified procedure by Janssen et al.<sup>121</sup>

To a solution of catechol (20 g, 0.1816 mol) in dry DMF (100 ml) was added 1-bromooctane (0.4168 mol, 80.5 g, 72 mL) and  $\text{K}_2\text{CO}_3$  (76 g, 0.55 mol). The mixture was stirred at 100 °C under a nitrogen atmosphere for 40 hours. After cooling the mixture to room temperature, 200 ml of water was added. The organic layer was separated and the aqueous layer was extracted with DCM. The combined organic phase was dried over  $\text{MgSO}_4$ . After filtration, the solvent was removed under vacuum. The product was recrystallized twice from ethanol to obtain the target product as needle like crystals (54.11 g, 89.1% yield). The product gave a single spot on TLC ( $R_f = 0.54$ ) (silica-gel plates - DCM / hexane (1 / 1)). M.p. 25- 26 °C (literature<sup>122</sup> m.p. 24-25 °C). Mass (EI); (m/z): 334 ( $M^+$ ).  $^1\text{H}$ NMR (250 MHz,  $\text{CDCl}_3$ )  $\delta_{\text{H}}$ /ppm: 6.92 (s, 4H), 4.02 (t,  $J = 6.65$  Hz, 4H), 1.91-1.78 (m, 4H), 1.61-1.22 (m, 20H), 0.92 (t, 6H).  $^{13}\text{C}$ NMR (250 MHz,  $\text{CDCl}_3$ )  $\delta_{\text{C}}$ /ppm: 149.3, 121.0, 114.2, 69.3, 31.8, 29.4, 29.3, 26.0, 22.6, 14.10. FT-IT (ATR): ( $\text{cm}^{-1}$ ) 2922, 2853, 2059, 1592, 1501, 1468, 1453, 1386, 1329, 1252, 1221, 1123, 1043, 902, 737.

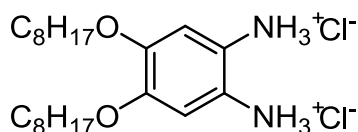
Elemental Analysis (%) calculated for  $C_{22}H_{38}O_2$ : C, 78.99; H, 11.45. Found: C, 78.65; H, 11.49.

### 3.3.13. 1,2-Dinitro-4,5-bis(octyloxy)benzene (**13**)



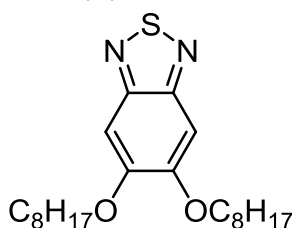
1,2-Dinitro-4,5-bis(octyloxy)benzene (**13**) was synthesised according to a modified procedure by Janssen et al.<sup>121</sup>

To a two neck round-bottom flask containing dichloromethane (560 ml), acetic acid (560 ml), and 1,2-bis(octyloxy)benzene (**12**) (30 g, 89.7 mmol) cooled to 0 °C was added dropwise 65% nitric acid (80 ml). The reaction was allowed to warm to room temperature and stirred for 1 hour. The mixture was again cooled to 0 °C and 100% nitric acid (200 ml) was added dropwise. The mixture was allowed to warm to room temperature and the mixture was stirred for 40 hours. After completion of the reaction, the reaction mixture was poured into ice-water and the dichloromethane layer separated. The water phase was extracted with dichloromethane. The combined organic phase was washed with water, NaHCO<sub>3</sub> (aq) and brine then dried over MgSO<sub>4</sub>. The solvent was removed in vacuo. The crude product was recrystallized from ethanol. The product was obtained as a yellow powder (35.31 g, 93% yield). M.p. 88-90 °C (literature<sup>122</sup> m.p. 87-87.5 °C). Mass (EI); (m/z) 424 (M<sup>+</sup>). <sup>1</sup>HNMR (250 MHz, CDCl<sub>3</sub>) δ<sub>H</sub>/ppm: 7.31 (s, 2H), 4.12 (t, *J* = 6.51 Hz, 4H), 1.96-1.82 (m, 4H), 1.56-1.22 (m, 20H), 0.90 (t, 6H). <sup>13</sup>CNMR (250 MHz, CDCl<sub>3</sub>) δ<sub>C</sub>/ppm: 151.8, 136.4, 107.9, 70.2, 31.7, 29.1, 28.7, 25.8, 22.6, 14.0. FT-IT (ATR): (cm<sup>-1</sup>) 3071, 2956, 2921, 2853, 2438, 2160, 2023, 1586, 1527, 1464, 1371, 1354, 1334, 1287, 1224, 1035, 992, 954, 909, 872, 827, 810, 750, 720. Elemental Analysis (%) calculated for  $C_{22}H_{38}O_2$ : C, 62.24; H, 8.55; N, 6.60. Found: C, 62.35; H, 8.64; N, 6.61.

**3.3.14. 4,5-Bis(octyloxy)benzene-1,2-diamonium chloride (14)**

4,5-Bis(octyloxy)benzene-1,2-diamonium chloride (**14**) was synthesised according to a modified procedure by Janssen et al.<sup>121</sup>

A mixture of 1,2-dinitro-4,5-bis-(octyloxy)-benzene (**13**) (5 g, 11.8 mmol) and Sn(II)Cl<sub>2</sub> (94.4 mmol, 17.87 g) in ethanol (175 ml) and conc. HCl (70 ml) was heated to 85 °C overnight. After cooling to room temperature the product was filtered and washed with water and methanol. Finally it was dried at RT under a stream of nitrogen and used directly (unstable). The product was obtained as an off-white solid (4.9 g, 95 % yield). M.p. 114-115 °C. Mass (EI); (m/z) 365 (M<sup>+</sup>). <sup>1</sup>HNMR (250 MHz, DMSO) δ<sub>H</sub>/ppm: 7.93 (s, 4H), 6.66 (s, 2H), 3.82 (t, *J* = 6.32 Hz, 4H), 1.76-1.59 (m, 4H), 1.48-1.15 (m, 20H), 0.86 (t, *J* = 6.83 Hz, 6H). <sup>13</sup>CNMR (250 MHz, CDCl<sub>3</sub>) δ<sub>C</sub>/ppm: 108.1, 69.62, 39.97, 39.76, 39.55, 39.34, 31.72, 29.45, 29.29, 29.22, 26.05, 22.58, 14.40. FT-IT (ATR): (cm<sup>-1</sup>) 3381, 3313, 2953, 2917, 2850, 2591, 2160, 2024, 1633, 1610, 1598, 1580, 1530, 1486, 1467, 1439, 1398, 1379, 1296, 1241, 1314, 1137, 1070, 1058, 1014, 998, 958, 920, 902, 859, 838, 793, 760, 723. Elemental Analysis (%) calculated for C<sub>22</sub>H<sub>42</sub>O<sub>2</sub>N<sub>2</sub>O<sub>2</sub>: C, 60.40; H, 9.68; N, 66.40; Cl, 16.21. Found: C, 64.18; H, 10.82; N, 6.84; Cl, 9.23.

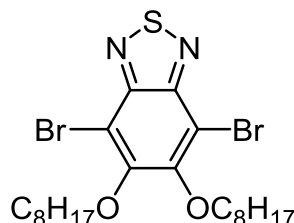
**3.3.15. 5,6-Bis(octyloxy)benzo[c][1,2,5]thiadiazole (15)**

5,6-Bis(octyloxy)benzo[c][1,2,5]thiadiazole (**15**) was synthesised according to a modified procedure by Janssen et al.<sup>121</sup>

To a mixture of 4,5-bis(octyloxy)-benzene-1,2-diaminium chloride (**14**) (4.9 g, 11.2 mmol) and triethylamine (16 ml, 25.1 mmol) in 180 ml dichloromethane was slowly added a solution of thionyl chloride (22.8 mmol, 2.7 g) in 22.4 ml

dichloromethane. After addition the mixture was heated to reflux for 6 hours. The reaction mixture was added to 300 ml water and 300 ml DCM was added. The organic layer was washed with water (300 ml x 3) then dried over  $\text{MgSO}_4$ . The solvent was removed using vacuum. The crude product was recrystallized from ethanol. The product was obtained as off white powder (5 g, 92% yield). M.p. 97-99 °C (literature<sup>122</sup> m.p. 96-98 °C). Mass (EI); (m/z) 392 ( $\text{M}^+$ ).  $^1\text{H}$ NMR (250 MHz,  $\text{CDCl}_3$ )  $\delta_{\text{H}}$ /ppm: 7.14 (s, 2H), 4.10 (t,  $J = 6.55$  Hz, 4H), 1.99-1.86 (m, 4H), 1.60-1.26 (m, 20H), 0.90 (t, 6H).  $^{13}\text{C}$ NMR (250 MHz,  $\text{CDCl}_3$ )  $\delta_{\text{C}}$ /ppm: 154.1, 151.4, 98.4, 69.1, 31.7, 29.3, 29.2, 28.7, 26.0, 22.6, 14.0. FT-IT (ATR): ( $\text{cm}^{-1}$ ) 3081, 3053, 2955, 2917, 2872, 2848, 2510, 2160, 2023, 1977, 1614, 1528, 1497, 1460, 1404, 1378, 1307, 1258, 1213, 1194, 1179, 1063, 1013, 998, 958, 937, 909, 851, 823, 753, 723. Elemental Analysis (%) calculated for  $\text{C}_{22}\text{H}_{36}\text{N}_2\text{O}_2\text{S}$ : C, 67.30; H, 9.24; N, 7.14 Found: C, 67.34; H, 9.59; N, 7.17.

### 3.3.16. 4,7-Dibromo-5,6-bis(octyloxy)benzo[c][1,2,5]thiadiazole (16)

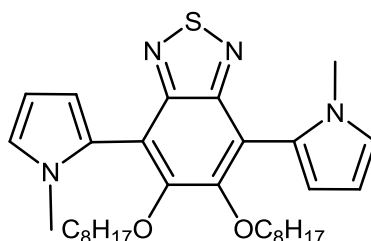


4,7-Dibromo-5,6-bis(octyloxy)benzo[c][1,2,5]thiadiazole (**16**) was synthesised according to a modified procedure by Janssen et al.<sup>121</sup>

To a solution of 5,6-bis(octyloxy)benzo[c][1,2,5]thiadiazole (**15**) (8.00 g, 14.3 mmol) in a mixture of dichloromethane (400 ml) and acetic acid (175 ml) was added bromine (5.3 ml, 103.11 mmol), and the resulting mixture was stirred in the dark for ca. 48 h at room temperature. The mixture was then poured in water (500 ml), extracted with dichloromethane, sequentially washed with water, saturated  $\text{NaHCO}_3$  (aq),  $\text{Na}_2\text{SO}_3$  (aq) and the solvents are evaporated under reduced pressure. The crude product was purified on a silica gel column chromatography eluting with petroleum ether. Recrystallization was carried out from ethanol to give the target product as white needles (8.2 g, 73 % yield). M.p. 44- 46 °C (literature<sup>122</sup> 44.5-45.6 °C). Mass (EI); (m/z) 558, 550, 552 ( $\text{M}^+$ ).  $^1\text{H}$ NMR (250 MHz,  $\text{CDCl}_3$ )  $\delta_{\text{H}}$ /ppm: 4.17 (t,  $J = 6.64$  Hz, 4H), 1.97-1.83 (m, 4H), 1.62-1.23 (m, 20H), 0.91 (t, 6H).  $^{13}\text{C}$ NMR

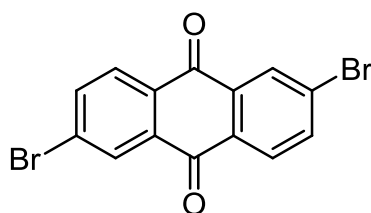
(250 MHz,  $CDCl_3$ )  $\delta_C$ /ppm: 154.5, 106.2, 75.1, 31.8, 30.2, 29.9, 29.2, 25.9, 22.6, 14.0. FT-IT (ATR): ( $cm^{-1}$ ) 2954, 2922, 2872, 2848, 2542, 2160, 2021, 1976, 1590, 1468, 1431, 1385, 1283, 1267, 1169, 1142, 1125, 1078, 1057, 1027, 1008, 992, 942, 908, 891, 882, 847, 840, 802, 772, 738, 710. Elemental Analysis (%) calculated for  $C_{22}H_{34}N_2O_2SBr_2$ : C, 48.01; H, 6.23; Br, 29.04; N, 5.09; O, 5.81; S, 5.83 Found: C, 47.72; H, 6.32; Br, 29.32; N, 5.04; O, 5.61; S, 5.81.

### 3.3.17. Attempted synthesis of 4,7-bis(1-methyl-1H-pyrrol-2-yl)-5,6-bis(octyloxy)benzo[c][1,2,5]thiadiazole (17)



To a solution of 1-methyl-2-(tributylstannyl)-1H-pyrrole (**9**) (2.01 g, 5.45 mmol) and 4,7-dibromo-5,6 bis(octyloxy)benzo[c][1,2,5]oxadiazole (**16**) (1 g, 1.82 mmol) in dry toluene (20 ml). A mixture of palladium acetate (57.1 mg, 0.254 mmol) and tri-*o*-tolylphosphine (232.22 mg, 0.763 mmol) was added under argon. The reaction mixture was degassed and heated under reflux for 72 h. The solvent was removed in vacuo and the residue was purified by column chromatography on silica gel (petroleum ether (40:60): ethyl acetate (9:1)), the  $^1H$ NMR and mass spectroscopy showed impure material so purification was undertaken using preparative HPLC eluted ( $H_2O$  : THF (30:70 %)) however the product could not be purified.

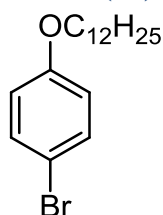
### 3.3.18. 2,6-Dibromoanthracene-9,10-dione (19)



The preparation of 2,6-dibromoanthracene-9,10-dione (**19**) was carried out according to a modified method by Vila et al.<sup>123</sup>

2,6-Diaminoanthraquinone (9.6 g, 40 mmol), *t*-Bu ONO (10.4 g, 100 mmol), CuBr<sub>2</sub> (22.2 g, 100 mmol), and CH<sub>3</sub>CN (170 mL) were added to a one-neck flask, and the mixture was heated at 65 °C for 2 h. The reaction was quenched by adding 35% HCl (aq) solution to the product mixture. The solution was filtered, washed with CH<sub>3</sub>CN, and the product was recrystallized from 1,4-dioxane. The product was obtained as a yellow powder (9.8 g, 67% yield). The product gave a single spot on TLC ( $R_f = 0.61$ ) (silica-gel plates - ethyl acetate/ petroleum ether (1/10) (v/v)). M.p. 284-285 °C (literature<sup>124</sup> m.p. 285-287 °C). Mass (EI); (m/z): 364, 366, 368 (M<sup>+</sup>). <sup>1</sup>HNMR (400 MHz, CDCl<sub>3</sub>)  $\delta_H$ /ppm: 8.46 (d,  $J = 1.99$  Hz, 2H), 8.20 (d,  $J = 8.31$  Hz, 2H), 7.97 (dd,  $J = 8.31, 2.02$  Hz, 2H). <sup>13</sup>CNMR (400 MHz, CDCl<sub>3</sub>)  $\delta_C$ /ppm: 137.4, 130.3, 129.1. FT-IT (ATR): (cm<sup>-1</sup>) 3080, 2447, 2160, 2022, 1963, 1708, 1674, 1570, 1386, 1338, 1307, 1283, 1245, 1161, 1106, 1067, 959, 910, 856, 847, 819, 730, 706. Elemental Analysis (%) calculated for C<sub>14</sub>H<sub>6</sub>O<sub>2</sub>Br<sub>2</sub>: C, 45.94; H, 1.65; Br, 43.66. Found: C, 45.87; H, 1.45; Br, 43.65.

### 3.3.19. 1-Bromo-4-(dodecyloxy)benzene (20)

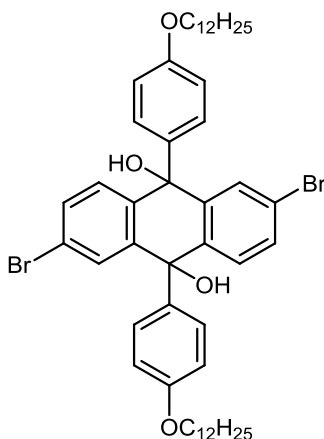


The preparation of 1-bromo-4-(dodecyloxy)benzene (**20**) was carried out according to a modified method by Nucklolls et al.<sup>125</sup>

4-Bromophenol (28.80 g, 170 mmol), NaOH (8.66 g, 220 mmol) and 1-bromododecane (40.00 g, 170 mmol) were added to DMSO (133 ml) in one neck round bottom flask. The mixture was stirred at 100 °C overnight, cooled and then 400 ml H<sub>2</sub>O was added. The product was extracted with diethyl ether (3 × 300ml) and dried over MgSO<sub>4</sub>. The solvent was evaporated and recrystallised from ethanol. The product was obtained as white crystals (43.54 g, 76.6% yield). The product gave a single spot on TLC ( $R_f = 0.78$ ) (silica-gel plates - ethyl acetate/ petroleum ether (1/10) (v/v)). M.p. 37-38 °C (literature<sup>126</sup> m.p. 38 °C). Mass (EI); (m/z): 340, 342 (M<sup>+</sup>). <sup>1</sup>HNMR (250 MHz, CDCl<sub>3</sub>)  $\delta_H$ /ppm: 7.38 (d,  $J = 9.03$  Hz, 2H), 6.79 (d,  $J = 9.02$  Hz, 2H), 3.93 (t,  $J = 6.55$  Hz, 2H), 1.85-1.72 (m, 2H), 1.49-1.24 (m, 18H),

0.90 (t,  $J = 6.57$  Hz, 6H).  $^{13}\text{C}$ NMR (250 MHz,  $\text{CDCl}_3$ )  $\delta_{\text{C}}/\text{ppm}$ : 158.2, 132.1, 116.3, 112.5, 68.3, 31.9, 29.6, 29.5, 29.5, 29.3, 29.1, 26.0, 22.6, 14.1. FT-IT (ATR): ( $\text{cm}^{-1}$ ) 2915, 2848, 2526, 2160, 2022, 1976, 1590, 1576, 1489, 1468, 1393, 1281, 1236, 1171, 1113, 1070, 1046, 1036, 1002, 977, 982, 819, 802, 792, 772, 719. Elemental Analysis (%) calculated for  $\text{C}_{18}\text{H}_{29}\text{OBr}$ : C, 63.34; H, 8.56; Br, 23.41. Found: C, 63.35; H, 8.33; Br, 23.46.

### 3.3.20. 2,6-Dibromo-9,10-bis(4-(dodecyloxy)phenyl)-9,10-dihydroanthracene-9,10-diol (**21**)

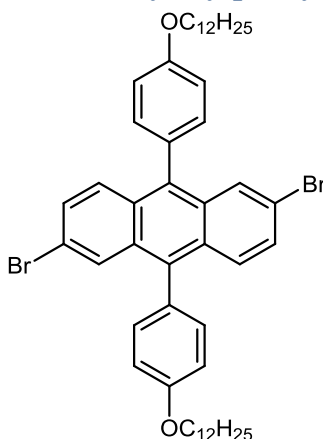


The preparation of 2,6-dibromo-9,10-bis(4-(dodecyloxy)phenyl)-9,10-dihydroanthracene-9,10-diol (**21**) was carried out according to a modified method by Wang et al.<sup>127</sup>

To a solution of 1-bromo-4-(dodecyloxy)benzene (**20**) (2.8 g, 8.2 mmol) in THF (50 mL) was added *t*-BuLi (3.8 mL, 5.56 mmol, 1.6 M in pentane) at  $-78$  °C. After 3 hours, 2,6-dibromoanthracene-9,10-dione (**19**) (1 g, 2.73 mmol) was added. The resulting mixture was allowed to warm to room temperature slowly. The mixture was poured into water, extracted with diethyl ether. The organic layer was washed with brine, dried over  $\text{MgSO}_4$ . The solvent was removed under high vacuum. The product was purified using column chromatography eluted ethyl acetate/ petroleum ether (1/10) (v/v) to obtain the target product as a yellow solid (5.2 g, 76.2% yield). The product gave a single spot on TLC ( $R_f = 0.39$ ) (silica-gel plates - ethyl acetate/ petroleum ether (1/10) (v/v)). M.p.  $101\text{--}102$  °C. Mass (EI); ( $m/z$ ): 888.2, 890.2, 892.2 ( $\text{M}^+$ ).  $^1\text{H}$ NMR (400 MHz,  $\text{CDCl}_3$ )  $\delta$  ppm 8.03 (s, 2H), 7.77 (d,  $J = 8.27$  Hz, 2H), 7.58 (dd,  $J = 8.30, 1.58$  Hz, 2H), 6.42 (bs, 4H), 6.18 (bs, 4H), 3.69 (t, 4H),

1.67 (m, 4H), 1.50-1.14 (m, 36H) , 0.90 (t,  $J = 6.78$  Hz, 6H).  $^{13}\text{C}$ NMR (400 MHz,  $\text{CDCl}_3$ )  $\delta_{\text{C}}/\text{ppm}$ : 142.9, 139.7, 130.8, 129.1, 128.3, 128.0, 122.1, 113.4, 74.4, 68.0, 31.9, 29.6, 29.6, 29.6, 29.4, 29.3, 29.2, 26.0, 22.7, 14.1. FT-IT (ATR): ( $\text{cm}^{-1}$ ) 3402, 2917, 2850, 1646, 1584, 1508, 1466, 1297, 1245, 1180, 1162, 1082, 1013, 825, 719. Elemental Analysis (%) calculated for  $\text{C}_{50}\text{H}_{66}\text{O}_4\text{Br}_2$ : C, 67.41; H, 7.47; Br, 17.94. Found: C, 67.05; H, 7.65; Br, 17.89.

### 3.3.21. 2,6-Dibromo-9,10-bis(4-(dodecyloxy)phenyl)anthracene (22)

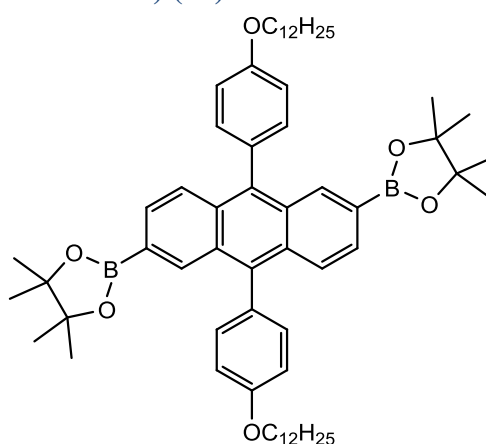


The preparation of 2,6-dibromo-9,10-bis(4-(dodecyloxy)phenyl)anthracene (**22**) was carried out according to a modified method by Wang et al.<sup>127</sup>

A mixture of 2,6-dibromo-9,10-bis(4-(dodecyloxy)phenyl)-9,10-dihydroanthracene-9,10-diol (**21**) (13.5 g, 15.20 mmol), KI (21.8 g, 131.48 mmol),  $\text{NaH}_2\text{PO}_2 \cdot x\text{H}_2\text{O}$  (15.4g, 175.4 mmol) and acetic acid (152 ml) was heated at reflux for 40 min. The precipitate was collected and dissolved in dichloromethane (DCM). The organic solution was washed with brine, dried over anhydrous  $\text{MgSO}_4$ . After solvent removal, the residue was purified by column chromatography on silica gel with petroleum ether:DCM (4:1) and then recrystallization from hexane to afford the target product (8.3 g, 63.4 % yield) as light yellow crystals. The product gave a single spot on TLC ( $R_f = 0.45$ ) (silica-gel plates - petroleum ether:DCM (4:1) (v/v)). M.p. 113-115 °C. Mass (EI); (m/z): 854.2, 856.3, 857.2 ( $\text{M}^+$ ).  $^1\text{H}$ NMR (250 MHz,  $\text{CDCl}_3$ )  $\delta$  ppm 7.89 (d,  $J = 1.85$  Hz, 2H), 7.61 (d,  $J = 9.32$  Hz, 2H), 7.37 (m, 6H), 7.15 (d,  $J = 8.63$  Hz, 4H), 4.13 (t,  $J = 6.50$  Hz, 4H), 1.92 (m, 4H), 1.46 (m, 36H), 0.91 (t,  $J = 6.52$  Hz, 6H).  $^{13}\text{C}$ NMR (400 MHz,  $\text{CDCl}_3$ )  $\delta_{\text{C}}/\text{ppm}$ : 158.9, 136.5,

132.2, 131.2, 129.4, 129.1, 129.0, 128., 128.8, 120.0, 120.0, 114.6, 68.1, 31.9, 29.7, 29.6, 29.5, 29.4, 29.4, 26.2, 22.7, 14.1. FT-IT (ATR): ( $\text{cm}^{-1}$ ) 2913, 2846, 2526, 2160, 2023, 1977, 1607, 1573, 1513, 1463, 1435, 1392, 1377, 1285, 1243, 1171, 1109, 1078, 1067, 1034, 1013, 995, 946, 915, 875, 824, 813, 805, 771, 754, 742, 721. Elemental Analysis (%) calculated for  $\text{C}_{50}\text{H}_{64}\text{O}_2\text{Br}_2$ : C, 70.09; H, 7.53; Br, 18.65. Found: C, 70.26; H, 7.68; Br, 18.66.

### 3.3.22. 2,2'-(9,10-Bis(4-(dodecyloxy)phenyl)anthracene-2,6-diyl)bis(4,4,5,5-tetramethyl-1,3,2-dioxaborolane) (**23**)

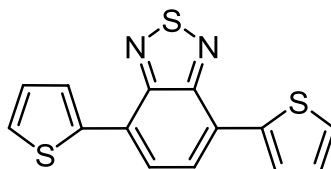


The preparation of 2,2'-(9,10-bis(4-(dodecyloxy)phenyl)anthracene-2,6-diyl)bis(4,4,5,5-tetramethyl-1,3,2-dioxaborolane) (**23**) was carried out according to a modified method by Jo et al.<sup>115</sup>

2,6-Dibromo-9,10-bis(4-(dodecyloxy)phenyl)-9,10-dihydroanthracene-9,10-diol (**22**) (3 g, 3.49 mmol), bis(pinacolato)diboron (4.33 g, 12.2 mmol), potassium acetate (2.06 g, 20.96 mmol) and  $\text{Pd}(\text{dppf})\text{Cl}_2$  (0.17 g, 0.022 mmol) in DMF (42  $\text{cm}^3$ ) was heated to 100 °C for 36 hours. The reaction mixture was cooled to room temperature, then poured into  $\text{H}_2\text{O}$  (100  $\text{cm}^3$ ) and extracted with diethyl ether (3  $\times$  100  $\text{cm}^3$ ). The organic phases were combined, then washed with  $\text{H}_2\text{O}$  (5  $\times$  100  $\text{cm}^3$ ) and dried over  $\text{MgSO}_4$ . The crude product was purified *via* recrystallisation, the crude product was dissolved in the minimum amount of diethyl ether and then precipitated in hot methanol which had been ran through a basic column. The product was obtained as light yellow crystals (2.3 g, 69.1 % yield). M.p. 109-110 °C. Mass (EI); ( $m/z$ ): 950.5( $\text{M}^+$ ).  $^1\text{H}$ NMR (400 MHz,  $\text{CDCl}_3$ )  $\delta$  ppm: 8.32 (s, 2H),

7.70 (d,  $J = 7.00$  Hz, 2H), 7.66 (d,  $J = 7.00$  Hz, 2H), 7.40 (d,  $J = 8.54$  Hz, 4H), 7.17 (d,  $J = 8.59$  Hz, 4H), 4.17 (t,  $J = 6.59$  Hz, 4H), 1.99-1.88 (m, 4H), 1.66-1.55 (m, 6H), 1.50-1.26 (m, 54H), 0.92 (t,  $J = 6.78$  Hz, 6H).  $^{13}\text{C}$ NMR (400 MHz,  $\text{CDCl}_3$ )  $\delta_{\text{C}}$ /ppm: 158.4, 137.7, 135.6, 132.5, 131.4, 130.7, 130.2, 128.8, 126.2, 114.4, 83.7, 68.2, 31.9, 29.7, 29.6, 29.5, 29.5, 29.3, 26.2, 24.8, 22.7, 14.1. FT-IT (ATR): ( $\text{cm}^{-1}$ ) 2918, 2851, 2518, 2160, 2941, 1977, 1621, 1606, 1572, 1512, 1473, 1370, 1340, 1309, 1267, 1240, 1173, 1148, 1137, 1108, 1076, 1026, 1004, 970, 909, 859, 838, 826, 770, 748, 723, 710. Elemental Analysis (%) calculated for  $\text{C}_{62}\text{H}_{88}\text{O}_6\text{B}_2$ : C, 78.30; H, 9.33. Found: C, 77.77; H, 9.58.

### 3.3.23. 4,7-Di(thiophen-2-yl)benzo[*c*][1,2,5]thiadiazole (**24**)

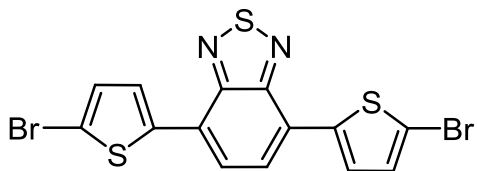


The preparation of 4,7-di(thiophen-2-yl)benzo[*c*][1,2,5]thiadiazole (**24**) was carried out according to a modified method by palama et al.<sup>128</sup>

4,7-Dibromo-1,2,5-benzothiadiazole (**8**) (3 g, 10.2 mmol) and tributyl(thiophen-2-yl)stannane (13.3 g, 35.7 mmol) were added to toluene (50 ml).  $\text{Pd}(\text{PPh}_3)_4$  (145.5 mg, 0.126 mmol) was added. The mixture was refluxed (120 °C) under argon atmosphere for 24 hours. Then, the residue was purified by column chromatography on silica gel (petroleum ether (40:60): toluene (2:1)). Recrystallization was carried out from ethanol, which gave the target product as orange crystals (2.6g, 75% yield). The product gave a single spot on TLC ( $R_f = 0.52$ ), silica-gel plates - petroleum ether (40:60): Toluene (2:1). M.p. 122-124 °C (literature<sup>129</sup> m.p. 123-125 °C). Mass (EI); ( $m/z$ ):. 300 ( $\text{M}^+$ ).  $^1\text{H}$ NMR (400 MHz,  $\text{CDCl}_3$ )  $\delta_{\text{H}}$ /ppm: 8.11 (dd,  $J = 3.71, 1.10$  Hz, 2H), 7.84 (s, 2H), 7.47 (dd,  $J = 5.10, 1.10$  Hz, 2H), 7.23 (dd,  $J = 5.10, 3.71$  Hz, 2H).  $^{13}\text{C}$ NMR (400 MHz,  $\text{CDCl}_3$ );  $\delta_{\text{C}}$ /ppm: 152.5, 139.3, 128.0, 127.5, 126.8, 125.9, 125.7. FT-IT (ATR): ( $\text{cm}^{-1}$ ) 3070, 2160, 2010, 1818, 1577, 1539, 1511, 1476, 1429, 1419, 1377, 1352, 1270, 1213, 1105, 1070, 1045, 918, 885, 874, 855,

842, 823, 808, 747, 702. Elemental Analysis (%) calculated for  $C_{14}H_8N_2S_3$ : C, 55.97; H, 2.68; N, 9.32; S, 32.02. Found: C, 56.05; H, 2.49; N, 9.21; S, 32.06.

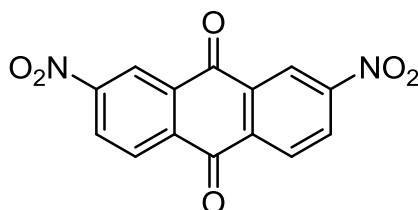
### 3.3.24. 4,7-Bis(5-bromothiophen-2-yl)benzo[c][1,2,5]thiadiazole (25)



4,7-Bis(5-bromothiophen-2-yl)benzo[c][1,2,5]thiadiazole (**25**) was synthesised according to a modified procedure by Zhang et al.<sup>120</sup>

4,7-Di(thiophen-2-yl)benzo[c][1,2,5]thiadiazole (**24**) (1 g, 3.33 mmol) was added to chlorobenzene (40 ml) in a 100 ml flask. The reaction mixture was heated to 50 °C and N-bromosuccinimide (NBS) (1.06 g, 5.99 mmol) was added in two portions (the second portion was added after one hour) for three hours. The reaction mixture was heated to 135 °C then cooled to room temperature. The product was filtered and washed with water and methanol. The target product was obtained as red crystals (1.2 g 80 % yield). M.p. 255-258 °C (literature<sup>130</sup> m.p. 256-258 °C). Mass (EI); (m/z) 456, 458, 460 ( $M^+$ ). <sup>1</sup>HNMR (400 MHz,  $CDCl_3$ )  $\delta_H$ /ppm: 7.84 (d,  $J = 3.97$  Hz, 1H), 7.82 (s, 1H), 7.19 (d,  $J = 3.98$  Hz, 1H). FT-IT (ATR): ( $cm^{-1}$ ) 3090, 2160, 2007, 1746, 1528, 1480, 1415, 1368, 1308, 1273, 1211, 1097, 1071, 969, 884, 871, 845, 830, 781, 738. Elemental Analysis (%) calculated for  $C_{14}H_6N_2Br_2S_3$ : C, 36.70; H, 1.32; N, 6.11; Br, 34.88; S, 20.99. Found: C, 37.04; H, 0.83; N, 6.11; Br, 34.88; S, 20.99.

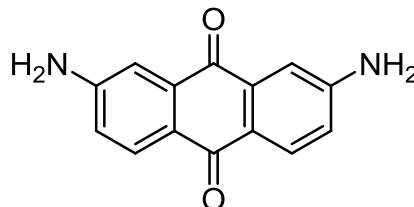
### 3.3.25. 2,7-Dinitro-9,10-anthraquinone (26)



The preparation of 2,7-dinitro-9,10-anthraquinone (**26**) was carried out according to a modified method by Yang et al.<sup>131</sup>

Anthrone (20 g, 104 mmol) was added slowly with stirring to fuming nitric acid (160 mL) at 0 °C. Subsequently, acetic acid (400 ml) was added slowly to the reaction mixture with cooling. The resulting solution was allowed to stand at room temperature for 1 week. At the end of the period, the yellow precipitate was collected by filtration, washed with acetic acid (100 ml) and hexane (100 ml), and dried under vacuum. The crude product was recrystallized twice from acetic acid then recrystallised from nitrobenzene/ acetic acid (1:1 v/v) to obtain the target product as yellow crystals (9.2 g, 23% yield). M.p. 289-291 °C (literature<sup>132</sup> m.p. 290-291 °C). Mass (EI); (m/z) 299 (M<sup>+</sup>). <sup>1</sup>HNMR (400 MHz, DMSO-*d*<sub>6</sub>) δ ppm: 8.84 (d, *J* = 1.99 Hz, 1H), 8.72 (dd, *J* = 8.36, 1.95 Hz, 1H), 8.49 (d, *J* = 8.51 Hz, 1H). FT-IT (ATR): (cm<sup>-1</sup>) 3091, 3073, 3040, 2448, 2160, 2024, 1975, 1673, 1604, 1587, 1539, 1523, 1435, 1352, 1326, 1299, 1274, 1249, 1164, 1121, 1084, 995, 948, 928, 902, 886, 864, 838, 815, 789, 868, 707. Elemental Analysis (%) calculated for C<sub>14</sub>H<sub>6</sub>N<sub>2</sub>O<sub>6</sub>: C, 56.39; H, 2.03; N, 9.39. Found: C, 56.44; H, 1.77; N, 9.61.

### 3.3.26. 2,7-Diaminoanthracene-9,10-dione (27)

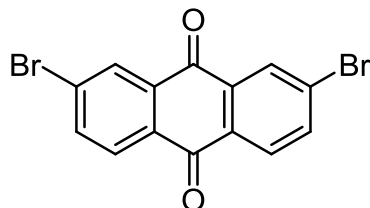


The preparation of 2,7-diaminoanthracene-9,10-dione (**27**) was carried out according to a modified method by Yang et al.<sup>131</sup>

2,7-Dinitroanthracene-9,10-dione (**26**) (8 g, 26.65 mmol) in ethanol (290 ml) was added to a solution of sodium sulfide nonahydrate (28.8 g, 120 mmol) and sodium hydroxide (11.4 g, 285.12 mmol) in water (500 ml). The mixture was heated at reflux for 6 h and left to stand overnight. The ethanol was removed in vacuum and the residue cooled to 0-5 °C. The resulting precipitate was collected by filtration, repeatedly washed with water, and dried. Recrystallization from ethanol afforded the target product as an orange/red solid (5.7g, 90% yield). Mass (EI); (m/z): 238 (M<sup>+</sup>). Mp 335-337 °C (literature<sup>132</sup> m.p. 337-339 °C). <sup>1</sup>HNMR (400 MHz, DMSO-*d*<sub>6</sub>) δ ppm: 7.84 (d, *J* = 8.47 Hz, 2H), 7.23 (d, *J* = 2.40 Hz, 2H), 6.89 (dd, *J* = 8.50,

2.43 Hz, 2H), 6.42 (s, N-H, 4H).  $^{13}\text{C}$ NMR (400 MHz,  $\text{DMSO}-d_6$ );  $\delta_{\text{C}}/\text{ppm}$ : 184.7, 179.7, 155.1, 152.3, 135.0, 129.3. FT-IT (ATR): ( $\text{cm}^{-1}$ ) 3344, 3223, 2502, 2160, 2022, 1976, 1671, 1623, 1581, 1553, 1499, 1458, 1338, 1312, 1245, 1206, 1191, 1130, 1088, 1001, 930, 889, 853, 772, 745, 715. Elemental Analysis (%) calculated for  $\text{C}_{14}\text{H}_{10}\text{N}_2\text{O}_2$ : C, 70.58; H, 4.23; N, 11.76. Found: C, 70.28; H, 3.82; N, 11.57.

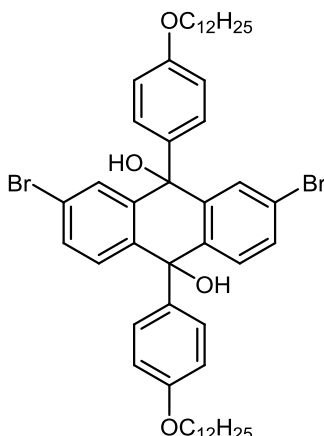
### 3.3.27. 2,7-Dibromoanthracene-9,10-dione (**28**)



The preparation of 2,7-dibromoanthracene-9,10-dione (**28**) was carried out according to a modified method by Vila et al.<sup>123</sup>

2,7-Diaminoanthraquinone (**27**) (3 g, 12.6 mmol), *t*-Bu ONO (3.2 g, 31.5 mmol),  $\text{CuBr}_2$  (7.03 g, 31.5 mmol), and  $\text{CH}_3\text{CN}$  (54 ml) were placed in a one-neck flask, and the mixture was heated at 65 °C for 2 h. The reaction was quenched by adding 35% HCl (aq) solution to the product mixture. The solution was filtered, washed with  $\text{CH}_3\text{CN}$ , and the product was recrystallized from 1,4-dioxane. The product was obtained as a yellow powder (3.4 g, 75% yield). The product gave a single spot on TLC ( $R_f = 0.46$ ) (silica-gel plates - ethyl acetate/ petroleum ether (1/10) (v/v)). M.p. 249-250 °C (literature<sup>131</sup> m.p. 248-250 °C). Mass (EI); ( $m/z$ ): 364, 366, 367 ( $\text{M}^+$ ).  $^1\text{H}$ NMR (400 MHz,  $\text{CDCl}_3$ )  $\delta_{\text{H}}/\text{ppm}$ : 8.45 (d,  $J = 1.98$  Hz, 2H), 8.20 (d,  $J = 8.31$  Hz, 2H), 7.97 (dd,  $J = 8.31, 2.03$  Hz, 2H).  $^{13}\text{C}$ NMR (400 MHz,  $\text{CDCl}_3$ )  $\delta_{\text{C}}/\text{ppm}$ : 137.5, 134.1, 131.8, 130.3, 130.0, 129.1. FT-IT (ATR): ( $\text{cm}^{-1}$ ) 3083, 2445, 2160, 2034, 1977, 1670, 1574, 1415, 1309, 1287, 1267, 1249, 1204, 1171, 1105, 1068, 924, 910, 865, 821, 772, 730, 713, 705. Elemental Analysis (%) calculated for  $\text{C}_{14}\text{H}_6\text{O}_2\text{Br}_2$ : C, 45.94; H, 1.65; Br, 43.66. Found: C, 46.44; H, 1.44; Br, 41.92.

### 3.3.28. 2,7-Dibromo-9,10-bis(4-(dodecyloxy)phenyl)-9,10-dihydroanthracene-9,10-diol (29)

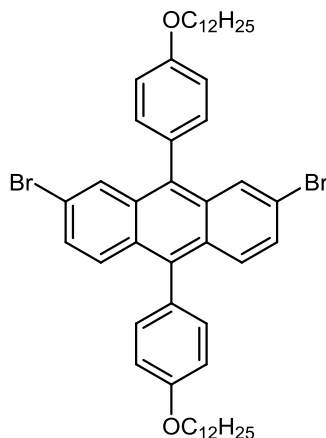


The preparation of 2,7-dibromo-9,10-bis(4-(dodecyloxy)phenyl)-9,10-dihydroanthracene-9,10-diol (**29**) was carried out according to a modified method by Wang et al.<sup>127</sup>

To a solution of 1-bromo-4-(dodecyloxy)benzene (**20**) ( 11.95 g, 32.8 mmol) in THF (250 ml) was added *t*-BuLi ( 16.1 ml, 27.3 mmol, 1.6 M in pentane) at -78 °C. After 3 hours, 2,7-dibromoanthracene-9,10-dione (**28**) (4 g, 10.93 mmol) was added. The resulting mixture was allowed to warm to room temperature slowly. After stirring overnight, the mixture was poured into water and extracted with diethyl ether. The organic layer was washed with brine and dried over MgSO<sub>4</sub>. The solvent was removed under high vacuum. The product was purified using column chromatography eluted ethyl acetate/ petroleum ether (1/10) (v/v) to obtain the target product as yellow solid (6.3 g, 65 % yield). The product gave a single spot on TLC ( $R_f = 0.31$ ) (silica-gel plates - ethyl acetate/ petroleum ether (1/10) (v/v)). M.p. 105-106 °C. Mass (EI); (m/z): 888, 890, 890, 892 ( $M^+$ ). <sup>1</sup>HNMR (250 MHz, CDCl<sub>3</sub>)  $\delta$  ppm: 8.03 (s, 2H), 7.75 (d,  $J = 8.34$  Hz, 2H), 7.57 (dd,  $J = 8.33, 1.84$  Hz, 2H), 6.40 (bs, 4H), 6.18 (bs, 4H), 3.68 (s, 4H), 1.75-1.54 (m, 4H), 1.46-1.15 (m, 36H), 0.89 (t,  $J = 6.56$  Hz, 6H). <sup>13</sup>CNMR (250 MHz, CDCl<sub>3</sub>)  $\delta_C$ /ppm: 157.7, 142.8, 139.8, 130.8, 129.1, 128.3, 128.0, 122.0, 113.5, 113.4, 76.9, 76.4, 74.5, 74.3, 68.1, 68.0, 31.9, 29.6, 29.4, 29.3, 29.2, 26.0, 22.6, 14.0. FT-IT (ATR): (cm<sup>-1</sup>) 3306, 2918, 2851, 2535, 2160, 2023, 1609, 1584, 1507, 1460, 1415, 1390, 1299, 1245, 1182, 1164, 1139, 1119, 1104, 1081, 1018, 957, 919, 877, 823, 810, 771, 748, 719.

Elemental Analysis (%) calculated for  $C_{14}H_{6}O_2Br_2$ : C, 67.41; H, 7.47; Br, 17.94.  
Found: C, 67.37; H, 7.44; Br, 18.07.

### 3.3.29. 2,7-Dibromo-9,10-bis(4-(dodecyloxy)phenyl)anthracene (30)

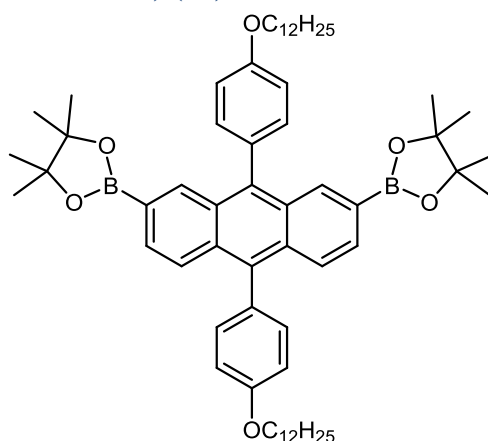


The preparation of 2,7-dibromo-9,10-bis(4-(dodecyloxy)phenyl)anthracene (**30**) was carried out according to a modified method by Wang et al.<sup>127</sup>

A mixture of 2,7-dibromo-9,10-bis(4-(dodecyloxy)phenyl)-9,10-dihydroanthracene-9,10-diol (**29**) (7.1 g, 8.01 mmol), KI (11.50 g, 69.23 mmol),  $NaH_2PO_2 \cdot xH_2O$  (8.12g, 92.3 mmol) and acetic acid (80 ml) was heated at reflux for 40 min. The precipitate was collected and dissolved in dichloromethane (DCM). The organic solution was washed with brine, dried over anhydrous  $MgSO_4$ . After solvent removal, the residue was purified by column chromatography on silica gel with petroleum ether : DCM (4:1) and then recrystallization from hexane to afford the target product (5.5 g, 80 % yield) as light yellow crystals. The product gave a single spot on TLC ( $R_f=0.46$ ) (silica-gel plates - petroleum ether: DCM (4:1) (v/v)). M.p. 110-111 °C. Mass (EI); (m/z): 854.6, 856.5, 857.6 ( $M^+$ ).  $^1H$ NMR (250 MHz,  $CDCl_3$ )  $\delta$  ppm: 7.88 (d,  $J = 1.78$  Hz, 2H), 7.61 (d,  $J = 9.32$  Hz, 2H), 7.41 (d,  $J = 1.99$  Hz, 2H), 7.36 (dd,  $J = 4.52, 1.93$  Hz, 2H), 7.32 (d,  $J = 1.90$  Hz, 2H), 7.15 (dd,  $J = 8.61, 5.84$  Hz, 4H), 4.13 (q,  $J = 6.65$  Hz, 4H), 2.02-1.80 (m, 4H), 1.68-1.17 (m, 36H), 0.91 (t,  $J = 6.57$  Hz, 6H).  $^{13}C$ NMR (400 MHz,  $CDCl_3$ )  $\delta_C$ /ppm: 159.0, 158.9, 137.7, 135.3, 132.2, 132.1, 131.7, 129.6, 129.3, 129.1, 128.7, 128.7, 120.3, 114.7, 114.5, 68.2, 31.9, 29.7, 29.6, 29.5, 29.4, 29.3, 26.2, 26.1, 22.7, 14.1. FT-IT (ATR): ( $cm^{-1}$ ) 3070, 2955, 2933, 2913, 2871, 2849, 2525, 2160, 2025, 1977, 1607, 1570, 1513, 1471, 1434, 1411, 1396, 1374, 1319, 1304, 1279, 1239, 1106, 1063,

1048, 1035, 1003, 959, 945, 925, 877, 823, 811, 774, 758, 741, 716. Elemental Analysis (%) calculated for  $C_{14}H_{16}O_2Br_2$ : C, 70.09; H, 7.53; Br, 18.65. Found: C, 70.03; H, 7.62; Br, 18.82.

### 3.3.30. 2,2'-(9,10-Bis(4-(dodecyloxy)phenyl)anthracene-2,7-diyl)bis(4,4,5,5-tetramethyl-1,3,2-dioxaborolane) (31)

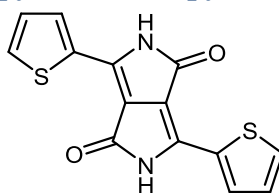


The preparation of 2,2'-(9,10-bis(4-(dodecyloxy)phenyl)anthracene-2,7-diyl)bis(4,4,5,5-tetramethyl-1,3,2-dioxaborolane) (**31**) was carried out according to a modified method by Jo et al.<sup>115</sup>

2,7-Dibromo-9,10-bis(4-(dodecyloxy)phenyl)-9,10-dihydroanthracene-9,10-diol (**30**) (3 g, 3.49 mmol), bis(pinacolato)diboron (4.33 g, 12.2 mmol), potassium acetate (2.06 g, 20.96 mmol) and  $Pd(dppf)Cl_2$  (0.17 g, 0.022 mmol) in DMF (42  $cm^3$ ) was heated to 100 °C for 36 hours. The reaction mixture was cooled to room temperature, then poured into  $H_2O$  (100  $cm^3$ ) and extracted with diethyl ether (3  $\times$  100  $cm^3$ ). The organic phases were combined, then washed with  $H_2O$  (5  $\times$  100  $cm^3$ ) and dried over  $MgSO_4$ . The crude product was purified *via* recrystallisation, the crude product was dissolved in the minimum amount of diethyl ether and then precipitated in hot methanol which had been ran through a basic column. The product was obtained as light yellow crystals. (2.0 g, 60.6 % yield). M.p. 110-112 °C. Mass (EI); (m/z): 950.9 ( $M^+$ ).  $^1H$ NMR (400 MHz,  $CDCl_3$ )  $\delta$  ppm: 8.32 (s, 2H), 7.72 – 7.68 (dd, 4H), 7.44 (d,  $J = 8.58$  Hz, 2H), 7.37 (d,  $J = 8.59$  Hz, 2H), 7.20 (d,  $J = 8.63$  Hz, 2H), 7.15 (d,  $J = 8.63$  Hz, 2H), 4.20 (t,  $J = 6.65$  Hz, 2H), 4.14 (t,  $J = 6.54$  Hz, 2H), 2.04-1.83 (m, 2H), 1.66-1.52 (m, 2H), 1.52-1.25 (m, 60H), 0.92 (t,  $J = 6.73$  Hz, 6H).  $^{13}C$ NMR (400 MHz,  $CDCl_3$ )  $\delta_C$ /ppm: 159.2, 159.1, 136.1, 132.7,

132.4, 132.0, 130.5, 129.6, 129.3, 125.9, 114.4, 114.3, 83.7, 77.0, 76.7, 68.2, 68.1, 31.9, 29.7, 29.6, 29.5, 29.4, 26.2, 24.8, 22.7, 14.1. FT-IT (ATR): ( $\text{cm}^{-1}$ ) 2918, 2851, 2161, 2021, 1607, 1513, 1493, 1472, 1371, 1349, 1322, 1276, 1241, 1175, 1143, 1127, 1107, 1078, 1031, 1003, 985, 951, 917, 891, 857, 834, 824, 802, 719, 710. Elemental Analysis (%) calculated for  $\text{C}_{14}\text{H}_6\text{O}_2\text{Br}_2$ : C, 78.30; H, 9.33. Found: C, 77.81; H, 9.41.

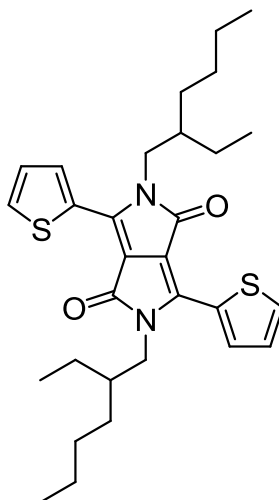
### 3.3.31. 3,6-Di(thiophen-2-yl)pyrrolo[3,4-c]pyrrole-1,4(2H,5H)-dione (32)



The preparation of 3,6-di(thiophen-2-yl)pyrrolo[3,4-c]pyrrole-1,4(2H,5H)-dione (**32**) was carried out according to a modified method by Chen et al.<sup>133</sup>

A mixture of Na (0.98 g, 42.6 mmol) and  $\text{FeCl}_3$  (0.1 g, 0.616 mmol) was dissolved in tert-amyl alcohol (20 ml) by heating at 90 °C for 2 h. After cooling to 50 °C, thiophene-2-carbonitrile (2.344, 21.2 mmol) was added and then the mixture was again heated at 90 °C. A solution of dimethyl succinate (2.23 g, 0.105 mmol) in tert-amyl alcohol (10 ml) was added dropwise over 2 h and then the mixture was maintained at 90 °C for 20 h. After cooling to 50 °C, glacial AcOH was added and then the mixture was heated under reflux for 10 min before being filtered. The residue was washed several times with hot MeOH and water, and then the solid was dried under vacuum to obtain the target product as a red solid (5.76 g, 90% yield). This compound was used directly in the next step without purification. M.p. 204–207 °C. Mass (EI); ( $m/z$ ) 300 ( $\text{M}^+$ ).  $^1\text{H}$ NMR (250 MHz, *DMSO*)  $\delta_{\text{H}}$ /ppm: 11.25 (bs, 2H), 8.20 (bs, 2H), 7.96 (bs, 2H), 7.30 (bs, 2H).  $^{13}\text{C}$ NMR (250 MHz, *CDCl}\_3*);  $\delta_{\text{C}}$ /ppm: 162.1, 136.6, 133.1, 131.7, 131.2, 129.2. FT-IT (ATR): ( $\text{cm}^{-1}$ ) 3275, 3125, 2989, 2160, 2024, 1704, 1679, 1640, 1594, 1498, 1439, 1415, 1361, 1313, 1289, 1229, 1181, 1127, 1099, 1056, 998, 940, 877, 857, 836, 789, 777, 747, 725. Elemental Analysis (%) calculated for  $\text{C}_{14}\text{H}_8\text{N}_2\text{S}_3\text{O}_2$ : C, 55.98; H, 2.68; N, 9.33; S, 21.35. Found: C, 48.59; H, 3.76; N, 6.37; S, 15.04.

### 3.3.32. 2,5-Bis(2-ethylhexyl)-3,6-di(thiophen-2-yl)pyrrolo[3,4-c]pyrrole-1,4(2H,5H)-dione (33)

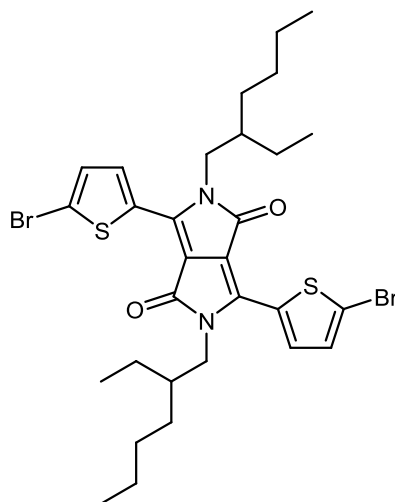


The preparation of 3,6-di(thiophen-2-yl)pyrrolo[3,4-c]pyrrole-1,4(2H,5H)-dione (**33**) was carried out according to a modified method by Chen et al.<sup>133</sup>

A solution of 2-ethylhexyl bromide (4.89 ml, 27.5 mmol) in DMF (30 ml) was added dropwise to a mixture of 3,6-di(thiophen-2-yl)pyrrolo[3,4-c]pyrrole-1,4(2H,5H)-dione (**32**) (2.50 g, 8.33 mmol),  $K_2CO_3$  (3.83 g, 27.8 mmol), and 18-crown-6 (0.25 g, 0.95 mmol) in DMF (50 ml) at 120 °C and then the mixture was maintained at 120 °C overnight. After cooling to room temperature, the product was dissolved in  $CHCl_3$  washed with water (3 × 300 ml), and then dried ( $MgSO_4$ ). The solvent was evaporated under reduced pressure and precipitated in methanol. The crude product was purified through chromatography using chloroform to obtain the target product as a red solid (1.4 g, 32 % yield). The product gave a single spot on TLC ( $R_f = 0.64$ ), silica-gel plates eluted with chloroform. M.p. 125-127 °C (literature<sup>134</sup> m.p. 125 °C). Mass (EI); (m/z) 524 ( $M^+$ ).  $^1H$ NMR (400 MHz,  $CDCl_3$ )  $\delta_H$ /ppm: 8.92 (dd,  $J = 3.87, 0.98$  Hz, 2H), 7.65 (dd,  $J = 5.00, 0.96$  Hz, 2H), 7.29 (dd,  $J = 4.93, 3.98$  Hz, 2H), 4.11-3.98 (m, 4H), 1.94-1.83 (m, 2H), 1.43-1.19 (m, 16H), 0.94-0.83 (m, 12H).  $^{13}C$ NMR (400 MHz,  $CDCl_3$ );  $\delta_C$ /ppm: 161.7, 140.4, 135.2, 130.5, 129.8, 128.4, 107.9, 45.8, 39.0, 30.2, 28.3, 23.5, 23.0, 14.0, 10.4. FT-IT (ATR): ( $cm^{-1}$ ) 3096, 3081, 2954, 2926, 2857, 2466, 2161, 2024, 1976, 1663, 1566, 1503, 1449, 1417, 1401, 1359, 1321, 1273, 1229, 1169, 1155, 1096, 1064, 1027, 958, 918, 894, 847, 804, 774, 751, 734, 710. Elemental Analysis (%)

calculated for  $C_{30}H_{40}N_2O_2S_2$ : C, 68.66; H, 7.68; N, 5.34; S, 12.22. Found: C, 67.94; H, 7.96; N, 5.15; S, 12.52.

### 3.3.33. 3,6-Bis(5-bromothiophen-2-yl)-2,5-bis(2-ethylhexyl)pyrrolo[3,4-c]pyrrole-1,4(2H,5H)-dione (34)



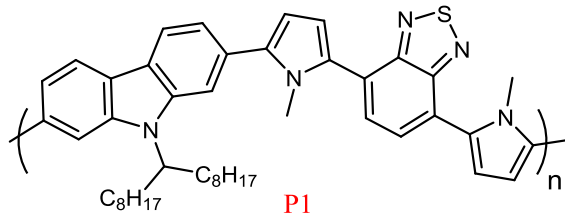
The preparation of 3,6-bis(5-bromothiophen-2-yl)-2,5-bis(2-ethylhexyl)pyrrolo[3,4-c]pyrrole-1,4(2H,5H)-dione (**34**) was carried out according to a modified method by Chen et al.<sup>133</sup>

NBS (0.45 g, 2.53 mmol) was added to a solution of 3,6-di(thiophen-2-yl)pyrrolo[3,4-c]pyrrole-1,4(2H,5H)-dione (**33**) (0.70 g, 1.33 mmol) in  $CHCl_3$  (40 ml) in a one neck round-bottom flask. After stirring at room temperature for 48 h and in the dark, the reaction mixture was poured into water (300 ml) and extracted with  $CHCl_3$  ( $3 \times 100$  ml). The organic layer was dried ( $MgSO_4$ ) and the solvent was evaporated under reduced pressure. The crude product was purified through chromatography using chloroform to obtain the target product as a red solid (0.74 g, 82 % yield). The product gave a single spot on TLC ( $R_f = 0.64$ ), silica-gel plates eluted with chloroform. M.p. 155-158 °C. Mass (EI); ( $m/z$ ) 680, 682, 684 ( $M^+$ ).  $^1H$ NMR (400 MHz,  $CDCl_3$ )  $\delta_H$ /ppm: 8.67 (d,  $J = 4.18$  Hz, 2H), 7.24 (d,  $J = 4.18$  Hz, 2H), 4.01-3.89 (m, 4H), 1.91-1.79 (m, 2H), 1.43-1.20 (m, 16H), 0.95-0.83 (m, 12H).  $^{13}C$ NMR (250 MHz,  $CDCl_3$ );  $\delta_C$ /ppm: 161.4, 139.4, 135.4, 131.4, 131.1, 119.0, 107.9, 45.9, 39.0, 30.14, 28.3, 23.5, 23.0, 14.0, 10.4. FT-IT (ATR): ( $cm^{-1}$ ) 3085, 2958, 2926, 2858, 2541, 3160, 2026, 1926, 1653, 1555, 1504, 1448, 1411,

1398, 1378, 1356, 1336, 1310, 1259, 1235, 1169, 1156, 1101, 1081, 1067, 1026, 969, 924, 896, 833, 801, 774, 730, 711. Elemental Analysis (%) calculated for  $C_{30}H_{38}N_2O_2S_2Br_2$  : C, 52.79; H, 5.61; N, 4.10; S, 9.40; Br, 23.41. Found: C, 52.50; H, 5.75; N, 4.05; S, 9.04; Br, 25.20.

### 3.4. Synthesis of Polymers

#### 3.4.1. Poly [9-(heptadecan-9-yl)-9H-carbazole-2,7-diyl-alt-(4',7'-bis(1-methyl-1H-pyrrol-2'-yl)-2',1',3'-benzothiadiazole)-5,5-diyl] (P1)



#### Method 1: Polymerisation in toluene using tetraethylammonium hydroxide as a base

A solution of 9-(heptadecan-9-yl)-2,7-bis(4,4,5,5-tetramethyl-1,3,2-dioxaborolan-2-yl)-9H-carbazole (**7**) (0.4 g, 0.608 mmol) and 4,7-bis(5-bromo-1-methyl-1H-pyrrol-2-yl)benzo[c][1,2,5]thiadiazole (**11**) (0.275 g, 0.608 mmol) in dry toluene (10 ml) in a 100 ml one-necked round bottom flask and under argon was degassed. To the reaction mixture was added a 20 % w/w aqueous solution of tetraethylammonium hydroxide (2.1 ml) and the reaction mixture was degassed. To the reaction mixture, Pd(OAc)<sub>2</sub> (7 mg, 0.031 mmol) and tri-*o*-tolylphosphine (19 mg, 0.055 mmol) were added and degassed then heated to 90 °C for 24 hours. After cooling the reaction mixture to room temperature, the polymer was end-capped with the addition of 1-bromobenzene (0.1 ml, 0.74 mmol) and degassed then heated to 90 °C for 1 hour. Again, the reaction mixture was cooled to room temperature and the polymer was end-capped with phenyl boronic acid (0.15 g, 0.1 mmol) and degassed, then the mixture was heated to 90 °C for 3 hours. The reaction mixture was cooled to room temperature, then dissolved in CHCl<sub>3</sub> (300 ml) and to this solution was added an ammonium hydroxide solution (28 % in H<sub>2</sub>O, 50 ml), followed by stirring overnight. Then, the organic layer was separated and washed with distilled water. The organic layer was concentrated to about 50 ml and poured into methanol:water (10:1, 300 ml). The resulting mixture was stirred overnight and filtered through a membrane filter. The collected solid was cleaned using soxhlet extraction with solvents in order methanol (250 ml), acetone (250 ml), hexane (250 ml) and toluene (250 ml). The toluene fraction was concentrated to about 50 ml and then poured into degassed methanol (300 ml). The resulting mixture was stirred overnight and the solid collected by filtration through a membrane filter to afford

polymer **P1** as a red powder ( 117 mg , 27 % yield). GPC (1,2,4-trichlorobenzene at 140 °C):  $M_w = 8100$ ,  $M_n = 2600$ , PD = 3.1. Elemental Analysis (%) calculated for  $C_{45}H_{53}N_2S$ : C, 77.66; H, 7.68; N, 10.06; S, 4.90. Found: C, 76.27; H, 7.29 ; N, 8.97 ; S, 3.18.

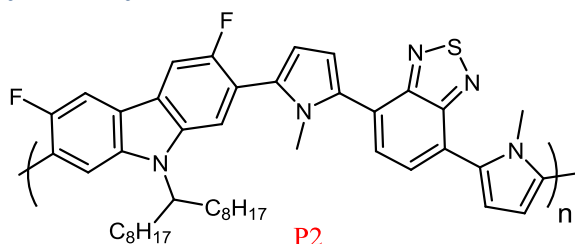
### **Method 2: polymerisation in THF using $NaHCO_3$ as base**

A solution of 9-(heptadecan-9-yl)-2,7-bis(4,4,5,5-tetramethyl-1,3,2-dioxaborolan-2-yl)-9H-carbazole (**7**) (0.35 g, 0.532 mmol) and 4,7-bis(5-bromo-1-methyl-1H-pyrrol-2-yl)benzo[c][1,2,5]thiadiazole (**11**) (0.24 g, 0.532 mmol) in dry THF (10 ml) in a 100 ml one-necked round bottom flask and under argon was degassed. To the reaction mixture was added a saturated solution of  $NaHCO_3$  (2 ml) and the reaction mixture was degassed. To the reaction mixture,  $Pd(OAc)_2$  (8.3 mg, 0.036 mmol) and tri-*o*-tolylphosphine (22.5 mg, 0.066 mmol) were added and degassed then heated to 90 °C for 24 hours. After cooling the reaction mixture to room temperature, the polymer was end-capped with the addition of 1-bromobenzene (0.1 ml, 0.74 mmol) and degassed then heated to 90 °C for 1 hour. Again, the reaction mixture was cooled to room temperature and the polymer was end-capped with phenyl boronic acid (0.15 g, 0.1 mmol) and degassed, then the mixture was heated to 90 °C for 3 hours. The reaction mixture was cooled to room temperature, then dissolved in  $CHCl_3$  (300 ml) and to this solution was added an ammonium hydroxide solution (28 % in  $H_2O$ , 50 ml), followed by stirring overnight. Then, the organic layer was separated and washed with distilled water. The organic layer was concentrated to about 50 ml and poured into methanol:water (10:1, 300 ml). The resulting mixture was stirred overnight and filtered through a membrane filter. The collected solid was cleaned using soxhlet extraction with solvents in order methanol (250 ml), acetone (250 ml), hexane (250 ml) and toluene (250 ml). The toluene fraction was concentrated to about 50 ml and then poured into degassed methanol (300 ml). The resulting mixture was stirred overnight and the solid collected by filtration through a membrane filter to afford polymer **P1** as a red powder (189 mg , 42 % yield). GPC (1,2,4-trichlorobenzene at 140 °C):  $M_w = 15300$ ,  $M_n = 14100$ , PD = 1.08. Elemental Analysis (%) calculated for  $C_{45}H_{53}N_5S$ : C, 77.66; H, 7.68; N,

---

10.6; S, 4.90. Found: C, 60.00; H, 7.76; N, 4.50 ; S, 2.64.  $^1\text{H NMR}$  (500 MHz,  $\text{C}_2\text{D}_2\text{Cl}_4$ , 80 °C)  $\delta_{\text{H}}/\text{ppm}$ : 8.00 (d,  $J = 7.98$  Hz, H), 7.74-7.54 (m, 4H), 7.42 (d,  $J = 7.91$  Hz, 2H), 7.24 (d, 2H), 6.94 (s, 2H), 4.64-4.55 (bs, 1H), 3.75 (s, 6H), 2.42-2.26 (m, 2H), 2.07-1.91 (m, 2H), 1.67-1.50 (m, 2H), 1.37-0.99 (m, 20H), 0.77 (t,  $J = 6.68$  Hz, 6H)

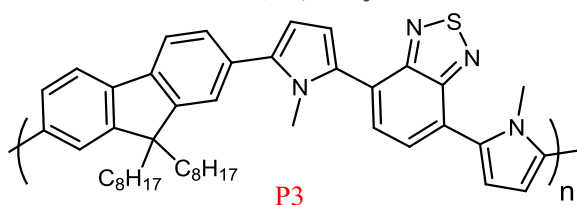
### 3.4.2. Poly[3,6-difluoro-9-(heptadecan-9-yl)-9H-carbazole-2,7-diyl-alt-(4',7'-bis(1-methyl-1H-pyrrol-2'-yl)-2',1',3'-benzothiadiazole)-5,5-diyl]



A solution of 3,6-difluoro-9-(heptadecan-9-yl)-2,7-bis(4,4,5,5-tetramethyl-1,3,2-dioxaborolan-2-yl)-9H-carbazole (**35**) (0.3 g, 0.432 mmol) and 4,7-bis(5-bromo-1-methyl-1H-pyrrol-2-yl)benzo[*c*][1,2,5]thiadiazole (**11**) (0.1956 g, 0.432 mmol) in dry THF (9 ml) in a 100 ml one-necked round bottom flask and under argon was degassed. To the reaction mixture was added a saturated solution of  $\text{NaHCO}_3$  (2 ml) and the reaction mixture was degassed. To the reaction mixture,  $\text{Pd}(\text{OAc})_2$  (6.86 mg, 0.03 mmol) and tri-*o*-tolylphosphine (22.5 mg, 0.066 mmol) were added and degassed then heated to 90 °C for 24 hours. After cooling the reaction mixture to room temperature, the polymer was end-capped with the addition of 1-bromobenzene (0.1 ml, 0.74 mmol) and degassed then heated to 90 °C for 1 hour. Again, the reaction mixture was cooled to room temperature and the polymer was end-capped with phenyl boronic acid (0.15 g, 0.1 mmol) and degassed, then the mixture was heated to 90 °C for 3 hours. The reaction mixture was cooled to room temperature, then dissolved in  $\text{CHCl}_3$  (300 ml) and to this solution was added an ammonium hydroxide solution (28 % in  $\text{H}_2\text{O}$ , 50 ml), followed by stirring overnight. Then, the organic layer was separated and washed with distilled water. The organic layer was concentrated to about 50 ml and poured into methanol:water (10:1, 300 ml). The resulting mixture was stirred overnight and filtered through a membrane filter. The collected solid was cleaned using soxhlet extraction with

solvents in order methanol (250 ml), acetone (250 ml), hexane (250 ml) and toluene (250 ml). The toluene fraction was concentrated to about 50 ml and then poured into degassed methanol (300 ml). The result mixture was stirred overnight and the solid collected by filtration through a membrane filter. Polymer **P2** was obtained as a red powder (163 mg, 43.6 % yield). GPC (1,2,4-trichlorobenzene at 140 °C):  $M_w = 8400$ ,  $M_n = 3500$ , PD = 2.4. Elemental Analysis (%) calculated for  $C_{45}H_{51}N_5SF_2$ : C, 73.84; H, 7.02; N, 9.57; S, 4.38. Found: C, 72.66; H, 6.53; N, 9.23; S, 4.07.  $^1\text{H NMR}$  (500 MHz,  $C_2D_2Cl_4$ , 80 °C)  $\delta_H$ /ppm: 7.78-7.49 (m, 4H), 7.40 (d,  $J = 16.30$  Hz, 2H), 7.23 (s, 2H), 6.98 (d,  $J = 10.78$  Hz, 2H), 4.55-4.45 (bs, 1H), 3.75 (s, 6H), 2.33-2.17 (m, 2H), 2.00-1.85 (m, 2H), 1.31-0.96 (m, 22H), 0.76 (t, 6H).

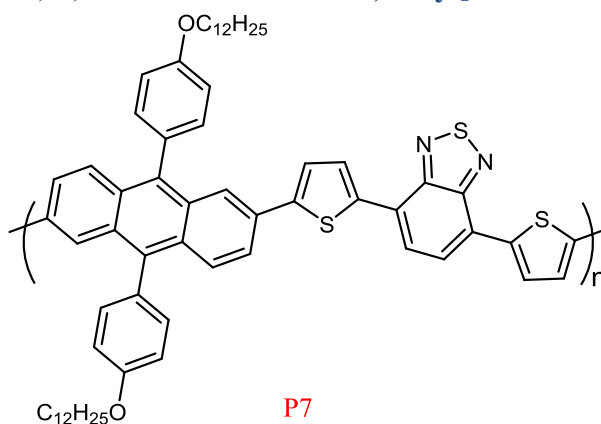
### 3.4.3. Poly [9,6-dioctyl-9H-fluorene-2,7-diyl-alt-(2',7'-bis(1-methyl-1H-pyrrol-2-yl)-2',1',3'-benzothiadiazole)-5,5-diyl]



A solution of 9,9-dioctylfluorene-2,7-diboronic acid bis(1,3-propanediol) ester (**36**) (0.247 g, 0.4423 mmol) and 4,7-bis(5-bromo-1-methyl-1H-pyrrol-2-yl)benzo[*c*][1,2,5]thiadiazole (**11**) (0.2 g, 0.4424 mmol) in dry THF (9 ml) in a 100 ml one-necked round bottom flask and under argon was degassed. To the reaction mixture was added a saturated solution of  $\text{NaHCO}_3$  (2 ml) and the reaction mixture was degassed. To the reaction mixture,  $\text{Pd}(\text{OAc})_2$  (7 mg, 0.031 mmol) and tri-*o*-tolylphosphine (19 mg, 0.062 mmol) were added and degassed then heated to 90 °C for 24 hours. After cooling the reaction mixture to room temperature, the polymer was end-capped with the addition of 1-bromobenzene (0.1 ml, 0.74 mmol) and degassed then heated to 90 °C for 1 hour. Again, the reaction mixture was cooled to room temperature and the polymer was end-capped with phenyl boronic acid (0.15 g, 0.1 mmol) and degassed, then the mixture was heated to 90 °C for 3 hours. The reaction mixture was cooled to room temperature, then dissolved in  $\text{CHCl}_3$  (300ml) and to this solution was added an ammonium hydroxide solution (28 % in  $\text{H}_2\text{O}$ , 50 ml), followed by stirring overnight. Then, the organic layer was separated and

washed with distilled water. The organic layer was concentrated to about 50 ml and poured into methanol:water (10:1, 300 ml). The resulting mixture was stirred overnight and filtered through a membrane filter. The collected solid was cleaned using soxhlet extraction with solvents in order methanol (250 ml), acetone (250 ml), hexane (250 ml) and toluene (250 ml). The toluene fraction was concentrated to about 50 ml and then poured into degassed methanol (300 ml). The resulting mixture was stirred overnight and the solid collected by filtration through a membrane filter. Polymer **P3** was obtained as a red powder (196 mg, 61.8 % yield). GPC (1,2,4-trichlorobenzene at 140 °C):  $M_w = 6300$ ,  $M_n = 3300$ , PD = 1.9 Elemental Analysis (%) calculated for  $C_{45}H_{52}N_4S$ : C, 79.37; H, 7.70; N, 8.23; S, 4.71. Found: C, 74.90; H, 7.38 ; N, 6.63 ; S, 3.86.  $^1\text{H NMR}$  (500 MHz,  $C_2D_2Cl_4$ , 80 °C)  $\delta_H$ /ppm: 7.79-7.41 (m, 6H), 7.27-7.16 (m, 4H), 6.91 (bs, 2H), 3.72 (s, 6H), 2.14-1.85 (m, 2H), 1.74-1.49 (m, 2H), 1.32-0.90 (m, 24H), 0.77 (t, 6H).

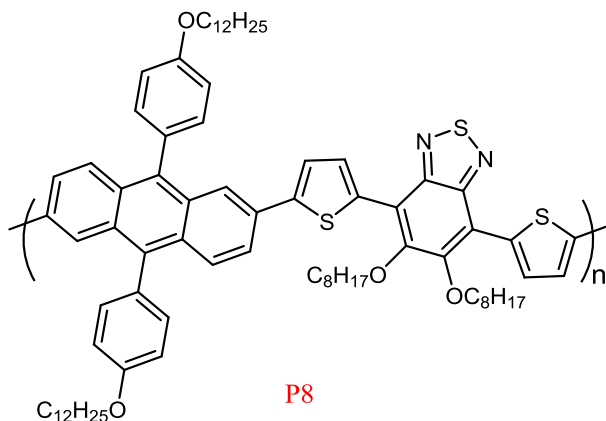
#### 3.4.4. Poly(9,10-bis(4-(dodecyloxy)phenyl)-anthracene-2,6-diyl-alt-(4,7-dithiophen-2-yl)- 2',1',3'-benzothiadiazole-5,5-diyl]



A solution of 2,6-bis-(4,4,5,5-tetramethyl-[1,3,2]dioxaborolan-2-yl)-9,10-bis(4-(dodecyloxy)phenyl)anthracene (**23**) (0.35 g, 0.367 mmol) and 4,7-bis(5-bromothiophen-2-yl)benzo[c][1,2,5]thiadiazole (**25**) (0.1683 g, 0.367 mmol) in dry toluene (9 ml) in a 100 ml one-necked round bottom flask and under argon was degassed. To the reaction mixture was added a 20 % w/w aqueous solution of tetraethylammonium hydroxide (2.1 ml, 2.85 mmol) and the reaction mixture was degassed. To the reaction mixture,  $\text{Pd}(\text{OAc})_2$  (6.3 mg, 0.028 mmol) and tri-*o*-

tolyphosphine (17.2 mg, 0.0565 mmol) were added and degassed then heated to 90 °C for 24 hours. After cooling the reaction mixture to room temperature, the polymer was end-capped with the addition of 1-bromobenzene (0.1 ml, 0.94 mmol) and degassed then heated to 90 °C for 1 hour. Again, the reaction mixture was cooled to room temperature was end-capped with phenyl boronic acid (0.15 g, 1.23 mmol) and degassed, then the mixture was heated to 90 °C for 3 hours. The reaction mixture was cooled to room temperature, then dissolved in CHCl<sub>3</sub> (300 ml) and to this solution was added an ammonium hydroxide solution (28 % in H<sub>2</sub>O, 50 ml), followed by stirring overnight. Then, the organic layer was separated and washed with distilled water. The organic layer was concentrated to about 50 ml and poured into methanol:water (10:1, 300 ml). The resulting mixture was stirred overnight and filtered through a membrane filter. The collected solid was cleaned using soxhlet extraction with solvents in order methanol (250 ml), acetone (250 ml), hexane (250 ml), toluene (250 ml), chloroform (250 ml) and chlorobenzene (250 ml). The toluene, chloroform and chlorobenzene fractions were concentrated to about 50 ml and then poured into degassed methanol (300 ml). The resulting mixtures were stirred overnight and the solids collected by filtration through a membrane filter. The different fractions of polymer **P7** were obtained as purple powder. Toluene fraction (128 mg, 35%), GPC (1,2,4-trichlorobenzene at 140 °C):  $M_w = 3800$ ,  $M_n = 3000$ , PD = 1.2. Chloroform fraction (162 mg, 44.2%), GPC (1,2,4-trichlorobenzene at 140 °C):  $M_w = 4900$ ,  $M_n = 3500$ , PD = 1.4. Chlorobenzene fraction (45 mg, 12%). GPC (1,2,4-trichlorobenzene at 140 °C):  $M_w = 9100$ ,  $M_n = 7800$ , PD = 1.1. Elemental Analysis (%) calculated for C<sub>64</sub>H<sub>70</sub>N<sub>2</sub>S<sub>3</sub>O<sub>2</sub>: C, 77.22; H, 7.09; N, 2.81; S, 9.66. Found: C, 60.33; H, 6.02 ; N, 2.75 ; S, 10.27. <sup>1</sup>HNMR (500 MHz, C<sub>2</sub>D<sub>2</sub>Cl<sub>4</sub>, 100 °C) δ<sub>H</sub>/ppm: 8.07 (d,  $J = 3.86$  Hz, 2H), 7.84 (s, 2H), 7.66 (d,  $J = 7.29$  Hz, 4H), 7.44 (d,  $J = 6.37$  Hz, 2H), 7.37 (d,  $J = 5.87$ , 1.62 Hz, 2H), 7.29 (d,  $J = 7.34$  Hz, 4H), 7.19 (d,  $J = 7.81$  Hz, 4H), 4.15 (t,  $J = 5.92$  Hz, 4H), 1.94-1.84 (m, 4H), 1.60-1.18 (m, 36H), 0.85 (t,  $J = 6.51$  Hz, 6H).

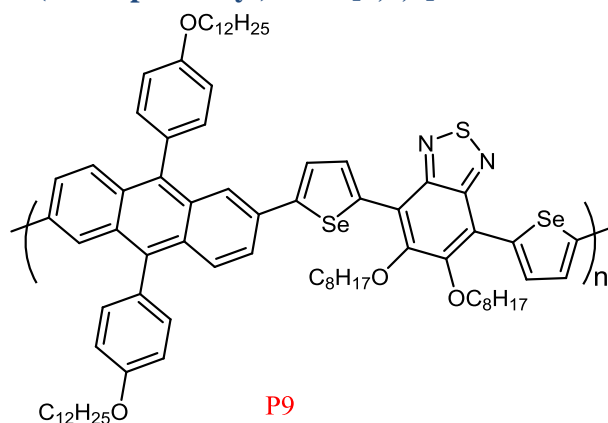
### 3.4.5. Poly(9,10-bis(4-(dodecyloxy)phenyl)anthracene-2,6-diyl-alt-(5,6-bis(octyloxy)-4,7-di(thiophen-2-yl)benzo[1,2,5]thiadiazole-5,5-diyl))



A solution of 2,6-bis-(4,4,5,5-tetramethyl-[1,3,2]dioxaborolan-2-yl)-9,10-bis(4-(dodecyloxy)phenyl)anthracene (**23**) (0.35 g, 0.367 mmol) and 4,7-bis(5-bromothiophen-2-yl)-5,6-bis(octyloxy)benzo[*c*][1,2,5]thiadiazole (**37**) (0.2625 g, 0.367 mmol) in dry toluene (9 ml) in a 100 ml one-necked round bottom flask and under argon was degassed. To the reaction mixture was added a 20 % w/w aqueous solution of tetraethylammonium hydroxide (2.1 ml, 2.85 mmol) and the reaction mixture was degassed. To the reaction mixture, Pd(OAc)<sub>2</sub> (6.3 mg, 0.028 mmol) and tri-*o*-tolylphosphine (17.2 mg, 0.0565 mmol) were added and degassed then heated to 90 °C for 24 hours. After cooling the reaction mixture to room temperature, the polymer was end-capped with the addition of 1-bromobenzene (0.1 ml, 0.94 mmol) and degassed then heated to 90 °C for 1 hour. Again, the reaction mixture was cooled to room temperature and the polymer was end-capped with phenyl boronic acid (0.15 g, 1.23 mmol) and degassed, then the mixture was heated to 90 °C for 3 hours. The reaction mixture was cooled to room temperature, then dissolved in CHCl<sub>3</sub> (300 ml) and to this solution was added an ammonium hydroxide solution (28 % in H<sub>2</sub>O, 50 ml), followed by stirring overnight. Then, the organic layer was separated and washed with distilled water. The organic layer was concentrated to about 50 ml and poured into methanol:water (10:1, 300 ml). The resulting mixture was stirred overnight and filtered through a membrane filter. The collected solid was cleaned using soxhlet extraction with solvents in order methanol (250 ml), acetone (250 ml), hexane (250 ml), toluene (250 ml), chloroform (250 ml). The toluene and chloroform fractions were concentrated to about 50 ml and

then poured into degassed methanol (300 ml). The resulting mixtures were stirred overnight and the solids collected by filtration through a membrane filter. The different fractions of P8 were obtained as purple powder. Toluene fraction (136 mg, 29.5%), GPC (1,2,4-trichlorobenzene at 140 °C):  $M_w = 12600$ ,  $M_n = 9100$ , PD = 1.38. Chloroform fraction (250 mg, 54 %), GPC (1,2,4-trichlorobenzene at 140 °C):  $M_w = 33900$ ,  $M_n = 25000$ , PD = 1.35. Elemental Analysis (%) calculated for  $C_{80}H_{102}N_2S_3O_4$ : C, 76.75; H, 8.21; N, 2.24; S, 7.68. Found: C, 73.35; H, 8.28 ; N, 1.28 ; S, 5.60.  $^1\text{H NMR}$  (500 MHz,  $C_2D_2Cl_4$ , 100 °C)  $\delta_H$ /ppm: 8.38 (d,  $J = 21.74$  Hz, 4H), 8.09 (s, 2H), 7.80 (d,  $J = 7.50$  Hz, 2H), 7.67 (d,  $J = 5.82$  Hz, 2H), 7.56-7.33 (m, 4H), 7.25-7.10 (m, 4H), 4.19-4.06 (bs, 8H), 1.96-1.80 (bs, 8H), 1.61-1.17 (m, 56H), 0.91-0.78 (m, 12H).

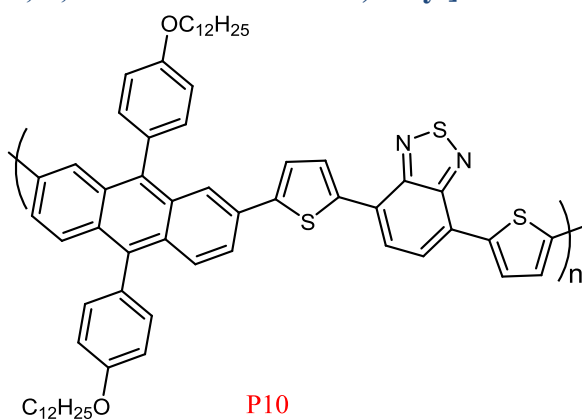
### 3.4.6. Poly(9,10-bis(4-(dodecyloxy)phenyl)-anthracene-2,6-diyl-alt-(5,6-bis(octyloxy)-4,7-di(selenophen-2-yl)benzo[1,2,5]thiadiazole-5,5-diyl)



A solution of 2,6-bis-(4,4,5,5-tetramethyl-[1,3,2]dioxaborolan-2-yl)-9,10-bis(4-(dodecyloxy)phenyl)anthracene (**23**) (0.177 g, 0.1855 mmol) and 4,7-bis(5-bromoselenophen-2-yl)-5,6-bis(octyloxy)benzo[*c*][1,2,5]thiadiazole (**38**) (0.15 g, 0.1855 mmol) in dry toluene (5 ml) in a 100 ml one-necked round bottom flask and under argon was degassed. To the reaction mixture was added a 20 % w/w aqueous solution of tetraethylammonium hydroxide (1 ml, 1.35 mmol) and the reaction mixture was degassed. To the reaction mixture,  $\text{Pd}(\text{OAc})_2$  (3.2 mg, 0.015 mmol) and tri-*o*-tolylphosphine (8.6 mg, 0.028 mmol) were added and degassed then heated to 90 °C for 24 hours. After cooling the reaction mixture to room temperature, the

polymer was end-capped with the addition of 1-bromobenzene (0.1 ml, 0.94 mmol) and degassed then heated to 90 °C for 1 hour. Again, the reaction mixture was cooled to room temperature and the polymer was end-capped with phenyl boronic acid (0.15 g, 1.23 mmol) and degassed, then the mixture was heated to 90 °C for 3 hours. The reaction mixture was cooled to room temperature, then dissolved in  $\text{CHCl}_3$  (300 ml) and to this solution was added an ammonium hydroxide solution (28 % in  $\text{H}_2\text{O}$ , 50 ml), followed by stirring overnight. Then, the organic layer was separated and washed with distilled water. The organic layer was concentrated to about 50 ml and poured into methanol:water (10:1, 300 ml). The resulting mixture was stirred overnight and filtered through a membrane filter. The collected solid was cleaned using soxhlet extraction with solvents in order methanol (250 ml), acetone (250 ml), hexane (250 ml), toluene (250 ml), chloroform (250 ml). The chloroform fraction was concentrated to about 50 ml and then poured into degassed methanol (300 ml). The resulting mixture was stirred overnight and the solid collected by filtration through a membrane filter to afford polymer **P9** as a purple powder. Chloroform fraction (231 mg, 92 %), GPC (1,2,4-trichlorobenzene at 140 °C):  $M_w = 101400$ ,  $M_n = 48700$ ,  $PD = 2.08$ . Elemental Analysis (%) calculated for  $\text{C}_{80}\text{H}_{102}\text{N}_2\text{O}_4\text{SSe}_2$ : C, 71.40; H, 7.64; N, 2.08; S, 2.38. Found: C, 70.35; H, 7.53; N, 1.92; S, 3.24.  $^1\text{HNMR}$  (500 MHz,  $\text{C}_2\text{D}_2\text{Cl}_4$ , 100 °C)  $\delta_{\text{H}}$ /ppm: ) 8.77 (s, 2H), 8.03 (bs, 2H), 7.76 (bs, 2H), 7.58 (dd,  $J = 36.16, 4.31$  Hz, 4H), 7.45 (d,  $J = 7.95$  Hz, 4H), 7.18 (d,  $J = 7.95$  Hz, 4H), 4.14 (bs, 8H), 2.05-1.82 (m, 8H), 1.61-1.13 (m, 56H), 0.94-0.76 (m, 12H).

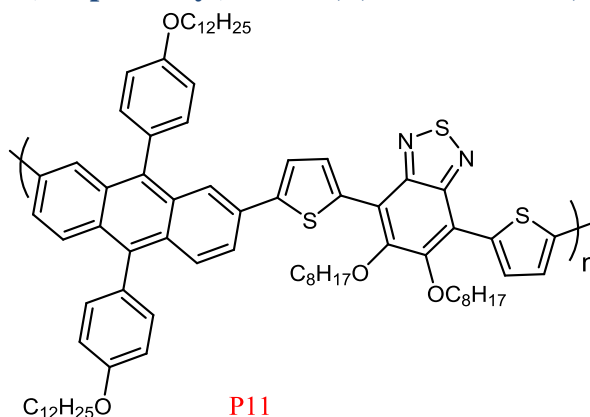
### 3.4.7. Poly(9,10-bis(4-(dodecyloxy)phenyl)-anthracene-2,7-diyl-alt-(4,7-dithiophen-2-yl)- 2',1',3'-benzothiadiazole-5,5-diyl]



A solution of 2,6-bis-(4,4,5,5-tetramethyl-[1,3,2]dioxaborolan-2-yl)-9,10-bis(4-(dodecyloxy)phenyl)anthracene (**31**) (0.3 g, 0.315 mmol) and 4,7-bis(5-bromothiophen-2-yl)benzo[c][1,2,5]thiadiazole (**25**) (0.144 g, 0.315 mmol) in dry toluene (8 ml) in a 100 ml one-necked round bottom flask and under argon was degassed. To the reaction mixture was added a 20 % w/w aqueous solution of tetraethylammonium hydroxide (1.7 ml, 2.3 mmol) and the reaction mixture was degassed. To the reaction mixture, Pd(OAc)<sub>2</sub> (5.4 mg, 0.024 mmol) and tri-*o*-tolylphosphine (15 mg, 0.044 mmol) were added and degassed then heated to 90 °C for 24 hours. After cooling the reaction mixture to room temperature, the polymer was end-capped with the addition of 1-bromobenzene (0.1 ml, 0.94 mmol) and degassed then heated to 90 °C for 1 hour. Again, the reaction mixture was cooled to room temperature and the polymer was end-capped with phenyl boronic acid (0.15 g, 1.23 mmol) and degassed, then the mixture was heated to 90 °C for 3 hours. The reaction mixture was cooled to room temperature, then dissolved in CHCl<sub>3</sub> (300 ml) and to this solution was added an ammonium hydroxide solution (28 % in H<sub>2</sub>O, 50 ml), followed by refluxing for three hours. The mixture was cooled to room temperature and the organic layer was separated, 400 mg of disodium ethylenediaminetetraacetate were added and the mixture was stirred overnight. Then the suspension was extracted three times with 500 ml of distilled water. The organic layer was concentrated to about 50 ml and poured into methanol:water (10:1, 300 ml). The resulting mixture was stirred overnight and filtered through a membrane filter. The collected solid was cleaned using soxhlet extraction with solvents in order methanol (250 ml), acetone (250 ml), hexane (250 ml), toluene (250 ml) and chloroform (250 ml). The toluene and chloroform fractions were concentrated to about 50 ml and then poured into degassed methanol (300 ml). The resulting mixtures were stirred overnight and the solids collected by filtration through membrane filters. The different fractions of polymer **P10** were collected as a purple powder. Toluene fraction (152 mg, 48.5%), GPC (1,2,4-trichlorobenzene at 140 °C): M<sub>w</sub> = 6400, M<sub>n</sub> = 4700, PD = 1.36. Chloroform fraction (55 mg, 17.5%), GPC (1,2,4-trichlorobenzene at 140 °C): M<sub>w</sub> = 20100, M<sub>n</sub> = 13700, PD = 1.46. Elemental Analysis (%) calculated for C<sub>64</sub>H<sub>70</sub>N<sub>2</sub>S<sub>3</sub>O<sub>2</sub>: C, 77.22; H, 7.09; N, 2.81; S, 9.66. Found: C, 61.12; H, 7.12 ; N, 2.64 ; S, 7.83. <sup>1</sup>HNMR (500 MHz, C<sub>2</sub>D<sub>2</sub>Cl<sub>4</sub>, 100

$^{\circ}\text{C}$ )  $\delta_{\text{H}}$ /ppm: ppm 8.08 (bs, 4H), 7.85-7.75 (m, 4H), 7.63 (d,  $J = 7.87$  Hz, 2H), 7.50 (d,  $J = 7.29$  Hz, 2H), 7.41 (d,  $J = 7.27$  Hz, 2H), 7.34 (d,  $J = 7.29$  Hz, 2H), 7.23 (d,  $J = 6.96$  Hz, 2H), 7.15 (d,  $J = 6.99$  Hz, 2H), 4.17 (m, 4H), 1.97-1.83 (m, 4H), 1.63-1.49 (m, 4H), 1.49-1.18 (m, 32H), 0.93-0.77 (m, 6H).

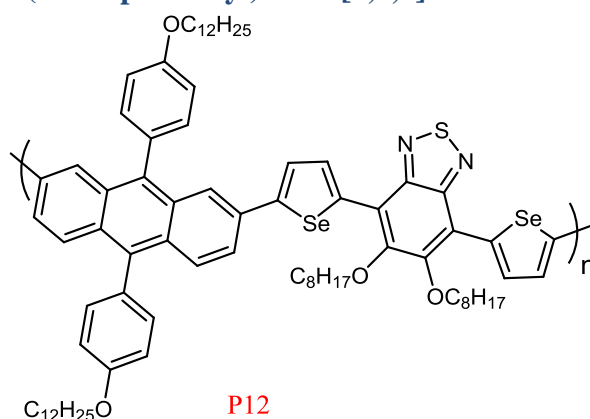
### 3.4.8. Poly(9,10-bis(4-(dodecyloxy)phenyl)anthracene-2,7-diyl-alt-(5,6-bis(octyloxy)-4,7-di(thiophen-2-yl)benzo[1,2,5]thiadiazole-5,5-diyl)



A solution of 2,7-bis-(4,4,5,5-tetramethyl-[1,3,2]dioxaborolan-2-yl)-9,10-bis(4-(dodecyloxy)phenyl)anthracene (**31**) (0.3 g, 0.314 mmol) and 4,7-bis(5-bromothiophen-2-yl)-5,6-bis(octyloxy)benzo[*c*][1,2,5]thiadiazole (**37**) (0.225 g, 0.314 mmol) in dry toluene (8 ml) in a 100 ml one-necked round bottom flask and under argon was degassed. To the reaction mixture was added a 20 % w/w aqueous solution of tetraethylammonium hydroxide (1.7 ml, 2.3 mmol) and the reaction mixture was degassed. To the reaction mixture, Pd(OAc)<sub>2</sub> (5.4 mg, 0.024 mmol) and tri-*o*-tolylphosphine (17.2 mg, 0.043 mmol) were added and degassed then heated to 90  $^{\circ}\text{C}$  for 24 hours. After cooling the reaction mixture to room temperature, the polymer was end-capped with the addition of 1-bromobenzene (0.1 ml, 0.94 mmol) and degassed then heated to 90  $^{\circ}\text{C}$  for 1 hour. Again, the reaction mixture was cooling to room temperature and the polymer was end-capped with phenyl boronic acid (0.15 g, 1.23 mmol) and degassed, then the mixture was heated to 90  $^{\circ}\text{C}$  for 3 hours. The reaction mixture was cooled to room temperature, then dissolved in CHCl<sub>3</sub> (300 ml) and to this solution was added an ammonium hydroxide solution (28 % in H<sub>2</sub>O, 50 ml), followed by refluxing for three hours. The mixture was cooled to room temperature and the organic layer was separated,

400 mg of disodium ethylenediaminetetraacetate were added and the mixture was stirred overnight. Then the suspension was extracted three times with 500 mL of distilled water. The organic layer was concentrated to about 50 ml and poured into methanol:water (10:1, 300 ml). The resulting mixture was stirred overnight and filtered through a membrane filter. The collected solid was cleaned using soxhlet extraction with solvents in order methanol (250 ml), acetone (250 ml), hexane (250 ml), toluene (250 ml) and chloroform (250 ml). The chloroform fraction was concentrated to about 50 ml and then poured in to degassed methanol (300 ml). The resulting mixture stirred overnight and the solid collected by filtration through a membrane filter. Polymer **P11** was obtained as a purple powder. Chloroform fraction (311 mg, 78.9 %), GPC (1,2,4-trichlorobenzene at 140 °C):  $M_w = 35400$ ,  $M_n = 21700$ , PD = 1.63. Elemental Analysis (%) calculated for  $C_{80}H_{102}N_2S_3O_4$ : C, 76.75; H, 8.21; N, 2.24; S, 7.68. Found: C, 74.19; H, 8.35 ; N, 2.06 ; S, 6.81.  $^1\text{H NMR}$  (500 MHz,  $C_2D_2Cl_4$ , 100 °C)  $\delta_H$ /ppm: 8.40 (s, 2H), 8.11 (s, 2H), 7.79 (d,  $J = 8.59$  Hz, 2H), 7.67 (d,  $J = 8.49$  Hz, 2H), 7.51 (d,  $J = 7.58$  Hz, 2H), 7.42 (d,  $J = 7.09$  Hz, 2H), 7.37 (d,  $J = 7.08$  Hz, 2H), 7.21 (d,  $J = 6.62$  Hz, 2H), 7.16 (d,  $J = 6.64$  Hz, 2H), 4.15 (m, 8H), 1.97-1.82 (m, 8H), 1.61-1.17 (m, 56H), 0.91-0.77 (m, 12H).

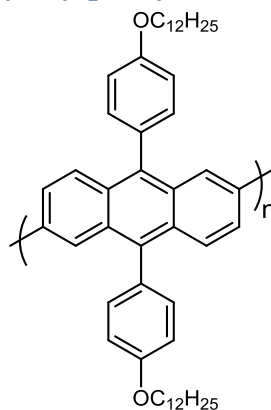
### 3.4.9. Poly(9,10-bis(4-(dodecyloxy)phenyl)-anthracene-2,7-diyl-alt-(5,6-bis(octyloxy)-4,7-di(selenophen-2-yl)benzo[1,2,5]thiadiazole-5,5-diyl))



A solution of 2,7-bis-(4,4,5,5-tetramethyl-[1,3,2]dioxaborolan-2-yl)-9,10-bis(4-(dodecyloxy)phenyl)anthracene (**31**) (0.235 g, 0.247 mmol) and 4,7-bis(5-

bromoselenophen-2-yl)-5,6-bis(octyloxy)benzo[c][1,2,5]thiadiazole (**38**) (0.20 g, 0.247 mmol) in dry toluene (6 ml) in a 100 ml one-necked round bottom flask and under argon was degassed. To the reaction mixture was added a 20 % w/w aqueous solution of tetraethylammonium hydroxide (1.3 ml, 1.76 mmol) and the reaction mixture was degassed. To the reaction mixture, Pd(OAc)<sub>2</sub> (4.2 mg, 0.018 mmol) and tri-*o*-tolylphosphine (11.56 mg, 0.033 mmol) were added and degassed then heated to 90 °C for 24 hours. After cooling the reaction mixture to room temperature, the polymer was end-capped with the addition of 1-bromobenzene (0.1 ml, 0.94 mmol) and degassed then heated to 90 °C for 1 hour. Again, the reaction mixture was cooled to room temperature and the polymer was end-capped with phenyl boronic acid (0.15 g, 1.23 mmol) and degassed, then the mixture was heated to 90 °C for 3 hours. The reaction mixture was cooled to room temperature, then dissolved in CHCl<sub>3</sub> (300 ml) and to this solution was added an ammonium hydroxide solution (28 % in H<sub>2</sub>O, 50 ml), followed by refluxing for three hours. The mixture was cooled to room temperature and the organic layer was separated, 400 mg of disodium ethylenediaminetetraacetate were added and the mixture was stirred overnight. Then the suspension was extracted three times with 500 mL of distilled water. The organic layer was concentrated to about 50 ml and poured into methanol:water (10:1, 300 ml). The resulting mixture was stirred overnight and filtered through a membrane filter. The collected solid was cleaned using soxhlet extraction with solvents in order methanol (250 ml), acetone (250 ml), hexane (250 ml), toluene (250 ml) and chloroform (250 ml). The chloroform fraction was concentrated to about 50 ml and then poured into degassed methanol (300 ml). The resulting mixture was stirred overnight and the solid collected by filtration through a membrane filter. Polymer **P12** was obtained as a purple powder. Chloroform fraction (285 mg, 85.6 %), GPC (1,2,4-trichlorobenzene at 140 °C): M<sub>w</sub> = 52200, M<sub>n</sub> = 33300, PD = 1.56. Elemental Analysis (%) calculated for C<sub>80</sub>H<sub>102</sub>N<sub>2</sub>O<sub>4</sub>SSe<sub>2</sub>: C, 71.40; H, 7.64; N, 2.08; S, 2.38. Found: C, 56.50; H, 7.94 ; N, 1.21 ; S, 1.78. <sup>1</sup>HNMR (500 MHz, C<sub>2</sub>D<sub>2</sub>Cl<sub>4</sub>, 100 °C) δ<sub>H</sub>/ppm: ) 8.73 (d, *J* = 20.28 Hz, 4H), 8.06 (bs, 2H), 7.76 (d, *J* = 8.19 Hz, 2H), 7.62 (s, 2H), 7.48 (d, *J* = 7.93 Hz, 2H), 7.41 (d, *J* = 7.89 Hz, 2H), 7.21 (d, *J* = 7.30 Hz, 2H), 7.15 (d, *J* = 7.32 Hz, 2H), 4.16 (m, 8H), 2.04-1.80 (m, 8H), 1.61-1.17 (m, 56H), 0.91-0.78 (m, 12H).

### 3.4.10. Poly[9,10-bis(4-(dodecyloxy)phenyl)-anthracene-2,6-diyl]

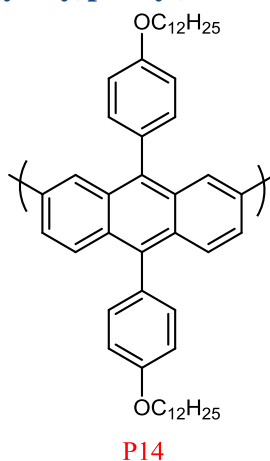


P13

A solution of 2,6-bis-(4,4,5,5-tetramethyl-[1,3,2]dioxaborolan-2-yl)-9,10-bis(4-(dodecyloxy)phenyl)anthracene (**23**) (0.20 g, 0.210 mmol) and 2,6-dibromo-9,10-bis(4-(dodecyloxy)phenyl)anthracene (**22**) (0.18 g, 0.210 mmol) in dry toluene (5.2 ml) in a 100 ml one-necked round bottom flask and under argon was degassed. To the reaction mixture was added a 20 % w/w aqueous solution of tetraethylammonium hydroxide (1.1 ml, 1.49 mmol) and the reaction mixture was degassed. To the reaction mixture, Pd(OAc)<sub>2</sub> (3.6 mg, 0.016 mmol) and tri-*o*-tolylphosphine (12.6 mg, 0.029 mmol) were added and degassed then heated to 90 °C for 24 hours. After cooling the reaction mixture to room temperature, the polymer was end-capped with the addition of 1-bromobenzene (0.1 ml, 0.94 mmol) and degassed then heated to 90 °C for 1 hour. Again, the reaction mixture was cooled to room temperature and the polymer was end-capped with phenyl boronic acid (0.15 g, 1.23 mmol) and degassed, then the mixture was heated to 90 °C for 3 hours. The reaction mixture was cooled to room temperature, then dissolved in CHCl<sub>3</sub> (300 ml) and to this solution was added an ammonium hydroxide solution (28 % in H<sub>2</sub>O, 50 ml), followed by refluxing for three hours. The mixture was cooled to room temperature and the organic layer was separated, 400 mg of disodium ethylenediaminetetraacetate were added and the mixture was stirred overnight. Then the suspension was extracted three times with 500 mL of distilled water. The organic layer was concentrated to about 50 ml and poured into methanol:water (10:1, 300 ml). The resulting mixture was stirred overnight and filtered through a membrane filter. The collected solid was cleaned using soxhlet extraction with solvents in order methanol (250 ml), acetone (250 ml), hexane (250

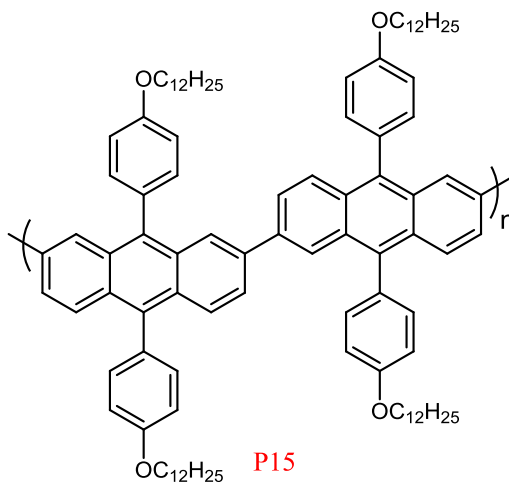
ml), toluene (250 ml) and chloroform (250 ml). The toluene and chloroform fractions were concentrated to about 50 ml and then poured into degassed methanol (300 ml). The resulting mixtures were stirred overnight and the solids collected by filtration through a membrane filter. The different fractions of **P13** were obtained yellow powders. Toluene fraction (136 mg, 46.5 %), GPC (1,2,4-trichlorobenzene at 140 °C):  $M_w = 35300$ ,  $M_n = 21600$ , PD = 1.6. Chloroform fraction (145 mg, 49.6 %), GPC (1,2,4-trichlorobenzene at 140 °C):  $M_w = 74900$ ,  $M_n = 50800$ , PD = 1.47. Elemental Analysis (%) calculated for  $C_{50}H_{64}O_2$ : C, 86.15; H, 9.25. Found: C, 80.53; H, 9.15.  $^1\text{H}$ NMR (500 MHz,  $C_2D_2CL_4$ , 100 °C)  $\delta_H$ /ppm: 7.96 (s, 2H), 7.76 (d,  $J = 7.21$  Hz, 2H), 7.55 (d,  $J = 7.97$  Hz, 2H), 7.35 (d,  $J = 7.85$  Hz, 4H), 7.11 (d,  $J = 7.41$  Hz, 4H), 4.14 (t, 4H), 1.94-1.83 (m, 4H), 1.61-1.50 (m, 4H), 1.48-1.20 (m, 32H), 0.86 (t,  $J = 5.95$  Hz, 6H).

### 3.4.11. Poly[9,10-bis(4-(dodecyloxy)phenyl)-anthracene-2,7-diyl]



A solution of 2,7-bis-(4,4,5,5-tetramethyl-[1,3,2]dioxaborolan-2-yl)-9,10-bis(4-(dodecyloxy)phenyl)anthracene (**31**) (0.30 g, 0.314 mmol) and 2,7-dibromo-9,10-bis(4-(dodecyloxy)phenyl)anthracene (**30**) (0.269 g, 0.314 mmol) in dry toluene (7.7 ml) in a 100 ml one-necked round bottom flask and under argon was degassed. To the reaction mixture was added a 20 % w/w aqueous solution of tetraethylammonium hydroxide (1.1 ml, 2.30 mmol) and the reaction mixture was degassed. To the reaction mixture,  $Pd(OAc)_2$  (5.4 mg, 0.024 mmol) and tri-*o*-tolylphosphine (14.7 mg, 0.043 mmol) were added and degassed then heated to 90 °C for 24 hours. After cooling the reaction mixture to room temperature, the

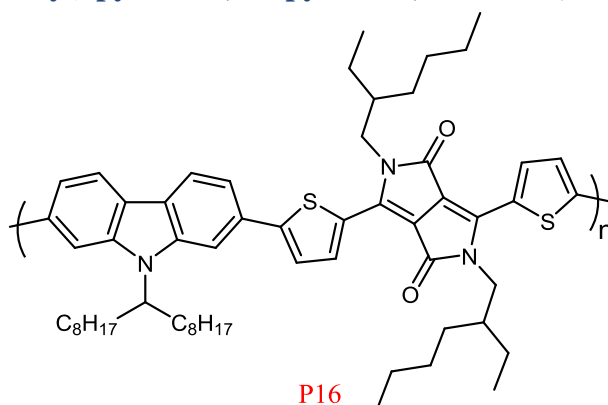
polymer was end-capped with the addition of 1-bromobenzene (0.1 ml, 0.94 mmol) and degassed then heated to 90 °C for 1 hour. Again, the reaction mixture was cooled to room temperature and the polymer was end-capped with phenyl boronic acid (0.15 g, 1.23 mmol) and degassed, then the mixture was heated to 90 °C for 3 hours. The reaction mixture was cooled to room temperature, then dissolved in CHCl<sub>3</sub> (300 ml) and to this solution was added an ammonium hydroxide solution (28 % in H<sub>2</sub>O, 50 ml), followed by refluxing for three hours. The mixture was cooled to room temperature and the organic layer was separated, 400 mg of disodium ethylenediaminetetraacetate were added and the mixture was stirred overnight. Then the suspension was extracted three times with 500 mL of distilled water. The organic layer was concentrated to about 50 ml and poured into methanol:water (10:1, 300 ml). The resulting mixture was stirred overnight and filtered through a membrane filter. The collected solid was cleaned using soxhlet extraction with solvents in order methanol (250 ml), acetone (250 ml), hexane (250 ml) and toluene (250 ml). The toluene fraction was concentrated to about 50 ml and then poured into degassed methanol (300 ml). The resulting mixture was stirred overnight and the solid collected by filtration through a membrane filter. Polymer **P14** was obtained as a yellow powder. Toluene fraction (404 mg, 92 %), GPC (1,2,4-trichlorobenzene at 140 °C):  $M_w = 40700$ ,  $M_n = 24900$ , PD = 1.63. Elemental Analysis (%) calculated for C<sub>50</sub>H<sub>64</sub>O<sub>2</sub>: C, 86.15; H, 9.25. Found: C, 82.98; H, 9.46. <sup>1</sup>HNMR (500 MHz, C<sub>2</sub>D<sub>2</sub>Cl<sub>4</sub>, 100 °C) δ<sub>H</sub>/ppm: 7.96 (s, 2H), 7.75 (d,  $J = 8.71$  Hz, 2H), 7.53 (d,  $J = 8.12$  Hz, 2H), 7.35 (m, 4H), 7.11 (m, 4H), 4.11 (t, 4H), 1.92-1.82 (m, 4H), 1.60-1.47 (m, 4H), 1.47-1.16 (m, 32H), 0.91-0.78 (m, 6H).

**3.4.12. Poly [9,10-bis(4-(dodecyloxy)phenyl)-anthracene-2,6-diyl-alt-9,10-bis(4-(dodecyloxy)phenyl)-anthracene-2,7-diyl]**

A solution of 2,7-bis-(4,4,5,5-tetramethyl-[1,3,2]dioxaborolan-2-yl)-9,10-bis(4-(dodecyloxy)phenyl)anthracene (**31**) (0.20 g, 0.210 mmol) and 2,6-dibromo-9,10-bis(4-(dodecyloxy)phenyl)anthracene (**22**) (0.180 g, 0.210 mmol) in dry toluene (5.2 ml) in a 100 ml one-necked round bottom flask and under argon was degassed. To the reaction mixture was added a 20 % w/w aqueous solution of tetraethylammonium hydroxide (1.1 ml, 2.30 mmol) and the reaction mixture was degassed. To the reaction mixture, Pd(OAc)<sub>2</sub> (3.6 mg, 0.016 mmol) and tri-*o*-tolylphosphine (14.7 mg, 0.029 mmol) were added and degassed then heated to 90 °C for 24 hours. After cooling the reaction mixture to room temperature, the polymer was end-capped with the addition of 1-bromobenzene (0.1 ml, 0.94 mmol) and degassed then heated to 90 °C for 1 hour. Again, the reaction mixture was cooled to room temperature and the polymer was end-capped with phenyl boronic acid (0.15 g, 1.23 mmol) and degassed, then the mixture was heated to 90 °C for 3 hours. The reaction mixture was cooled to room temperature, then dissolved in CHCl<sub>3</sub> (300 ml) and to this solution was added an ammonium hydroxide solution (28 % in H<sub>2</sub>O, 50 ml), followed by refluxing for three hours. The mixture was cooled to room temperature and the organic layer was separated, 400 mg of disodium ethylenediaminetetraacetate were added and the mixture was stirred overnight. Then the suspension was extracted three times with 500 mL of distilled water. The organic layer was concentrated to about 50 ml and poured into methanol:water (10:1, 300 ml). The resulting mixture was stirred overnight and

filtered through a membrane filter. The collected solid was cleaned using soxhlet extraction with solvents in order methanol (250 ml), acetone (250 ml), hexane (250 ml) and toluene (250 ml). The toluene fraction was concentrated to about 50 ml and then poured into degassed methanol (300 ml). The resulting mixture was stirred overnight and the solid collected by filtration through a membrane filter. Polymer **P15** was obtained as a yellow powder. Toluene fraction (155 mg, 39 %), GPC (1,2,4-trichlorobenzene at 140 °C):  $M_w = 46300$ ,  $M_n = 29000$ , PD = 1.63. Elemental Analysis (%) calculated for  $C_{100}H_{128}O_4$ : C, 86.15; H, 9.25. Found: C, 83.62; H, 9.57.  $^1\text{H NMR}$  (500 MHz,  $C_2D_2Cl_4$ , 100 °C)  $\delta_{\text{H}}$ /ppm: 7.94 (bs, 4H), 7.74 (d,  $J = 8.70$  Hz, 4H), 7.54 (d,  $J = 4.77$  Hz, 4H), 7.35 (d,  $J = 8.84$  Hz, 8H), 7.11 (bs, 8H), 4.12 (m, 8H), 1.95-1.82 (m, 8H), 1.61-1.48 (m, 8H), 1.47-1.14 (m, 64H), 0.91-0.78 (m, 12H).

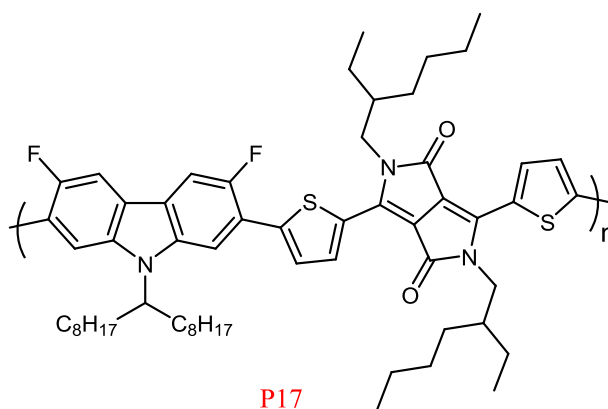
### 3.4.13. Poly [9-(heptadecan-9-yl)-9H-carbazole-2,7-diyl-alt-3,6-bis(thiophen-5-yl)-2,5-di(2-ethylhexyl)pyrrolo[3,4-c]pyrrole-1,4-dione-5',5'-diyl]



A solution of 9-(heptadecan-9-yl)-2,7-bis(4,4,5,5-tetramethyl-1,3,2-dioxaborolan-2-yl)-9H-carbazole (**7**) (0.1926 g, 0.293 mmol) and 3,6-bis(5-bromothiophen-2-yl)-2,5-bis(2-ethylhexyl)pyrrolo[3,4-c]pyrrole-1,4(2H,5H)-dione (**34**) (0.20 g, 0.293 mmol) in dry toluene (7 ml) in a 100 ml one-necked round bottom flask and under argon was degassed. To the reaction mixture was added a 20 % w/w aqueous solution of tetraethylammonium hydroxide (1.55 ml, 2.1 mmol) and the reaction mixture was degassed. To the reaction mixture,  $\text{Pd}(\text{OAc})_2$  (4.65 mg, 0.021 mmol) and tri-*o*-tolylphosphine (12.6 mg, 0.037 mmol) were added and degassed then heated to 90 °C for 24 hours. After cooling the reaction mixture to room

temperature, the polymer was end-capped with the addition of 1-bromobenzene (0.1 ml, 0.94 mmol) and degassed then heated to 90 °C for 1 hour. Again, the reaction mixture was cooled to room temperature and the polymer was end-capped with phenyl boronic acid (0.15 g, 1.23 mmol) and degassed, then the mixture was heated to 90 °C for 3 hours. The reaction mixture was cooled to room temperature, then dissolved in CHCl<sub>3</sub> (300 ml) and to this solution was added an ammonium hydroxide solution (28 % in H<sub>2</sub>O, 50 ml), followed by refluxing for three hours. The mixture was cooled to room temperature and the organic layer was separated, 400 mg of disodium ethylenediaminetetraacetate were added and the mixture was stirred overnight. Then the suspension was extracted three times with 500 mL of distilled water. The organic layer was concentrated to about 50 ml and poured into methanol:water (10:1, 300 ml). The resulting mixture was stirred overnight and filtered through a membrane filter. The collected solid was cleaned using soxhlet extraction with solvents in order methanol (250 ml), acetone (250 ml), hexane (250 ml), toluene (250 ml) and chloroform (250 ml). The chloroform fraction was concentrated to about 50 ml and then poured into degassed methanol (300 ml). The resulting mixture was stirred overnight and the solid collected by filtration through a membrane filter. Polymer **P16** was obtained as a green powder. Chloroform fraction (182 mg, 67.1 %), GPC (1,2,4-trichlorobenzene at 140 °C):  $M_w = 78800$ ,  $M_n = 39600$ , PD = 1.99. Elemental Analysis (%) calculated for C<sub>59</sub>H<sub>79</sub>N<sub>3</sub>O<sub>2</sub>S<sub>2</sub>: C, 76.40; H, 8.60; N, 4.54; S, 6.92. Found: C, 73.70; H, 8.49; N, 4.27; S, 7.07. <sup>1</sup>HNMR (500 MHz, C<sub>2</sub>D<sub>2</sub>Cl<sub>4</sub>, 100 °C) δ<sub>H</sub>/ppm: 8.91 (s, 2H), 8.09 (d,  $J = 8.09$  Hz, 2H), 7.77 (bs, 2H), 7.55 (s, 4H), 4.61 (d, 1H), 4.10 (bs, 4H), 2.32 (bs, 2H), 2.02 (s, 4H), 1.52-1.06 (m, 40H), 0.97 (t,  $J = 6.77$  Hz, 6H), 0.88 (t,  $J = 6.22$  Hz, 6H), 0.78 (t,  $J = 6.66$  Hz, 6H).

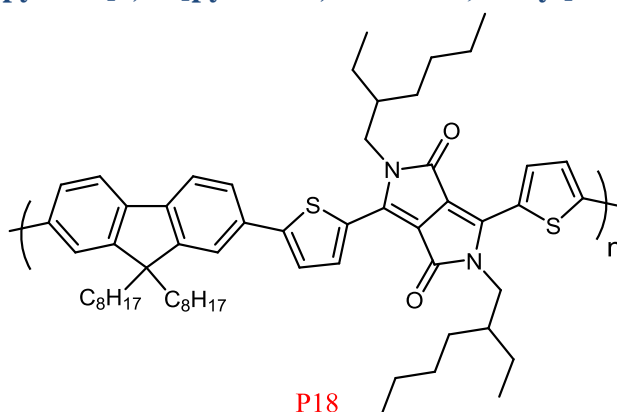
**3.4.14. Poly [3,6-difluoro-9-(heptadecan-9-yl)-9H-carbazole-2,7-diyl-alt-3,6-bis(thiophen-5-yl)-2,5-di(2-ethylhexyl)-pyrrolo[3,4-c]pyrrole-1,4-dione-5',5'-diyl]**



A solution of 3,6-difluoro-9-(heptadecan-9-yl)-2,7-bis(4,4,5,5-tetramethyl-1,3,2-dioxaborolan-2-yl)-9H-carbazole (**35**) (0.203 g, 0.293 mmol) and 3,6-bis(5-bromothiophen-2-yl)-2,5-bis(2-ethylhexyl)pyrrolo[3,4-c]pyrrole-1,4(2H,5H)-dione (**34**) (0.20 g, 0.293 mmol) in dry toluene (7 ml) in a 100 ml one-necked round bottom flask and under argon was degassed. To the reaction mixture was added a 20 % w/w aqueous solution of tetraethylammonium hydroxide (1.55 ml, 2.1 mmol) and the reaction mixture was degassed. To the reaction mixture, Pd(OAc)<sub>2</sub> (4.65 mg, 0.021 mmol) and tri-*o*-tolylphosphine (12.6 mg, 0.037 mmol) were added and degassed then heated to 90 °C for 24 hours. After cooling the reaction mixture to room temperature, the polymer was end-capped with the addition of 1-bromobenzene (0.1 ml, 0.94 mmol) and degassed then heated to 90 °C for 1 hour. Again, the reaction mixture was cooled to room temperature and the polymer was end-capped with phenyl boronic acid (0.15 g, 1.23 mmol) and degassed, then the mixture was heated to 90 °C for 3 hours. The reaction mixture was cooled to room temperature, then dissolved in CHCl<sub>3</sub> (300 ml) and to this solution was added an ammonium hydroxide solution (28 % in H<sub>2</sub>O, 50 ml), followed by refluxing for three hours. The mixture was cooled to room temperature and the organic layer was separated, 400 mg of disodium ethylenediaminetetraacetate were added and the mixture was stirred overnight. Then the suspension was extracted three times with 500 mL of distilled water. The organic layer was concentrated to about 50 ml and poured into methanol:water (10:1, 300 ml). The resulting mixture was stirred overnight and filtered through a membrane filter. The collected solid was cleaned

using soxhlet extraction with solvents in order methanol (250 ml), acetone (250 ml), hexane (250 ml) and toluene (250 ml). The toluene fraction was concentrated to about 50 ml and then poured into degassed methanol (300 ml). The resulting mixture was stirred overnight and the solid collected by filtration through a membrane filter. Polymer **P17** was obtained as a green powder. Toluene fraction (35 mg, 12.4 %), GPC (1,2,4-trichlorobenzene at 140 °C):  $M_w = 17100$ ,  $M_n = 12200$ , PD = 1.4. Elemental Analysis (%) calculated for  $C_{59}H_{77}N_3O_2S_2F_2$ : C, 76.63; H, 8.06; N, 3.95; S, 6.66. Found: C, 73.61; H, 8.81; N, 4.16; S, 6.39.  $^1\text{H NMR}$  (500 MHz,  $C_2D_2Cl_4$ , 100 °C)  $\delta_{\text{H}}$ /ppm: 9.07 (d,  $J = 7.45$  Hz, 2H), 8.95 (d,  $J = 7.38$  Hz, 2H), 7.94-7.73 (m, 2H), 7.53 (s, 2H), 4.62 (m, 1H), 4.16 (d, 4H), 2.35 (bs, 1H), 2.17-1.97 (m, 4H), 1.72-1.12 (m, 40H), 1.10-0.84 (m, 18H).

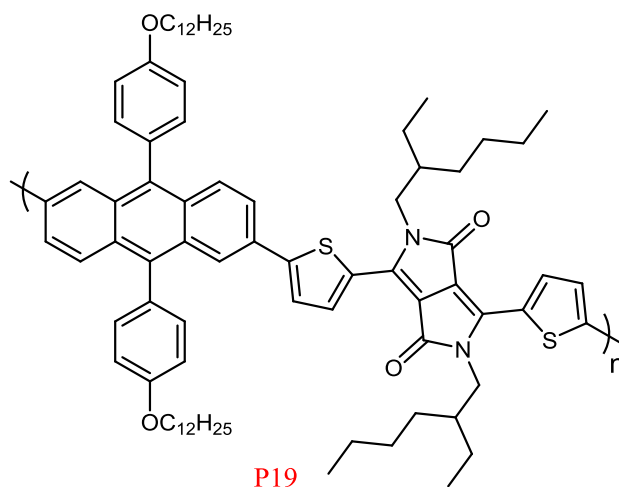
### 3.4.15. Poly [9,6-dioctyl-9H-fluorene-2,7-diyl-alt-3,6-bis(thiophen-5-yl)-2,5-di(2-ethylhexyl)-pyrrolo[3,4-c]pyrrole-1,4-dione-5',5'-diyl]



A solution of 9,9-dioctylfluorene-2,7-diboronic acid bis(1,3-propanediol) ester (**36**) (0.163 g, 0.293 mmol) and 3,6-bis(5-bromothiophen-2-yl)-2,5-bis(2-ethylhexyl)pyrrolo[3,4-c]pyrrole-1,4(2H,5H)-dione (**34**) (0.20 g, 0.293 mmol) in dry toluene (7 ml) in a 100 ml one-necked round bottom flask and under argon was degassed. To the reaction mixture was added a 20 % w/w aqueous solution of tetraethylammonium hydroxide (1.55 ml, 2.1 mmol) and the reaction mixture was degassed. To the reaction mixture,  $\text{Pd}(\text{OAc})_2$  (4.65 mg, 0.021 mmol) and tri-*o*-tolylphosphine (12.6 mg, 0.037 mmol) were added and degassed then heated to 90 °C for 24 hours. After cooling the reaction mixture to room temperature, the polymer was end-capped with the addition of 1-bromobenzene (0.1 ml, 0.94 mmol)

and degassed then heated to 90 °C for 1 hour. Again, the reaction mixture was cooled to room temperature and the polymer was end-capped with phenyl boronic acid (0.15 g, 1.23 mmol) and degassed, then the mixture was heated to 90 °C for 3 hours. The reaction mixture was cooled to room temperature then dissolved in CHCl<sub>3</sub> (300 ml) and to this solution was added an ammonium hydroxide solution (28 % in H<sub>2</sub>O, 50 ml), followed by refluxing for three hours. The mixture was cooled to room temperature and the organic layer was separated, 400 mg of disodium ethylenediaminetetraacetate were added and the mixture was stirred overnight. Then the suspension was extracted three times with 500 mL of distilled water. The organic layer was concentrated to about 50 ml and poured into methanol:water (10:1, 300 ml). The resulting mixture was stirred overnight and filtered through a membrane filter. The collected solid was cleaned using soxhlet extraction with solvents in order methanol (250 ml), acetone (250 ml), hexane (250 ml), toluene (250 ml) and chloroform (250 ml). The chloroform fraction was concentrated to about 50 ml and then poured into degassed methanol (300 ml). The resulting mixture was stirred overnight and the solid collected by filtration through a membrane filter. Polymer **P18** was obtained as a green powder. Chloroform fraction (90 mg, 33.7 %), GPC (1,2,4-trichlorobenzene at 140 °C):  $M_w = 40100$ ,  $M_n = 25400$ , PD = 1.57. Elemental Analysis (%) calculated for C<sub>59</sub>H<sub>78</sub>N<sub>2</sub>O<sub>2</sub>S<sub>2</sub>: C, 77.75; H, 8.63; N, 3.07; S, 7.04. Found: C, 75.05; H, 8.91; N, 2.83; S, 6.69. <sup>1</sup>HNMR (500 MHz, C<sub>2</sub>D<sub>2</sub>Cl<sub>4</sub>, 100 °C) δ<sub>H</sub>/ppm: 8.96 (s, 2H), 7.84 (s, 2H), 7.75 (d,  $J = 18.04$  Hz, 4H), 7.61 (s, 2H), 4.18 (d, 4H), 2.11 (d,  $J = 37.70$  Hz, 6H), 1.61-1.10 (m, 40H), 1.04 (m, 6H), 0.97 (m, 6H), 0.89 (m, 6H).

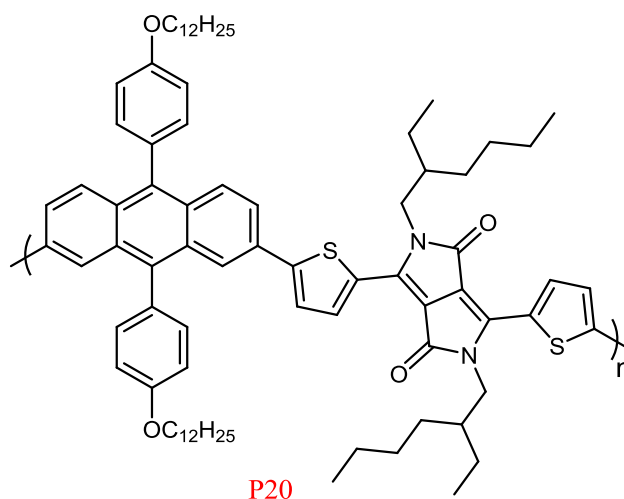
**3.4.16. Poly [9,10-bis(4-(dodecyloxy)phenyl)-anthracene-2,6-diyl-alt-3,6-bis(thiophen-5-yl)-2,5-di(2-ethylhexyl)-pyrrolo[3,4-c]pyrrole-1,4-dione-5',5'-diyl]**



A solution of 2,6-bis-(4,4,5,5-tetramethyl-[1,3,2]dioxaborolan-2-yl)-9,10-bis(4-(dodecyloxy)phenyl)anthracene (**23**) (0.279 g, 0.293 mmol) and 3,6-bis(5-bromothiophen-2-yl)-2,5-bis(2-ethylhexyl)pyrrolo[3,4-c]pyrrole-1,4(2H,5H)-dione (**34**) (0.20 g, 0.293 mmol) in dry toluene (7 ml) in a 100 ml one-necked round bottom flask and under argon was degassed. To the reaction mixture was added a 20 % w/w aqueous solution of tetraethylammonium hydroxide (1.55 ml, 2.1 mmol) and the reaction mixture was degassed. To the reaction mixture, Pd(OAc)<sub>2</sub> (4.65 mg, 0.021 mmol) and tri-*o*-tolylphosphine (12.6 mg, 0.037 mmol) were added and degassed then heated to 90 °C for 24 hours. After cooling the reaction mixture to room temperature, the polymer was end-capped with the addition of 1-bromobenzene (0.1 ml, 0.94 mmol) and degassed then heated to 90 °C for 1 hour. Again, the reaction mixture was cooled to room temperature and the polymer was end-capped with phenyl boronic acid (0.15 g, 1.23 mmol) and degassed, then the mixture was heated to 90 °C for 3 hours. The reaction mixture was cooled to room temperature, then dissolved in CHCl<sub>3</sub> (300 ml) and to this solution was added an ammonium hydroxide solution (28 % in H<sub>2</sub>O, 50 ml), followed by refluxing for three hours. The mixture was cooled to room temperature and the organic layer was separated, 400 mg of disodium ethylenediaminetetraacetate were added and the mixture was stirred overnight. Then the suspension was extracted three times with 500 mL of distilled water. The organic layer was concentrated to about 50 ml and

poured into methanol:water (10:1, 300 ml). The resulting mixture was stirred overnight and filtered through a membrane filter. The collected solid was cleaned using soxhlet extraction with solvents in order methanol (250 ml), acetone (250 ml), hexane (250 ml), toluene (250 ml) and chloroform (250 ml). The chloroform fraction was concentrated to about 50 ml and then poured into degassed methanol (300 ml). The resulting mixture was stirred overnight and the solid collected by filtration through a membrane filter. Polymer **P19** was obtained as a green powder. Chloroform fraction (208 mg, 58.2 %), GPC (1,2,4-trichlorobenzene at 140 °C):  $M_w = 12600$ ,  $M_n = 9100$ , PD = 1.4. Elemental Analysis (%) calculated for  $C_{80}H_{102}N_2O_4S_2$ : C, 78.77; H, 8.43; N, 2.30; S, 5.26. Found: C, 76.27; H, 8.52; N, 2.16; S, 4.98.  $^1H$ NMR (500 MHz,  $C_2D_2Cl_4$ , 100 °C)  $\delta_H$ /ppm: 8.88 (s, 2H), 8.09 (s, 2H), 7.82 (d,  $J = 8.94$  Hz, 2H), 7.60 (d,  $J = 9.06$  Hz, 2H), 7.41 b(s, 6H), 7.16 (d,  $J = 7.59$  Hz, 4H), 4.13 (m, 4H), 3.98 (m, 4H), 1.90 (bs, 6H), 1.62-1.12 (m, 52H), 0.95-0.73 (m, 18H).

### 3.4.17. Poly [9,10-bis(4-(dodecyloxy)phenyl)-anthracene-2,7-diyl-alt-3,6-bis(thiophen-5-yl)-2,5-di(2-ethylhexyl)-pyrrolo[3,4-c]pyrrole-1,4-dione-5',5'-diyl]



A solution of 2,7-bis-(4,4,5,5-tetramethyl-[1,3,2]dioxaborolan-2-yl)-9,10-bis(4-(dodecyloxy)phenyl)anthracene (**31**) (0.20 g, 0.210 mmol) and 3,6-bis(5-bromothiophen-2-yl)-2,5-bis(2-ethylhexyl)pyrrolo[3,4-c]pyrrole-1,4(2H,5H)-dione (**34**) (0.143 g, 0.210 mmol) in dry toluene (5 ml) in 100ml one-necked round bottom flask and under argon was degassed. To the reaction mixture was added a

20 % w/w aqueous solution of tetraethylammonium hydroxide (1.55 ml, 1.49 mmol) and degassed. To the reaction mixture mixture, Pd(OAc)<sub>2</sub> (3.4 mg, 0.015 mmol) and tri-*o*-tolylphosphine (9.3 mg, 0.027 mmol) were added and degassed then heated to 90 °C for 24 hours. After cooling the reaction mixture to the room temperature was end-capped with the addition of 1-bromobenzene (0.1 ml, 0.94 mmol) and degassed then heated 90 C for 1 hour. Again, the reaction mixture was cooling to room temperature was end-caped with phenyl boronic acid (0.15 g, 1.23 mmol) and degassed, then the mixture was heated to 90 °C for 3 hours. The reaction mixture was cooled to room temperature then dissolved in CHCl<sub>3</sub> (300 ml) and to this solution was added an ammonium hydroxide solution (28 % in H<sub>2</sub>O, 50 ml), followed by refluxing for three hours. The mixture was cooled to room temperature and the organic layer was separated, 400 mg of disodium ethylenediaminetetraacetate were added and the mixture was stirred overnight. Then the suspension was extracted three times with 500 mL of distilled water. The organic layer was concentrated to about 50 ml and poured into methanol:water (10:1, 300 ml). The result mixture was stirred overnight and filtered through a membrane filter. The collection solid was cleaned using a soxhlet extraction with solvents in order methanol (250 ml), acetone (250 ml), hexane (250 ml), toluene (250 ml) and chloroform (250 ml). The chloroform fraction was concentrated to about 50 ml and then poured in to degassed methanol (300 ml). The result mixture stirred overnight and the solid collected by filtration through membrane filter. The fraction was green powders. Chloroform fraction (0.196 mg, 76.5 %), GPC (1,2,4-trichlorobenzene at 140 °C): M<sub>w</sub> = 12700, M<sub>n</sub> = 9100, PD = 1.4. Elemental Analysis (%) calculated for C<sub>80</sub>H<sub>102</sub>N<sub>2</sub>O<sub>4</sub>S<sub>2</sub>: C, 78.77; H, 8.43; N, 2.30; S, 5.26. Found: C, 74.77; H, 8.50; N, 2.07; S, 4.57. <sup>1</sup>HNMR (500 MHz, C<sub>2</sub>D<sub>2</sub>CL<sub>4</sub>, 100 °C) δ<sub>H</sub>/ppm: 8.98 (d, *J* = 8.94 Hz, 2H), 8.20 (d, *J* = 10.85 Hz, 2H), 7.89 (d, *J* = 8.51 Hz, 2H), 7.68 (d, *J* = 8.64 Hz, 2H), 7.49 (m, 6H), 7.24 (m, 4H), 4.22 (m, 4H), 4.08 (m, 4H), 1.99 (bs, 6H), 1.74-1.22 (m, 52H), 1.06-0.84 (m, 18H).

## Chapter Four: Results and Discussion – Monomers

## 4.1. Synthesis of monomers for polymers P1, P2 and P3

In order to prepare polymers **P1**, **P2** and **P3**, monomers **(7)** and **(11)** as shown in Figure 32 were prepared successfully. In addition, monomer **(35)** was prepared by A. Alghamdi of the Iraqi group using the same preparation route to monomer **(7)**. Moreover, monomer **(36)** was bought from Sigma Aldrich.

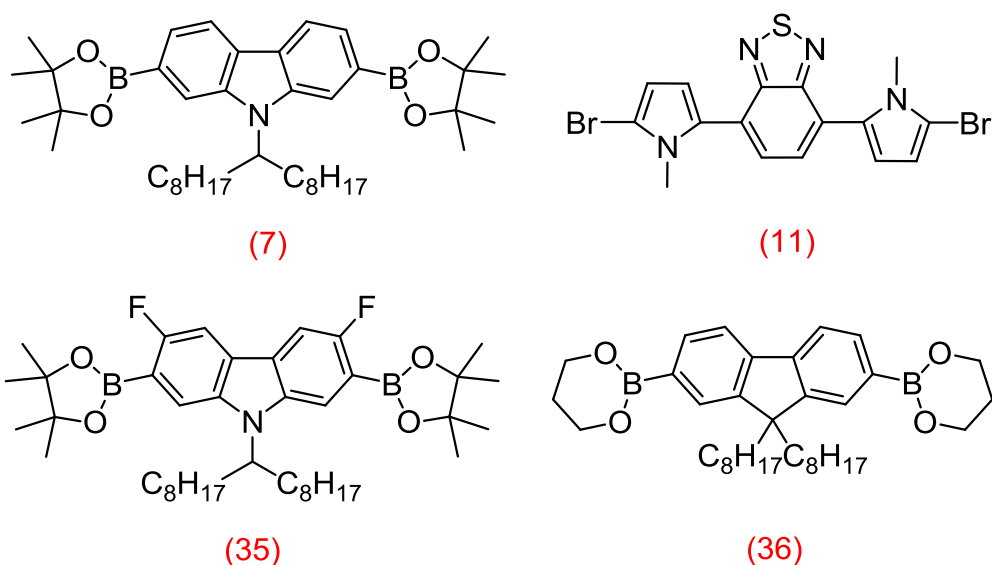
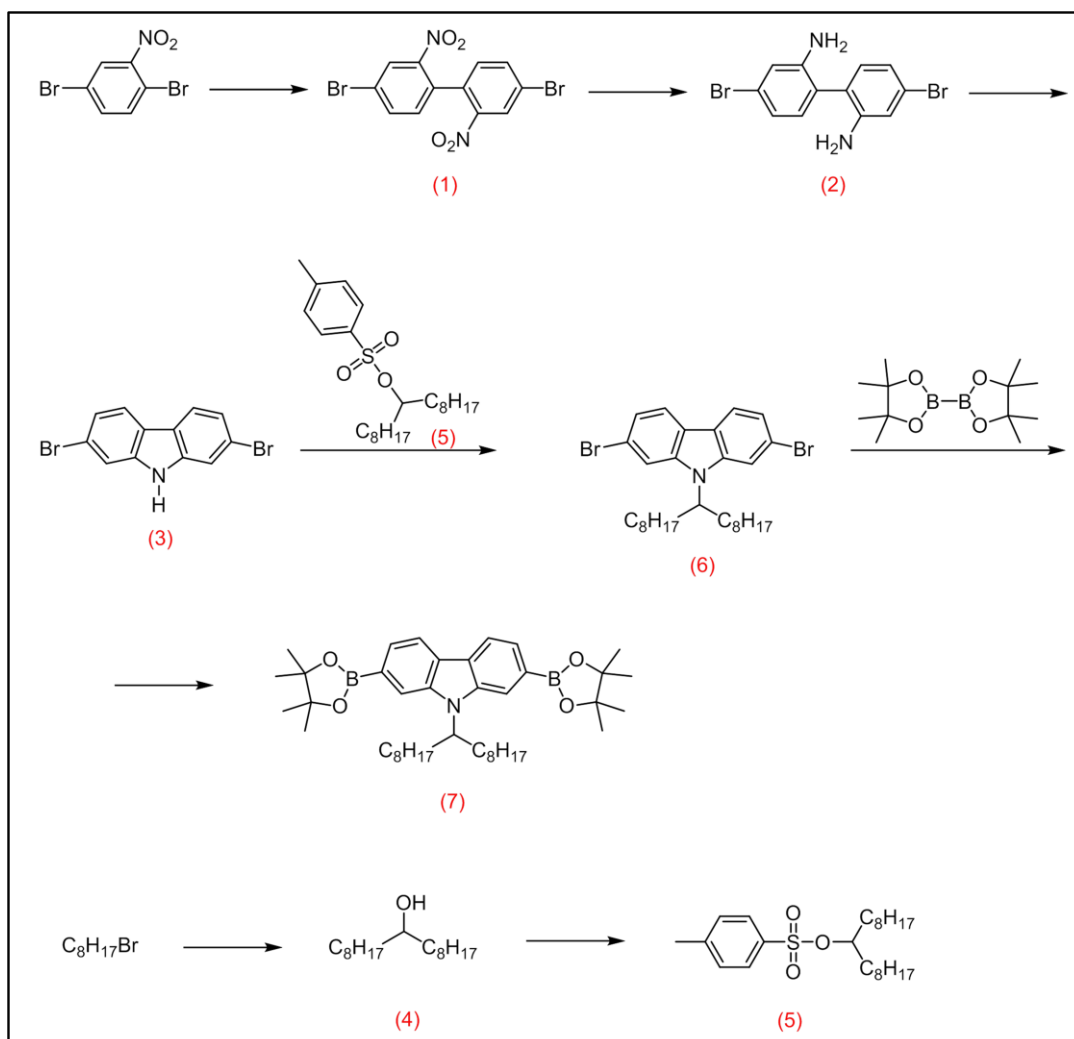


**Figure 32. Monomers required for the preparation of polymers P1, P2 and P3.**

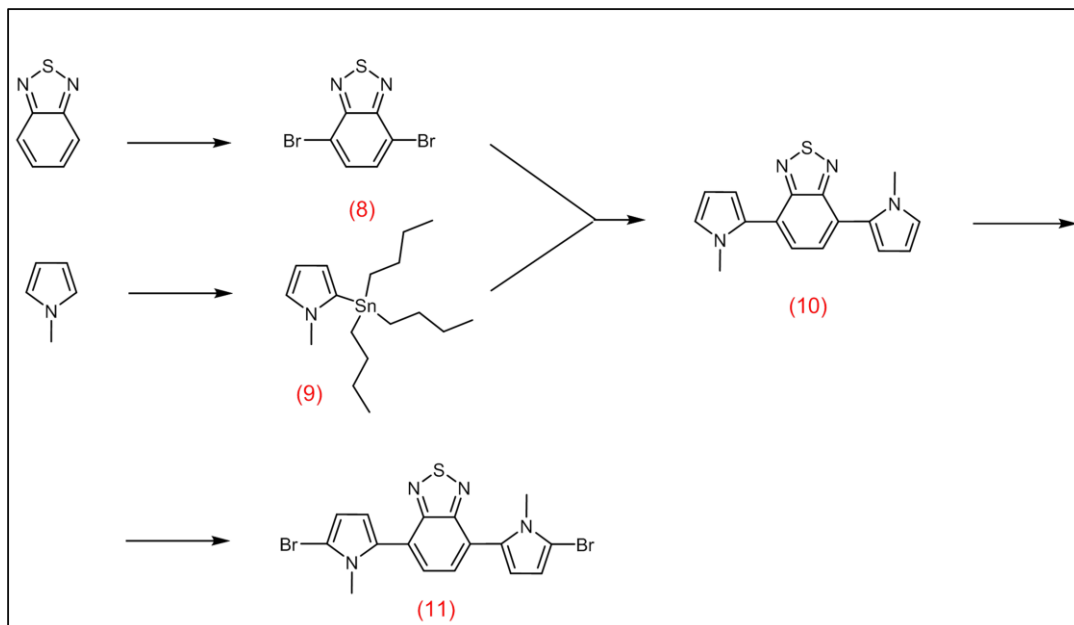
A series intermediates were prepared successfully in order to prepare **(7)** and **(11)**, and their's structure and purity were confirmed by TLC, <sup>1</sup>HNMR, <sup>13</sup>CNMR, elemental analysis, mass spectrometry, melting point, and FT-IR.

9-(Heptadecan-9-yl)-2,7-bis(4,4,5,5-tetramethyl-1,3,2-dioxaborolan-2-yl)-9H-carbazole **(7)** was prepared in seven steps as shown in Scheme 1 starting from 1,4-dibromo-2-nitrobenzene.



**Scheme 1. The preparation route for 9-(heptadecan-9-yl)-2,7-bis(4,4,5,5-tetramethyl-1,3,2-dioxaborolan-2-yl)-9H-carbazole (7).**

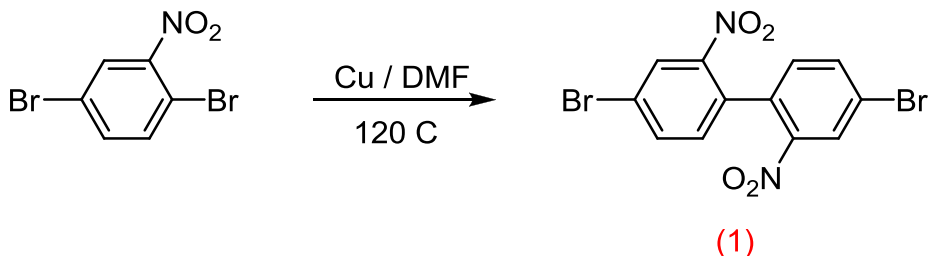
On the other hand, 4,7-bis(5-bromo-1-methyl-1H-pyrrol-2-yl)benzo[*c*][1,2,5]thiadiazole (11) was prepared in four steps as shown in Scheme 2, starting from *N*-methyl-pyrrole and benzo[*c*][1,2,5]thiadiazole.



**Scheme 2.** The preparation route for 4,7-bis(5-bromo-1-methyl-1H-pyrrol-2-yl)benzo[*c*][1,2,5]thiadiazole (11).

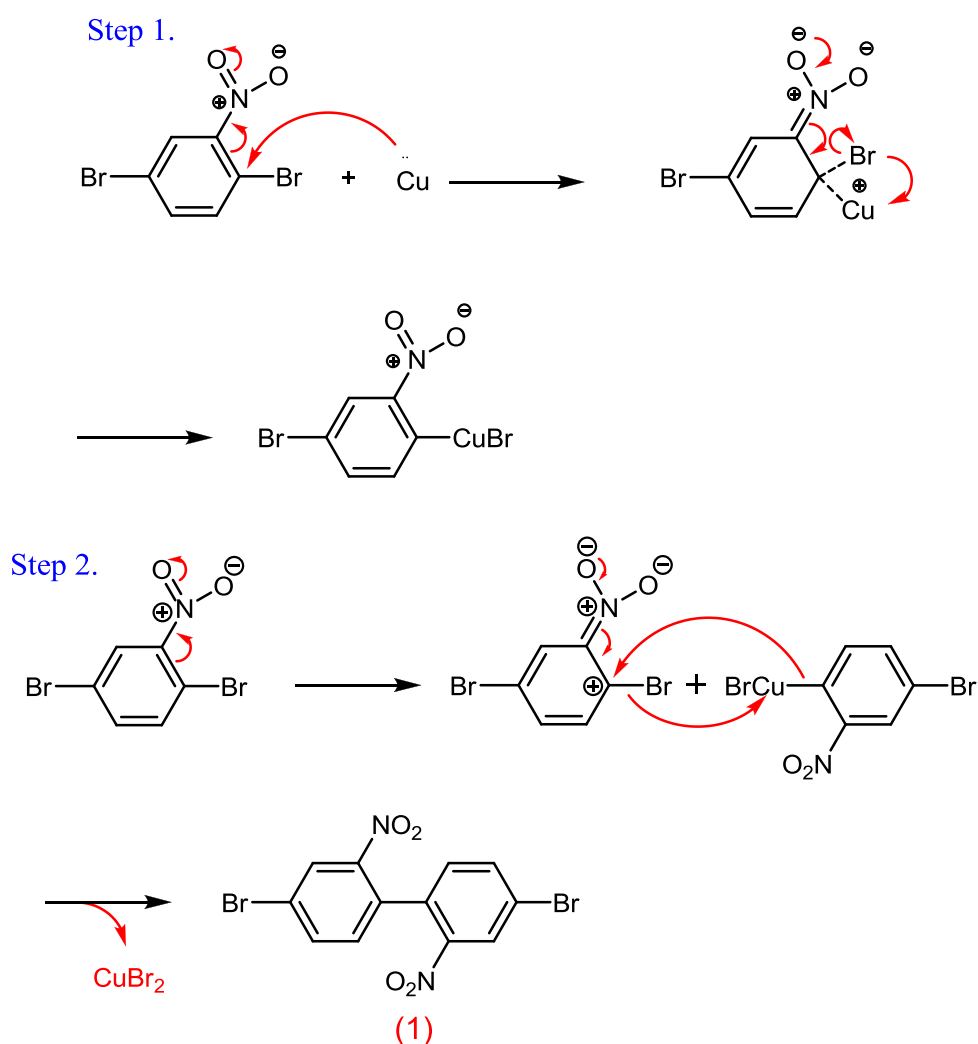
#### 4.1.1. 4,4'-Dibromo-2,2'-dinitrobiphenyl (1)

The preparation of 4,4'-dibromo-2,2'-dinitrobiphenyl (**1**) was carried out according to a modified method by Yamoto et al.<sup>111</sup>. The reaction was performed by heating a mixture of 1,4-dibromo-2-nitrobenzene and copper powder in DMF at 120 °C for three hours as shown in Scheme 3. In addition, the purification was carried out using recrystallization from ethanol to obtain the target product (**1**) as yellow crystals. The TLC gave a single spot and the yield was 95%.



**Scheme 3.** Synthesis of 4,4'-dibromo-2,2'-dinitrobiphenyl (1).

The reaction was performed using the Ullman coupling which is a coupling reaction between aryl halides using copper<sup>135</sup>. The reaction goes through two steps. The first step is a nucleophilic attack of copper to the C-Br bond on the phenyl ring which is activated by the nitro group in the ortho position which leads to the creation of copper bromide complex in the ring. The second step is a nucleophilic substitution due to the effect of copper bromide. The complex which results from the first step attacks C-Br bond in the position 1 in the second molecule (1,4-dibromo-2-nitrobenzene).



**Scheme 4. The mechanism of preparation of 4,4'-dibromo-2,2'-dinitrobiphenyl (1).**

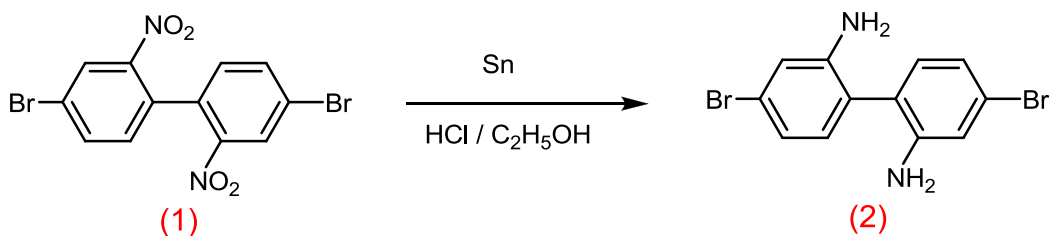
The structure and purity of the target product **(1)** were confirmed by TLC, <sup>1</sup>H NMR, <sup>13</sup>C NMR, elemental analysis, mass spectrometry, melting point and FT-IR.

The TLC gave a single spot and the melting point (146-148 °C) is in agreement with literature value 148 °C<sup>112</sup>. The elemental analysis for CHNBr confirmed the structure of the target product. The mass spectra illustrates the main integer masses of **(1)**, which are obtained at 400, 402, 404 (M<sup>+</sup>) in 1:2:1 intensities because of the bromine isotopes (<sup>81</sup>Br and <sup>79</sup>Br).

The <sup>1</sup>HNMR spectrum shows the aromatic peaks, doublet at 8.40 ppm, doublet of doublet at 8.85 ppm and doublet at 7.19 ppm. The <sup>13</sup>CNMR spectra illustrated six peaks in the aromatic region from 147.3 to 122.9. The FT-IR of the target product illustrates the stretching vibration bands for the aromatic nitro group at 1977 cm<sup>-1</sup> and 1336 cm<sup>-1</sup>. The stretch vibration at 3100 cm<sup>-1</sup> is correlated to aromatic C – H bond. The C-Br stretching vibration is displayed at 1097 cm<sup>-1</sup>.

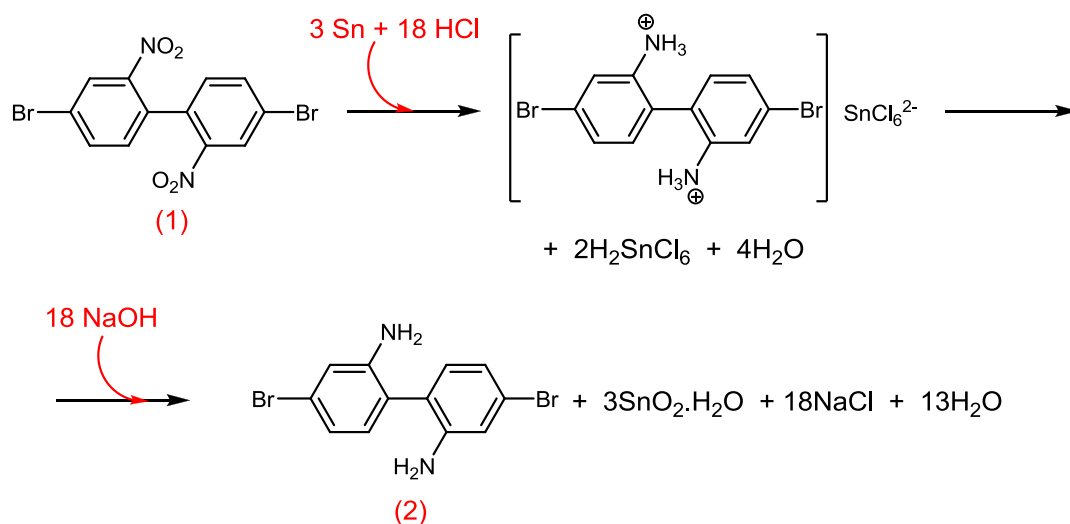
#### 4.1.2. 4,4'-dibromobiphenyl-2,2'-diamine (**2**)

The preparation of 4,4'-dibromobiphenyl-2,2'-diamine (**2**) was carried out according to a modified method by Yamoto et al<sup>111</sup>. The reaction was performed by refluxing a mixture of 4,4'-dibromo-2,2'-dinitrobiphenyl (**1**) and tin powder in a mixture solution of ethanol and HCl for 150 minutes as shown in Scheme 5. The starting material (4,4'-dibromo-2,2'-dinitrobiphenyl (**1**)) has a low solubility in the mixture of HCl and ethanol while the product is soluble. Thus, tin powder was added within two portions because after 90 minutes, there was still heterogeneous mixture which indicates that the starting material had not been consumed. In addition, the purification was carried out using recrystallization from ethanol to obtain the target product (**2**) as a yellow powder. The TLC gave single spot and the yield was 89.6%.



Scheme 5. Preparation of 4,4'-dibromobiphenyl-2,2'-diamine (**2**).

The mechanism of this reaction is proposed by Morrison and Bayd<sup>136</sup>. The reduction of nitro groups to the amino groups takes place within two steps as shown in Scheme 6. The first step is the creation of protonated amine under acidic condition followed by reduction reaction. The second step is a basification reaction by treatment with base which leads to the generation of the amine.



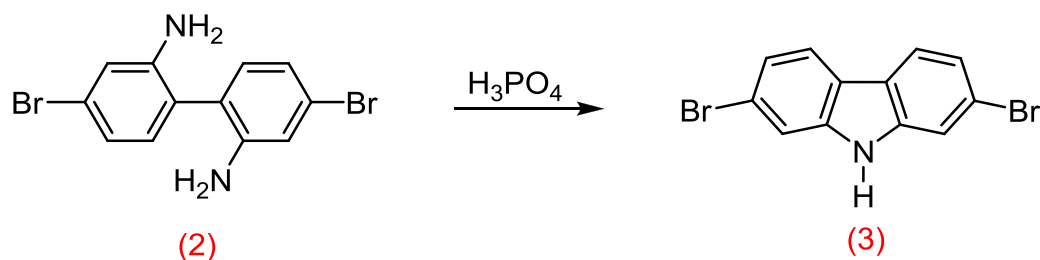
**Scheme 6. The mechanism of preparation of 4,4'-dibromobiphenyl-2,2'-diamine (2).**

The structure and purity of the target product (**2**) were confirmed by TLC,  $^1\text{H}$  NMR,  $^{13}\text{C}$  NMR, elemental analysis, mass spectrometry, melting point and FT-IR. The TLC gave a single spot and the melting point ( $191\text{-}193\text{ }^\circ\text{C}$ ) is in agreement with literature value  $192^\circ\text{C}$ <sup>112</sup>. The elemental analysis for  $\text{CHNBr}$  confirmed the structure of the target product. The mass spectra illustrates the main integer masses of (**2**), which are obtained at 340, 342 and 344 ( $\text{M}^+$ ) in 1:2:1 intensities because of the bromine isotopes ( $^{81}\text{Br}$  and  $^{79}\text{Br}$ ).

The  $^1\text{HNMR}$  spectrum shows a singlet peak at 6.95 ppm for the aromatic protons. In addition, the spectrum show a broad singlet peak at 3.76 ppm which corresponds to the N – H protons. The  $^{13}\text{CNMR}$  spectrum illustrated six peaks in the aromatic region from 145.4 ppm to 118.1 ppm which correspond very well with the structure of the target product.

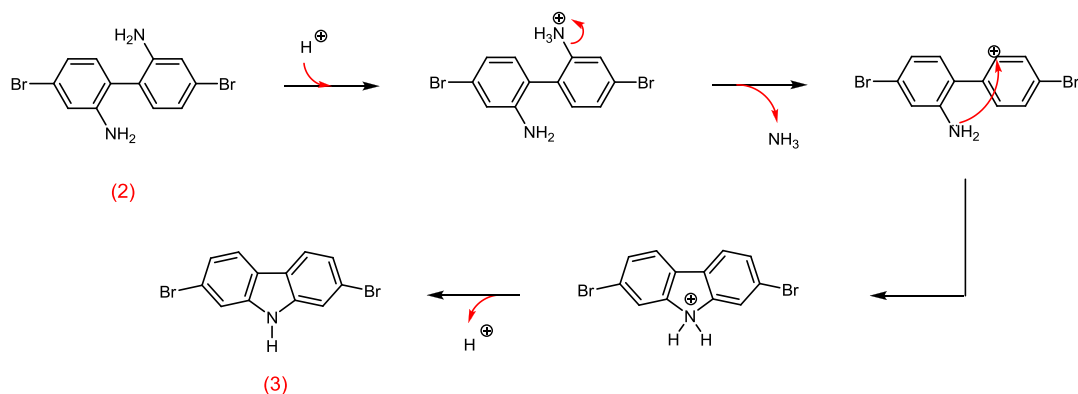
### 4.1.3. 2,7-Dibromo-9H-carbazole (3)

The preparation of 2,7-dibromo-9H-carbazole (**3**) was carried out according to a modified method by Sonntaq et al <sup>113</sup>. The reaction was performed by heating 4,4'-dibromobiphenyl-2,2'-diamine (**2**) in concentrated phosphoric acid at 190 °C overnight as shown in Scheme 7. In addition, the purification was carried out using recrystallization from a mixture of toluene and hexane (10:1) to obtain the target product (**3**) as white crystals. The TLC gave a single spot and the yield was 60%.



Scheme 7. The preparation of 2,7-dibromo-9H-carbazole (**3**).

2,7-Dibromo-9H-carbazole was formed via a cyclisation reaction. The mechanism of its preparation is not fully understood. The proposed mechanism might consist of two steps as shown in Scheme 8. The first step of the mechanism is the protonation of the  $-NH_2$  under acidic conditions to form  $NH_3^+$  on one of the biphenyl rings. The second step is elimination of  $NH_3^+$  (a good leaving group) which requires very high temperature then cyclisation takes place.



Scheme 8. The mechanism of preparation of 2,7-dibromo-9H-carbazole (**3**).

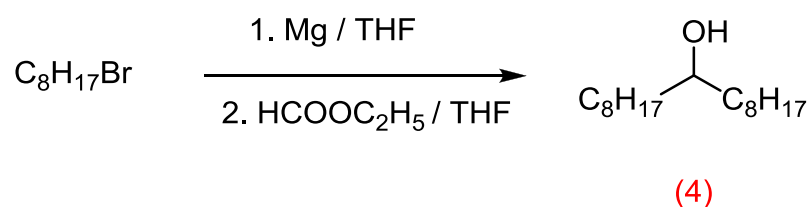
The structure and purity of the target product (**3**) were confirmed by TLC,  $^1H$ NMR,  $^{13}C$ NMR, elemental analysis, mass spectrometry, melting point and FT-IR. The

TLC gave a single spot and the melting point (229-230 °C) is in agreement with the literature value (230-232 °C)<sup>114</sup>. The elemental analysis for CHNBr confirmed the structure of the target product. The mass spectrum illustrates the main integer masses of (**3**) which are obtained at 323, 325, 327 ( $M^+$ ) in 1:2:1 intensities because of the bromine isotopes ( $^{81}\text{Br}$  and  $^{79}\text{Br}$ ).

The  $^1\text{H}$ NMR spectrum shows aromatic peaks; doublet peaks at 7.89, 7.58 and doublet of doublet at 7.38 ppm. The spectrum shows a broad singlet peak at 8.06 ppm which is related to the N - H proton. The  $^{13}\text{C}$ NMR spectrum illustrates six peaks in the aromatic region from 140.2 ppm to 113.8 ppm which correspond very well with the structure of the target product. The FT-IR of the target product illustrates the stretching vibration bands for (N - H) group at  $3315\text{ cm}^{-1}$ , the stretching vibration bands for (C - N) group appears at  $1241\text{ cm}^{-1}$ . The C-H stretching vibration is displayed at 2596, 2916, 2872 and  $2848\text{ cm}^{-1}$ .

#### 4.1.4. Heptadecan-9-ol (**4**)

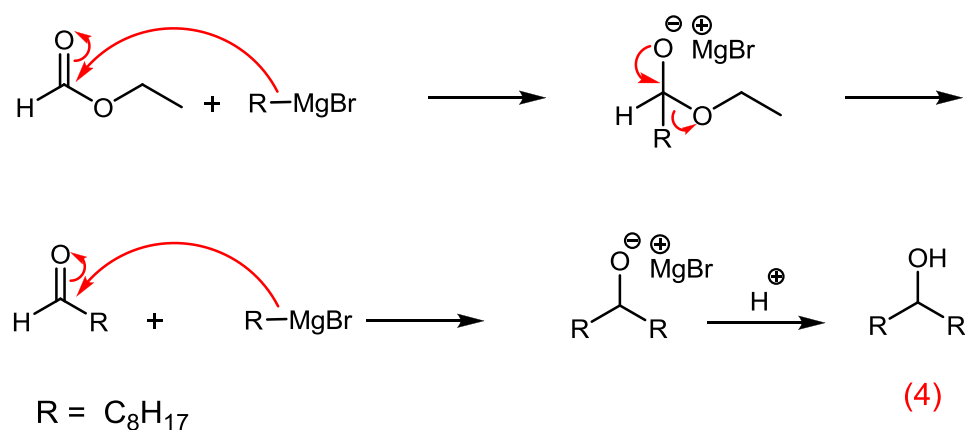
The preparation of heptadecan-9-ol (**4**) was performed according to the method by Leclerc et al.<sup>11b</sup> using a reaction of octylmagnesium bromide first prepared by adding a solution of bromooctane in THF to magnesium in THF. The reaction mixture was added drop wise to a solution of ethyl formate in THF at  $-78\text{ }^\circ\text{C}$  as shown in Scheme 9. The reaction was quenched by adding a mixture solution of methanol and  $\text{NH}_4\text{Cl}$ . The product did not require purification and it was used directly in the next step as a colourless oil, the yield is 90.6%.



**Scheme 9. The preparation of heptadecan-9-ol (**4**).**

The preparation of heptadecan-9-ol (**4**) goes through two steps. The first step is formation of Grignard reagent ( $\text{RMgX}$ ). The second step involves a nucleophilic

attack of the first Grignard reagent on the carbonyl group in the ethyl formate form an aldehyde. The carbonyl group in aldehyde is more reactive than before (the carbonyl in the ethyl formate), as a result, the second nucleophilic attack by Grignard reagent takes place, then a hydrolysis reaction results in formation of the target product (4).



**Scheme 10.** The mechanism of preparation of heptadecan-9-ol (4).

The structure of the target product (4) was confirmed by TLC, <sup>1</sup>HNMR, <sup>13</sup>CNMR, elemental analysis, mass spectrometry, melting point and FT-IR. The TLC gave a single spot and the melting point (29-30 °C) is in agreement with the literature value (28-31 °C) <sup>11b</sup>. The elemental analysis for CH confirmed the structure of the target product. The mass spectrum illustrates the main integer mass of (4) at 256 (M<sup>+</sup>) which is in agreement with the proposed structure.

The <sup>1</sup>HNMR spectrum shows the assumed peaks, a broad peak at 3.59 ppm can be assigned to the (O - H) proton, a multiplet at 1.40 ppm corresponds to the alkyl chain and a triplet at 0.90 ppm is related to the (CH<sub>3</sub>) protons at the end of the alkyl chains. The <sup>13</sup>CNMR spectrum shows nine peaks from 72.0 ppm to 14.12 ppm. The FT-IR of the target product illustrates the stretching vibration bands for the hydroxyl group (O - H) at 3315 cm<sup>-1</sup>, the stretching vibration bands for (C - O) group appears at 1241 cm<sup>-1</sup>. The C-H stretching vibration bands are displayed at 2996, 2916, 2872 and 2848 cm<sup>-1</sup>, the bending vibration at 1465 and 1375 are related to CH<sub>2</sub> and CH<sub>3</sub> bends respectively.

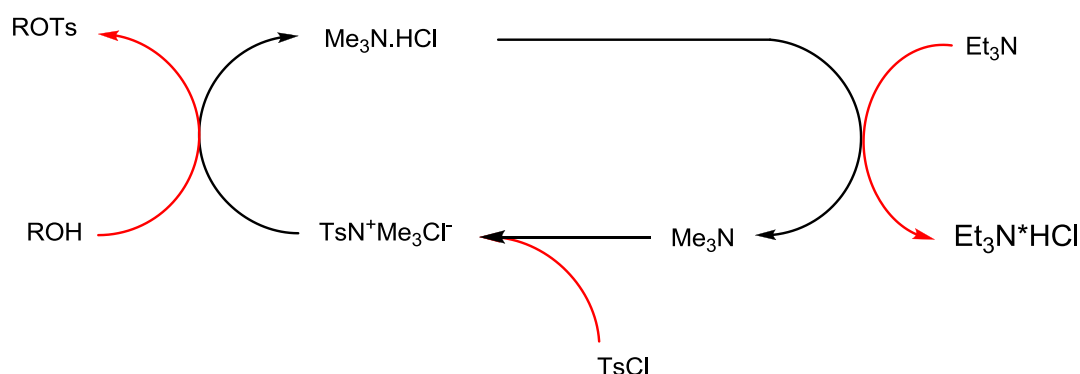
## 4.1.5. Heptadecan-9-yl 4-methylbenzenesulfonate (5)

The preparation of heptadecan-9-yl 4-methylbenzenesulfonate (5) was carried out according to a modified method by Leclerc et al <sup>11b</sup>. The reaction was performed by adding a solution of p – toluene sulfonyl chloride in DCM to a mixture of heptadecan-9-ol, triethylamine and Me<sub>3</sub>N.HCl in DCM at 0 °C as shown in Scheme 11. In addition, the purification was carried out using silica gel column chromatography in 89:9:2 petroleum ether (40:60) / ethyl acetate / triethyl amine to obtain the target product (5) as a white solid, triethylamine was added to the column chromatography to avoid the product degradation due to silica gel acidity. The TLC gave a single spot and the yield was 75%.



**Scheme 11. The preparation of heptadecan-9-yl 4-methylbenzenesulfonate (5).**

This is a tosylation reaction in which the trimethylamine hydrochloride salt acts as a catalyst in presence of the base (triethylamine). Thus, Me<sub>3</sub>N.HCl reacts with Et<sub>3</sub>N forming Me<sub>3</sub>N which reacts with TsCl and generates the tosylate reagent (TsN<sup>+</sup>Me<sub>3</sub>Cl). Then, the tosylate reagent reacts with heptadecan-9-ol (4) to obtain the target product and Me<sub>3</sub>N.HCl which starts new cycle as shown in Scheme 12.



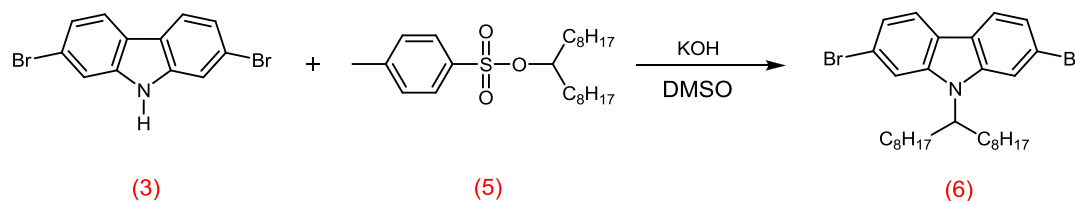
**Scheme 12. The mechanism of preparation of heptadecan-9-yl 4-methylbenzenesulfonate (5).**

The structure of the target product (**5**) were confirmed by TLC,  $^1\text{H}$ NMR,  $^{13}\text{C}$ NMR, elemental analysis, mass spectrometry, melting point and FT-IR. The TLC gave a single spot and the melting point ( $32\text{ }^\circ\text{C}$ ) is in agreement with the literature value ( $31\text{-}32\text{ }^\circ\text{C}$ )<sup>11b</sup>. The elemental analysis for CH confirmed the structure of the target product. The mass spectrum illustrate the main integer mass of (**5**) at  $410\text{ (M}^+)$  which is in agreement with the proposed structure.

The  $^1\text{H}$ NMR spectrum confirms the proposed structure with a multiplet peak at 3.59 ppm which corresponds to the (O - C - H) proton and a triplet peak at 0.90 ppm which can be assigned to  $\text{CH}_3$  protons at the end of alkyl chains. The  $^{13}\text{C}$ NMR spectrum illustrate fourteen peaks from 144.2 ppm to 14.0 ppm, which corresponds very well with the structure of target product. The FT-IR of the target product shows that the stretching vibration bands for the hydroxyl group (O - H) at  $3315\text{ cm}^{-1}$  for Heptadecan-9-ol (**4**) disappeared, a stretch vibration band at  $2954\text{ cm}^{-1}$  for aromatic C - H is observed. The C - H bend is displayed at  $881, 766, \text{ and } 741\text{ cm}^{-1}$ .

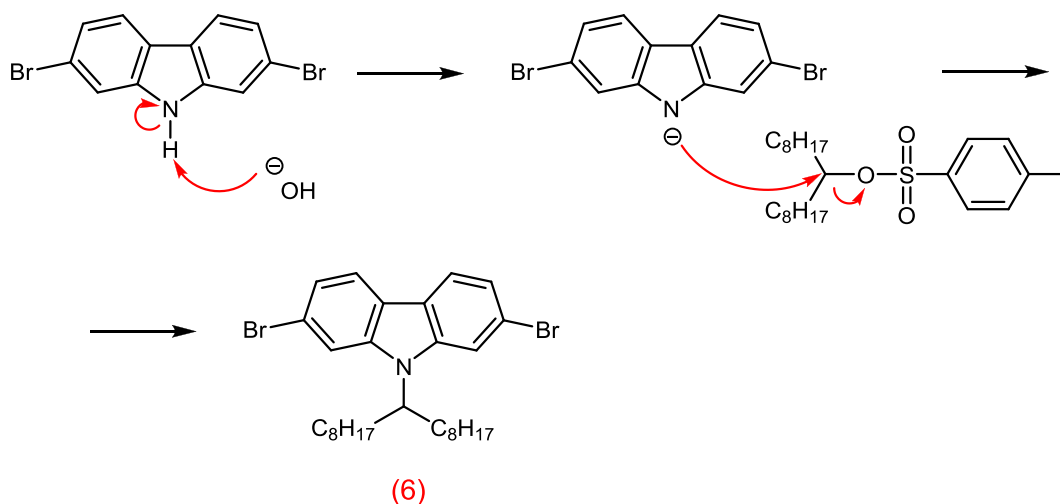
#### 4.1.6. 2,7-Dibromo-9-(heptadecan-9-yl)-9H-carbazole (**6**)

2,7-Dibromo-9-(heptadecan-9-yl)-9H-carbazole (**6**) was synthesised according to a modified procedure by Leclerc et al<sup>11b</sup>. The reaction was performed by adding a solution of heptadecan-9-yl 4-methylbenzenesulfonate (**5**) in dry DMSO dropwise to a mixture of 2,7-dibromocarbazole and KOH in DMSO as shown in Scheme 13. The purification was carried out using silica gel column chromatography with the crude product pre-absorbed onto silica gel and eluted with petroleum ether (40-60%) to obtain the target product as white crystals. The TLC gave a single spot and the yield was 57.7%.



Scheme 13. The preparation of 2,7-dibromo-9-(heptadecan-9-yl)-9H-carbazole (**6**)

The reaction involved a deprotonation of the  $-NH$  group with the base (KOH) which gives the anion on the nitrogen. The next step is nucleophilic attack on the carbon attached to the tosylate group (which is a good leaving group) to give the target product (**6**) as shown in Scheme 14.



**Scheme 14. The mechanism for the preparation of 2,7-dibromo-9-(heptadecan-9-yl)-9H-carbazole (**6**).**

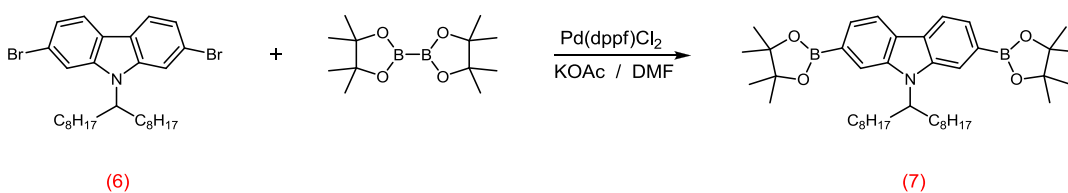
The structure of the target product (**6**) was confirmed by TLC,  $^1\text{H}$ NMR,  $^{13}\text{C}$ NMR, elemental analysis, mass spectrometry, melting point and FT-IR. The TLC gave a single spot and the melting point (59-60 °C) is in agreement with literature value (59-61 °C) <sup>11b</sup>. The elemental analysis for  $\text{CHNBr}$  confirmed the structure of the target product. The mass spectrum illustrates the main integer mass of (**6**) at 563, 565, 567 ( $\text{M}^+$ ) in 1:2:1 intensities because of the bromine isotopes ( $^{81}\text{Br}$  and  $^{79}\text{Br}$ ).

The  $^1\text{H}$ NMR spectrum illustrated the aromatic peaks; a triplet peak at 7.92 ppm, singlet peaks at 7.71 and 7.56 ppm, a doublet peak at 7.35 ppm which are related to the carbazole protons. In addition, the spectrum shows a multiplet peak at 4.43 ppm which is related to (N - C - H) proton and the triplet peak at 0.85 ppm which can be assigned to the  $\text{CH}_3$  groups at the end of the alkyl chain. The broadening of the peaks in the  $^{13}\text{C}$ NMR is due to a phenomenon known as atropisomerism <sup>137</sup>, which leads to multiple peaks. This phenomenon was first reported by Christie in 1922, atropisomerism arises when rotation around a single bond is restricted <sup>115</sup>. The FT-

IR of the target product illustrates that the stretching vibration bands for (N - H) group displays at  $3315\text{ cm}^{-1}$  in 2, 7-dibromo-9H-carbazole (**3**) disappeared.

#### 4.1.7. 9-(Heptadecan-9-yl)-2,7-bis(4,4,5,5-tetramethyl-1,3,2-dioxaborolan-2-yl)-9H-carbazole (**7**)

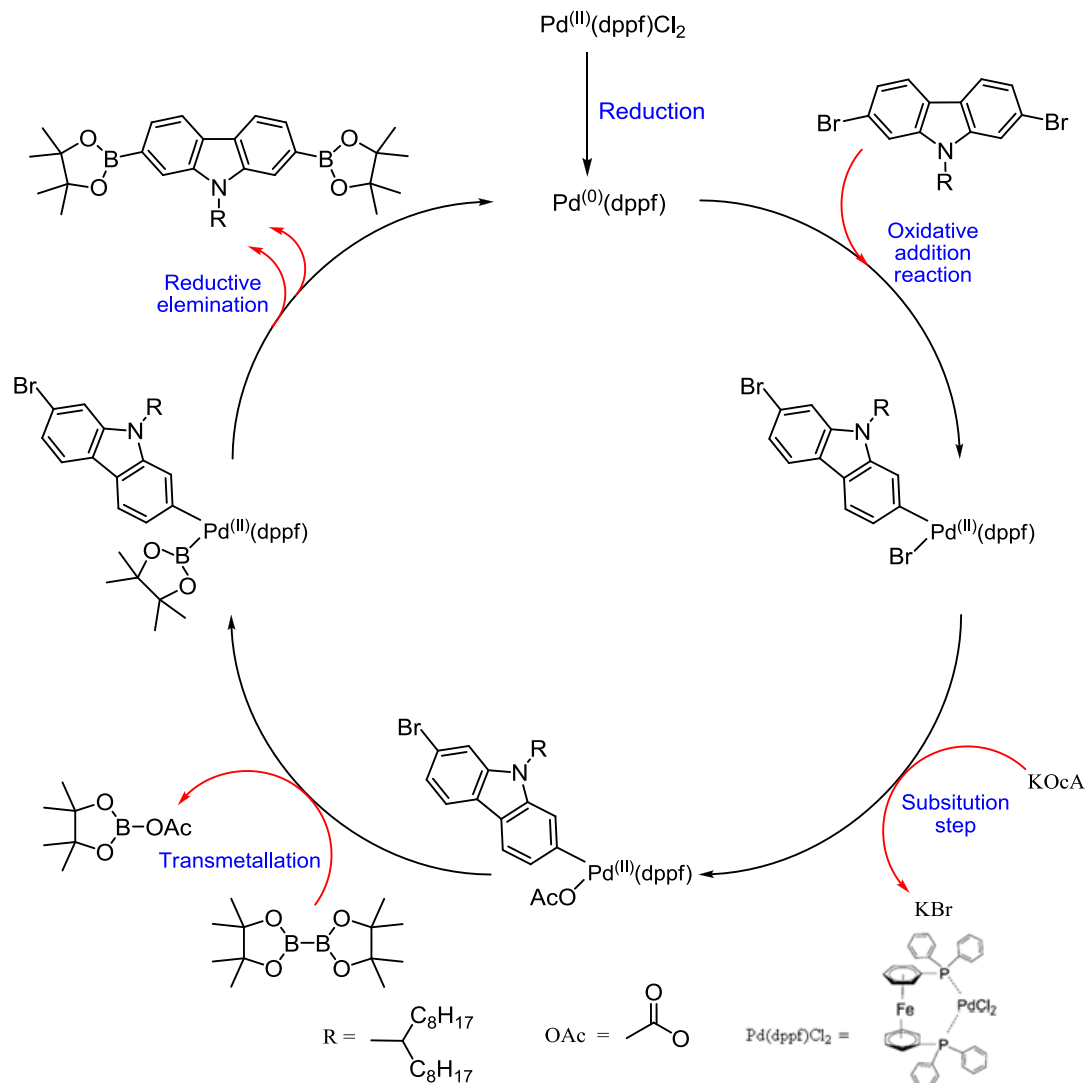
The preparation of 9-(heptadecan-9-yl)-2,7-bis(4,4,5,5-tetramethyl-1,3,2-dioxaborolan-2-yl)-9H-carbazole (**7**) was carried out using a modified procedure by Jo et al <sup>115</sup>. The reaction was performed by heating mixture of 2,7-dibromo-9-(heptadecan-9-yl)-9H-carbazole (**6**), bis(pinacolato) diboron, potassium acetate and the [1,1'-bis(diphenylphosphino)ferrocene] dichloropalladium (II) ( $\text{Pd}(\text{dppf})\text{Cl}_2$ ) in DMF at  $100\text{ }^\circ\text{C}$  for 36 hours as shown in Scheme 15. An excess of bis(pinacolato) diboron was used to prevent the creation of oligomers. The colour of the reactive mixture changed to black during the reaction. Recrystallization was carried out using diethyl ether and methanol. Firstly, methanol was passed through basic alumina column to remove any acidic trace because the boronic ester is very sensitive to acids. The product was dissolved in the minimum amount of diethyl ether and added to the hot methanol so diethyl ether was evaporated and the target product precipitated and the impurities were dissolved in methanol. The target product was obtained with 60% yield as white crystals.



**Scheme 15. The preparation of 9-(heptadecan-9-yl)-2,7-bis(4,4,5,5-tetramethyl-1,3,2-dioxaborolan-2-yl)-9H-carbazole (**7**).**

The mechanism of this reaction is similar to the Suzuki cross coupling mechanism and it consists of five steps as shown in Scheme 16. The first step is reduction of  $\text{Pd}(\text{dppf})\text{Cl}_2$  from Pd (II) to Pd (0). The second step is oxidative addition reaction that couples the Pd(dppf) to the 2,7-dibromo-9-(heptadecan-9-yl)-9H-carbazole (**6**) which forms a palladium(II) complex. The third step is activation of this complex

by using potassium acetate and the bromide group is substituted with an acetate group. The fourth step is transmetalation that bis(pinacolate) diboron is reacted with the palladium complex which generates the boron palladium complex. The last step is reductive elimination to obtain the target product and regeneration the Pd(dppf) again which starts a new catalytic cycle.



**Scheme 16.** The mechanism of preparation of 9-(heptadecan-9-yl)-2,7-bis(4,4,5,5-tetramethyl-1,3,2-dioxaborolan-2-yl)-9H-carbazole (7).

The structure of the target product (7) was confirmed by  $^1\text{H}$ NMR,  $^{13}\text{C}$ NMR, elemental analysis, mass spectrometry, melting point and FT-IR. The melting point (127-128 °C) is in agreement with literature value (128-130 °C)<sup>115</sup>. The elemental analysis for CHN confirmed the structure of the target product. The mass spectrum

illustrates the main integer mass of (7) at 657.5 ( $M^+$ ) which is in agreement with the proposed structure. The  $^1\text{H}$ NMR spectrum confirms the structure of 9-(heptadecan-9-yl)-2,7-bis(4,4,5,5-tetramethyl-1,3,2-dioxaborolan-2-yl)-9H-carbazole (7) as shown in Figure 33. The spectrum shows broad peaks at 8.15, 8.05 and 7.91 ppm which are related to the carbazole protons in the positions (a) and (b). It is interesting to note that the carbazole protons in the position (a) are displayed in two different environments as a result of restricted rotation at the C-N bond. The doublet peak at 7.69 ppm can be assigned to the carbazole protons in the position (c). The multiplet peak at 4.72 ppm can be assigned to the ( $\text{R}_2\text{CHN}$ ) proton in the position (d). The multiplet peaks at 2.36, 1.97 and 1.22 ppm correspond to the alkyl chain protons that are attached to the carbazole in the positions ((e) to (k)). The triplet peak at 0.84 ppm is related to the six protons on the  $\text{CH}_3$  groups at the end of the alkyl chains that are attached to the carbazole. The singlet peak observed at 1.42 ppm can be assigned to the methyl group of the boronic ester protons in the positions (m). The  $^{13}\text{C}$ NMR also confirms the structure of (7).

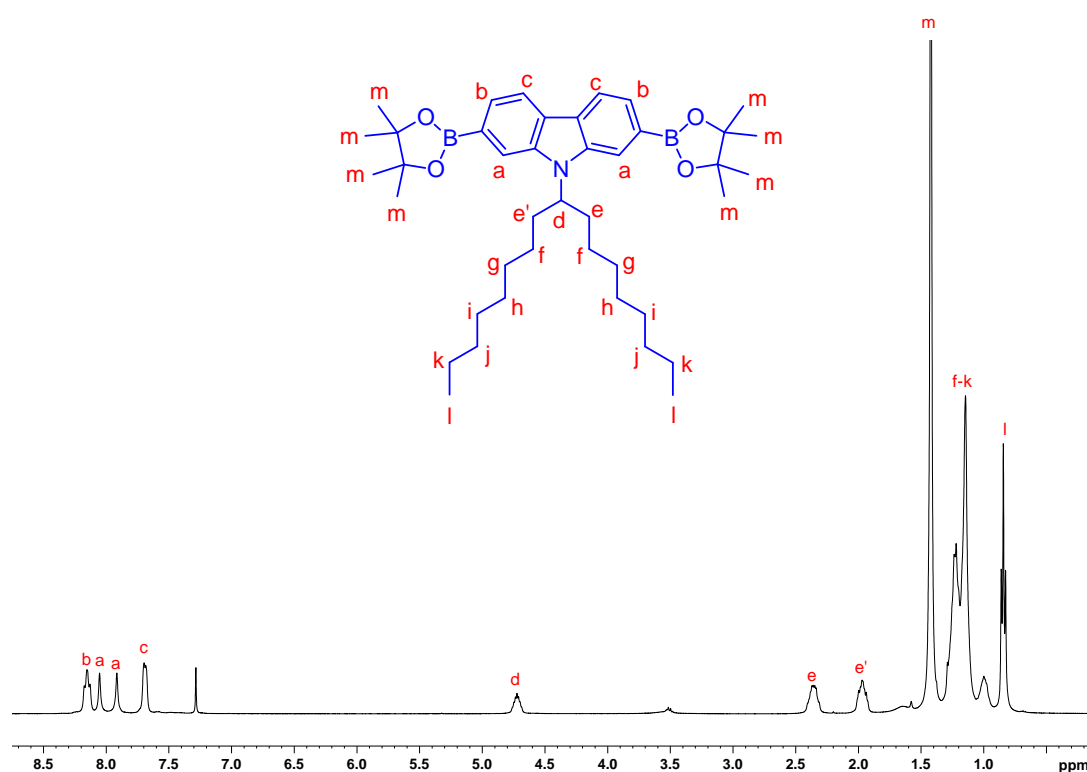
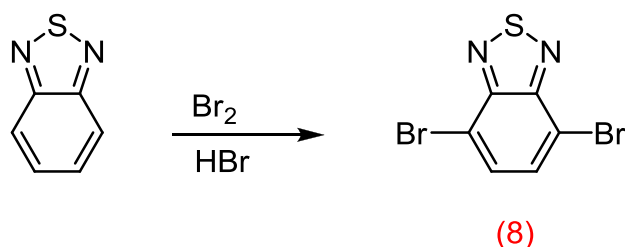


**Figure 33.** The  $^1\text{H}$ NMR spectrum of 9-(heptadecan-9-yl)-2,7-bis(4,4,5,5-tetramethyl-1,3,2-dioxaborolan-2-yl)-9H-carbazole (7).

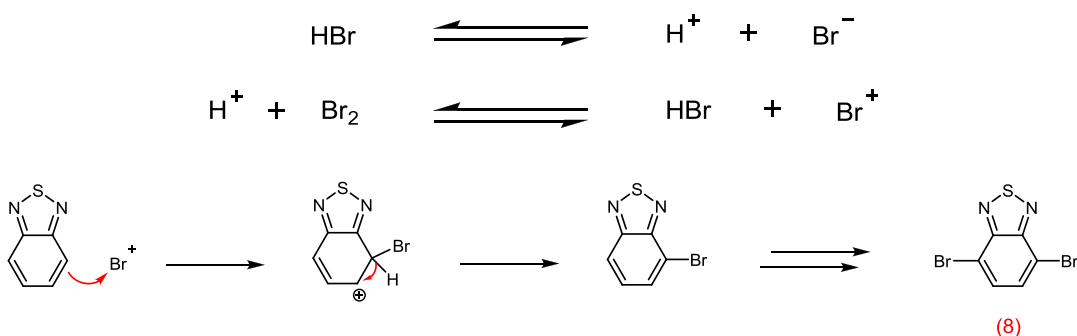
## 4.1.8. 4,7-Dibromobenzo[c][1,2,5]thiadiazole (8)

The preparation of 4,7-dibromobenzo[c][1,2,5]thiadiazole (**8**) was carried out according to a modified procedure by Zoombelt et al <sup>116</sup>. The reaction was performed by heating 1,2,5-benzothiadiazole in hydrogen bromide at 110 °C and bromine was added dropwise within 90 minutes. Also, further hydrogen bromide was added to the reaction mixture in order to facilitate stirring toward the end of reaction as shown in Scheme 17. The purification was carried out by In recrystallization from a mixture of THF : methanol (1:1) to obtain the target product as white needles with 81.4% yield.



Scheme 17. The preparation of 4,7-dibromobenzo[c][1,2,5]thiadiazole (**8**).

The reaction was performed by electrophilic substitution to the 4- and 7- positions which are activated by nitrogen atoms. However, when the substitution in the positions 4- and 7- occur, the 5- and 6- positions are activated by the neighbouring bromine substituents and so a small amount of tris- and tetrakis- bromine substituted products might be formed which can be removed easily by recrystallization.

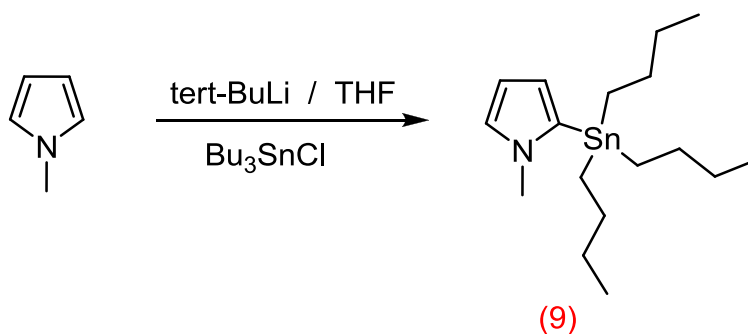


Scheme 18. The mechanism of the preparation of 4,7-dibromobenzo[c][1,2,5]thiadiazole (**8**).

The structure of the target product (**8**) was confirmed by  $^1\text{H}$ NMR,  $^{13}\text{C}$ NMR, elemental analysis, mass spectrometry, melting point and FT-IR. The TLC gave a single spot and the melting point (189-191  $^\circ\text{C}$ ) is in agreement with literature value <sup>117</sup>. The elemental analysis for  $\text{CHNBr}$  confirmed the structure of the target product. The mass spectrum illustrates the main integer masses of (**8**) at 292, 294, 296 ( $\text{M}^+$ ) in 1:2:1 intensities because of the bromine isotopes ( $^{81}\text{Br}$  and  $^{79}\text{Br}$ ).

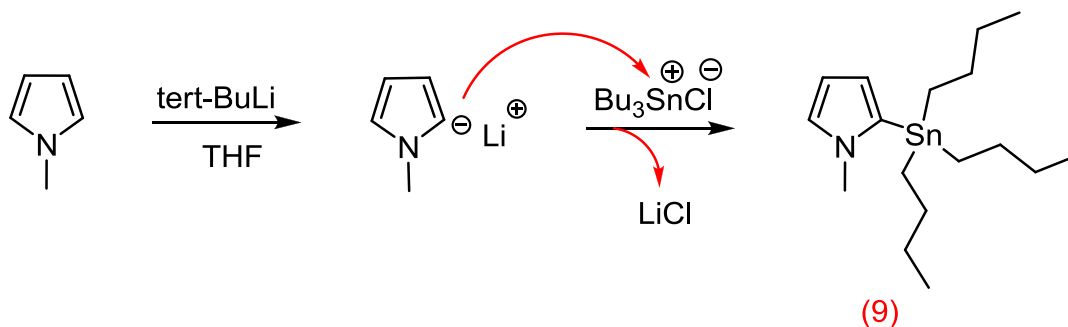
#### 4.1.9. 1-Methyl-2-(tributylstannyl)-1H-pyrrole (**9**)

The preparation of 1-methyl-2-(tributylstannyl)-1H-pyrrole (**9**) was carried out according to a modified procedure by Torum et al <sup>118</sup>. The reaction was performed by adding *tert*-butyl lithium drop wise to a solution of N-methyl pyrrole in THF at -78  $^\circ\text{C}$ . The reaction mixture was stored for 16 hours at -15  $^\circ\text{C}$  and then  $\text{Bu}_3\text{SnCl}$  was added as shown in Scheme 19. The product was obtained as a yellow oil with 84% yield.



**Scheme 19. The preparation of 1-methyl-2-(tributylstannyl)-1H-pyrrole (**9**).**

The mechanism of the reaction involves deprotonation of the 2-position of methylpyrrole followed by nucleophilic substitution of chlorine in tributyl tin chloride as illustrated in the Scheme 20.

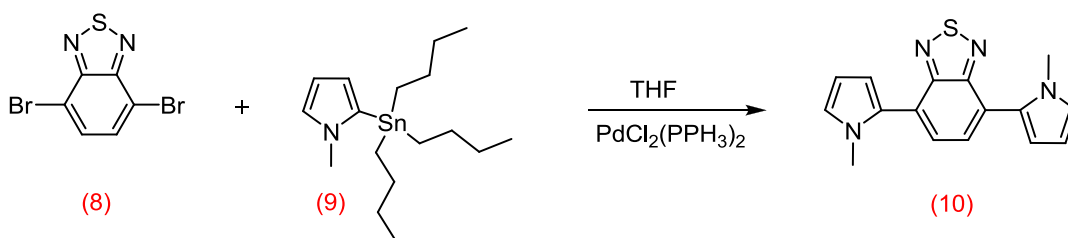


**Scheme 20.** The mechanism of preparation of 1-methyl-2-(tributylstannyl)-1H-pyrrole (9).

The structure and purity of the target product (9) were confirmed by  $^1\text{H}$ NMR,  $^{13}\text{C}$ NMR, elemental analysis, mass spectrometry and FT-IR. The elemental analysis for CHN confirmed the structure of the target product. The mass spectrum illustrates the main integer masses of (9) at 371 ( $\text{M}^+$ ) which is in agreement with the proposed structure.

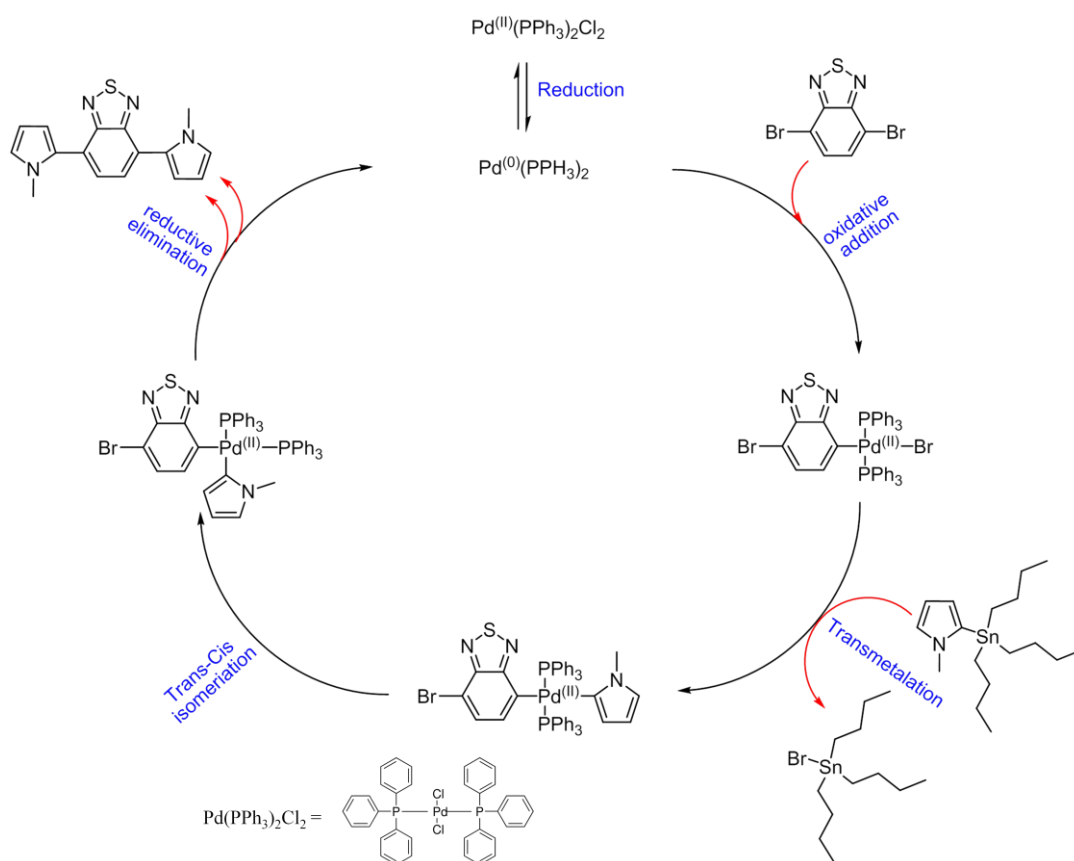
#### 4.1.10. 4,7-Bis(1-methyl-1H-pyrrol-2-yl)benzo[*c*][1,2,5]thiadiazole (10)

4,7-Bis(1-methyl-1H-pyrrol-2-yl)benzo[*c*][1,2,5]thiadiazole (10) was synthesised according to a modified procedure by Kim et al.<sup>119</sup>. The reaction was performed by heating a mixture of 4,7-dibromobenzo[*c*][1,2,5]thiadiazole (8) and 1-methyl-2-(tributylstannyl)-1H-pyrrole (9) in THF at 75 °C in the presence of an amount of catalyst  $\text{PdCl}_2(\text{PPh}_3)_2$  overnight. The purification was carried out using silica gel column chromatography eluted with petroleum ether (40:60) : ethyl acetate (9:1) then recrystallization from ethanol was carried out. The TLC gave a single spot and the yield was 74.9%.



**Scheme 21.** The preparation of 4,7-bis(1-methyl-1H-pyrrol-2-yl)benzo[*c*][1,2,5]thiadiazole (10).

There are two suggested mechanisms, the first one suggested by Stille<sup>39</sup>. The second was suggested by Espinet which is discussed in more detail.<sup>138</sup> Stille suggested that the mechanism consists of four steps (Scheme 22). The first step is oxidative addition that couples the palladium (0) catalyst to 2,7-dibromobenzo[c][1,2,5]thiadiazole (**8**) which leads to oxidation of the palladium to Pd (II). The second step is a transmetalation reaction that involves 1-methyl-2-(tributylstannyl)-1H-pyrrole (**9**) which reacts with the palladium halide complex which generates a palladium complex with methyl-pyrrole and benzothiadiazole groups. The third step is *trans-cis* isomerisation and the last step is elimination which regenerates the palladium (0) which starts again in the catalytic cycle<sup>39,138</sup>.



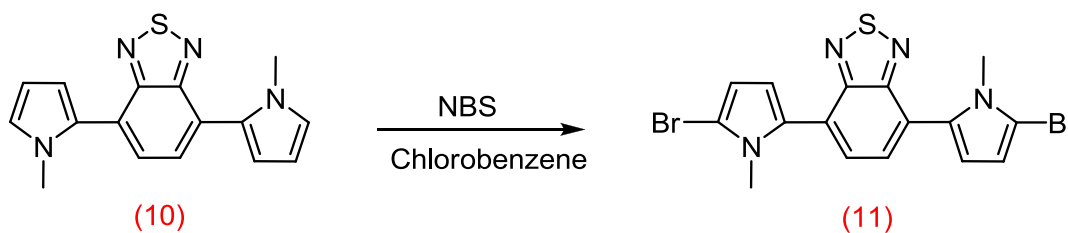
**Scheme 22. The mechanism of preparation of 4,7-bis(1-methyl-1H-pyrrol-2-yl)benzo[c][1,2,5]thiadiazole according to Stille (10).**

The structure and purity of the target product (**10**) were confirmed by TLC, <sup>1</sup>HNMR, <sup>13</sup>CNMR, elemental analysis, mass spectrometry and FT-IR. The TLC gave a single spot. The elemental analysis for CHN confirmed the structure of the

target product. The mass spectrum illustrate the main integer mass of **(10)** at 294(M<sup>+</sup>).

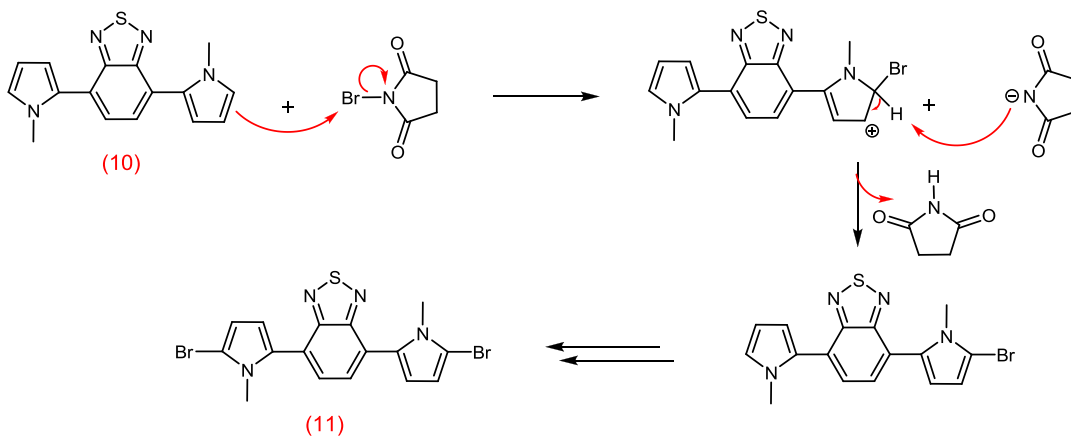
#### 4.1.11. 4,7-Bis(5-bromo-1-methyl-1H-pyrrol-2-yl)benzo[c][1,2,5]thiadiazole (**11**)

4,7-Bis(5-bromo-1-methyl-1H-pyrrol-2-yl)benzo[c][1,2,5]thiadiazole (**11**) was synthesised according to a modified procedure by Zhang et al <sup>120</sup>. The reaction was performed by heating 4,7-bis(1-methyl-1H-pyrrol-2-yl)benzo[c][1,2,5]thiadiazole (**10**) in chlorobenzene at 55 °C, NBS was added in two portions as shown in Scheme 23. The purification was carried out using silica gel column chromatography eluted with petroleum ether (60:40) : ethyl acetate (5:1). The TLC gave a single spot and the product was obtained as orange powder with 26.6% yield.



**Scheme 23. The preparation of 4,7-bis(5-bromo-1-methyl-1H-pyrrol-2-yl)benzo[c][1,2,5] thiadiazole (**11**).**

The reaction proceeds through an electrophilic substitution on the 5-position of the methyl-pyrrole units which is activated by the nitrogen atom. The reaction is very sensitive to light and so was carried out in the dark. In addition, the amount of NBS is crucial in this reaction, thus 1.95 equivalents of NBS were used to avoid forming tri- and tetra brominated products which can be difficult to separate by column chromatography from the desired product.



**Scheme 24.** The mechanism of the formation of 4,7-bis(5-bromo-1-methyl-1H-pyrrol-2-yl)benzo[c][1,2,5]thiadiazole (**11**).

The structure and purity of the target product (**11**) were confirmed by TLC,  $^1\text{H}$ NMR,  $^{13}\text{C}$ NMR, elemental analysis, mass spectrometry and FT-IR. The TLC gave a single spot and the elemental analysis for  $\text{CHNBr}$  confirmed the structure of the target product. The mass spectrum illustrates the main integer masses of (**11**), which are obtained at 450, 452, 454 ( $\text{M}^+$ ) in 1:2:1 ratio because of the bromine isotopes ( $^{81}\text{Br}$  and  $^{79}\text{Br}$ ).

The  $^1\text{H}$ NMR spectrum confirms the chemical structure of 4,7-bis(5-bromo-1-methyl-1H-pyrrol-2-yl)benzo[c][1,2,5]thiadiazole (**11**) as shown in Figure 34. It can be seen that the singlet peak at 7.58 ppm is related to the benzothiadiazole protons in the position (a) and doublet peaks at 6.88 and 6.56 ppm can be assigned to the methyl-pyrrole protons in positions (b) and (c). The singlet peak at 3.67 ppm can be assigned to the methyl group protons on position (d). The  $^{13}\text{C}$ NMR spectrum illustrates seven peaks in the aromatic region from 153.8 to 95.7 which corresponds very well with the structure of the target product. The FT-IR of the target product illustrates the stretching vibration bands for the aromatic C-Br at  $1082\text{ cm}^{-1}$ .

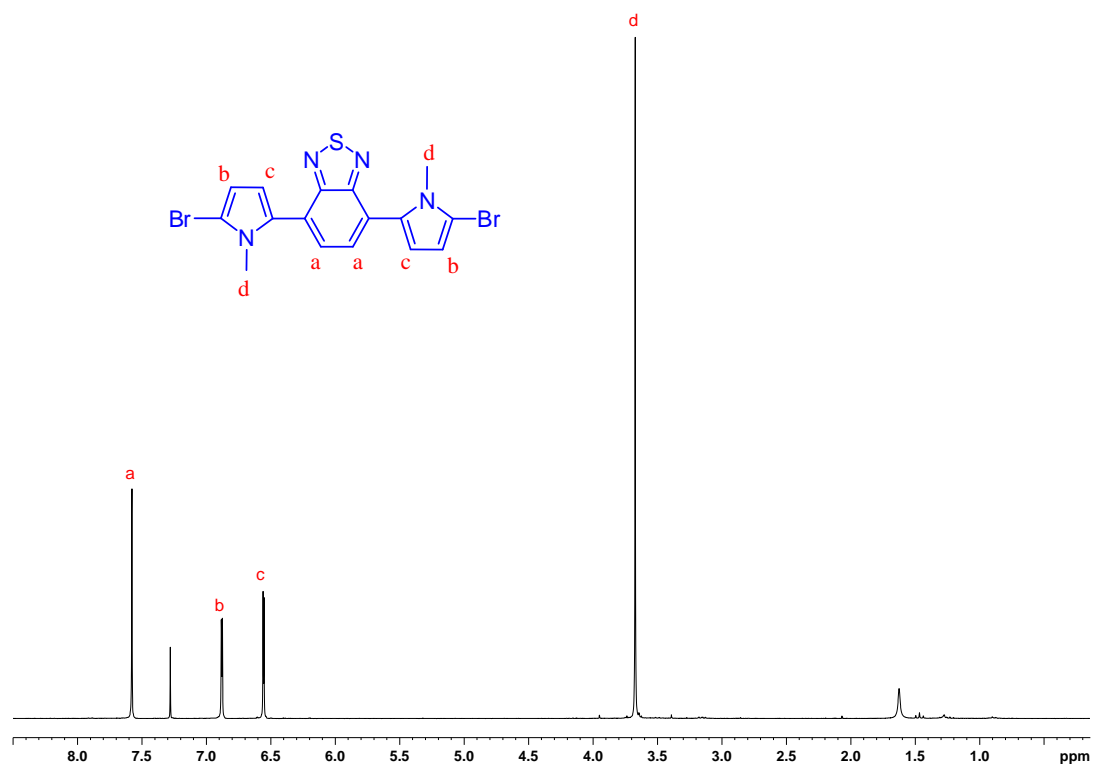


Figure 34. The <sup>1</sup>H NMR spectrum for 4,7-bis(5-bromo-1-methyl-1H-pyrrol-2-yl)benzo[c][1,2,5]thiadiazole (11).

## 4.2. Synthesis of monomers of polymers (P4, P5 and P6)

In order to prepare **P4**, **P5** and **P6**, monomers (**7**), (**18**), (**35**) and (**36**) (Figure 35) were needed. Monomer (**35**) was prepared by S. Alfifi of the Iraqi group and monomer (**36**) was bought from Sigma Aldrich.

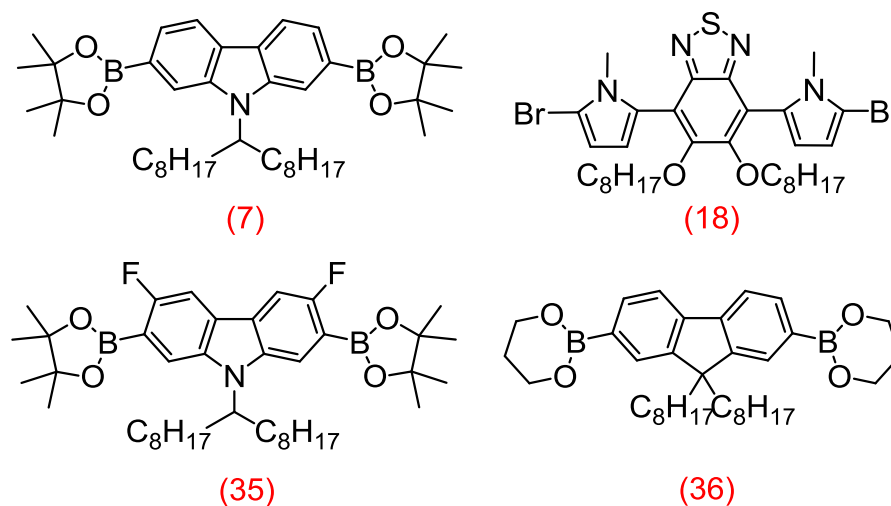
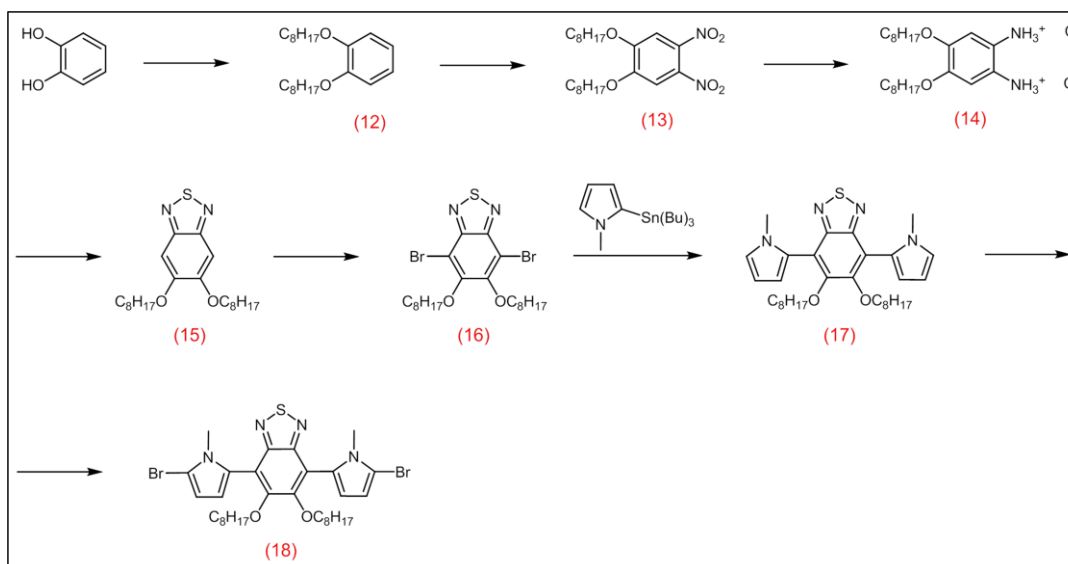


Figure 35. Monomers required for preparing P4, P5 and P6.

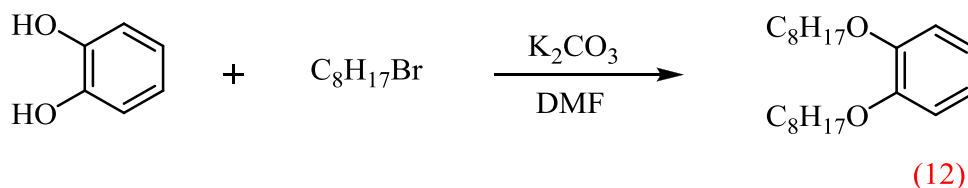
The preparation route of 4,7-bis(5-bromo-1-methyl-1H-pyrrol-2-yl)-5,6-bis(octyloxy)benzo[*c*][1,2,5]thiadiazole (**18**) consists of eight steps starting from starting from catechol as shown in Scheme 25.



Scheme 25. The preparation route of 4,7-bis(5-bromo-1-methyl-1H-pyrrol-2-yl)-5,6-bis(octyloxy)benzo[*c*][1,2,5]thiadiazole.

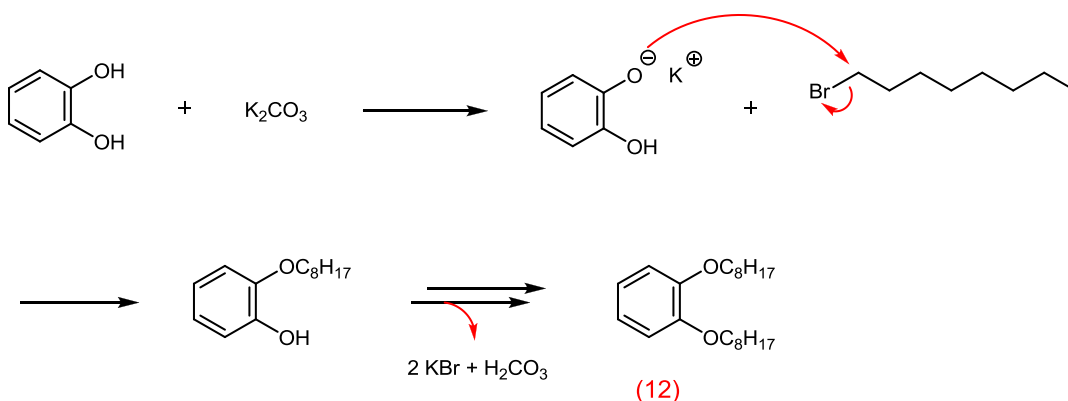
4.2.1. 1,2-Bis(octyloxy)benzene (**12**)

1,2-Bis(octyloxy)benzene (**12**) was synthesised according to a modified procedure by Janssen et al <sup>120</sup>. The reaction was performed by heating a mixture of catechol, 1-bromooctane and  $K_2CO_3$  in DMF at 100 °C for 40 hours as shown in Scheme 26. The crude product was recrystallised twice from ethanol to obtain the target product as needle like crystals. The TLC gave a single spot and the yield was 89.1%.



**Scheme 26. The preparation of 1,2-bis(octyloxy)benzene (**12**).**

The mechanism of the reaction proceeds via a nucleophilic substitution ( $S_N2$ ). The first step is deprotonation of the hydroxyl group with the  $K_2CO_3$  base then nucleophilic attack on the alkyl bromide to afford the target product as illustrated in Scheme 27.



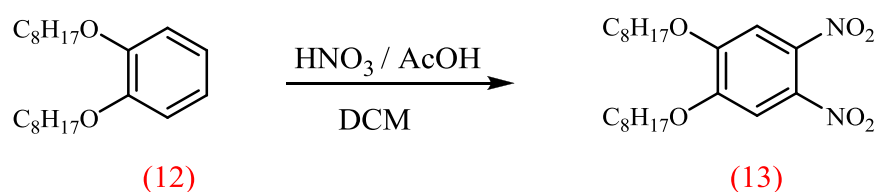
**Scheme 27. The mechanism of the preparation of 1,2-bis(octyloxy)benzene (**12**).**

The structure of the target product (**12**) was confirmed by TLC,  $^1H$ NMR,  $^{13}C$ NMR, elemental analysis, mass spectrometry, melting point and FT-IR. The melting point (25- 26 °C) is in agreement with literature value <sup>139</sup>. The elemental analysis for CH confirmed the structure of the target product. The mass spectrum illustrate the main integer mass of (**12**) at 334 ( $M^+$ ) and it is in agreement with proposed structure.

The  $^1\text{H}$ NMR spectrum shows a singlet aromatic peak at 6.92 ppm related to the four protons on the phenyl ring and triplet peaks at 4.02 and 0.92 ppm corresponding to the ( $\text{OCH}_2$ ) and ( $\text{CH}_3$ ) protons on the alkyl chains respectively. The FT-IR of the target product illustrates the stretching vibration bands at 2922 and 2853  $\text{cm}^{-1}$  for  $\text{CH}_3$  group, the stretching vibration bands for ( $\text{C} - \text{O}$ ) group appears at 1252  $\text{cm}^{-1}$ . The bending vibration at 1468 and 1386  $\text{cm}^{-1}$  are related to  $\text{CH}_2$  and  $\text{CH}_3$  bends respectively. The spectrum do not show any absorption band in the range 3100 – 3700  $\text{cm}^{-1}$  which belong to the stretching vibration bands for ( $\text{OH}$ ) group.

#### 4.2.2. 1,2-Dinitro-4,5-bis(octyloxy)benzene (13)

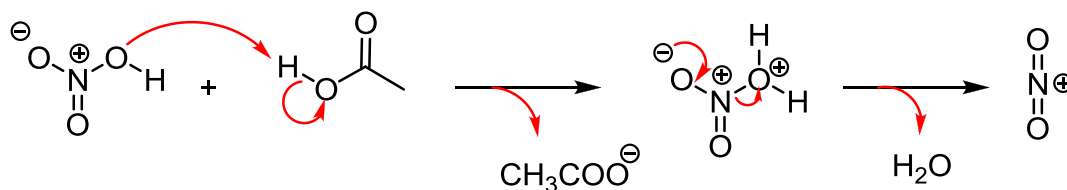
1,2-Dinitro-4,5-bis(octyloxy)benzene (**13**) was synthesised according to a modified procedure by Janssen et al <sup>120</sup>. The reaction was performed by adding nitric acid (65%) dropwise to a mixture of 1,2-bis(octyloxy)benzene (**12**) and acetic acid in DCM at 0 °C. The reaction mixture was allowed to warm to the room temperature then cooled to 0 °C and nitric acid (100%) was added dropwise. In addition, the purification was carried out using recrystallization from ethanol to obtain the target product as a yellow powder with 93% yield.



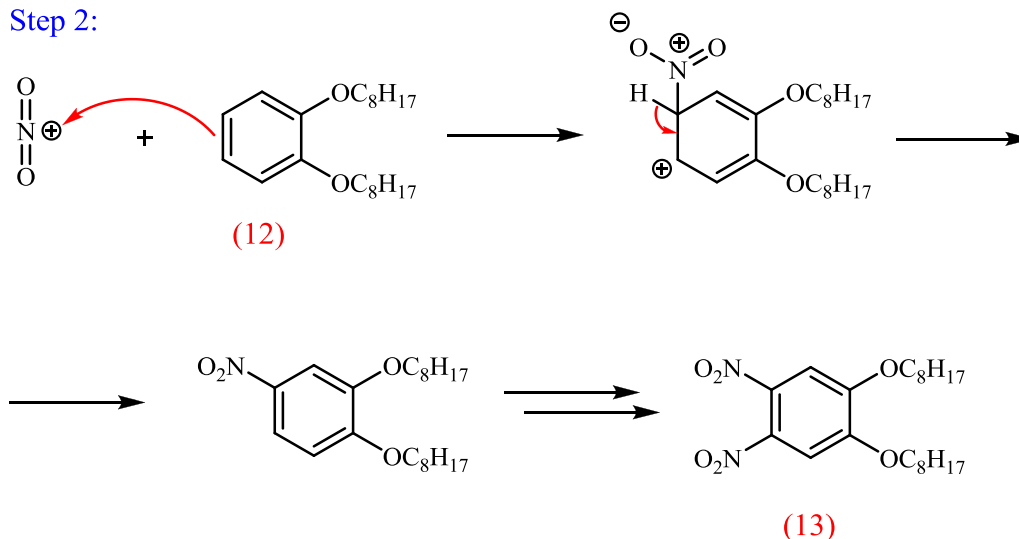
**Scheme 28. The preparation of 1,2-dinitro-4,5-bis(octyloxy)benzene (13).**

The mechanism of the reaction proceeds through two steps. The first step is generation of nitronium cation ( $\text{NO}_2^+$ ) by reacting nitric acid with acetic acid. The second step is electrophilic attack of nitronium cation on the aromatic ring at the 4- and 5- positions which are activated by the octyloxy groups as shown in Scheme 29.

Step 1:



Step 2:

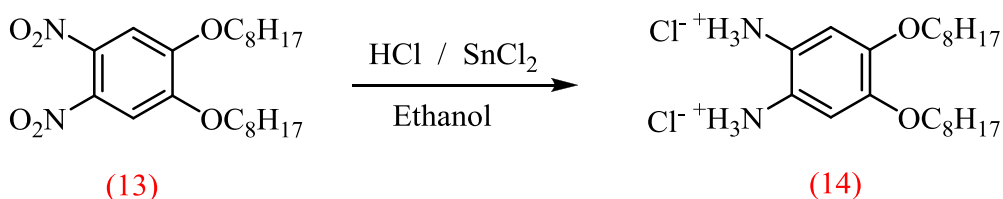


**Scheme 29. The mechanism of the preparation of 1,2-dinitro-4,5-bis(octyloxy)benzene (13)**

The structure and purity of the target product (**13**) were confirmed by  $^1\text{H}$ NMR,  $^{13}\text{C}$ NMR, elemental analysis, mass spectrometry, melting point and FT-IR. The melting point (88-90 °C) is in agreement with literature <sup>122</sup>. The elemental analysis for CHN confirmed the structure of the target product. The mass spectrum illustrates the main integer mass of (**13**) at 424 ( $M^+$ ), which is in agreement with proposed structure. The  $^1\text{H}$ NMR spectrum showed a singlet aromatic peak at 7.31 ppm as expected along with signals from the octyloxy groups. The FT-IR of the target product illustrates the stretching vibration bands for the aromatic nitro group at 2023  $\text{cm}^{-1}$  and 1354  $\text{cm}^{-1}$ . The stretch vibration band at 3071  $\text{cm}^{-1}$  is correlated to aromatic C – H bond. The bending vibration of  $\text{CH}_2$  and  $\text{CH}_3$  are displayed at 1464 and 1371  $\text{cm}^{-1}$  respectively.

### 4.2.3. 4,5-Bis(octyloxy)benzene-1,2-diaminium chloride (14)

4,5-Bis(octyloxy)benzene-1,2-diaminium chloride (**14**) was synthesised according to a modified procedure by Janssen et al <sup>120</sup>. The reaction was performed by heating a mixture of 1,2-dinitro-4,5-bis(octyloxy)benzene (**13**), SnCl<sub>2</sub>, ethanol and HCl at 85 °C overnight. The product is unstable and so it was dried under a stream of nitrogen and used directly in the next step without purification, the yield was 95 %.

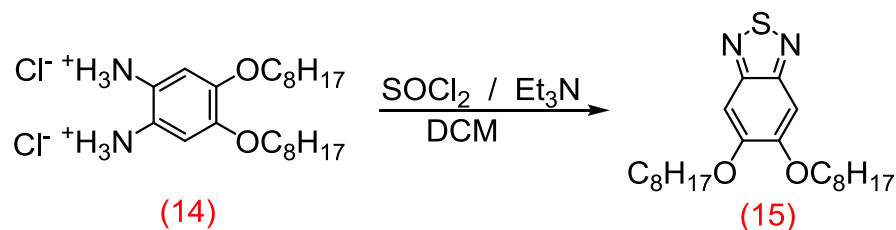


**Scheme 30. The preparation of 4,5-bis(tetradecyloxy)benzene-1,2-diaminium chloride (14).**

The structure of the target product (**14**) was confirmed by <sup>1</sup>HNMR, <sup>13</sup>CNMR, elemental analysis, mass spectrometry and FT-IR. The mass spectrum illustrate the main integer mass of (**14**) at 365 (M<sup>+</sup>), while the molecular weight for the proposed structure (**14**) is 437 g/mol due to 2 × HCl were not detected by Mass (EI<sup>+</sup>) analysis. The <sup>1</sup>HNMR spectrum showed the assumed a singlet aromatic peak at 6.66 ppm for ring protons and a broad singlet peak at 7.93 ppm for (N - H) protons and the signals of octyloxy groups were observed as expected.

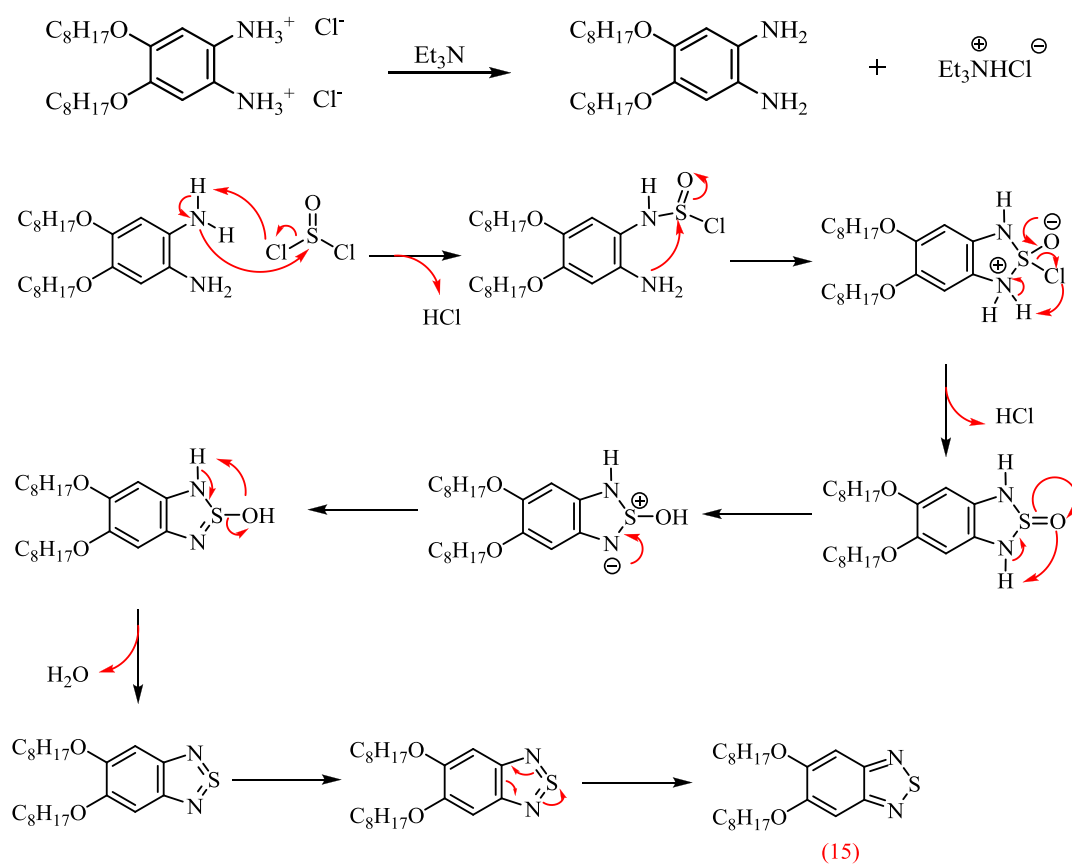
### 4.2.4. 5,6-Bis(octyloxy)benzo[c][1,2,5]thiadiazole (15)

5,6-Bis(octyloxy)benzo[c][1,2,5]thiadiazole (**15**) was synthesised according to a modified procedure by Janssen et al <sup>120</sup>. The reaction was performed by adding a solution of thionyl chloride in DCM to a mixture of 4,5-bis(octyloxy)-benzene-1,2-diaminium chloride (**14**) and triethylamine in DCM. Then the reaction mixture was heated to reflux for 6 hours. The crude product was purified by recrystallization from ethanol and the pure product was obtained as an off white powder with 92 % yield.



**Scheme 31. The preparation of 5,6-bis(octyloxy)benzo[c][1,2,5]thiadiazole (15).**

The mechanism involves two steps as shown in Scheme 32. In the first step, (14) reacts with triethyl amine which generates the diamine. The second step involves nucleophilic attack of the diamine on the sulphur of the thionyl chloride generate  $2 \times \text{HCl}$  and  $\text{H}_2\text{O}$ , and then the cyclisation occur.



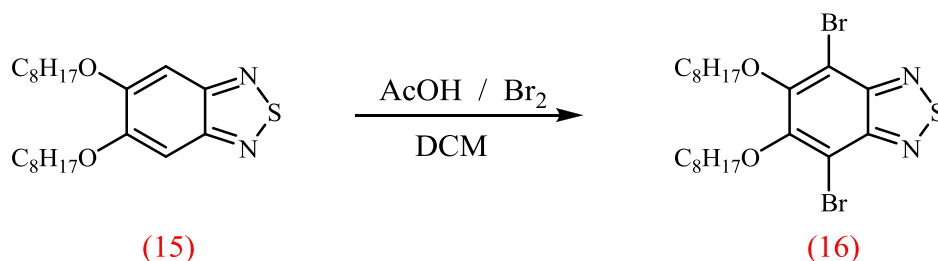
**Scheme 32. The mechanism for the preparation of (15).**

The structure and purity of the target product (15) were confirmed by  $^1\text{H}$ NMR,  $^{13}\text{C}$ NMR, elemental analysis, mass spectroscopy, melting point and FT-IR. The melting point (97-99 °C) is in agreement with literature value <sup>122</sup>. The elemental

analysis for CHN confirmed the structure of the target product. The mass spectrum illustrate the main integer mass of **(15)**, at 392 ( $M^+$ ), which is in agreement with proposed structure.

#### 4.2.5. 4,7-Dibromo-5,6-bis(octyloxy)benzo[c][1,2,5]thiadiazole (**16**)

4,7-Dibromo-5,6-bis(octyloxy)benzo[c][1,2,5]thiadiazole (**16**) was synthesised according to a modified procedure by Janssen et al <sup>120</sup>. The reaction was performed by adding bromine to a solution of 5,6-bis(octyloxy)benzo[c][1,2,5]thiadiazole (**15**) in a mixture of dichloromethane and acetic acid. The reaction mixture was stirred in the dark for 48 h at room temperature as shown in Scheme 33. The crude product was purified using column chromatography eluted with petroleum ether (40:60) then recrystallization was carried out from ethanol. The pure product (**16**) was obtained as white needles with 73%.

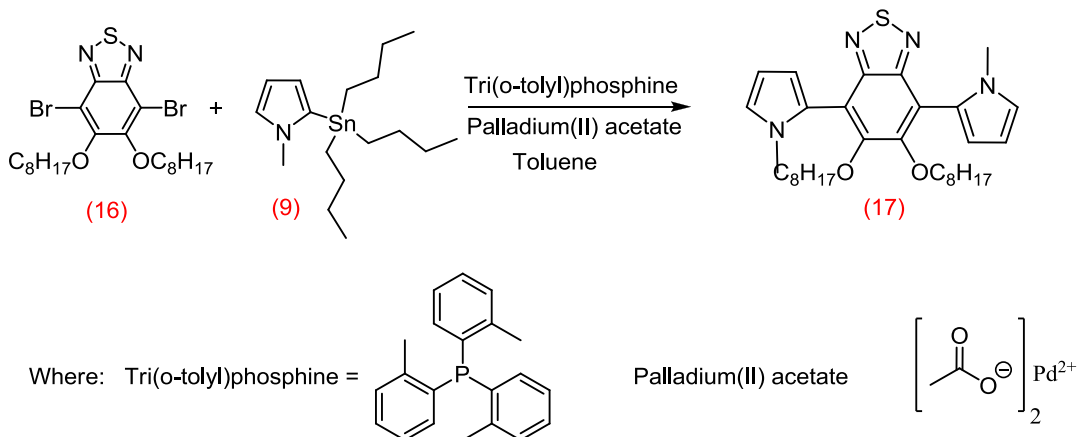


**Scheme 33. The preparation of 4,7-dibromo-5,6-bis(octyloxy)benzo[c][1,2,5]thiadiazole (**16**).**

The structure and purity of the target product (**16**) were confirmed by TLC,  $^1H$ NMR,  $^{13}C$ NMR, elemental analysis, mass spectrometry, melting point, and FT-IR. The melting point (44- 46 °C) is in agreement with literature value <sup>122</sup>. The elemental analysis for CHNBrOS confirmed the structure of the target product. The mass spectrum illustrates the main integer masses of (**16**), which are obtained at 558, 550, 552 ( $M^+$ ) in 1:2:1 intensities because of the bromine isotopes ( $^{81}Br$  and  $^{79}Br$ ).

#### 4.2.6. 4,7-Bis(1-methyl-1H-pyrrol-2-yl)-5,6-bis(octyloxy)benzo[c][1,2,5]thiadiazole (17)

4,7-Bis(1-methyl-1H-pyrrol-2-yl)-5,6-bis(octyloxy)benzo[c][1,2,5]thiadiazole (17) was synthesised according to a modified procedure by Jiang et al <sup>140</sup>. The reaction was carried out using Stille cross coupling by adding a mixture of palladium acetate and tri-*o*-tolylphosphine to a solution of 1-methyl-2-(tributylstannyl)-1H-pyrrole (9) and 4,7-dibromo-5,6 bis(octyloxy)benzo[c][1,2,5]oxadiazole (16) in dry toluene. The reaction mixture was degassed then heated under reflux for 72 h under argon.



**Scheme 34. The preparation of 4,7-bis(1-methyl-1H-pyrrol-2-yl)-5,6-bis(octyloxy)benzo[c][1,2,5]thiadiazole (17).**

The residue was purified by column chromatography on silica gel (petroleum ether (40:60): ethyl acetate (9:1)). The <sup>1</sup>HNMR and mass spectrometry show impure material so purification using HPLC eluting with H<sub>2</sub>O: THF (30:70 %) was carried out, but the product could not be purified. Pure product is crucial at this step because it is followed by a bromination step which requires accurate calculation in order to avoid over bromination which could result in mixture that is very difficult to purify and so 4,7-bis(5-bromo-1-methyl-1H-pyrrol-2-yl)-5,6-bis(octyloxy)benzo[c][1,2,5]thiadiazole (18), **P4**, **P5** and **P6** could not be prepared and this section of project was then abandoned.

## 4.3. Synthesis of monomers for copolymers (P7, P8 and P9)

In order to prepare **P7**, **P8** and **P9**, monomers (**23**) and (**25**) (Figure 36) were prepared successfully. In addition, (**37**) and (**38**) were prepared by S. Alfifi and A. Alghamdi of the Iraqi group respectively, using the same preparation route that used for 4,7-bis(5-bromo-1-methyl-1H-pyrrol-2-yl)-5,6-bis(octyloxy)benzo[c][1,2,5]thiadiazole (**18**) as shown in Figure 36.

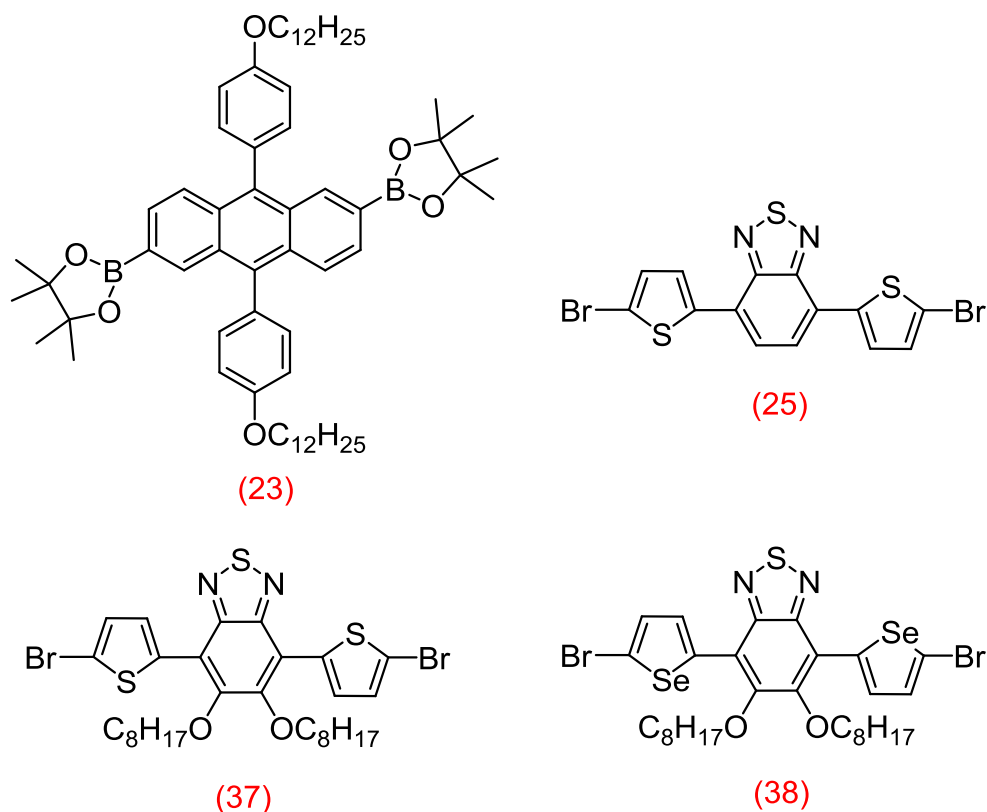
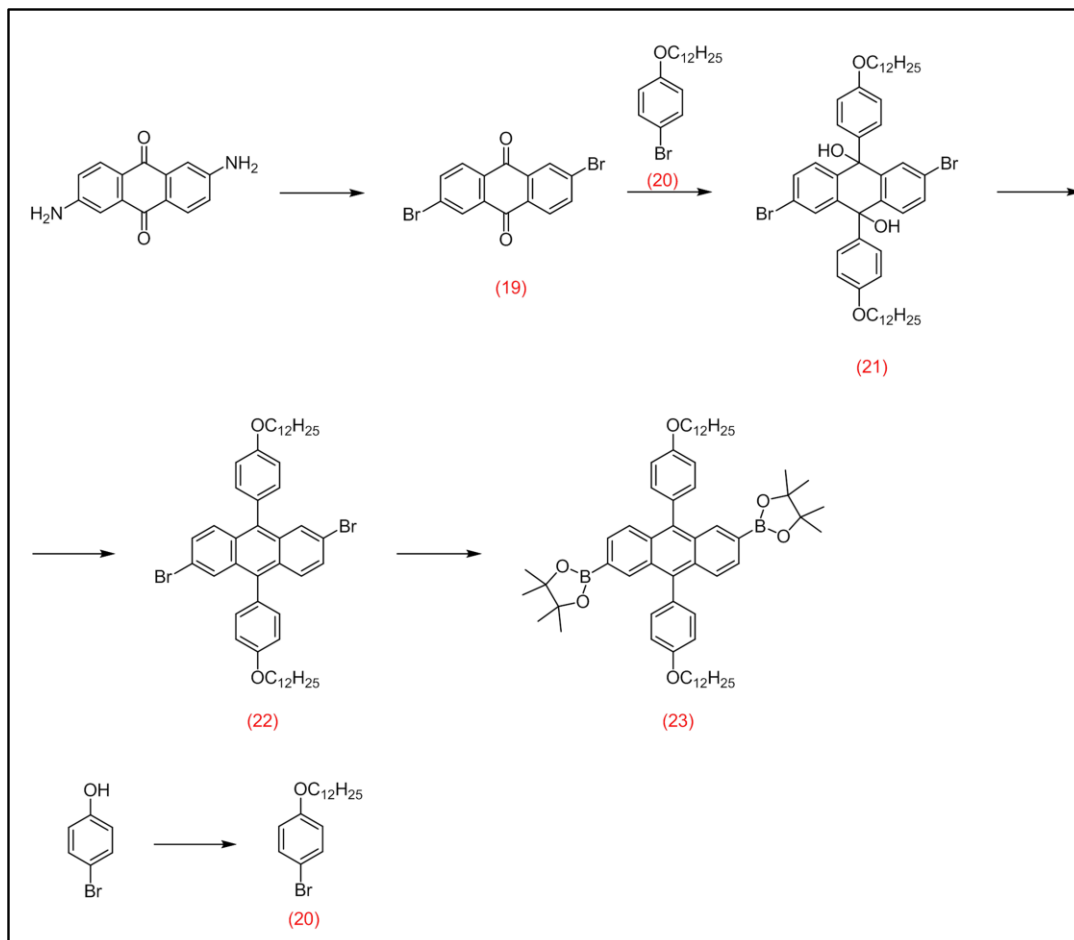


Figure 36. Monomers required for preparing P7, P8 and P9.

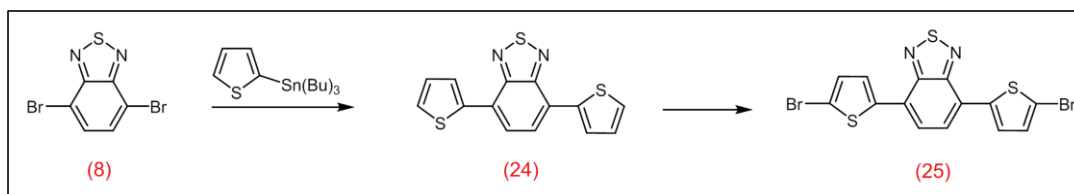
A series of intermediates were prepared successfully in order to prepare 2,2'-(9,10-bis(4-(dodecyloxy)phenyl)anthracene-2,6-diyl)bis(4,4,5,5-tetramethyl-1,3,2-dioxaborolane) (**23**) and 4,7-bis(5-bromothiophen-2-yl)benzo[c][1,2,5]thiadiazole (**25**), and their structure and purity were confirmed by by TLC,  $^1\text{H}$ NMR,  $^{13}\text{C}$ NMR, elemental analysis, mass spectrometry, melting point, and FT-IR.

Monomer (**23**) was prepared in five steps as shown in Scheme 35 starting from 2,6-diaminoanthraquinone.



**Scheme 35.** The preparation route of 2,2'-(9,10-bis(4-(dodecyloxy)phenyl)anthracene-2,6-diyl)bis(4,4,5,5-tetramethyl-1,3,2-dioxaborolane) (23).

Monomer (25) was prepared in two steps as shown in Scheme 36 starting from 4,7-dibromobenzo[c][1,2,5]thiadiazole and tributyl(thiophen-2-yl)stannane.

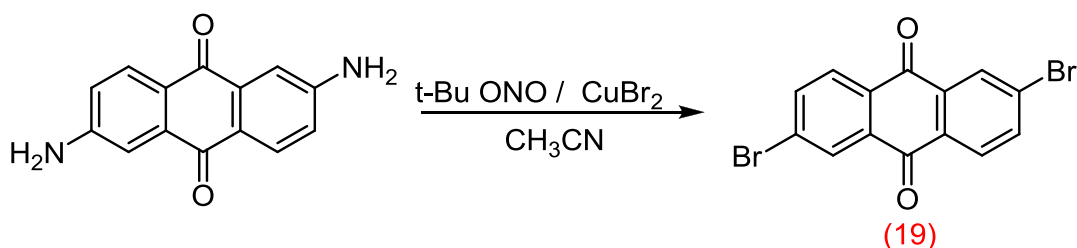


**Scheme 36.** The preparation route of 4,7-bis(5-bromothiophen-2-yl)benzo[c][1,2,5]thiadiazole (25).

The preparations of the various intermediates toward (23) and (25) are discussed below.

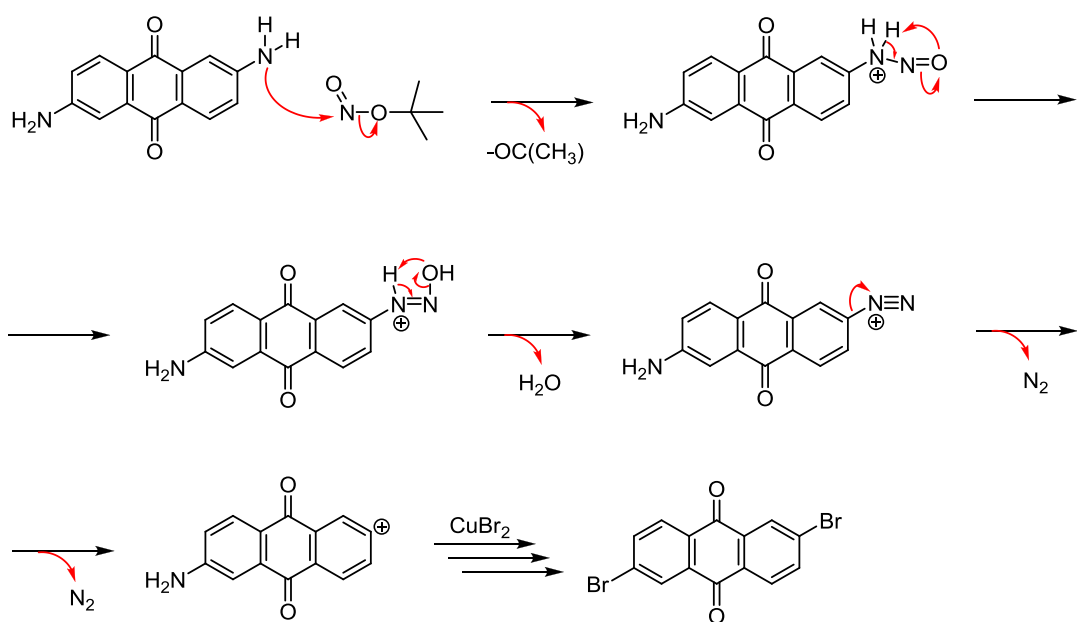
### 4.3.1. 2,6-Dibromoanthracene-9,10-dione (19)

The preparation of 2,6-dibromoanthracene-9,10-dione (**19**) was carried out according to a modified method by Vila et al <sup>123</sup>. The reaction was performed by heating a mixture of 2,6-diaminoanthraquinone, t-Bu ONO, CuBr<sub>2</sub> in acetonitrile for two hours as shown in Scheme 37. In addition, the purification was carried out using recrystallization from 1,4-dioxane to obtain the target product (**18**) as yellow crystals. The TLC gave a single spot and the yield was 85%.



**Scheme 37.** The preparation of 2,6-dibromoanthracene-9,10-dione (**19**).

The reaction proceeds through a Sandmeyer reaction which is used to prepare aryl halide from aryl diazonium salts <sup>141</sup>. The reaction involves two steps. The first step is reaction between amine in 2,6-diaminoanthraquinone and nitrite which forms an aryl diazonium salt. In second step, the result complex from the first step reacts with copper bromide to obtain the target product.



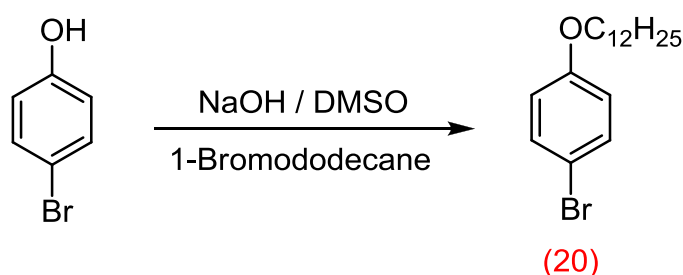
**Scheme 38.** The mechanism of the preparation of 2,6-dibromoanthracene-9,10-dione.

The structure and purity of the target product (**19**) were confirmed by TLC,  $^1\text{H}$ NMR,  $^{13}\text{C}$ NMR, elemental analysis, mass spectrometry, melting point and FT-IR. The TLC gave a single spot and the melting point (284-285 °C) is in agreement with literature value <sup>124</sup>. The elemental analysis for CHBr confirmed the structure of the target product. The mass spectrum illustrates the main integer masses of (**19**) at 364, 366, 368 ( $\text{M}^+$ ) in 1:2:1 intensities because of the bromine isotopes ( $^{81}\text{Br}$  and  $^{79}\text{Br}$ ).

The  $^1\text{H}$ NMR spectrum confirm the structure of the target product (**19**). It shows doublet signals at 8.46 and 8.20 ppm as well as a doublet of doublet at 7.97 ppm in the aromatic region. The FT-IR of the target product shows the stretching vibration bands for the (C-Br) bond at  $1067\text{ cm}^{-1}$ .

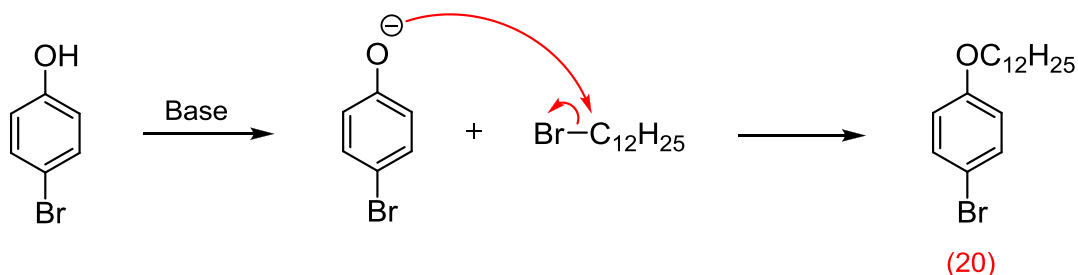
#### 4.3.2. 1-Bromo-4-(dodecyloxy)benzene (**20**)

The preparation of 1-bromo-4-(dodecyloxy)benzene (**20**) was carried out according to a modified method by Nucklolls et al <sup>125</sup>. The reaction was performed by heating a mixture of 4-bromophenol, NaOH and 1-bromododecane in DMSO overnight (Scheme 39). The purification was carried out using recrystallization from ethanol to obtain the target product (**19**) as white crystals. The TLC gave a single spot and the yield was 76.6%.



**Scheme 39. The preparation of 1-bromo-4-(dodecyloxy)benzene (**20**).**

The reaction proceeds through two steps. The first step is deprotonation of the phenol with the base then nucleophilic attack on the alkyl bromide which leads to the formation of the target product.

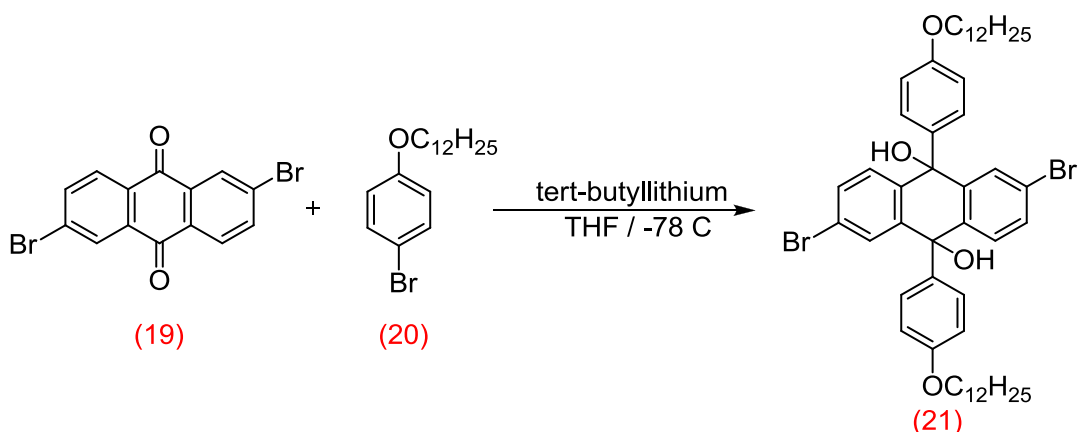


**Scheme 40.** The mechanism of the preparation of 1-bromo-4-(dodecyloxy)benzene.

The structure and purity of the target product **(20)** were confirmed by TLC,  $^1\text{H}$ NMR,  $^{13}\text{C}$ NMR, elemental analysis, mass spectrometry, melting point and FT-IR. The TLC gave a single spot and the melting point (37-38 °C) is in agreement with literature value <sup>126</sup>. The mass spectrum illustrate the main integer masses of **(19)**, at 340, 342 ( $\text{M}^+$ ), which is in agreement with proposed structure.

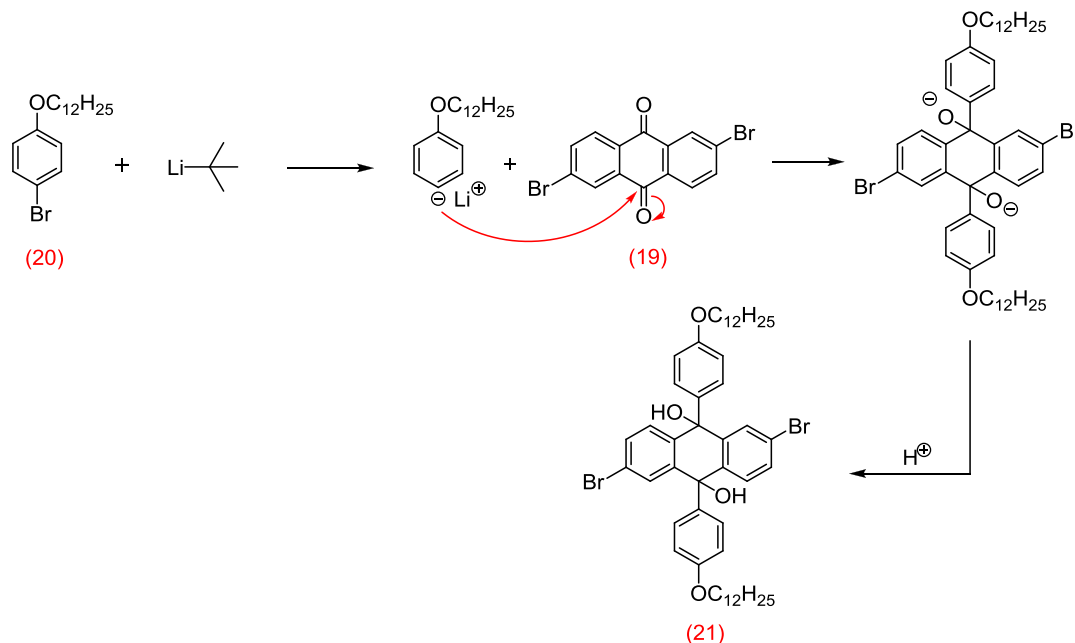
#### 4.3.3. 2,6-Dibromo-9,10-bis(4-(dodecyloxy)phenyl)-9,10-dihydroanthracene 9,10-diol (**21**)

The preparation of 2,6-dibromo-9,10-bis(4-(dodecyloxy)phenyl)-9,10-dihydroanthracene-9,10-diol (**21**) was performed according to a modified method by Wang et al <sup>127</sup>, that by adding *t*-BuLi to a solution of **(20)** in THF at  $-78\text{ }^\circ\text{C}$  then **(19)** was added to the mixture. In addition, the purification was carried out using column chromatography with ethyl acetate/ petroleum ether (1/10) (v/v).



**Scheme 41.** The preparation of 2,6-dibromo-9,10-bis(4-(dodecyloxy)phenyl)-9,10-dihydroanthracene-9,10-diol (**21**).

The reaction proceeds through two steps. The first step is a lithiation reaction and the second step is nucleophilic attack of dodecyloxy phenyl on the positions 9- and 10- in 2,6-dibromoanthracene-9,10-dione.



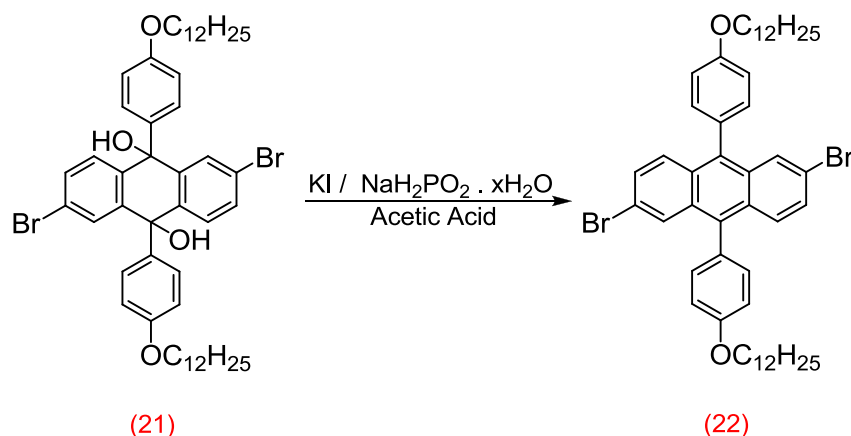
**Scheme 42.** The mechanism of the preparation of 2,6-dibromo-9,10-bis(4-(dodecyloxy)phenyl)-9,10-dihydroanthracene-9,10-diol (**21**).

The structure and purity of the target product **(21)** were confirmed by TLC,  $^1H$ NMR,  $^{13}C$ NMR, elemental analysis, mass spectrometry and FT-IR. The TLC gave a single spot and the elemental analysis for  $CHBr$  confirmed the structure of the target product. The mass spectrum illustrate the main integer masses of **(21)** at 888.2, 890.2, 892.2 ( $M^+$ ) in 1:2:1 intensities because of the bromine isotopes ( $^{81}Br$  and  $^{79}Br$ ).

#### 4.3.4. 2,6-Dibromo-9,10-bis(4-(dodecyloxy)phenyl)anthracene (**22**)

The preparation of 2,6-dibromo-9,10-bis(4-(dodecyloxy)phenyl)anthracene (**22**) was carried out according to a modified method by Wang et al <sup>127</sup>. The reaction was performed by heating a mixture of 2,6-dibromo-9,10-bis(4-(dodecyloxy)phenyl)-9,10-dihydroanthracene-9,10-diol (**19**), KI,  $NaH_2PO_2 \cdot H_2O$  in

acetic acid for 40 minutes as shown in Scheme 43. The purification was carried out using column chromatography eluting with DCM/ petroleum ether (1/4) (v/v) then recrystallisation from hexane to obtain the target product as a yellow solid. The TLC gave single spot and the yield was 63.4 %.



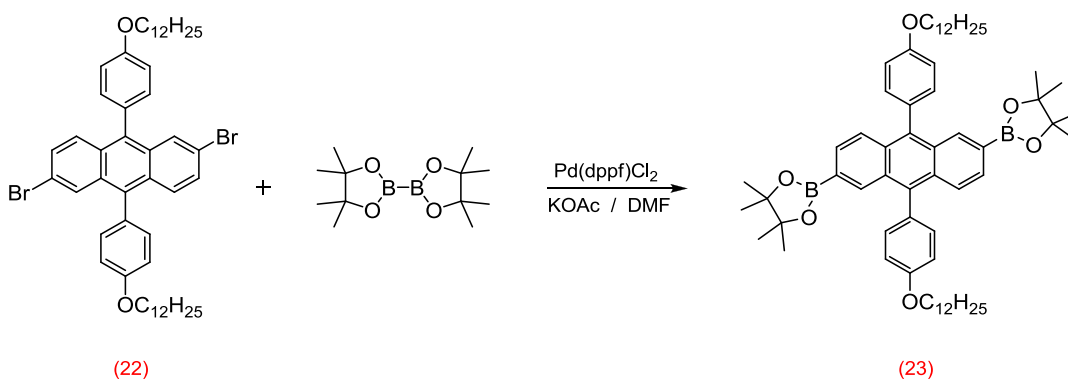
**Scheme 43. The preparation of 2,6-dibromo-9,10-bis(4-(dodecyloxy)phenyl)anthracene (22).**

The structure and purity of the target product (22) were confirmed by TLC, <sup>1</sup>HNMR, <sup>13</sup>CNMR, elemental analysis, mass spectrometry, and FT-IR. The TLC gave a single spot and the elemental analysis for CHBr confirmed the structure of the target product. The mass spectrum illustrate the main integer masses of (22) at 854.2, 856.3, 857.2 (M<sup>+</sup>)<sup>+</sup> in 1:2:1 intensities because of the bromine isotopes (<sup>81</sup>Br and <sup>79</sup>Br). The <sup>1</sup>HNMR, <sup>13</sup>CNMR and FT-IR correspond very well with the structure of target product. The FT-IR around (O - H) group at 3402 cm<sup>-1</sup> and the aromatic (C - O) stretch vibration at 1180 cm<sup>-1</sup> disappeared.

#### 4.3.5. 2,2'-(9,10-Bis(4-(dodecyloxy)phenyl)anthracene-2,6-diyl)bis(4,4,5,5-tetramethyl-1,3,2-dioxaborolane) (23)

The preparation of 2,2'-(9,10-bis(4-(dodecyloxy)phenyl)anthracene-2,6-diyl)bis(4,4,5,5-tetramethyl-1,3,2-dioxaborolane) (23) was carried out according to a modified method by Jo et al <sup>115</sup>. The reaction was performed by heating a mixture of 2,6-dibromo-9,10-bis(4-(dodecyloxy)phenyl)anthracene (22), bis(pinacolate)

diboron, potassium acetate and Pd(dppf)Cl<sub>2</sub> in DMF at 100 °C for 36 hours as shown in Scheme 44. An excess of bis(pinacolato) diboron was used to prevent the creation of oligomers. The colour change to a dark black solution was noticed during the reaction. The purification was carried out using recrystallization from diethyl ether and methanol. Firstly, methanol was passed through a basic alumina column to remove any acidic traces in the solvent as boronic esters are very sensitive to acids (lead to degradation). The product was dissolved in the lowest amount of diethyl ether and added to the hot methanol so diethyl ether was evaporated and the target product precipitate and the impurities were dissolved in methanol. The target product was obtained as yellow powder with 69.1 % yield.



**Scheme 44. The preparation of 2,2'-(9,10-bis(4-(dodecyloxy)phenyl)anthracene-2,6-diyl)bis(4,4,5,5-tetramethyl-1,3,2-dioxaborolane) (23).**

The structure and purity of the target product (**23**) were confirmed by <sup>1</sup>HNMR, <sup>13</sup>CNMR, elemental analysis, mass spectrometry and FT-IR. The elemental analysis for CH confirmed the structure of the target product. The mass spectrum illustrates the main integer masses of (**23**) at 950.5 (M<sup>+</sup>). The <sup>1</sup>HNMR spectrum confirms the chemical structure of the target monomer. The spectrum shows a singlet peak at 8.32 ppm which corresponds to the protons on position (a) in the anthracene. Also, the spectrum reveal two doublet peaks at 7.70 and 7.66 ppm which are related to the anthracene protons in the positions (b) and (c) respectively. It can be seen that the doublet peaks at 7.40, 7.17 ppm can be assigned to the attached phenyl group protons on positions (d) and (e) respectively. The broad singlet peak at 4.17 ppm corresponds to the protons on the carbon which is bonded directly to the oxygen atom of the phenyl in the position (f). The triplet peak at 0.92 ppm can be assigned

to the six protons on the CH<sub>3</sub> group at the end of the alkyl chain. In addition, the spectrum shows a singlet absorption at 1.32 ppm for methyl protons of the boronic ester group as shown in Figure 37. The FT-IR of the target product illustrates the stretching vibration bands for the (B - O) at 1370 and 1340 cm<sup>-1</sup> and the stretch vibration at 1076 cm<sup>-1</sup> which is correlated to the C-B bond.

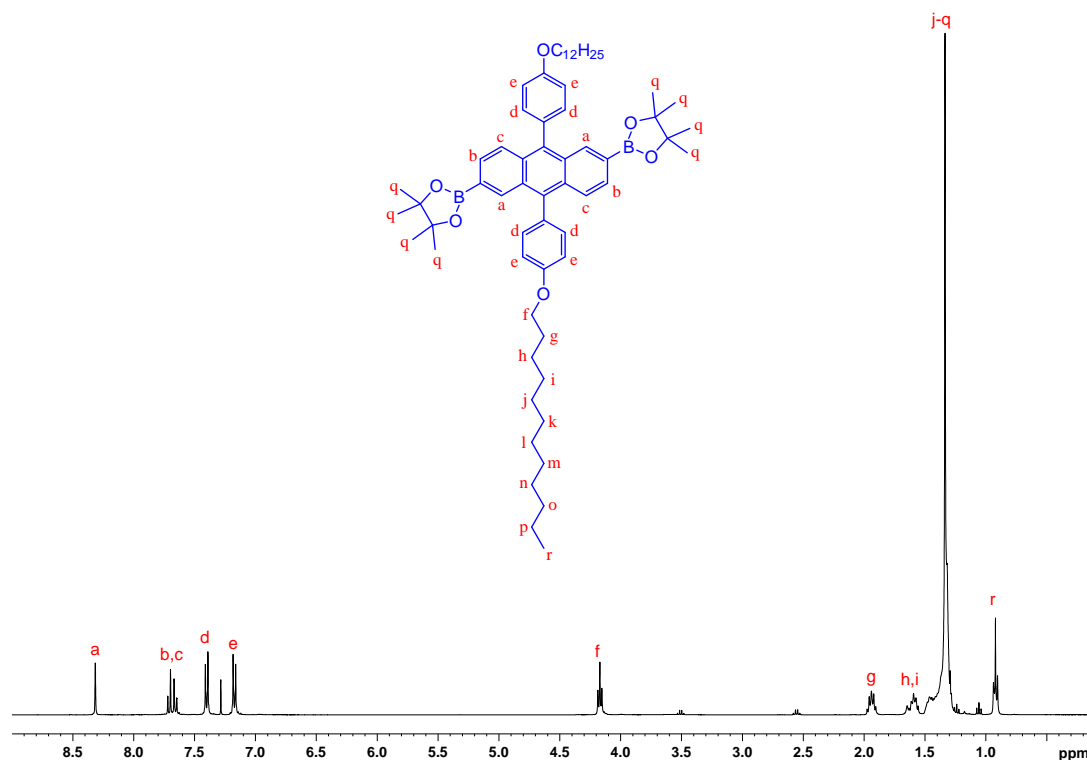
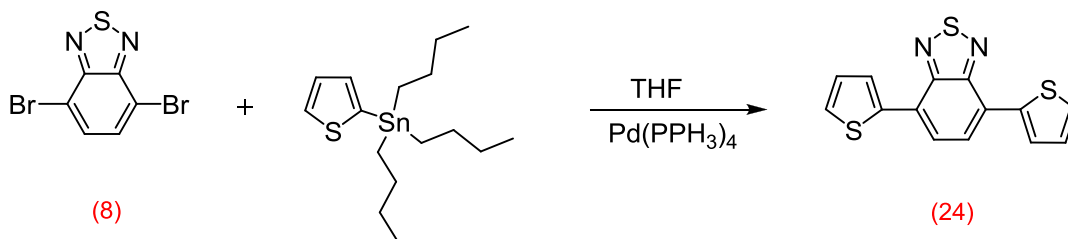


**Figure 37.** The <sup>1</sup>H NMR spectrum of 2,2'-(9,10-bis(4-(dodecyloxy)phenyl)anthracene-2,6-diyl)bis(4,4,5,5-tetramethyl-1,3,2-dioxaborolane) (**23**)

#### 4.3.6. 4,7-Di(thiophen-2-yl)benzo[c][1,2,5]thiadiazole (**24**)

The preparation of 4,7-di(thiophen-2-yl)benzo[c][1,2,5]thiadiazole (**24**) was performed according to a modified method by Palama et al.<sup>128</sup>. The reaction was carried out by heating a mixture of 4,7-dibromobenzo[c][1,2,5]thiadiazole (**8**) and tributyl(thiophen-2-yl)stannane in toluene at 120 °C in the presence of Pd(PPh<sub>3</sub>)<sub>4</sub> catalyst for 24 hours. The purification was carried out using silica gel column chromatography eluting with petroleum ether (40:60) : toluene (2:1) then recrystallization from ethanol. The TLC gave a single spot and the yield was 75%.

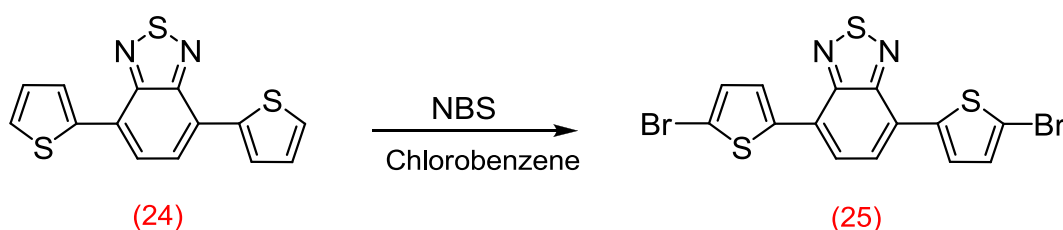


**Scheme 45. The preparation of 4,7-di(thiophen-2-yl)benzo[c][1,2,5]thiadiazole (24).**

The structure and purity of the target product (**24**) were confirmed by TLC,  $^1\text{H}$ NMR,  $^{13}\text{C}$ NMR, elemental analysis, mass spectroscopy and FT-IR. The TLC gave a single spot and the melting point (122-124 °C) is in a good agreement with the literature value <sup>129</sup>. The elemental analysis for CHN confirmed the structure of the target product. The mass spectrum shows the main integer mass of (**24**) at 300 ( $\text{M}^+$ ) and it corresponds very well with the proposed structure.

#### 4.3.7. 4,7-Bis(5-bromothiophen-2-yl)benzo[c][1,2,5]thiadiazole (25)

4,7-Bis(5-bromothiophen-2-yl)benzo[c][1,2,5]thiadiazole (**25**) was synthesised according to a modified procedure by Zhang et al <sup>120</sup>. The reaction was performed by heating 4,7-di(thiophen-2-yl)benzo[c][1,2,5]thiadiazole (**24**) in chlorobenzene at 55 °C, N-bromosuccinimide (NBS) was added in two portions. The crude product was purified via recrystallization from chlorobenzene. The product was obtained as red crystals with an 80% yield.



**Scheme 46. The preparation of 4,7-bis(5-bromothiophen-2-yl)benzo[c][1,2,5]thiadiazole (25).**

The structure and purity of the target product (**25**) were confirmed by  $^1\text{H}$ NMR,  $^{13}\text{C}$ NMR, elemental analysis, mass spectrometry and FT-IR. The elemental analysis for CHNBr confirmed the structure of the target product and the melting point (255-

258 °C) is in a good agreement with the literature value <sup>130</sup>. The mass spectrum illustrate that the main integer masses of (**25**) at 456, 458, 460 ( $M^+$ ) in 1:2:1 intensities because of the bromine isotopes (<sup>81</sup>Br and <sup>79</sup>Br). The <sup>1</sup>HNMR spectrum shows (Figure 38) a singlet peak at 7.82 ppm which corresponds to the benzothiadiazole protons. The doublet peaks at 7.84 and 7.19 ppm are related to thiophene protons in the positions (a) and (c) respectively.

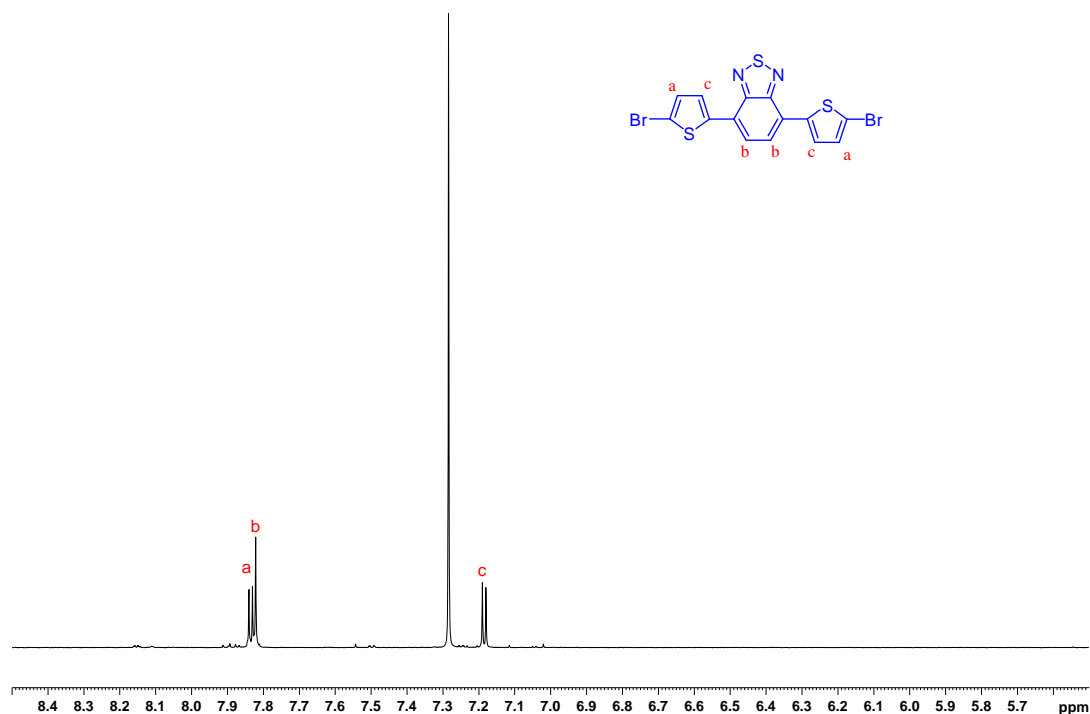


**Figure 38.** The <sup>1</sup>HNMR spectrum for 4,7-bis(5-bromothiophen-2-yl)benzo[c][1,2,5]thiadiazole (**25**).

#### 4.4. Synthesis of monomers for copolymers (P10, P11 and P12)

In order to prepare **P10**, **P11** and **P12**, monomer (**31**) (Figure 39) was required. In addition, monomers (**37**) and (**38**) were prepared by S. Alfifi and Dr. Y. Hunan of the Iraqi group respectively, using the same preparation route that used for (**18**).

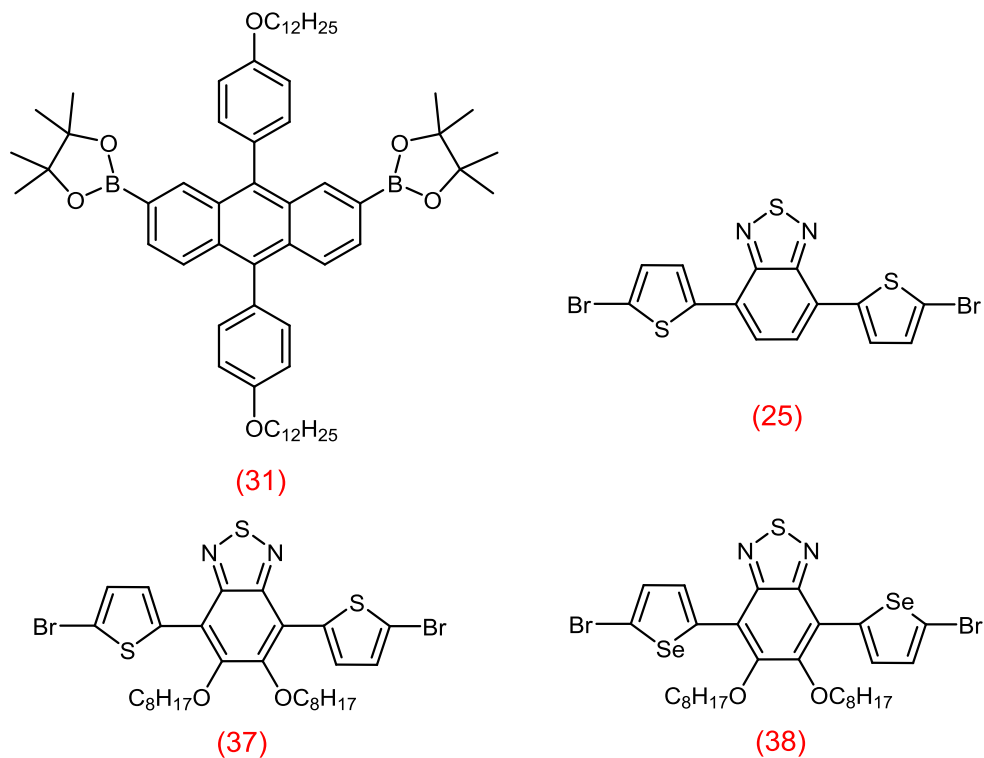
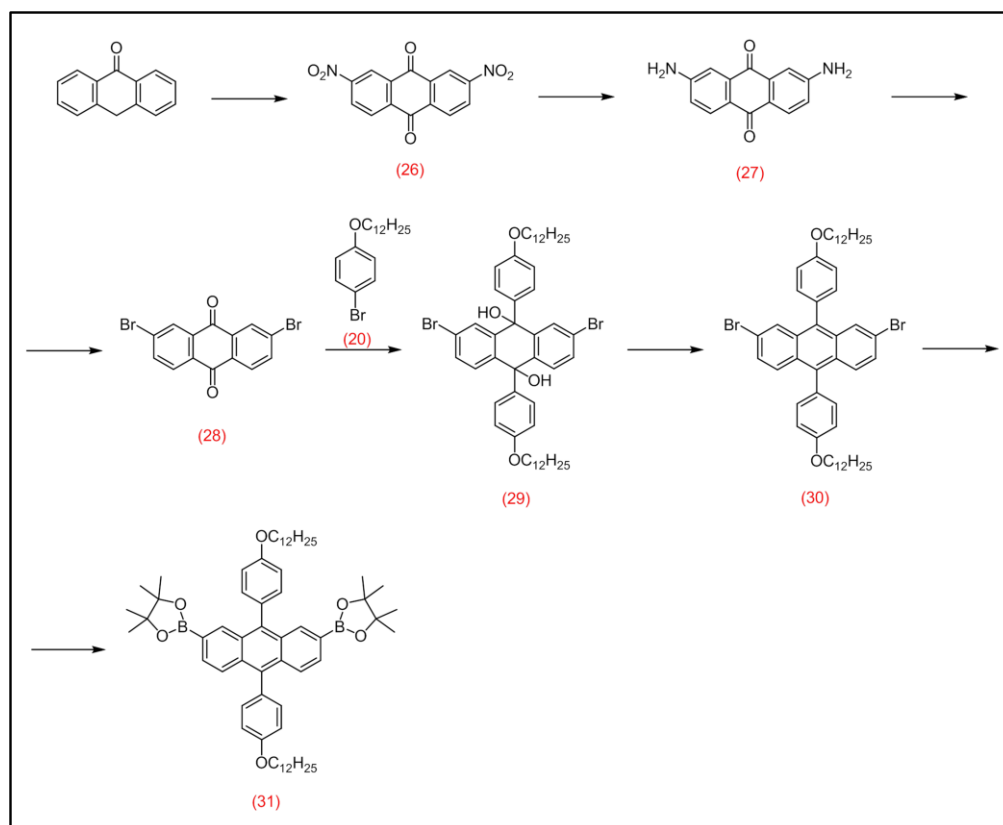


**Figure 39. Monomers required for preparing P10, P11 and P12.**

A series of intermediates for the monomers were prepared successfully in order to prepare 2,2'-(9,10-bis(4-(dodecyloxy)phenyl)anthracene-2,7-diyl)bis(4,4,5,5-tetramethyl-1,3,2-dioxaborolane) (**31**), and their structure and purity were confirmed by TLC, <sup>1</sup>HNMR, <sup>13</sup>CNMR, elemental analysis, mass spectroscopy, melting point, and FT-IR.

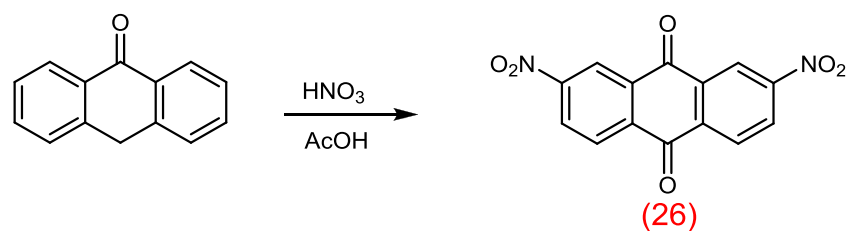
Monomer (**31**) was prepared in six steps as shown in Scheme 47, starting from anthrone.



Scheme 47. The preparation route of 2,2'-(9,10-bis(4-(dodecyloxy)phenyl)anthracene-2,7-diyl)bis(4,4,5,5-tetramethyl-1,3,2-dioxaborolane) (31).

#### 4.4.1. 2,7-Dinitro-9,10-anthraquinone (26)

The preparation of 2,7-dinitro-9,10-anthraquinone (**26**) was carried out according to a modified method by Yang et al.<sup>131</sup> The reaction was performed by adding anthrone to fuming nitric acid at 0 – 5 °C then acetic acid was added slowly to the reaction mixture with cooling as shown in Scheme 48. In addition, the crude product was recrystallised from acetic acid and then from a mixture of nitrobenzene / acetic acid (1/1) to obtain the target product as a yellow solid in a yield of 23%.

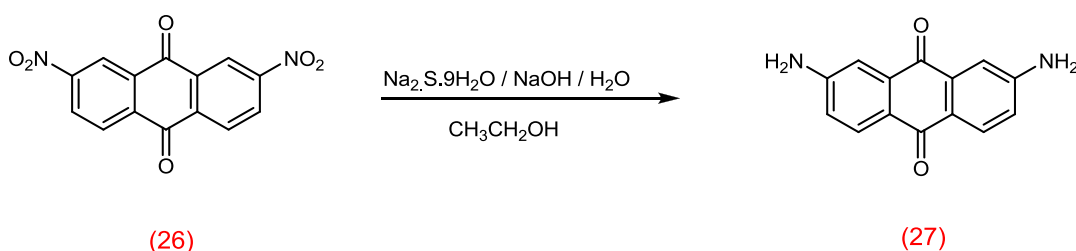


Scheme 48. The preparation of 2,7-dinitro-9,10-anthraquinone (26).

The structure and purity of the target product (**26**) were confirmed by  $^1\text{H}$ NMR, elemental analysis, mass spectrometry, melting point and FT-IR. The melting point (289-291 °C) is in agreement with literature value <sup>132</sup> and the elemental analysis for CHN confirmed the structure of the target product. The mass spectrum illustrate the main integer mass of (**26**) are obtained at 299 ( $\text{M}^+$ ) which is in agreement with the proposed structure.

#### 4.4.2. 2,7-Diaminoanthracene-9,10-dione (**27**)

The preparation of 2,7-diaminoanthracene-9,10-dione (**27**) was carried out according to a modified method by Yang et al <sup>131</sup>. The reaction was performed by adding 2,7-dinitroanthracene-9,10-dione (**26**) in ethanol to a mixture solution of sodium sulfide nonahydrate and sodium hydroxide in water. The mixture was heated at reflux for 6 h and left to stir overnight. The purification was carried out through recrystallization from ethanol to obtain the target product as an orange/red solid with 90% yield.



**Scheme 49. The preparation of 2,7-diaminoanthracene-9,10-dione (**27**).**

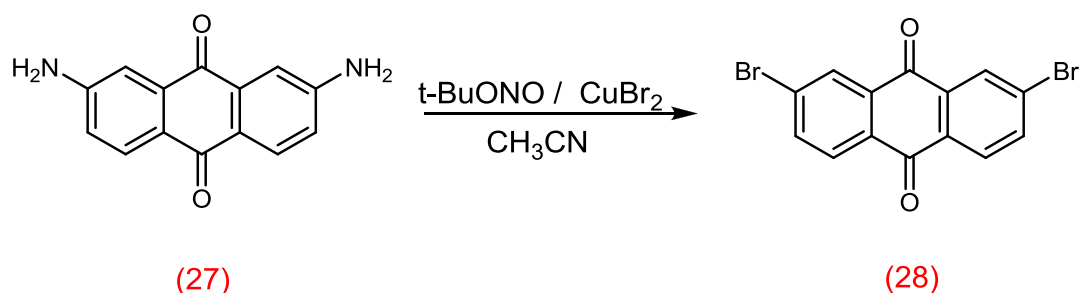
The structure and purity of the target product (**27**) were confirmed by  $^1\text{H}$ NMR,  $^{13}\text{C}$ NMR, elemental analysis, mass spectrometry, melting point and FT-IR. The melting point (335-337 °C) is in agreement with literature value <sup>132</sup>, the elemental analysis for CHN confirmed the structure of the target product. The mass spectrum illustrate the main integer masses of (**27**) at 238 ( $\text{M}^+$ ) which corresponds very well with proposed structure.

The  $^1\text{H}$ NMR spectrum illustrated the assumed aromatic peaks, doublet peaks at 7.84 and 7.23 ppm and a doublet of doublets peak at 6.89 ppm. In addition, the spectrum shows a singlet peak at 6.42 ppm which is related to the N – H proton. The FT-IR of the target product illustrates the stretching vibration bands for (N - H)

group at 3344 and 1623  $\text{cm}^{-1}$ , the stretching vibration bands for (C – N) group appears at 1338  $\text{cm}^{-1}$ . The C-H stretching vibration is displayed at 3223 $\text{cm}^{-1}$ , the stretch vibration at 1581, 1553 and 1499  $\text{cm}^{-1}$  are related to C = C stretch.

#### 4.4.3. 2,7-Dibromoanthracene-9,10-dione (28)

The preparation of 2,7-dibromoanthracene-9,10-dione (**28**) was carried out according to a modified method by Vila et al <sup>123</sup>. The reaction was performed by heating a mixture of 2,6-diaminoanthraquinone, t-BuONO, CuBr<sub>2</sub> in acetonitrile for two hours as shown in Scheme 50. In addition, the purification was carried out using recrystallization from 1,4-dioxane to obtain the target product (**18**) as yellow crystals. The TLC gave a single spot and the yield was 85%.



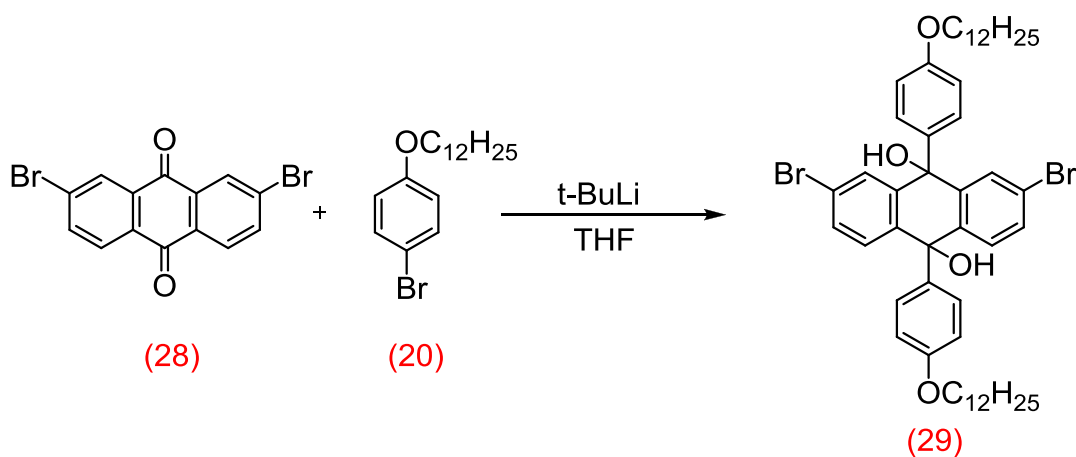
**Scheme 50.** The preparation of 2,7-dibromoanthracene-9,10-dione (**28**).

The structure and purity of the target product (**28**) were confirmed by <sup>1</sup>HNMR, <sup>13</sup>CNMR, elemental analysis, mass spectrometry, melting point and FT-IR. The melting point (249-250 °C) is in agreement with literature value <sup>131</sup>, the elemental analysis for CHBr confirmed the structure of the target product. The mass spectrum illustrate the main integer masses of (**28**) which are obtained at 364, 366, 367 (M<sup>+</sup>) in 1:2:1 intensities because of the bromine isotopes (<sup>81</sup>Br and <sup>79</sup>Br).

The <sup>1</sup>HNMR spectrum illustrated the assumed aromatic peaks, doublet peaks at 8.45 and 8.20 ppm, a doublet of doublet peak at 7.97 ppm which corresponds very well the proposed structure. The FT-IR of the target product illustrates the stretching vibration bands for (C - Br) bond at 1105  $\text{cm}^{-1}$ . While, the stretching vibration bands at 3344, 1623  $\text{cm}^{-1}$  for (N - H) bond and 1338  $\text{cm}^{-1}$  for (C – N) bond disappear.

#### 4.4.4. 2,7-Dibromo-9,10-bis(4-(dodecyloxy)phenyl)-9,10-dihydroanthracene-9,10-diol (29)

The preparation of 2,7-dibromo-9,10-bis(4-(dodecyloxy)phenyl)-9,10-dihydroanthracene-9,10-diol (**29**) was carried out according to a modified method by Wang et al.<sup>127</sup>. The reaction was performed by adding *t*-BuLi to a solution of 1-bromo-4-(dodecyloxy)benzene (**20**) in THF at -78 °C then 2,7-dibromoanthracene-9,10-dione (**28**) was added to the mixture. The purification was carried out using column chromatography eluted ethyl acetate/ petroleum ether (1/10) (v/v) to obtain target product as a yellow solid in 65% yield.



**Scheme 51.** The preparation of 2,7-dibromo-9,10-bis(4-(dodecyloxy)phenyl)-9,10-dihydroanthracene-9,10-diol (**29**).

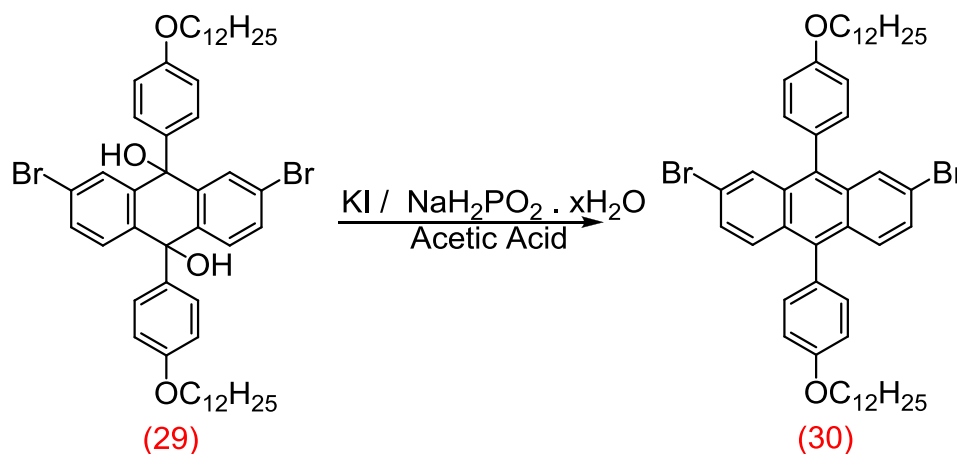
The structure and purity of the target product (**29**) were confirmed by TLC, <sup>1</sup>HNMR, <sup>13</sup>CNMR, elemental analysis, mass spectrometry and FT-IR. The TLC gave a single spot and the elemental analysis for CHBr confirmed the structure of the target product. The mass spectrum illustrate the main integer masses of (**28**) at 888, 890, 892 (M<sup>+</sup>) in 1:2:1 intensities because of the bromine isotopes (<sup>81</sup>Br and <sup>79</sup>Br).

The <sup>1</sup>HNMR spectrum confirm the structure of the target product. It shows three aromatic peaks at 8.03, 7.75 and 7.57 ppm which are related to the anthracene protons. Also, it shows two broad peaks at 6.40, 6.18 which can be assigned to the attached phenyl group protons. The alkyl chain protons are observed at 3.68 (s)

1.75-1.54 and 1.46-1.15 ppm. Finally, the triplet peak at 0.89 is related to the CH<sub>3</sub> group protons at the end of alkyl chains. The FT-IR of the target product illustrates the stretching vibration bands for (O - H) group at 3306 cm<sup>-1</sup> and the stretching vibration bands for (C - O) bond appears at 1164 cm<sup>-1</sup>. While, the stretching vibration bands at 1673 cm<sup>-1</sup> for (C = O) bond disappear.

#### 4.4.5. 2,7-Dibromo-9,10-bis(4-(dodecyloxy)phenyl)anthracene (30)

The preparation of 2,7-dibromo-9,10-bis(4-(dodecyloxy)phenyl)anthracene (**30**) was carried out according to a modified method by Wang et al.<sup>127</sup>. The reaction was performed by heating a mixture of 2,7-dibromo-9,10-bis(4-(dodecyloxy)phenyl)-9,10-dihydroanthracene-9,10-diol (**28**), KI, NaH<sub>2</sub>PO<sub>2</sub>·H<sub>2</sub>O in acetic acid for 40 minutes as shown in Scheme 52. In addition, the purification was performed via column chromatography eluting with DCM/ petroleum ether (1/4) (v/v) then recrystallisation from hexane to obtain the target product as a yellow solid. The TLC gave a single spot and the yield was 80 %.



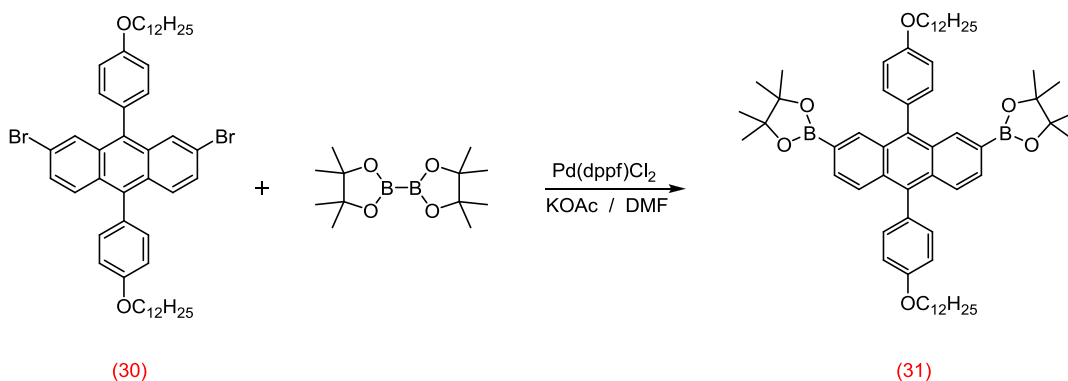
**Scheme 52. The preparation of 2,7-dibromo-9,10-bis(4-(dodecyloxy)phenyl)anthracene (30).**

The structure and purity of the target product (**30**) were confirmed by TLC, <sup>1</sup>HNMR, <sup>13</sup>CNMR, elemental analysis, mass spectrometry and FT-IR. The TLC gave a single spot elemental analysis for CHBr confirmed the structure of the target product. The mass spectrum illustrate the main integer masses of (**29**) which are

obtained at 854.6, 856.5, 857.6 ( $M^+$ ) in 1:2:1 intensities because of the bromine isotopes ( $^{81}\text{Br}$  and  $^{79}\text{Br}$ ). The  $^1\text{HNMR}$  and  $^{13}\text{CNMR}$  spectrums correspond very well with the structure of target product.

#### 4.4.6. 2,2'-(9,10-Bis(4-(dodecyloxy)phenyl)anthracene-2,7-diyl)bis(4,4,5,5-tetramethyl-1,3,2-dioxaborolane) (31)

The preparation of 2,2'-(9,10-bis(4-(dodecyloxy)phenyl)anthracene-2,6-diyl)bis(4,4,5,5-tetramethyl-1,3,2-dioxaborolane) (**31**) was carried out according to a modified method by Jo et al <sup>115</sup>. The reaction was performed by heating a mixture of 2,6-dibromo-9,10-bis(4-(dodecyloxy)phenyl)anthracene (**30**), bis(pinacolato) diboron, potassium acetate and  $\text{Pd}(\text{dppf})\text{Cl}_2$  in DMF at 100 °C for 36 hours as shown in Scheme 53. In addition, an excess of bis(pinacolato) diboron was used to prevent the creation of oligomers. The colour change to a dark black solution was noticed during the reaction. The purification was carried out using recrystallization from using diethyl ether and methanol. The target product was obtained as a yellow powder with 60.6 % yield.



**Scheme 53. The preparation of 2,2'-(9,10-bis(4-(dodecyloxy)phenyl)anthracene-2,7-diyl)bis(4,4,5,5-tetramethyl-1,3,2-dioxaborolane) (31).**

The structure and purity of the target product (**31**) were confirmed by  $^1\text{HNMR}$ ,  $^{13}\text{CNMR}$ , elemental analysis, mass spectrometry and FT-IR. The elemental analysis for CH confirmed the structure of the target product. The mass spectrum illustrate the main integer mass of (**31**) which are obtained at 950.5 ( $M^+$ ). The structure of

(31) was confirmed using  $^1\text{H}$ NMR as shown in Figure 40. The singlet peak at 8.32 ppm is related to the anthracene protons in the position (a). The four anthracene protons in the positions (b) and (c) are observed at 7.72 – 7.68 ppm. The structure of this anthracene version is not symmetrical; the attached phenyl group protons are displayed at different chemical environments. So, the spectrum shows two doublet peaks at 7.44 and 7.37 ppm which are related to the four protons in the attached phenyl group in the positions (d') and (d) respectively. Also, the two doublet peaks at 7.20 and 7.15 ppm are related to the phenyl group protons in the positions (e') and (e) respectively. The singlet peak at 1.34 ppm is related the  $\text{CH}_3$  protons in the position (q). The remaining peaks at 4.20, 4.14, 2.04-1.83, 1.66-1.52, 1.52-1.25 and 0.92 ppm are related to the aliphatic protons of the alkyl chain attached to the phenyl group. The FT-IR of the target product illustrates the stretching vibration bands for the (B - O) at 1371 and 1349  $\text{cm}^{-1}$  and the stretch vibration at 1078  $\text{cm}^{-1}$  which correlated to the C-B bond.

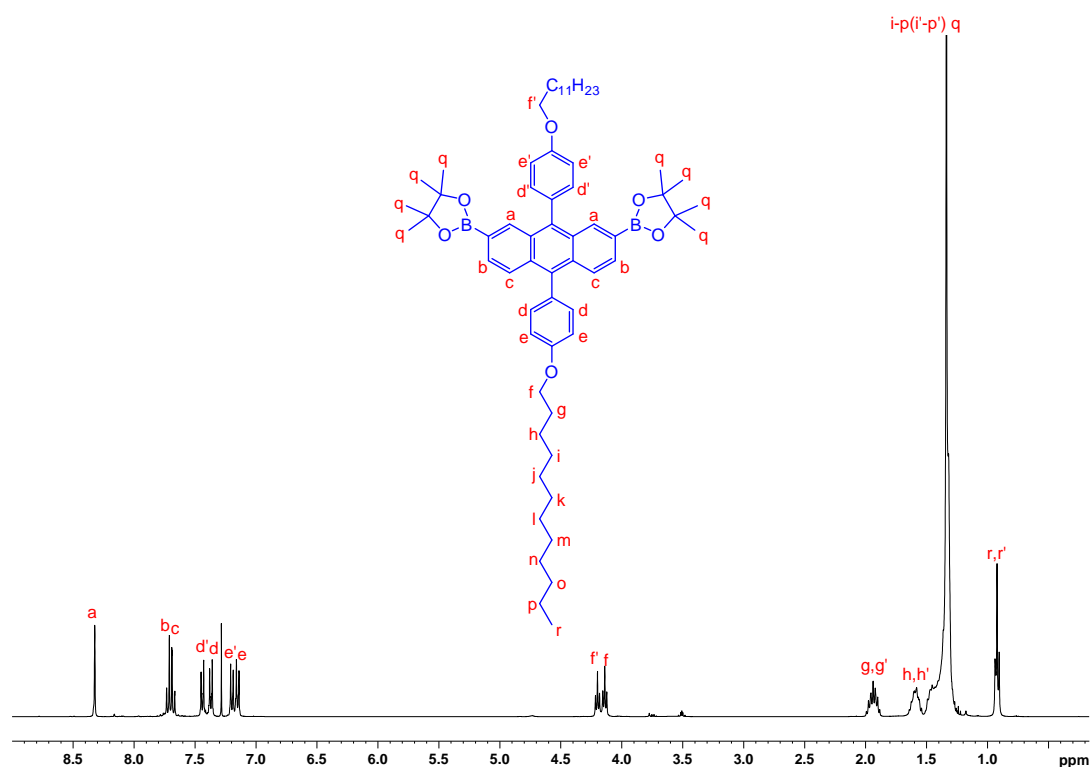


**Figure 40.** The  $^1\text{H}$ NMR spectrum for 2,2'-(9,10-bis(4-(dodecyloxy)phenyl)anthracene-2,7-diyl)bis(4,4,5,5-tetramethyl-1,3,2-dioxaborolane) (31).

## 4.5. Synthesis of monomers for polymers (P16, P17, P18, P19 and P20)

In order to prepare **P16**, **P17**, **P18**, **P19** and **P20**, monomers **(7)**, **(23)**, **(31)** and **(34)** (Figure 41) were required. In addition, monomer **(35)** was prepared by S. Alfifi of the Iraqi group using the same preparation route for monomer **(7)** and monomer **(36)** was bought from Sigma Aldrich.

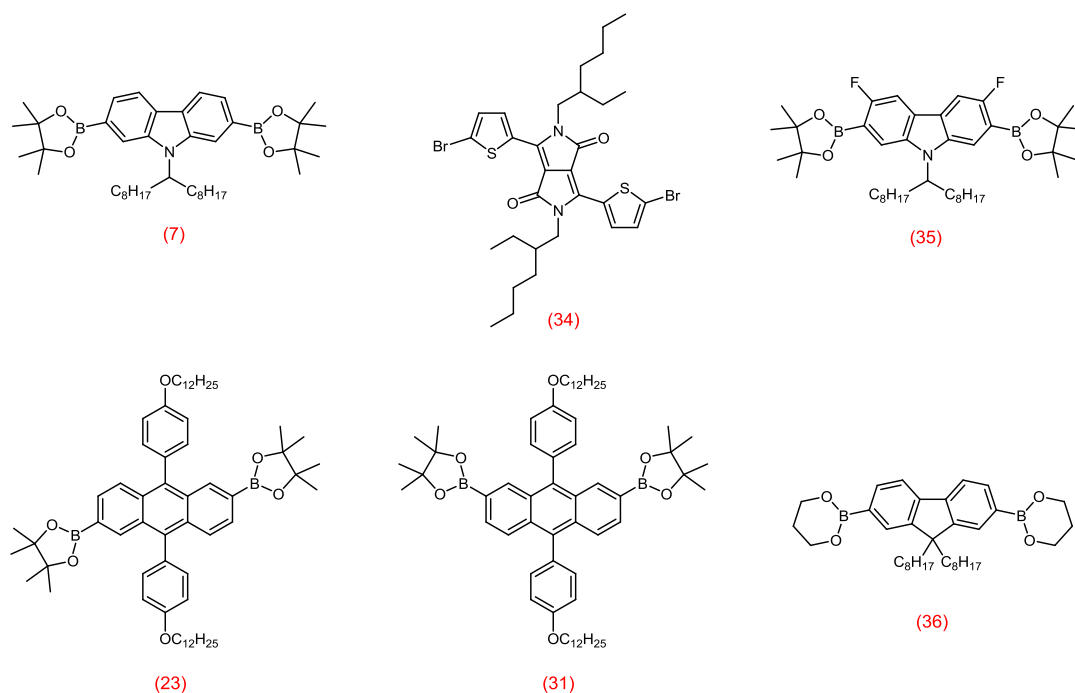
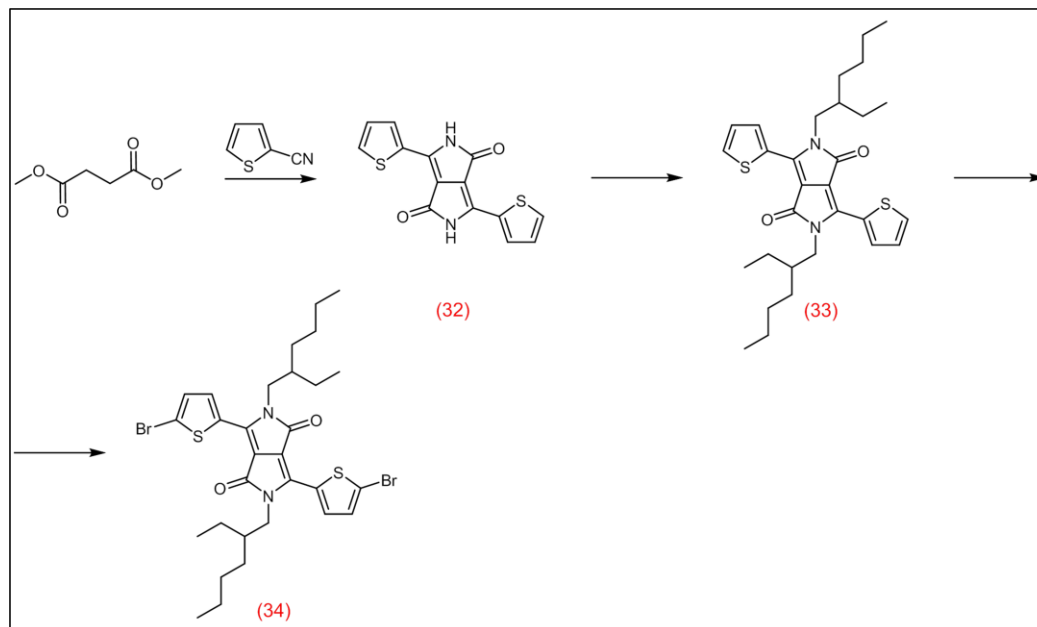


**Figure 41. Monomers required for preparing P16, P17 ,P18, P19 and P20.**

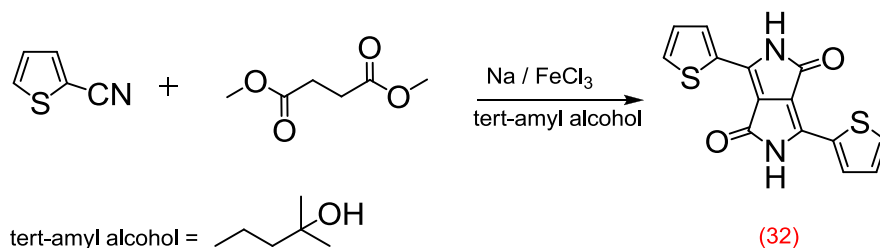
A series of intermediates were prepared successfully in order to prepare 3,6-bis(5-bromothiophen-2-yl)-2,5-bis(2-ethylhexyl)pyrrolo[3,4-c]pyrrole-1,4(2H,5H)-dione (**33**), and their structure and purity were confirmed by by TLC,  $^1H$ NMR,  $^{13}C$ NMR, elemental analysis, mass spectrometry, melting point, and FT-IR. It was prepared in three steps as shown in Scheme 54 starting from thiophene-2-carbonitrile and dimethyl succinate.



**Scheme 54. Preparation route to 3,6-bis(5-bromothiophen-2-yl)-2,5-bis(2-ethylhexyl) pyrrolo[3,4-c]pyrrole-1,4(2H,5H)-dione (34)**

#### 4.5.1. 3,6-Di(thiophen-2-yl)pyrrolo[3,4-c]pyrrole-1,4(2H,5H)-dione (32)

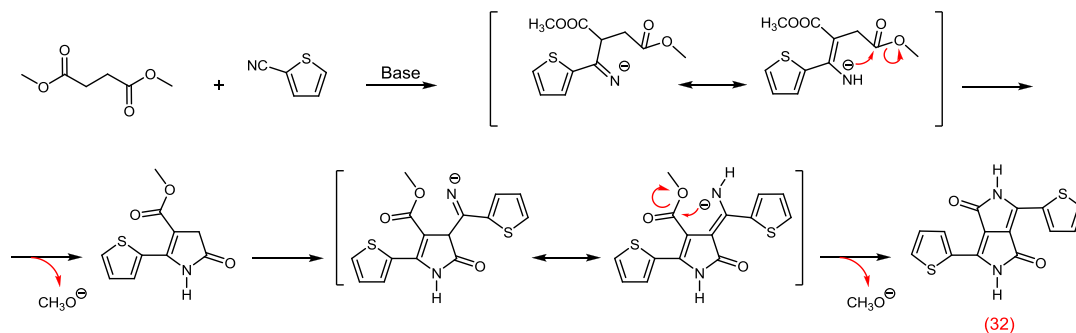
The preparation of 3,6-di(thiophen-2-yl)pyrrolo[3,4-c]pyrrole-1,4(2H,5H)-dione (**32**) was carried out according to a modified method by Chen et al.<sup>133</sup>. The reaction was performed by mixing Na and a catalytic amount of FeCl<sub>3</sub> in tert-amyl alcohol at 90 °C for 2 hours, then the reaction mixture was cooled to 50 °C and thiophene-2-carbonitrile was added to the mixture which was then again heated at 90 °C. A solution of dimethyl succinate in tert-amyl alcohol was added dropwise for two hours and then the mixture was maintained at 90 °C overnight. Again the reaction mixture was cooled to 50 °C and glacial AcOH was added, then the mixture was heated under reflux for 10 min before being filtered. The product did not require any purification and it was obtained as a red solid in 90% yield.



**Scheme 55. The preparation of 3,6-di(thiophen-2-yl)pyrrolo[3,4-c]pyrrole-1,4(2H,5H)-dione (32).**

The mechanism of the reaction is very complicated and not fully understood. It was proposed by Lenz and Wallquist<sup>102</sup>. The DPP are prepared by reacting two equivalent of aromatic nitrile with one equivalent of a succinic ester under strong basic media. In addition, a branched alcohol such as tert-amyl alcohol is used as a solvent and base to make the formation of the DPP easier. The first step of the mechanism involves formation of the amino cinnamic acid by condensation of the thiophene-2-carbonitrile with dimethyl succinate. There are two possible routes which might take place after this step. The first route involves condensation of the amino cinnamic acid with dimethyl succinate which leads to formation of a side product which has a major yield and it was confirmed experimentally by Lenz and Wallquist. The second route is cyclisation of the amino cinnamic acid and lactam formation. The second step involves another condensation of thiophene-2-carbonitrile with the intermediate resulted from the previous step and then followed by cyclisation which affords the target DPP product<sup>102</sup> as shown in Scheme 56.

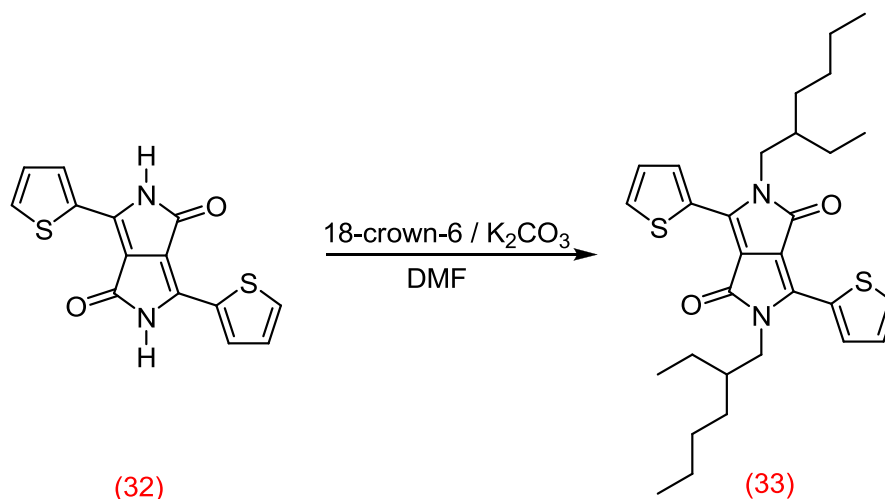
The structure and purity of the target product (**31**) were confirmed by <sup>1</sup>HNMR, <sup>13</sup>CNMR, mass spectroscopy and FT-IR. The mass spectrum illustrate the main integer mass of (**31**) which are obtained at 300 (M<sup>+</sup>). The <sup>1</sup>HNMR and <sup>13</sup>CNMR spectrums are in agreement with the literature<sup>142</sup>. The FT-IR of the target product illustrates the stretching vibration bands for (N - H) group at 3275 cm<sup>-1</sup>, the stretching vibration bands for (C - N) group appears at 1127 cm<sup>-1</sup>. The C = O stretching vibration is displayed at 1704 cm<sup>-1</sup>.



**Scheme 56. Proposed mechanism for the preparation of 3,6-di(thiophen-2-yl)pyrrolo[3,4-c]pyrrole-1,4(2H,5H)-dione (32) (adapted from Wallquist et al <sup>102</sup>)**

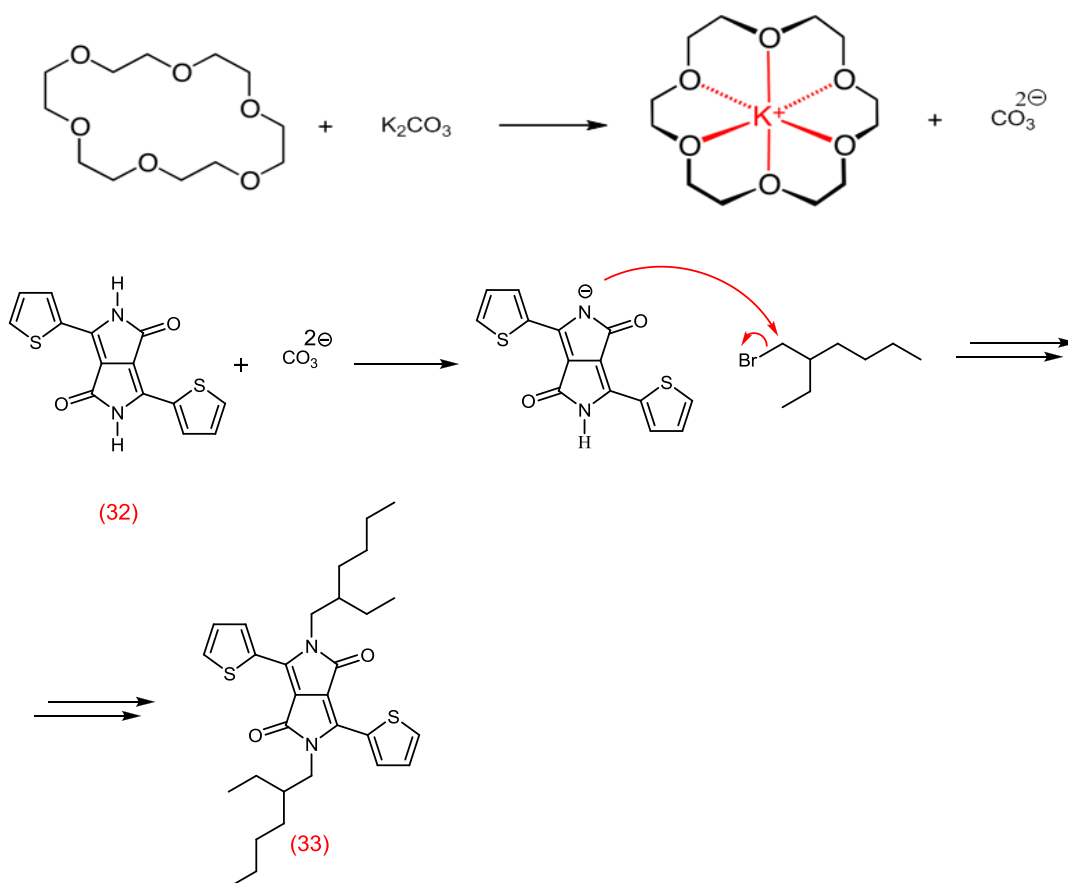
#### 4.5.2. 2,5-Bis(2-ethylhexyl)-3,6-di(thiophen-2-yl)pyrrolo[3,4-c]pyrrole-1,4(2H,5H)-dione (33)

The preparation of 2,5-bis(2-ethylhexyl)-3,6-di(thiophen-2-yl)pyrrolo[3,4-c]pyrrole-1,4(2H,5H)-dione (**33**) was carried out according to a modified method by Chen et al <sup>133</sup>. The reaction was performed by adding a solution of 2-ethylhexyl bromide in DMF dropwise to a mixture of (**32**),  $K_2CO_3$  and 18-crown-6 in DMF at 120 °C. The purification was carried out by precipitating the crude product in methanol then via column chromatography eluting with chloroform. The pure target product was obtained as red solid with 32 %.



**Scheme 57. The preparation of 3,6-di(thiophen-2-yl)pyrrolo[3,4-c]pyrrole-1,4(2H,5H)-dione (33).**

The reaction proceeds in two steps. 18 – Crown – 6 is a phase transfer catalyst and used to help in the displacement step. So, 18 – Crown – 6 chelates the potassium and form a carbonate anion. In the second step, the DPP is deprotonated by the bicarbonate anion which gives the ion on the nitrogen, then nucleophilic attack to ethyl hexyl.

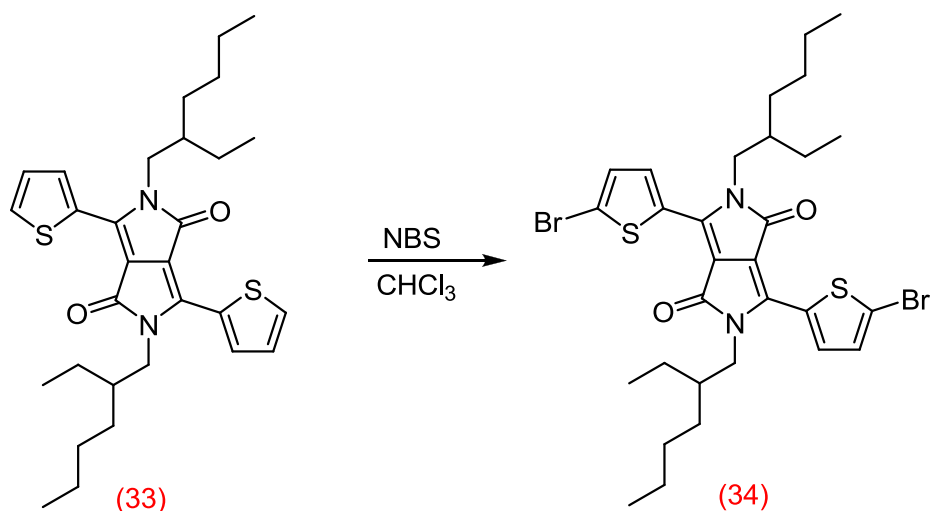


**Scheme 58. The mechanism of the preparation of 3,6-di(thiophen-2-yl)pyrrolo[3,4-c]pyrrole-1,4(2H,5H)-dione (33).**

The structure and purity of the target product **(33)** were confirmed by TLC,  $^1H$ NMR,  $^{13}C$ NMR, elemental analysis, mass spectrometry, melting point and FT-IR. The TLC gave a single spot and the melting point (125 - 127 °C) is in agreement with literature value (125 °C) <sup>134</sup>. The elemental analysis for CHN confirmed the structure of the target product. The mass spectrum illustrate the main integer masses of **(33)** which are obtained at 524 ( $M^+$ ).

**4.5.3. 3,6-Bis(5-bromothiophen-2-yl)-2,5-bis(2-ethylhexyl)pyrrolo[3,4-c]pyrrole-1,4(2H,5H)-dione (34)**

The preparation of 3,6-bis(5-bromothiophen-2-yl)-2,5-bis(2-ethylhexyl)pyrrolo[3,4-c]pyrrole-1,4(2H,5H)-dione (**34**) was carried out according to a modified method by Chen et al.<sup>133</sup>. The reaction was performed by adding NBS to a solution of 3,6-di(thiophen-2-yl)pyrrolo[3,4-c]pyrrole-1,4(2H,5H)-dione (**32**) in CHCl<sub>3</sub>. The reaction mixture was stirred for two days in the dark. The purification was carried out by column chromatography eluted with chloroform. The pure target product was obtained as a red solid with 82 % yield.



**Scheme 59.** The preparation of 3,6-bis(5-bromothiophen-2-yl)-2,5-bis(2-ethylhexyl)pyrrolo[3,4-c]pyrrole-1,4(2H,5H)-dione (**34**).

The structure and purity of the target product (**34**) were confirmed by TLC, <sup>1</sup>HNMR, <sup>13</sup>CNMR, elemental analysis, mass spectrometry and FT-IR. The TLC gave a single spot and elemental analysis for CHNSBr confirmed the structure of the target product. The mass spectrum illustrate the main integer masses of (**34**) which are obtained at 680, 682, 684 (M<sup>+</sup>) in 1:2:1 intensities that because of the bromine isotopes (<sup>81</sup>Br and <sup>79</sup>Br). The <sup>1</sup>HNMR spectrum confirms the chemical structure of (**34**) as shown in Figure 42. The doublet peaks at 8.67 and 7.24 ppm are related to the thiophene protons in the positions (a) and (b). The rest of peaks correspond to the alky chain protons.

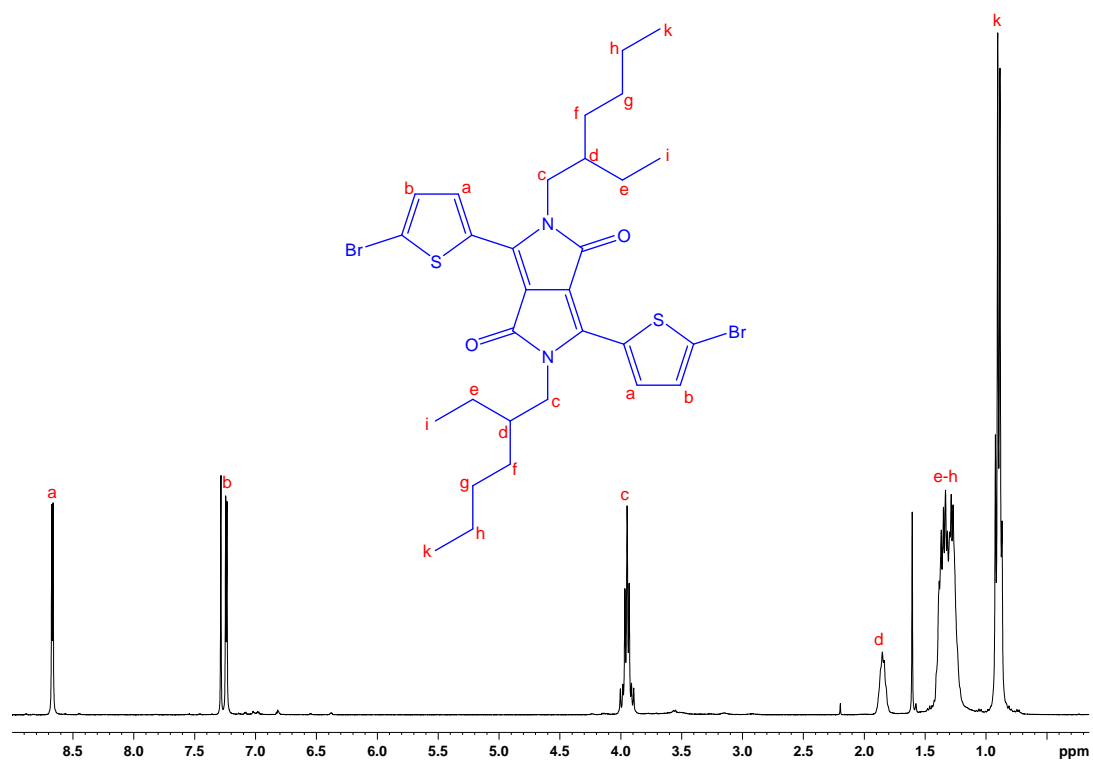


**Figure 42.** The <sup>1</sup>H NMR spectrum for 3,6-bis(5-bromothiophen-2-yl)-2,5-bis(2-ethylhexyl) pyrrolo[3,4-c]pyrrole-1,4(2H,5H)-dione (34).

## Chapter Five: Results and Discussion – Polymers

### 5.1. Carbazole – Pyrrole based copolymers (P1, P2, P3)

A range of 2,7-carbazole – pyrrole based copolymers were designed as alternating donor – acceptor systems in order to have low band gaps and so harvest more photons from sunlight. **P1**, **P2** and **P3** (Figure 43) were synthesised successfully using Suzuki cross coupling and analysed by  $^1\text{H}$ NMR, elemental analysis and GPC. The thermal stability was studied using TGA and the physical and electrical properties of these polymers were studied using UV-Vis spectroscopy and cyclic voltammetry.

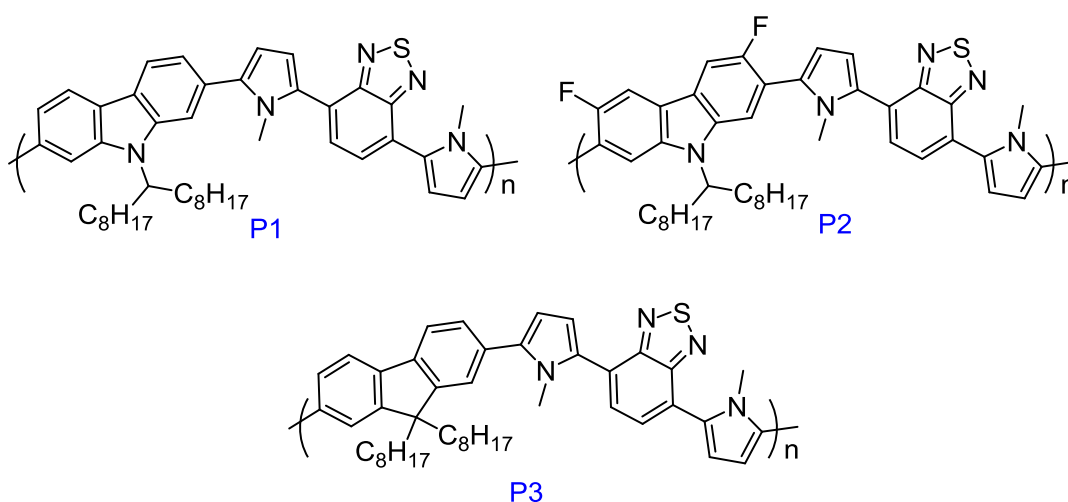
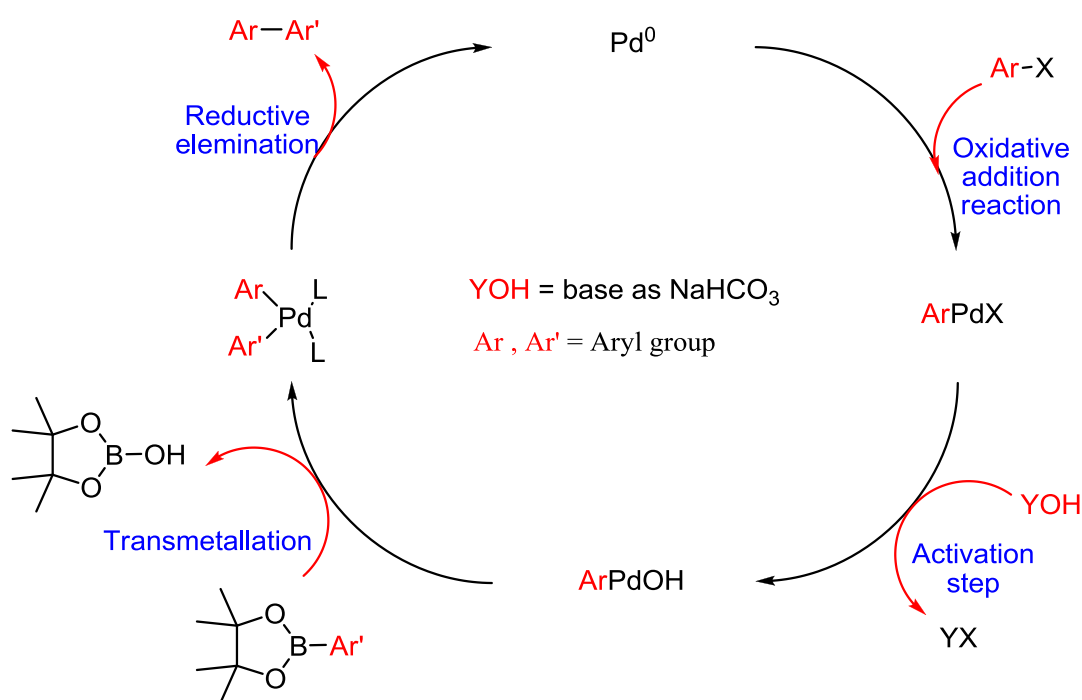


Figure 43. The chemical structure of P1 , P2 , P3.

#### 5.1.1. Preparation of P1, P2, P3

**P1**, **P2** and **P3** were prepared using Suzuki cross coupling polymerization reactions. The mechanism of Suzuki cross coupling consists of four steps, as shown in Figure 44. The first step is an oxidative addition reaction that couples the palladium (0) catalyst to the aryl halide which forms palladium (II) halide complex ( $\text{RPdXL}_2$ ). The complex forms in cis-conformation. The second step is activation the alkyl

palladium halide complex or organoboron compound for transmetalation using nucleophilic base. The third step is transmetalation when the organoborn compound reacts with palladium (II) complex and generates a boron complex and a palladium (II) complex (two organic groups are attached to palladium by palladium carbon bonds). The last step is reductive elemenation when the two organic groups are coupled with each other which generates the desired product and regenerates the palladium (0) which starts again in the catalyst cycle <sup>143</sup>.

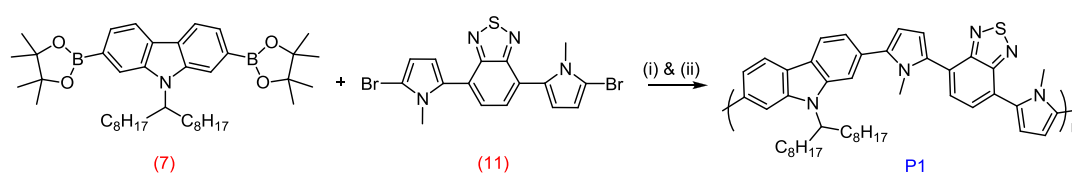


**Figure 44. The mechanism of Suzuki Cross Coupling.**

**P1** was prepared twice with different conditions, the first polymerization was carried out using toluene as solvent and tetraethylammonium hydroxide as a base, while the second polymerization was carried out in THF as solvent and NaHCO<sub>3</sub> as a base. The polymerization of **P2** and **P3** was carried out in THF as solvent and NaHCO<sub>3</sub> as a base. All of the polymerizations were carried out under argon. When the polymerization mixtures became viscous and the polymers dropped out of solutions, the polymers were end-capped with bromobenzene and phenyl boronic acid to increase the stability of the polymers in device operation. Then, the polymers were dissolved in chloroform and stirred with ammonium hydroxide

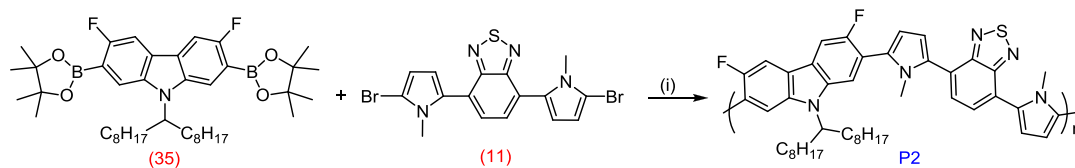
solution (28 % in H<sub>2</sub>O) overnight, in order to remove palladium catalyst impurities. It is reported that contamination of polymers with palladium particles leads to a break in voltage and circuit current. In addition, the palladium particles have negative effects on charge carrier mobility and lifetime<sup>144</sup>. After washing the polymers with ammonia solutions, the polymer solutions were washed with distilled water to remove the ammonia and concentrated to about 50 ml and then precipitated in a mixture of methanol: water (10:1). The solid crude polymers were collected through filtration with micropore membranes and transferred to a fiber glass thimble and washed with various solvents, in order methanol, acetone, hexane and toluene, using a soxhlet apparatus. The reason for washing with methanol, acetone and hexane is to remove monomers and the low molecular weight oligomers. The toluene fraction was concentrated and precipitated in methanol and collected through micropore membranes.

Poly [9-(1-octyl-nonyl)-9H-carbazole-2,7-diyl-alt-(4',7'-bis(1-methyl-1H-pyrrol-2'-yl)-2',1',3'-benzothiadiazole)-5,5-diyl] (**P1**) was prepared by reacting 9-(heptadecan-9-yl)-2,7-bis(4,4,5,5-tetramethyl-1,3,2-dioxaborolan-2-yl)-9H-carbazole (**7**) with 4,7-bis(5-bromo-1-methyl-1H-pyrrol-2-yl)benzo[c][1,2,5]thiadiazole (**11**) as shown in Scheme 60.



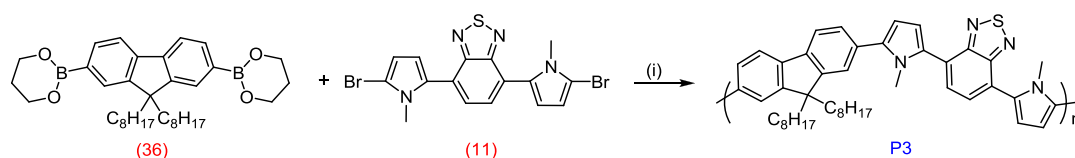
**Scheme 60. Preparation of P1. (i) Pd(AcO)<sub>2</sub>, tri-*o*-tolylphosphine, Toluene, tetraethylammonium hydroxide; (ii) Pd(AcO)<sub>2</sub>, tri-*o*-tolylphosphine, THF, NaHCO<sub>3</sub>.**

Poly[3,6-difluoro-9-(1-octyl-nonyl)-9H-carbazole-2,7-diyl-alt-(4',7'-bis(1-methyl-1H-pyrrol-2'-yl)-2',1',3'-benzothiadiazole)-5,5-diyl] (**P2**) was prepared by reacting 3,6-difluoro-9-(heptadecan-9-yl)-2,7-bis(4,4,5,5-tetramethyl-1,3,2-dioxaborolan-2-yl)-9H-carbazole (**35**) with 4,7-bis(5-bromo-1-methyl-1H-pyrrol-2-yl)benzo[c][1,2,5]thiadiazole (**11**) as shown in Scheme 61.



**Scheme 61. Preparation of P2. (i) Pd(AcO)<sub>2</sub>, tri-*o*-tolylphosphine, THF, NaHCO<sub>3</sub>.**

Poly [9,6-dioctyl-9H-fluorene-2,7-diyl-alt-(2',7'-bis(1-methyl-1H-pyrrol-2-yl)-2',1',3'-bezothiadiazole)-5,5-diyl] (**P3**) were prepared by reacting 9,9-dioctylfluorene-2,7-diboronic acid bis(1,3-propanediol) ester (**36**) with 4,7-bis(5-bromo-1-methyl-1H-pyrrol-2-yl)benzo[*c*] [1,2,5]thiadiazole (**11**) as shown in Scheme 62.



**Scheme 62. Preparation of P3. (i) Pd(AcO)<sub>2</sub>, tri-*o*-tolylphosphine, THF, NaHCO<sub>3</sub>.**

## 5.1.2. Characterization of P1, P2, P3

### 5.1.2.1. Gel Permeation Chromatography studies of P1, P2 and P3

All the GPC results are illustrated in Table 1, with the polydispersity (PD) and the degree of polymerization (DP).

Table 1. Yields and GPC results for P1, P2 and P3.

Polymer	Yield %	Solvent		$M_n$	$M_w$	PD	DP
		Fraction					
P 1(1)	27	Toluene		2600	8100	3.08	4
P1 (2)	42	Toluene		14100	15300	1.08	20
P2	43.6	Toluene		3500	8400	2.4	5
P3	61.8	Toluene		3300	6300	1.9	5

#### 5.1.2.2. $^1\text{H}$ NMR analysis of P1, P2 and P3

The  $^1\text{H}$ NMR analysis of polymers **P1**, **P2** and **P3** were carried out in  $\text{C}_2\text{D}_2\text{Cl}_4$  at 80 °C in order to avoid broad signal especially in the downfield region around (6 – 9 ppm) as a result of the phenomenon of atropisomerism and polymer aggregation<sup>145</sup>.

Figure 45 shows the  $^1\text{H}$ NMR of **P1** and it reveals six signals in the aromatic region for the carbazole, methylpyrrole and benzothiadiazole. The protons of the carbazole hydrogen with doublet peak at 8.00 ppm for the two protons on positions (a). The multiplet peaks around 7.74-7.54 ppm are related to the four protons on the positions (b) and (c) on the carbazole and the overlapping peaks are assigned to the end capping groups (phenyl protons) of the polymer. The doublet peaks at 7.42 and 7.24 ppm can be assigned to the four protons of the methyl pyrrole on the positions (d) and (e) respectively. The singlet peak around 6.94 ppm can be assigned to the benzothiadiazole hydrogens in the position (f). The broad singlet peak at 4.64-4.55 ppm is related to protons on the carbon which is bonded directly to the nitrogen atom of the carbazole (position f). It can be seen that this broad peak was observed in monomer (**7**) as a result of the atropisomerism phenomenon and it is still observed even at high temperature. The six protons of the methyl group of the methylpyrrole are displayed at 3.75 ppm which is a singlet peak. It is clear that the broad peaks noticed on the spectrum of monomer (**7**) are observed on this polymer

which result from restricted rotation at the C-N, these broad peaks are displayed at 2.42-2.26 and 2.07-1.91 corresponding to protons on the position (h and h') on the alkyl chain. The multiplet peaks at, 1.67-1.50 and 1.37-0.99 ppm correspond to the alkyl chain protons that are attached to the carbazole. The triplet peak at 0.77 ppm is related to the six protons on the CH<sub>3</sub> group at the end of the alkyl chains attached to the carbazole.

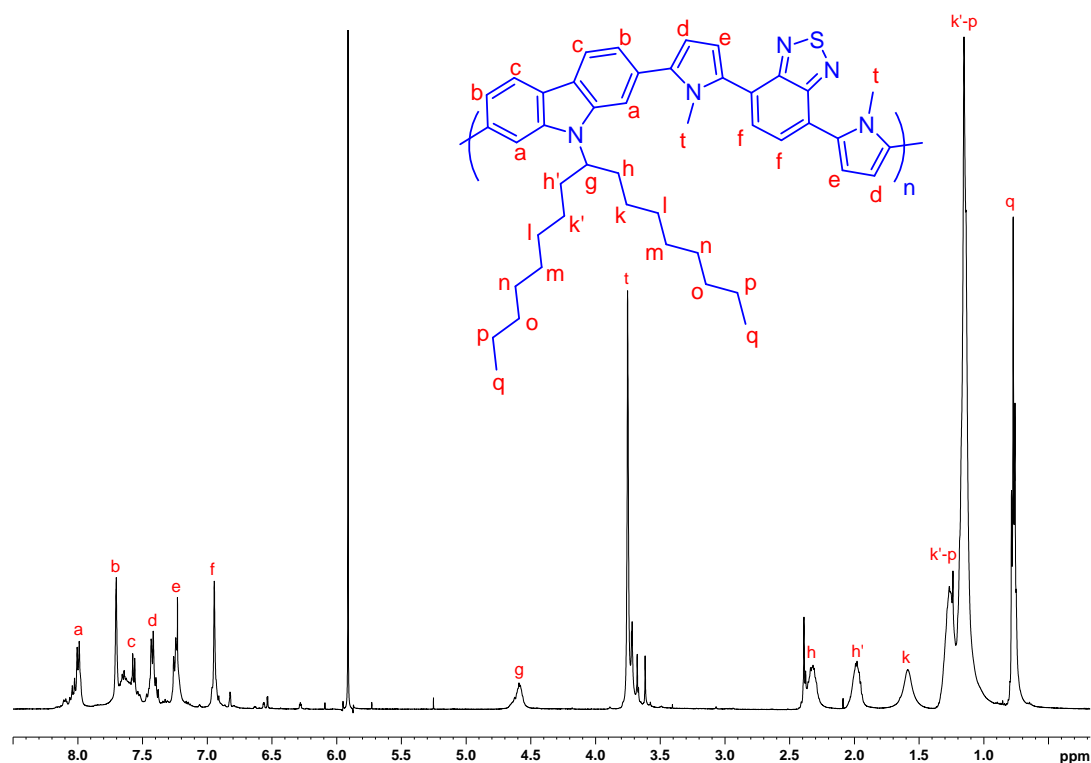


Figure 45. <sup>1</sup>H NMR spectrum of P1 in C<sub>2</sub>D<sub>2</sub>Cl<sub>4</sub> at 80 °C

Figure 46 reveals the <sup>1</sup>H NMR of **P2** and it can be seen that the protons for the carbazole hydrogen with multiplet peaks at 7.78-7.49 ppm attributed to the four protons on the positions (a) and (b) and the overlapping peaks possibly related to the end capping groups (phenyl protons) of the polymer. The doublet peak at 7.40 ppm is related to the two protons at positions (c) on the methyl pyrrole, while the doublet peak at 6.98 ppm are assigned to the other two protons on positions (d) on the methylpyrrole. The singlet peak around 7.23 ppm can be assigned to the benzothiadiazole hydrogens in the positions (e). The broad singlet peak at 4.55-4.45 ppm is related to protons on the carbon which is bonded directly to the nitrogen atom of the carbazole (position f). The six protons on the methyl group of

the methylpyrrole are displayed at 3.75 ppm which is a singlet peak. The broad peaks at 2.33-2.17 and 2.00-1.85 corresponding to protons on the position (h and h') on the alkyl chain. The peaks at 1.31-0.96 and 0.76 ppm correspond to the rest of the alkyl chain protons that are attached to the carbazole.

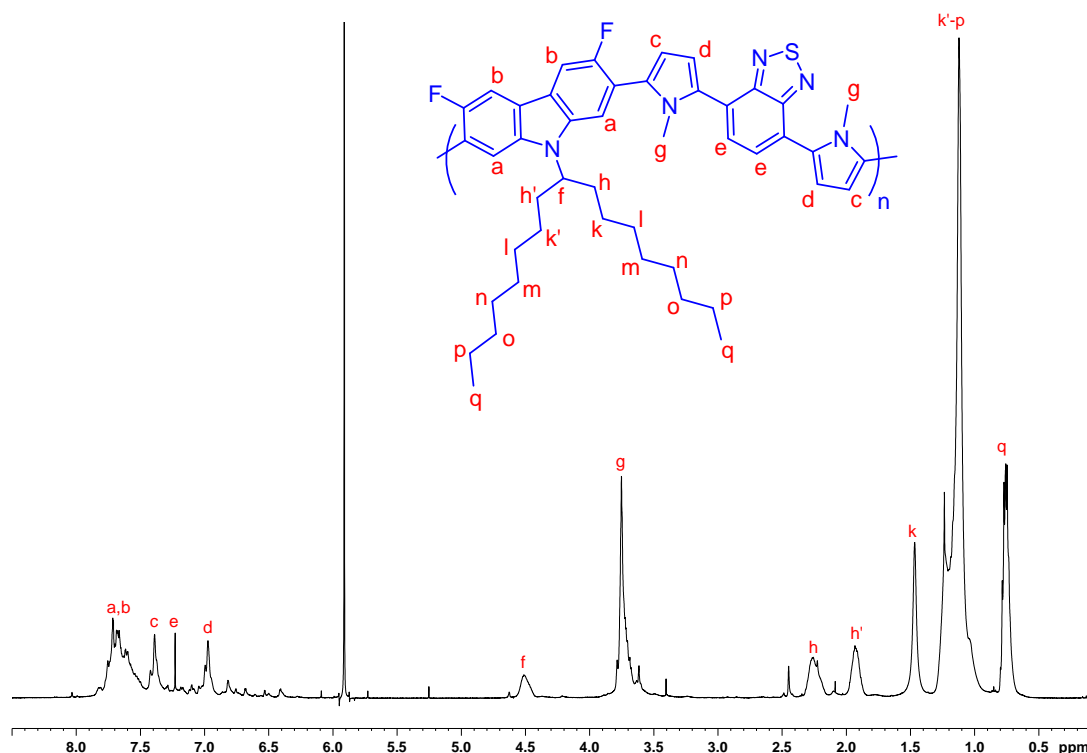


Figure 46.  $^1\text{H}$ NMR spectrum of P2 in  $\text{C}_2\text{D}_2\text{Cl}_4$  at 80 °C.

The  $^1\text{H}$ NMR spectrum of **P3** is shown in Figure 47. It shows four chemical environments in the aromatic region for the fluorene, methylpyrrole and benzothiadiazole protons. The broad singlet peak at 7.90 ppm is related the protons in positions (a) of the fluorene. The multiplet-peak at 7.79-7.41 ppm is related to the six protons on positions (b), (c) and (d) of the fluorene and methyl pyrrole. The singlet peak centred at 7.27 ppm is related to the two protons on the position (f) of the benzothiadiazole. The doublet peak at 6.91 ppm is related to the other two protons on position (e) of the methylpyrrole. The six protons on the methyl group of the methyl pyrrole are displayed at 3.72 ppm which is a singlet peak. The multiplet peaks at 2.14-1.85, 1.74-1.49 and 1.32-0.90 ppm are corresponded to the alkyl chain protons that attached to the fluorene. The triplet peak at 0.77 ppm is

related the six protons on the CH<sub>3</sub> group at the end of the alkyl chain that attached to the fluorene.

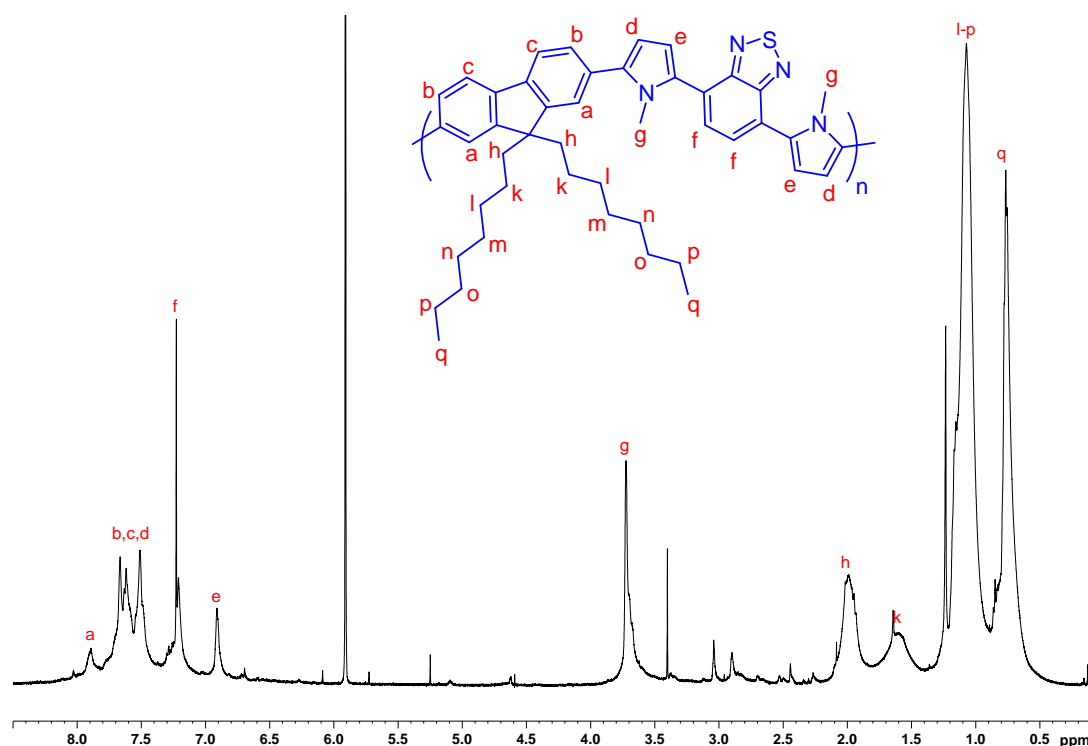
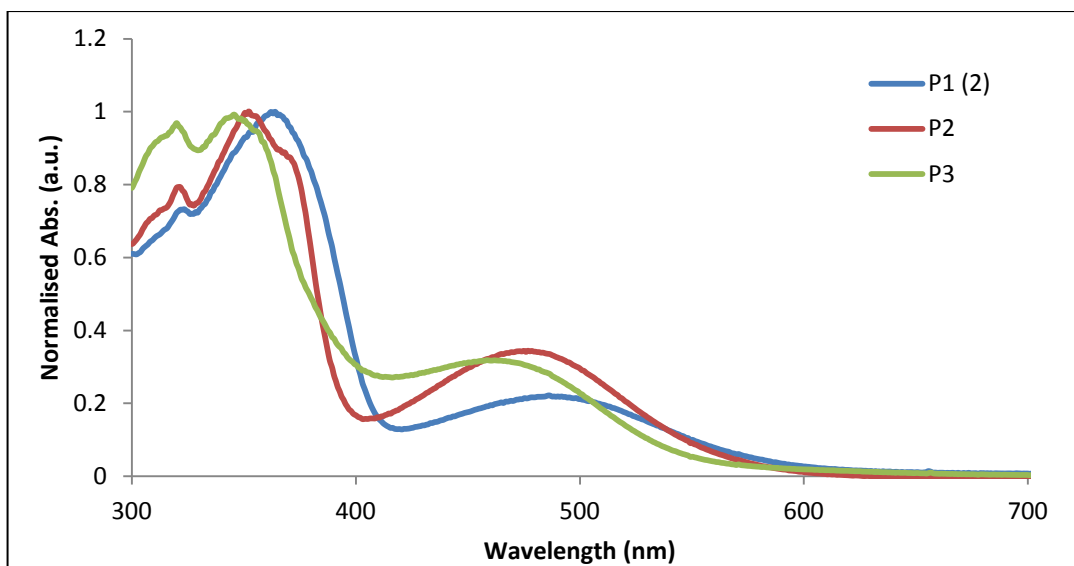


Figure 47. <sup>1</sup>H NMR spectrum of P3 in C<sub>2</sub>D<sub>2</sub>Cl<sub>4</sub> at 80 °C.

### 5.1.2.3. UV-visible absorption spectroscopy analysis of P1, P2 and P3

The UV-Visible absorption spectra of **P1**, **P2** and **P3** were performed in chloroform solutions and thin films at room temperature. Figure 48 shows the spectra of **P1(2)**, **P2** and **P3** in chloroform solutions. It can be seen that all polymers show two absorption bands with the first bands between 345 and 364 nm while the second bands are between 459 and 486 nm (Figure 48). A comparison of the absorption bands of **P1(2)** and **P2** indicates that they have comparable absorption bands maxima. The fluorene pyrrole based copolymer **P3** shows lower absorption maxima compared to other copolymers **P1(2)** and **P2** which is expected due to the weaker electron donating properties of fluorene compared to that of carbazole.



**Figure 48.** Absorption spectra of **P1(2)**, **P2** and **P3** in chloroform solutions.

Figure 49 shows the spectra of **P1(2)**, **P2** and **P3** as thin films. All polymers show two absorption bands, the shorter wavelength between 346 and 364 nm while the longer wavelength between 486 and 505 nm (Figure 49). The results indicate that there is a very small shift in the  $\lambda_{\max}$  values between solutions and solid state thin films which are assumed to be due to aggregation as in thin films polymers have more planar structure than in solution. The freedom of movement of polymer chains in solution leads to polymer chain twisting and so lead to lower conjugation. From the absorption onset of **P1(2)** (610 nm), the optical band gap energy is 2.03 eV. **P2** has an optical band gap energy of 2.05 eV (absorption onset at 604 nm) which is comparable to that of **P1(2)** even though **P1(2)** has a high molecular weight of (Table 1). This could be due to electrostatic interactions between fluorine substituents on the carbazole and hydrogens at the 4-position on the pyrrole units as shown in Figure 50. This interaction increases the planarity of the polymer structure and so increases the conjugation which results in a lower optical band gap energy. This phenomenon was reported by Hursthouse et al.<sup>146</sup> **P3** shows the larger optical band gap energy compared to that of the other two polymers (2.03 eV for **P1(2)**, 2.05 eV for **P2** vs 2.15 eV for **P3**) which is expected due to fluorene being a weaker electron donor compared to carbazole.

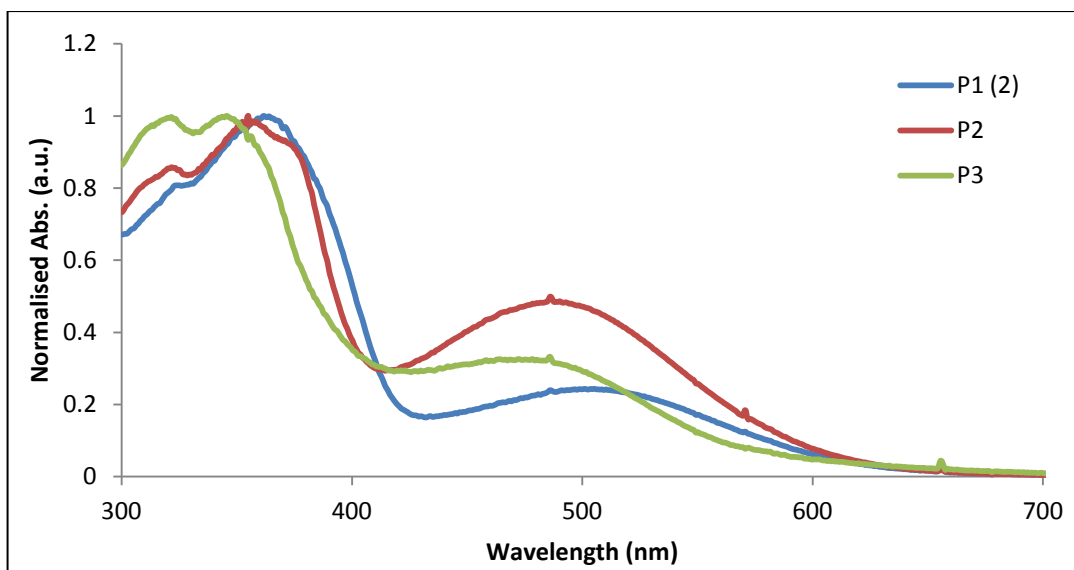


Figure 49. Absorption spectra of P1(2), P2 and P3 as a thin films.

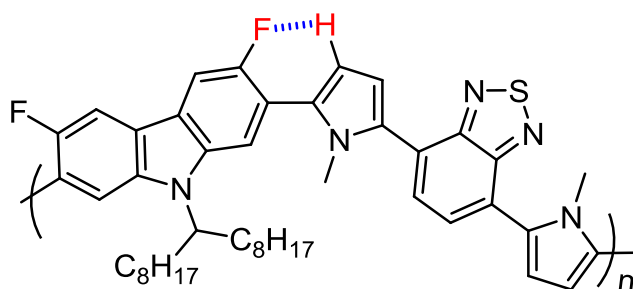
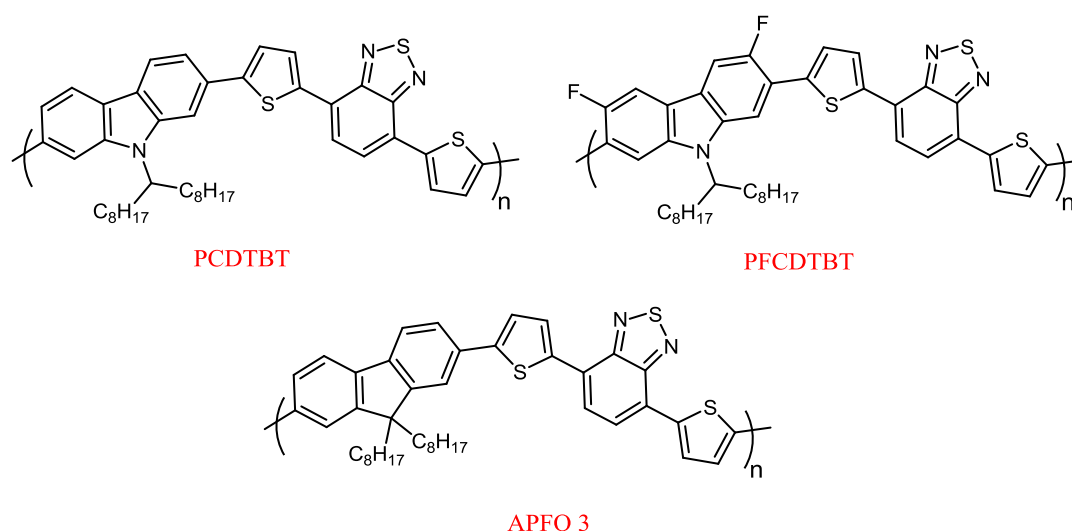


Figure 50. The H-F electrostatic interaction of P2.

A comparison of the absorption spectra of **P1(2)** with its analogous thiophene polymer **PCDTBT** which was reported by Leclerc et al.<sup>11b</sup> (the same structure but with methylpyrrole replaced with thiophene (Figure 51) indicates that the absorption bands for **PCDTBT** are at  $\lambda_{\max}$  390 and 545 nm for thin films, while the absorption bands for **P1(2)** are at  $\lambda_{\max}$  364 and 505 which indicates that **P1(2)** has a higher optical band gap than **PCDTBT** (**P1(2)** (2.03 eV for **P1(2)**) vs 1.88 eV for **PCDTBT**). In addition, a comparison of **P2** with its analogous polythiophene polymer **PFCDTBT**<sup>147</sup> (same chemical structure but methylpyrrole is replaced with thiophene (Figure 51) indicates a lower band gap for **PFCDTBT** (2.05 eV for **P2** vs 1.73 eV for **PFCDTBT**). In addition, the **PFCDTBT** gave absorption bands at  $\lambda_{\max}$  416 and 595 nm which means **PFCDTBT** is red shifted compared to **P2**. Moreover, a comparison of **P3** with its equivalent polythiophene polymer **APFO 3** which was

reported by Admassie et al.<sup>148</sup> (the same chemical structure but methyl pyrrole is replaced with thiophene (Figure 51) indicates that **APFO 3** has lower band gap energy with 1.80 eV. In addition, the absorption band at  $\lambda_{\max}$  for APFO 3 is red shifted compared to **P3** ( $\lambda_{\max}$ : 386 and 554 nm for **APFO 3** vs 345 and 486 for **P3**). It can be seen, the electronic delocalisation is clearly less pronounced on **P1(2)**, **P2** and **P3** compared to that of their thiophene analogous polymers. Such finding could be due to more twisting of the backbone of **P1(2)** out of the planarity when compared to that in thiophene analogue polymers possibly as a result of steric hindrance induced by the methyl groups on the nitrogen of pyrrole units on **P1(2)**, **P2** and **P3** and reducing the intramolecular charge transfer along the polymer backbone.



**Figure 51.** The chemical structure of PCDTBT, PFCDTBT and APFO 3.

#### 5.1.2.4. Cyclic Voltammetry (CV) analysis of P1, P2 and P3

In order to study the electrochemical properties of the polymers, Cyclic Voltammetry was carried out on drop-cast polymer films in acetonitrile and tetrabutylammonium perchlorate as electrolyte. The onset of oxidation and reduction can be obtained from cyclic voltammetry curve and used to assess the energy level of HOMO and LUMO (ferrocene has an ionisation potential of - 4.8 eV under vacuum level<sup>149</sup> and the oxidation takes place at 0.083 eV against the

Ag/Ag<sup>+</sup> reference couple). In addition, the electrochemical band gap energy can be calculated from the energy difference between the HOMO and LUMO levels.

Figure 52 shows the redox behaviour of **P1(2)**, **P2** and **P3**. As a result of having the same acceptor repeat units, they (**P1**, **P2**, **P3**) have comparable LUMO energy levels which is in the range (3.07-3.11 eV). In addition, **P3** has lower HOMO energy level compared to that of **P1(2)** and **P2** (-5.71 eV for **P1(2)**, -5.71 eV for **P2**, -5.81 eV for **P3**), this is because fluorene alternate repeat units are weaker electron donating groups than carbazole repeat units. A comparison of the electrochemical band gap energy indicates that **P3** has the widest band gap energy while **P1(2)** and **P2** have comparable electrochemical band gap energies (2.60 eV for **P1(2)**, 2.61 eV for **P2**, 2.75 eV for **P3**) despite the big difference in molecular weight (Table 1) which means the electrostatic interaction between fluorine substituents on the carbazole repeat units and hydrogens at the 4-position on the methylpyrrole repeat units (Figure 50) does exist in **P2**. It can be seen that there are differences between the optical and electrochemical band gap around (0.5 eV) as expected due to exciton binding energy which is in the range of (0.40 – 1.00 eV)<sup>150</sup>.

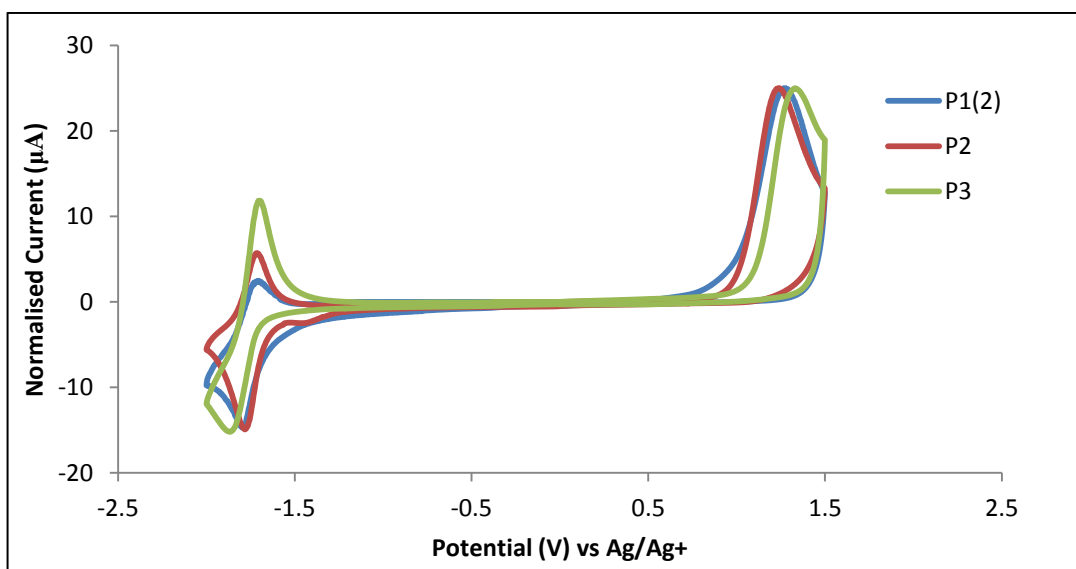


Figure 52. Cyclic voltammetry curves of **P1(2)**, **P2** and **P3** .

A comparison of the redox behaviour of **P1(2)** with its analogous thiophene copolymer **PCDTBT** reported by Leclerc et al.<sup>11b</sup> (Figure 51) indicates that **PCDTBT** has lower electrochemical band gap energy ( $E_{\text{elect}} = 1.90$  eV for

**PCDTBT**,  $E_{\text{elect}} = 2.60$  eV for **P1(2)**). In addition, a comparison of electronic properties of **P2** with its analogous thiophene copolymer **PFCDTBT** reported by Iraqi et al.<sup>147</sup> (Figure 51) indicates that **P2** has higher electrochemical band gap energy ( $E_{\text{elect}} = 1.80$  eV for **PFCDTBT**,  $E_{\text{elect}} = 2.64$  eV for **P2**). Also, **P3** has wider electrochemical band gap energy compared to that of analogous thiophene copolymer **APF03** reported by Admassie et al.<sup>148</sup> (Figure 51) indicating that **P3** has higher electrochemical band gap energy ( $E_{\text{elect}} = 2.00$  eV for **APF03**,  $E_{\text{elect}} = 2.75$  eV for **P3**). It is interesting to note that the reduction of electronic delocalisation along the polymer backbone of these version of polymers as a result of steric hindrance induced by the methyl groups on the nitrogen of pyrrole units on **P1(2)**, **P2** and **P3**.

**Table 2. Summary of photo-physical and electrochemical properties of P1, P2 and P3.**

Polymer	$\lambda_{\text{max}}$ (solution)	$\lambda_{\text{max}}$ (Thin Film)	$E_{\text{op}}$ (eV)	HOMO (eV)	LUMO (eV)	$E_{\text{elect}}$ (eV)
<b>P1(2)</b>	364, 486	364, 505	2.03	-5.71	-3.11	2.60
<b>P2</b>	352, 486	355, 490	1.85	-5.71	-3.09	2.62
<b>P3</b>	345, 459	346, 386	2.15	-5.81	-3.07	2.75

### 5.1.3. Thermal analysis of P1, P2, P3

The thermal stability of **P1**, **P2** and **P3** were studied using TGA as shown in Figure 53. It can be seen that all three polymers exhibit a high thermal stability up to 400 °C which is high enough for the requirements of solar cell applications. The degradation onset of **P1** occurred at 431 °C with a total weight loss percentage of 50.3% at 800 °C. In addition, the degradation onset of **P2** occurred at 434 °C with a total weight loss percentage of 48.36% at 800 °C. Finally, the degradation onset of **P3** occurred at 430 °C and the total weight loss percentage was 55.29% at 800 °C. It is clear, they all have similar degradation onset which indicates that the degradation can be assigned to the alkyl chain attached to the carbazole or fluorene units.

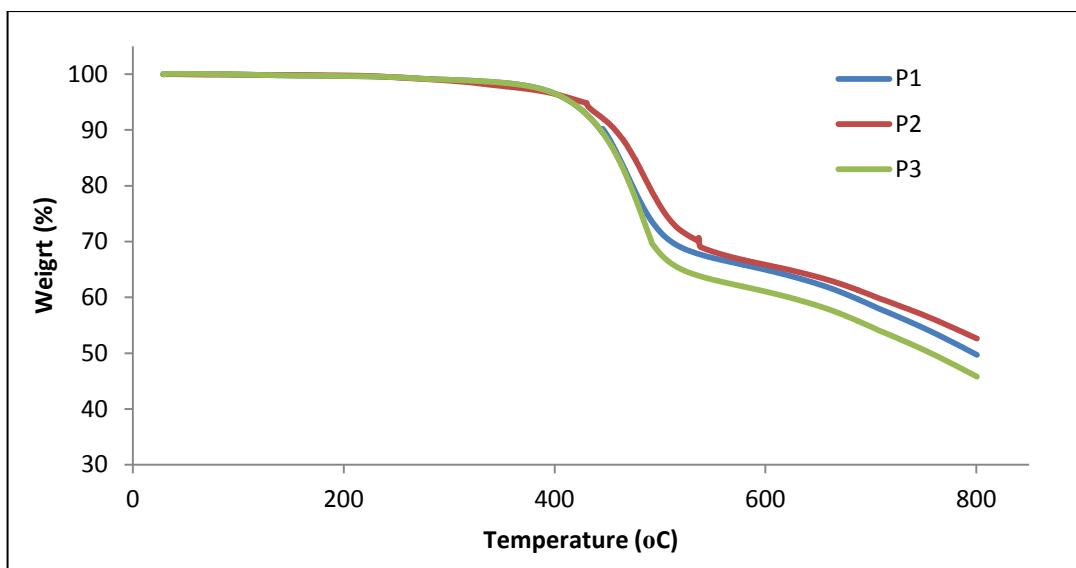
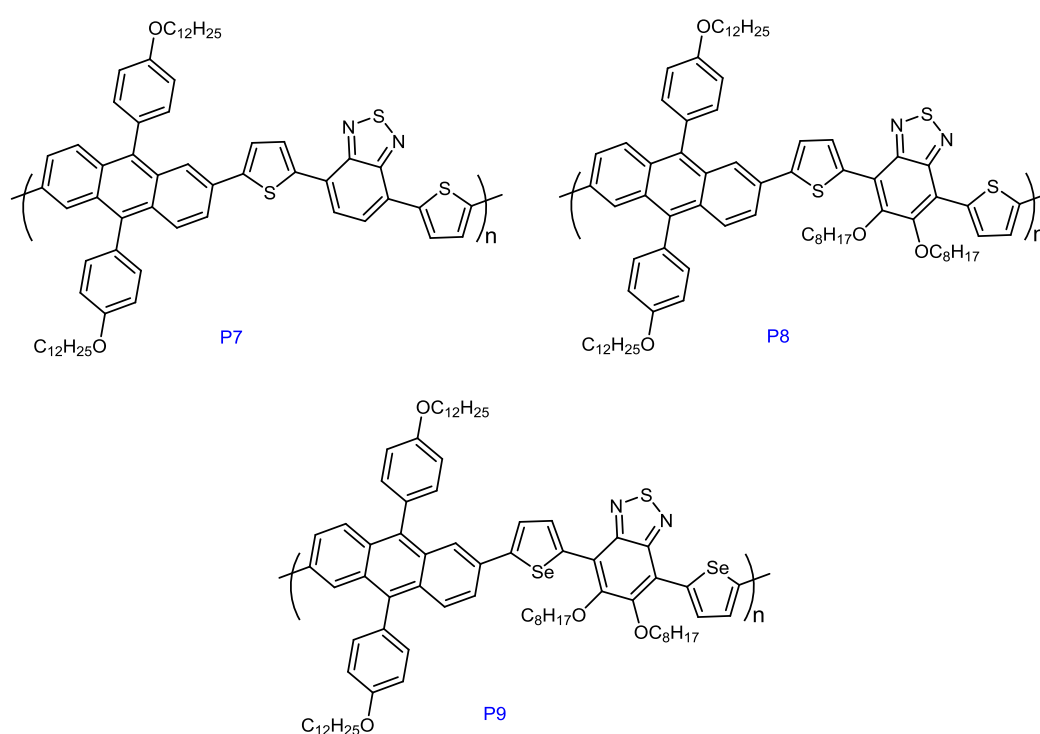


Figure 53. TGA curves of P1, P2 and P3.

### 5.2. 2,6- Linked anthracene based copolymer (P7, P8, P9)

A range of 2,6- linked anthracene based copolymers designed to be low band gap copolymers due to alternation of donor – acceptor groups along the polymer backbone were prepared. These copolymers should be able to harvest more photons from sunlight (Figure 54). The **P7**, **P8** and **P9** were synthesised successfully using Suzuki cross coupling and analysed by  $^1\text{H}$ NMR, elemental analysis and GPC. The thermal stability was studied using TGA and the physical and electrical properties of these polymers were studied using UV-Vis spectroscopy and cyclic voltammetry.



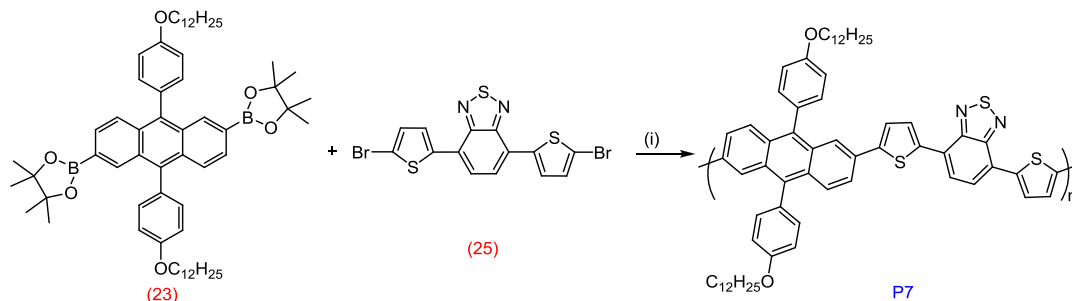
**Figure 54.** The chemical structure of **P7**, **P8**, **P9**.

#### 5.2.1. Preparation of P7, P8, P9

Preparation of **P7**, **P8** and **P9** were carried out using Suzuki cross coupling polymerization reactions. The mechanism of the reaction is illustrated in Figure 44.

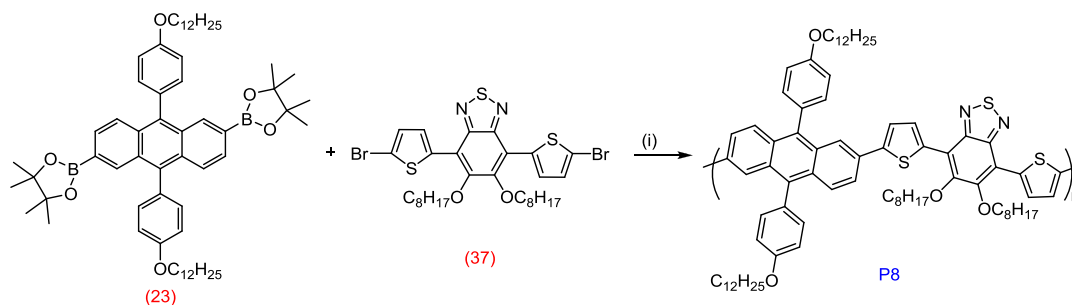
Poly(9,10-bis(4-(dodecyloxy)phenyl)-anthracene-2,6-diyl-alt-(4,7-dithiophen-2-yl)-2',1',3'-benzothiadiazole-5,5-diylium] (**P7**) was prepared by reacting 2,6-bis-(4,4,5,5-

tetramethyl-[1,3,2]dioxaborolan-2-yl)-9,10-bis(4-(dodecyloxy)phenyl) anthracene (**23**) with 4,7-bis(5-bromothiophen-2-yl)benzo[c][1,2,5]thiadiazole (**25**), as shown in Scheme 63.



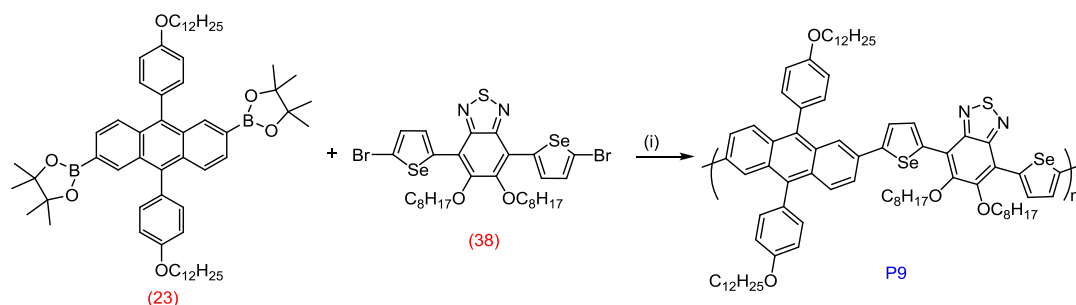
**Scheme 63. Preparation of P7. (i) Pd(AcO)<sub>2</sub>, tri-*o*-tolylphosphine, toluene, tetraethylammonium hydroxide.**

Poly(9,10-bis(4-(dodecyloxy)phenyl)-anthracene-2,6-diyl-alt-(5,6-bis(octyloxy)-4,7-di (thiophen-2-yl)benzo[1,2,5]thiadiazole-5,5-diyl) (**P8**) was prepared by reacting 2,6-bis-(4,4,5,5-tetramethyl-[1,3,2]dioxaborolan-2-yl)-9,10-bis(4-(dodecyloxy)phenyl)anthracene (**23**) with 4,7-bis(5-bromothiophen-2-yl)-5,6-bis(octyloxy)benzo[c][1,2,5]thiadiazole (**37**) as shown in Scheme 64.



**Scheme 64. Preparation of P8. (i) Pd(AcO)<sub>2</sub>, tri-*o*-tolylphosphine, toluene, tetraethylammonium hydroxide.**

Poly(9,10-bis(4-(dodecyloxy)phenyl)-anthracene-2,6-diyl-alt-(5,6-bis(octyloxy)-4,7-di(selenophen-2-yl)benzo[1,2,5]thiadiazole-5,5-diyl) (**P9**) was prepared by reacting 2,6-bis-(4,4,5,5-tetramethyl-[1,3,2]dioxaborolan-2-yl)-9,10-bis(4-(dodecyloxy)phenyl)anthracene (**23**) with 4,7-bis(5-bromoselenophen-2-yl)-5,6-bis(octyloxy)benzo[c][1,2,5]thiadiazole (**38**) as shown in Scheme 65.



**Scheme 65. Preparation of P9. (i) Pd(AcO)<sub>2</sub>, tri-*o*-tolylphosphine, toluene, tetraethylammonium hydroxide.**

## 5.2.2. Characterization of P7, P8, P9

### 5.2.2.1. Gel Permeation Chromatography studies of P7, P8 and P9

All the GPC results are illustrated in Table 3, with the polydispersity (PD) and the degree of polymerization (DP).

**Table 3. Yields and GPC results for P7, P8 and P9.**

Polymer	Yield %	Solvent				
		Fraction	M <sub>n</sub>	M <sub>w</sub>	PD	DP
P7	35	Toluene	3000	3800	1.2	3
	44.2	Chloroform	3500	4900	1.4	4
	12	Chlorobenzene	7800	9100	1.1	8
P8	29.5	Toluene	9100	12600	1.38	7
	54	Chloroform	25000	34000	1.35	20
P9	92	Chloroform	48700	101400	2.08	36

### 5.2.2.2. <sup>1</sup>HNMR analysis of P7, P8 and P9

The <sup>1</sup>HNMR analysis of polymers **P7**, **P8** and **P9** were carried out in C<sub>2</sub>D<sub>2</sub>Cl<sub>4</sub> at 80 °C in order to avoid broad signal especially in the down field region around (6 – 9 ppm) as a result of polymer aggregation.

The spectrum of **P7** illustrate in the aromatic region the protons of the anthracene hydrogens with a doublet peak at 8.07 ppm related to the two protons in the positions (a) (Figure 55). In addition, the doublet peaks which are observed at 7.66 ppm are related to the four protons on the positions (c) and (d) on the anthracene. The singlet peak at 7.84 ppm can be assigned to the benzothiazole aromatic protons (position (b)). The doublet peaks at 7.44 and 7.37 ppm are assigned to the thiophene protons on the positions (e) and (f) respectively. The spectrum also shows doublet peaks at 7.29 and 7.19 ppm which are related to the attached phenyl group on positions (g) and (h) respectively. The triplet peak at 4.15 ppm corresponds to the protons on the carbon which is bonded directly to the oxygen atom of the phenyl (position (i)). The multiplet peaks at, 1.94-1.84 and 1.60-1.18 ppm correspond to the alkyl chain protons (positions (j-s)). The triplet peak at 0.85 ppm can be assigned to the six protons on the CH<sub>3</sub> group at the end of the alkyl chain (position (t)).

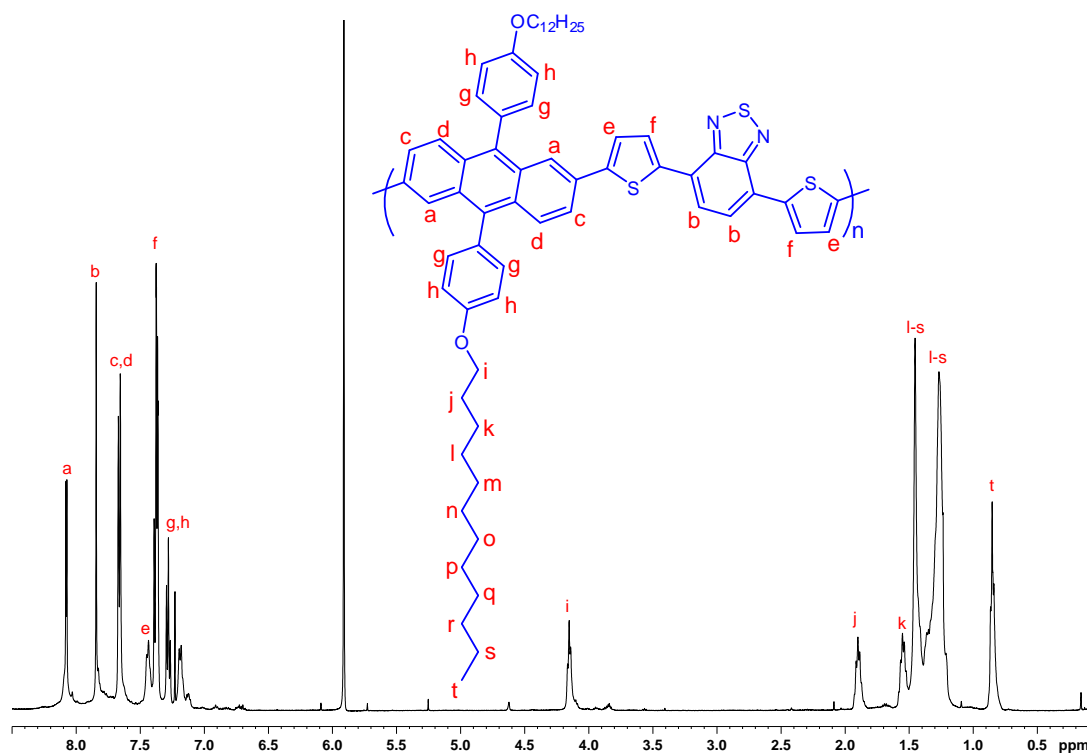


Figure 55. <sup>1</sup>H NMR spectrum of **P7** in C<sub>2</sub>D<sub>2</sub>Cl<sub>4</sub> at 80 °C.

The spectrum of the **P8** reveals six aromatic signals which are related to the anthracene and thiophene hydrogens as shown in Figure 56. The doublet peak at

8.38 ppm can be assigned to the four protons on the positions (a) and (b) on the anthracene. The singlet peak at 8.09 ppm is related to the two protons on the position (c) on the anthracene. The doublet peaks at 7.80 and 7.67 ppm correspond to the thiophene protons on the positions (d) and (e) respectively. The spectrum shows multiplet peaks at 7.56-7.33 and 7.25-7.10 ppm which correspond to the attached phenyl group protons on positions (f) and (g) respectively. The broad peak at 4.19-4.06 ppm is related to the protons on the carbon bonded directly to the oxygen atom of the phenyl groups attached to the anthracene (position (h)) and the protons on the carbon which is bonded to the oxygen on the benzothiadiazole (positions (i) and (i')). The multiplet peaks at 1.96-1.80 and 1.61-1.17 ppm correspond to the alkyl chain protons attached to the anthracene and benzothiadiazole (position (i) to (w)). The multiplet peak at 0.91-0.78 ppm is related to the twelve protons on the CH<sub>3</sub> groups at the end of the alkyl chain on anthracene and benzothiadiazole (positions (y) and (y')).

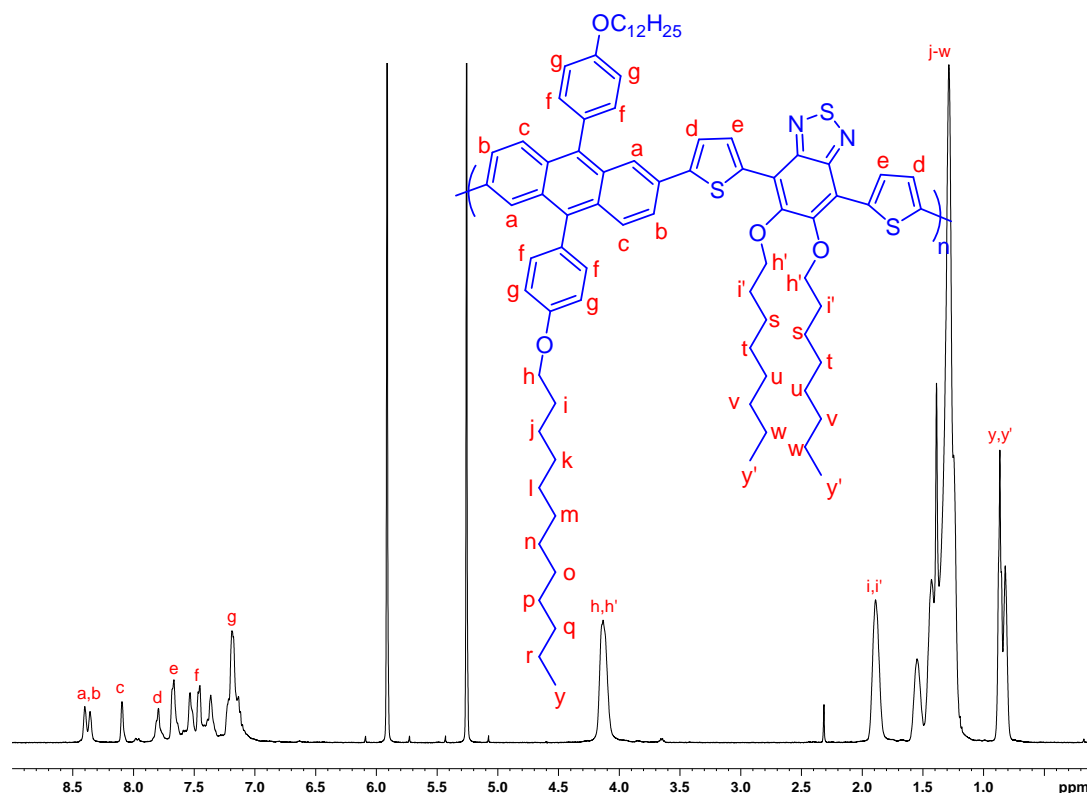


Figure 56. <sup>1</sup>H NMR spectrum of P8 in C<sub>2</sub>D<sub>2</sub>Cl<sub>4</sub> at 80 °C.

The  $^1\text{H}$ NMR spectrum of **P9** shows seven aromatic signals in the aromatic region (Figure 57). The broad singlet peak at 8.77 ppm can be assigned the two protons on the positions (a) on the anthracene. The broad singlet peaks at 8.03 and 7.76 ppm are related to the four protons on the position (b) and (c) on the anthracene. The doublet peak at 7.58 ppm corresponds to the selenophene protons on the positions (d) and (e) respectively. The spectrum shows multiplet peaks at 7.45 and 7.18 ppm which are related to the attached phenyl group on positions (f) and (g) respectively. Similarly to **P8**, the broad peak at 4.14 ppm corresponds to the protons on the carbon which is bonded directly to the oxygen atom of the phenyl group which attached to the anthracene and the protons on the carbon which is bonded to the oxygen on the benzothiadiazole (positions (h) and (h')). The multiplet peaks at 2.05-1.82 and 1.61-1.13 ppm correspond to the alkyl chain protons that attached to the anthracene and benzothiadiazole (positions (i), (i') and (k-w)). The multiplet peak at 0.94-0.76 ppm related the twelve protons on the  $\text{CH}_3$  group at the end of the alkyl chain on anthracene and benzothiadiazole (position (y) and (y')).

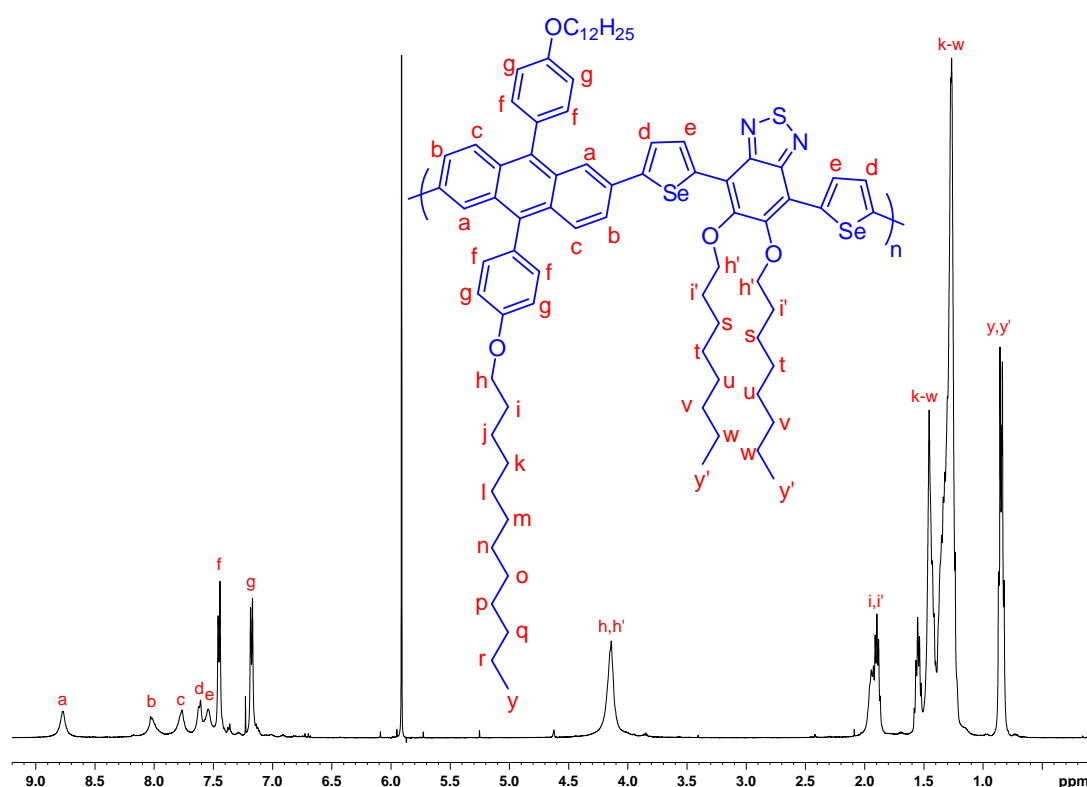
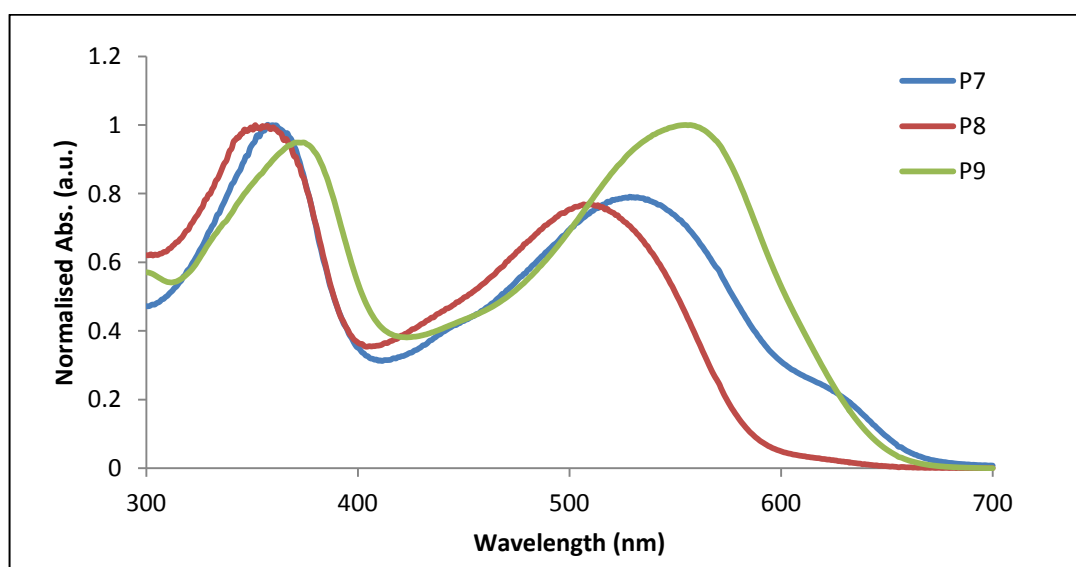


Figure 57.  $^1\text{H}$ NMR spectrum of **P9** in  $\text{C}_2\text{D}_2\text{Cl}_4$  at  $80\text{ }^\circ\text{C}$ .

### 5.2.2.3. The UV-visible absorption spectroscopy analysis of P7, P8 and P9

The UV-Visible absorption spectra of **P7** (chloroform fraction), **P8** (chloroform fraction) and **P9** were performed in chloroform solution and on thin films at room temperature.

Figure 58 shows the absorption spectra of **P7**, **P8** and **P9** in chloroform solutions. It is clear that they have different absorption band maxima ( $\lambda_{\text{max}}$ ) because they have different donor or acceptor repeat units along their polymer backbones. It can be seen that all polymers show two absorption bands, the first bands are between 352 and 375 nm while the second bands are between 507 and 555 nm. A comparison of the absorption bands at maxima of **P7** and **P8** indicates that **P7** is red shifted compared to that of **P8** as a result of the effect of octyloxy groups attached to the benzothiazole repeated units in **P8**. The spectrum indicate that **P9** is red shifted compared to that of **P7** and **P8** (360 and 532 nm for **P7** vs 352 and 507 nm for **P8** vs 375 and 555 nm for **P9**).



**Figure 58. Absorption spectra of P7, P8 and P9 in chloroform solutions.**

Figure 59 shows UV-Vis spectra for **P7**, **P8** and **P9** as solid thin films. Again, the thin film absorption spectra are red shifted compared to those of solutions due to aggregation and planarity of polymer chains. It is interesting to note the effect of octyloxy groups attached to the benzothiazole repeat units in polymer **P8** on the conjugation and

electronic properties. It can be seen that **P7** has higher absorption at  $\lambda_{\max}$  compared to that of **P8** (368 and 563 nm for **P7** vs 365 and 523 nm for **P8**). Also, the optical band gap energy for **P7** as measured from the onset of its absorption in film also emphasises a narrower gap than that of **P8** (1.84 eV for **P7** vs 1.96 eV for **P8**) which indicates that octyloxy groups have a negative impact on the conjugation properties of **P8**. The donating properties of the octyloxy substituent attached to the benzothiadiazole repeat units decrease their electron accepting properties and intramolecular charge transfer along the polymer backbone. Also, these substituents possibly affect the planarity of the polymer backbone due to steric hindrance and so lead to lowering the absorption maxima but they increase polymer solubility and so processability. In addition, a comparison of the absorption maxima of **P9** with that of **P8** indicates a red shift (379 and 569 nm for **P9** vs 365 and 523 nm for **P8**) and the optical band gap energy for **P9** is lower than **P8** (1.85 eV for **P9** vs 1.96 eV for **P8**). It is clear that replacing thiophene with selenophene leads to increasing the electron donating properties and the intramolecular charge transfer along the polymer backbone as a result of the intermolecular Se-Se interactions which could facilitate intramolecular charge transfer<sup>151</sup>. A comparison the optical band gap energy of **P7** and **P9** indicate that they have comparable optical band gap energy (1.85 eV for **P9** vs 1.84 eV for **P7**) but **P9** has higher absorption bands at  $\lambda_{\max}$  (379 and 569 nm for **P9** vs 368 and 563 nm for **P7**). It can be seen that replacing thiophene with selenophene would increase the extended conjugated along the polymer backbone even with the negative impact of the dioctyloxy substituents.

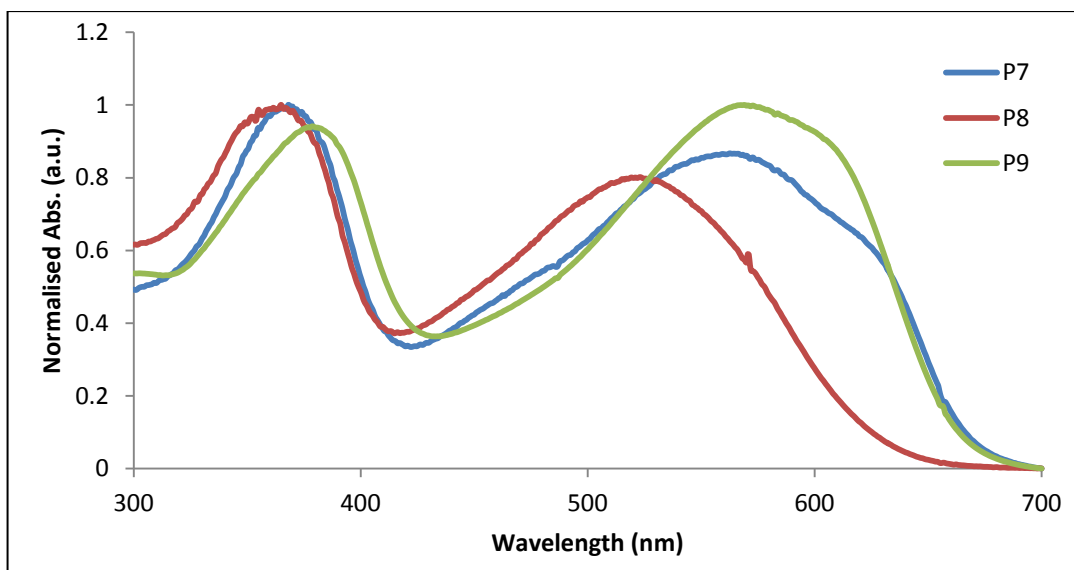


**Figure 59.** Absorption spectra of **P7**, **P8** and **P9** as thin films.

A comparison of **P7** with its carbazole analogous (**PCDTBT**) reported by Leclerc *et al.*<sup>11b</sup> (Figure 60) indicates that **P7** has slightly lower optical band gap energy (1.84 eV for **P7** vs 1.88 eV for **PCDTBT**) and higher absorption band at  $\lambda_{\max}$  (563 nm for **P7** vs 545 nm for **PCDTBT**). In addition, a comparison of **P8** (chloroform fraction) with its polycarbazole equivalent reported by Iraqi *et al.*<sup>93a</sup> (**PCDTOBT**) (Figure 60) indicates that they have the same optical band gap energy (1.98 eV for **P8** vs 1.98 eV for **PCDTOBT**) but the absorption band at  $\lambda_{\max}$  of **P8** is blue shifted compared to that of **PCDTOBT** (365 and 523 nm for **P8** vs 391 and 536 nm for **PCDTOBT**). Moreover, a comparison of **P9** with its equivalent carbazole polymer reported by Iraqi *et al.*<sup>152</sup> (**PCDSeOBT**) (Figure 60) which gave absorption band at  $\lambda_{\max}$  558 nm, indicates that **P9** absorption spectra is red shifted when compared with **PCDSeOBT** result. Also, **P9** has lower band gap energy compared to that of **PCDSeOBT** (1.85 eV for **P9** vs 1.94 eV for **PCDSeOBT**). These value emphasis that anthracene repeat units has higher higher electron donating properties compared to that of carbazole repeat units as a consequence to a strong intramolecular charge transfer along polymer backbone.

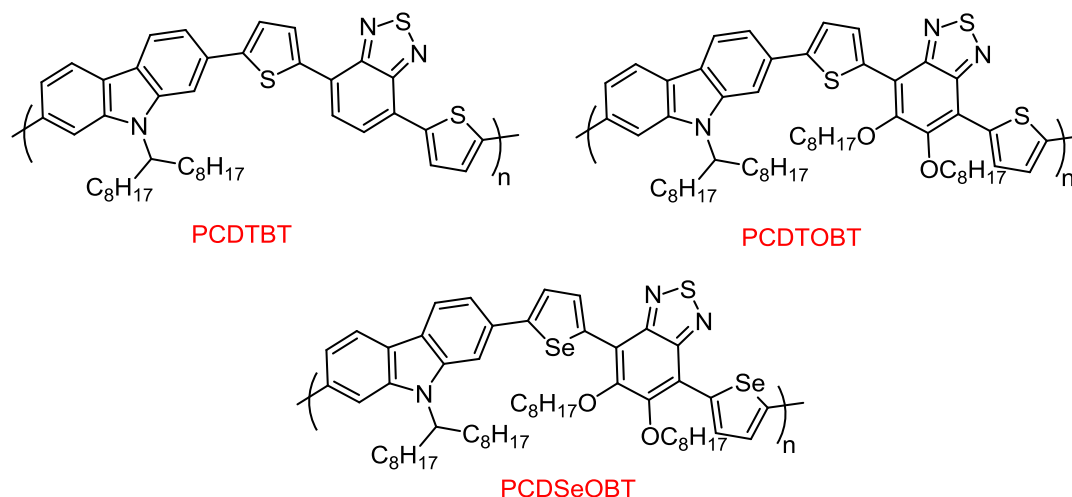


Figure 60. The chemical structure of PCDTBT, PCDOBT and PCDSeOBT.

#### 5.2.2.4. Cyclic Voltammetry (CV) analysis of P7, P8 and P9

In order to study the electrochemical properties of the polymers, Cyclic Voltammetry was carried out on drop-cast polymer films in acetonitrile and tetrabutylammonium perchlorate as electrolyte. The onset of oxidation and reduction can be obtained from cyclic voltammetry curves and used to assess the energy level of HOMO and LUMO (ferrocene has an ionisation potential of - 4.8 eV) under vacuum level <sup>149</sup> and the oxidation takes place at 0.083 eV against the Ag/Ag<sup>+</sup> reference couple). In addition, the electrochemical band gap energy can be calculated from the energy difference between HOMO and LUMO.

The cyclic voltammetry curves of **P7**, **P8** and **P9** are shown in Figure 61. A comparison of **P7** and **P8** indicates that they have very close HOMO energy levels (-5.44 eV for **P7** vs -5.48 eV for **P8**) because they have the same donor repeat units. On the other hand, **P8** has higher negative potential to that of **P7** due to the reduction of the extended conjugation along polymer backbone. The deeper LUMO energy level of **P7** compared to that of **P8** is possibly due to a reduction of the electron accepting ability of benzothiadiazole repeat units by attaching donating octyloxy substituents to them. The table shows that unlike the optical band gap energy, **P8** and **P9** have the same electrochemical band gap energy as a result of having comparable HOMO and LUMO energy levels. It can be seen that replacing

thiophene with selenophene has no clear effect on the HOMO and LUMO energy levels of **P8** and **P9**. It can be seen that **P7** has the lowest electrochemical band gap energy compared to that of **P8** and **P9** (2.20 eV for **P7** vs 2.34 eV for **P8** vs 2.33 eV for **P9**). Again, the optical band gap energies of these polymers (1.84-1.96 eV) are lower than their electrochemical band gap energy (2.30-2.34 eV) due to exciton binding energy which is in the range of (0.40 – 1.00 eV)<sup>150</sup>.

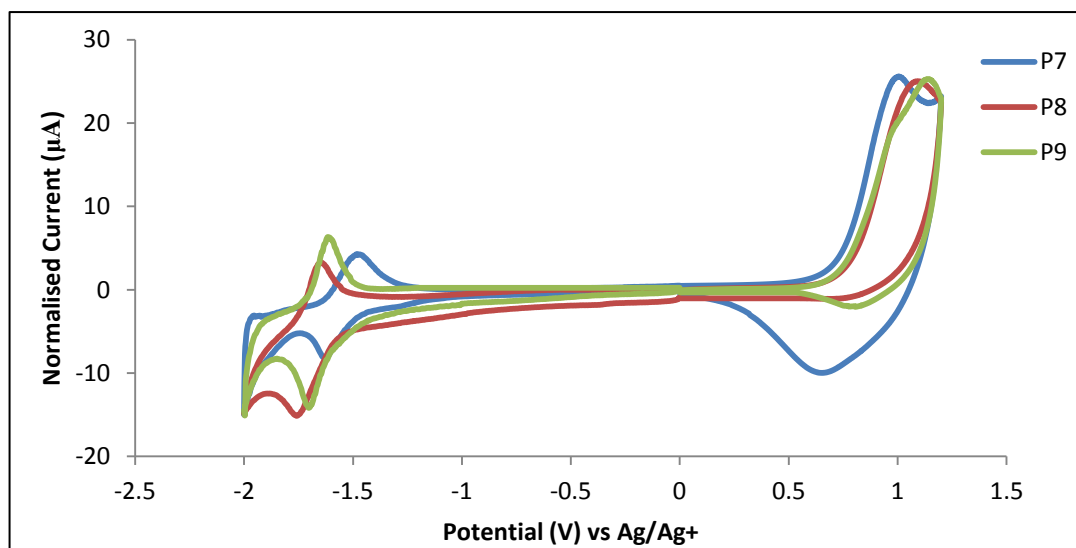


Figure 61. Cyclic voltammetry curves of **P7**, **P8** and **P9**.

A comparison of **P7** redox potential results to that of **PCDTBT** reported by Leclerc et al.<sup>11b</sup> (Figure 60) indicates that **PCDTBT** has lower electrochemical band gap energy (1.90 eV for **PCDTBT**, 2.20 eV for **P7**) but **P7** has lower optical band gap energy ( $E_{op}$  = 1.84 eV for **P7**,  $E_{op}$  = 1.88 eV for **PCDTBT**). Also, **P7** has higher HOMO energy level compared to that of **PCDTBT** which has HOMO energy level at (-5.44 eV for **P7** vs -5.5 eV for **PCDTBT**) while **PCDTBT** has deeper LUMO energy level compared to that of **P7** (-3.24 eV for **P7** vs -3.6 eV for **PCDTBT**). In addition, a comparison of **P8** with **PCDTOBT** reported by Iraqi et al.<sup>93a</sup> (Figure 60) indicates that **PCDTOBT** has lower electrochemical band gap energy (2.13 eV for **PCDTBT**, 2.34 eV for **P8**). In addition, they have comparable HOMO energy level (-5.40 eV for **PCDTOBT** vs -5.48 eV for **P8**) but **P8** displays higher LUMO level compared to that of **PCDTOBT** (-3.27 eV for **PCDTOBT** vs -3.14 eV for **P8**). Moreover, a comparison of **P9** with **PCDSeOBT** reported by Iraqi et al.<sup>152</sup>

(Figure 60) indicates that they have comparable electrochemical band gap energy (2.36 eV for **PCDSeOBT** vs 2.33 eV for **P9**). In addition, they have the same HOMO (-5.46 eV for **PCDSeOBT** vs -5.47 eV for **P9**) and LUMO energy levels (-3.10 eV for **PCDSeOBT** vs -3.14 eV for **P9**). According to the HOMO and LUMO energy levels, it is clear that ananthracene based polymers have higher open circuit voltage than carbazole analogous polymer which would harvest more photons from sunlight. The cyclic voltammetry result is affected by the thickness of the film, the film morphology and the exciton binding energies.

**Table 4. Summary of the photophysical and the electrochemical properties of P7, P8 and P9.**

Polymer	$\lambda_{\max}$ (solution)	$\lambda_{\max}$ (Thin Film)	$E_{\text{op}}$ (eV)	HOMO (eV)	LUMO (eV)	$E_{\text{elect}}$ (eV)
<b>P7</b>	360, 532	368, 563	1.84	-5.44	-3.21	2.20
<b>P8</b>	355, 507	365, 523	1.96	-5.48	-3.14	2.34
<b>P9</b>	375, 555	379, 569	1.85	-5.47	-3.14	2.33

### 5.2.3. Thermal analysis of P7, P8, P9

The thermal stability of **P7**, **P8** and **P9** were studied using TGA as shown in Figure 62. It can be seen that **P7** exhibits a high thermal stability up to 400 °C which is similar to the result obtained for **P1**, **P2** and **P3**. The degradation onset of **P7** occurred at 438 °C and then at 563 °C the degradation slightly falls, the total weight loss percentage of 75.2% at 800 °C. For **P8**, there are two main degradation onsets, the first one occurs at 340 °C and the second one takes place at 415 °C, the total weight loss percentage of 69 % at 800 °C. Finally, the degradation onset of **P9** occurs at 310 °C which is earlier than **P7** and **P8**, then at 360 °C the weight percentage starts to decrease gradually, the total weight loss percentage of 72.9 % at 800 °C. It is clear that the degradation of **P8** and **P9** start earlier than **P7** due to the loss of alkoxy groups which attached to the benzothiadiazole units. Thus, the alkyloxy group provides higher solubility but lower thermal stability.

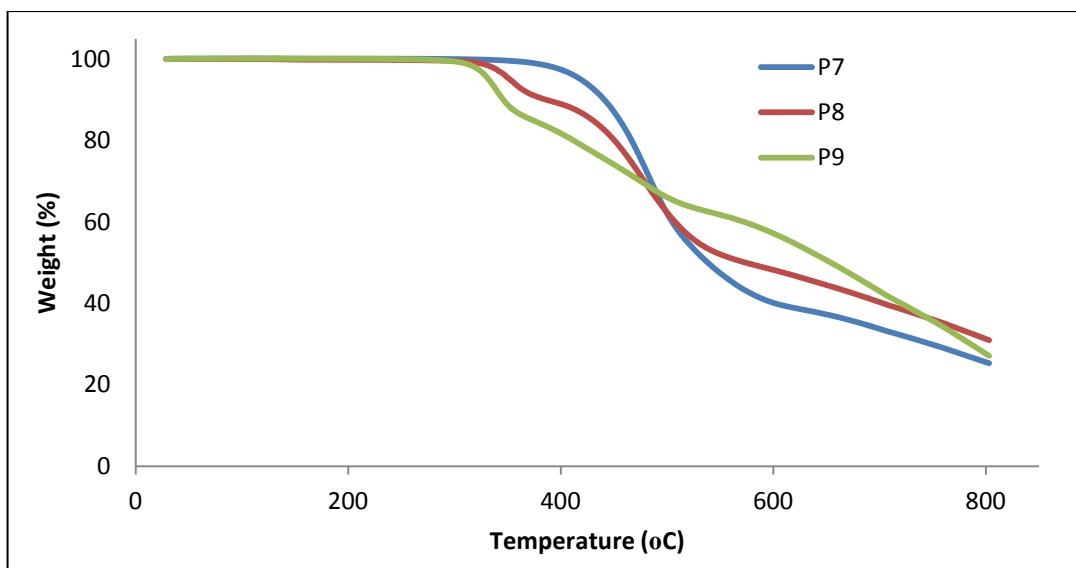
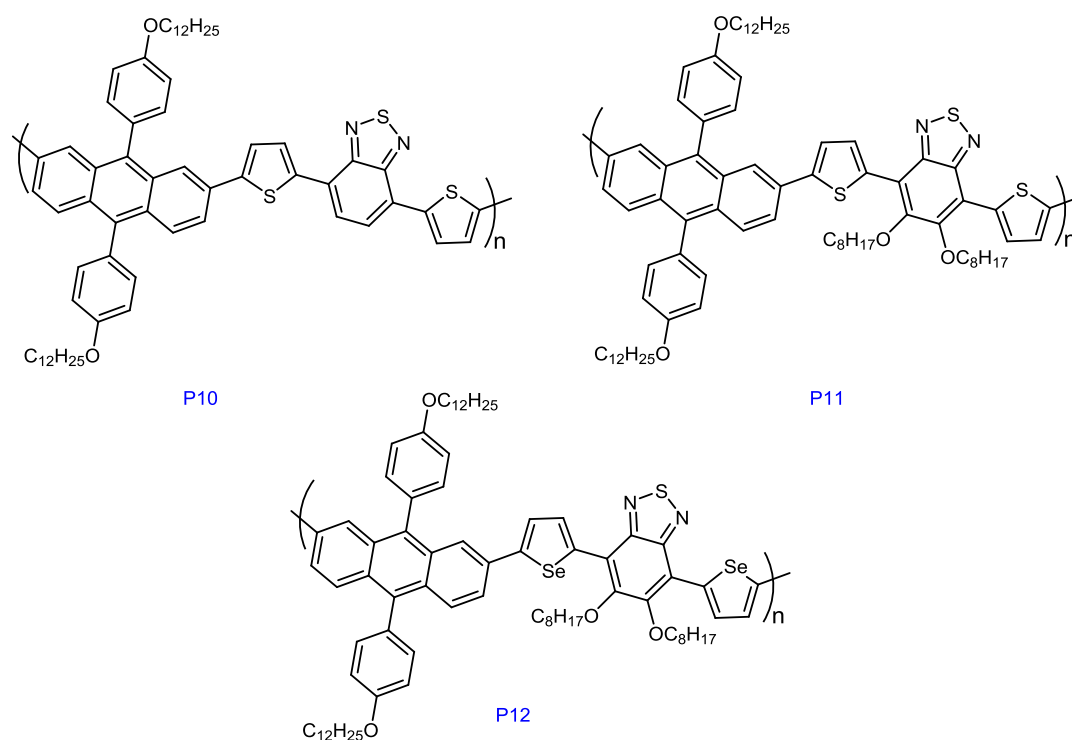


Figure 62. TGA curves of P7, P8 and P9.

### 5.3. 2,7- Linked anthracene based copolymers (P10, P11, P12)

2,6-Linked anthracene based polymers have been studied and the polymers displayed promising results for solar cell applications have. 2,7-Linked anthracene polymers have been suggested in order to study which anthracene structure provides more conjugation for solar cell application. The alternation of donor – acceptor repeat units along the polymer backbone should lead them to have a low band gap in order to harvest more photons from sunlight as shown in Figure 63. **P10**, **P11** and **P12** were synthesised successfully using Suzuki cross coupling and analysed by  $^1\text{H}$ NMR, elemental analysis and GPC. The thermal stability was studied using TGA and the physical and electrical properties of these polymers were studied using UV-Vis spectroscopy and cyclic voltammetry. In addition, a comparison of physical and electrochemical properties of 2,7-linked anthracene based polymers to that of 2,6-linked anthracene based polymers will be studied.



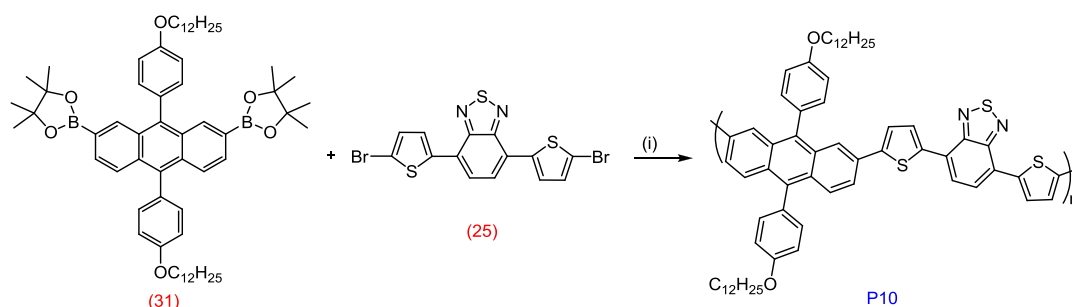
**Figure 63. Chemical structures of P10, P11 and P12.**

### 5.3.1. Preparation of P10 , P11 , P12

The preparation of **P10**, **P11** and **P12** were carried out using Suzuki cross coupling polymerization reactions. The mechanism of the reaction is illustrated in Figure 44.

For **P10**, **P11** and **P12**, palladium was removed in different ways in order to make sure there is not palladium impurities left in the polymers. Firstly, the crude polymers were dissolved in chloroform and ammonium hydroxide solution (28 % in H<sub>2</sub>O) was added. The mixtures were heated to reflux for three hours then cooled to room temperature. The organic layer was separated and disodium ethylenediaminetetraacetate was added and stirred for overnight. The mixture was washed with water several times then concentrated. It is reported that using this method reduces the amount of palladium residues to less than 9 ppm. As mentioned before removing palladium residues leads to higher charge mobility, avoidance of space charge carrier effect, reduces recombination (results from impurities) and improves the behaviour of polymers in devices<sup>153</sup>.

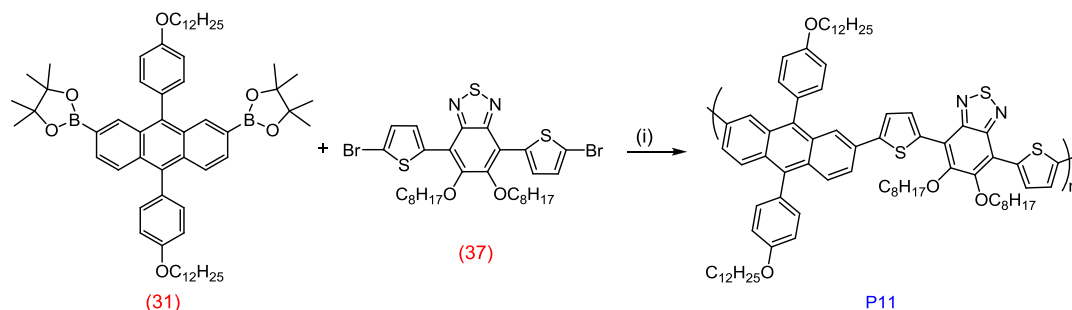
Poly(9,10-bis(4-(dodecyloxy)phenyl)-anthracene-2,7-diyl-alt-(4,7-dithiophen-2-yl)-2',1',3'-benzothiadiazole-5,5-diyl] (**P10**) was prepared by reacting 2,7-bis(4,4,5,5-tetramethyl-[1,3,2]dioxaborolan-2-yl)-9,10-bis(4-(dodecyloxy)phenyl)anthracene (**31**) with 4,7-bis(5-bromothiophen-2-yl)benzo[c][1,2,5]thiadiazole (**25**), as shown in Scheme 66.



**Scheme 66. Preparation of P10. (i) Pd(AcO)<sub>2</sub> , tri-*o*-tolyphosphine, Toluene, tetraethylammonium hydroxide.**

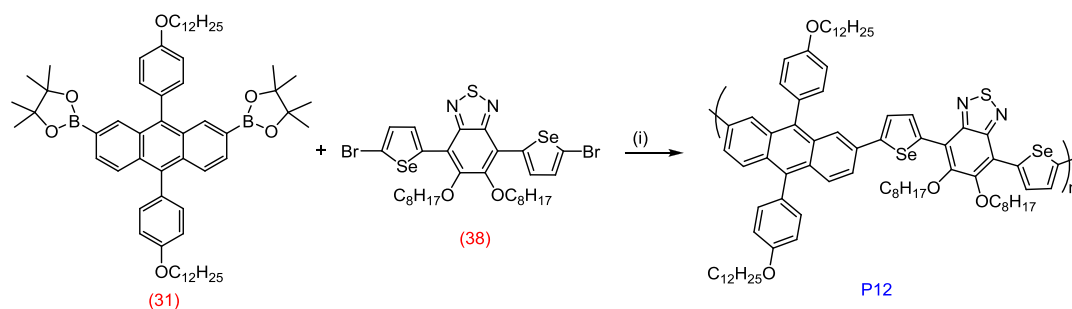
Poly(9,10-bis(4-(dodecyloxy)phenyl)-anthracene-2,7-diyl-alt-(5,6-bis(octyloxy)-4,7-di (thiophen-2-yl)benzo[1,2,5]thiadiazole-5,5-diyl] (**P11**) was prepared by

reacting 2,7-bis-(4,4,5,5-tetramethyl-[1,3,2]dioxaborolan-2-yl)-9,10-bis(4-(dodecyloxy)phenyl)anthracene (**31**) with 4,7-bis(5-bromothiophen-2-yl)-5,6-bis(octyloxy)benzo[*c*][1,2,5]thiadiazole (**37**) as shown in Scheme 67.



**Scheme 67. Preparation of P11. (i) Pd(AcO)<sub>2</sub>, tri-*o*-tolylphosphine, Toluene, tetraethylammonium hydroxide.**

Poly(9,10-bis(4-(dodecyloxy)phenyl)-anthracene-2,7-diyl-alt-(5,6-bis(octyloxy)-4,7-di(selenophen-2-yl)benzo[1,2,5]thiadiazole-5,5-diyl) (**P12**) was prepared by reacting 2,7-bis-(4,4,5,5-tetramethyl-[1,3,2]dioxaborolan-2-yl)-9,10-bis(4-(dodecyloxy)phenyl)anthracene (**22**) with 4,7-bis(5-bromoselenophen-2-yl)-5,6-bis(octyloxy)benzo[*c*][1,2,5]thiadiazole (**37**) as shown in Scheme 68.



**Scheme 68. Preparation of P12. (i) Pd(AcO)<sub>2</sub>, tri-*o*-tolylphosphine, Toluene, tetraethylammonium hydroxide.**

### 5.3.2. Characterization of P10, P11, P12

#### 5.3.2.1. Gel Permeation Chromatography studies of P10, P11 and P12

All the GPC results are illustrated in Table 5, with the polydispersity (PD) and the degree of polymerization (DP).

Table 5. Yields and GPC results for P10 , P11 and P12.

Polymer	Yield %	Solvent		M <sub>n</sub>	M <sub>w</sub>	PD	DP
		Fraction					
P10	48.5	Toluene		4700	6400	1.36	5
	17.5	Chloroform		13700	20100	1.46	11
P11	78.9	Chloroform		21700	35400	1.63	17
P12	85.6	Chloroform		33300	52200	1.56	25

### 5.3.2.2. <sup>1</sup>HNMR analysis of P10, P11 and P12

The <sup>1</sup>HNMR analysis of polymers **P10**, **P11** and **P12** were carried out in  $C_2D_2Cl_4$  at 100 °C in order to avoid broad signals especially in the downfield region around (6 – 9 ppm) as a result of polymer aggregation.

The <sup>1</sup>HNMR spectrum of **P10** show eight peaks in the aromatic region for anthracene, thiophene and benzothiadiazole protons (Figure 64). The broad singlet peak at 8.08 ppm corresponds to the four protons on position (a) on the anthracene and position (b) on the benzothiadiazole. Also, the rest of anthracene protons on position (c) and (d) are observed at 7.85-7.75 ppm which give multiplet peaks. The doublet peaks at 7.63 and 7.50 ppm are related to the thiophene protons on positions (e) and (f) respectively. It is clear that the 2,7-linked anthracene units do not show a symmetrical structure as the 2,6-linked anthracene units, so the attached phenyl groups have different chemical environments. The doublet peaks at 7.41 and 7.34 ppm are related to the phenyl group protons on the positions (g') and (g) respectively, while the doublet peaks at 7.23 and 7.15 ppm can be assigned to the other phenyl group protons in the other phenyl group in the positions (h') and (h) respectively. The singlet peaks at 4.20 and 4.14 ppm corresponds to the protons on the carbon which is bonded directly to the oxygen atom of the phenyl group which attached to the anthracene on the positions (k') and (k) respectively. The

multiplet peaks at, 1.97-1.83, 1.63-1.49 and 1.49-1.18 ppm correspond to the alkyl chain protons attached to the anthracene (l-u) and (l'-u'). The multiplet peak at 0.93-0.77 ppm can be assigned to the CH<sub>3</sub> group protons at the end of the alkyl chains.

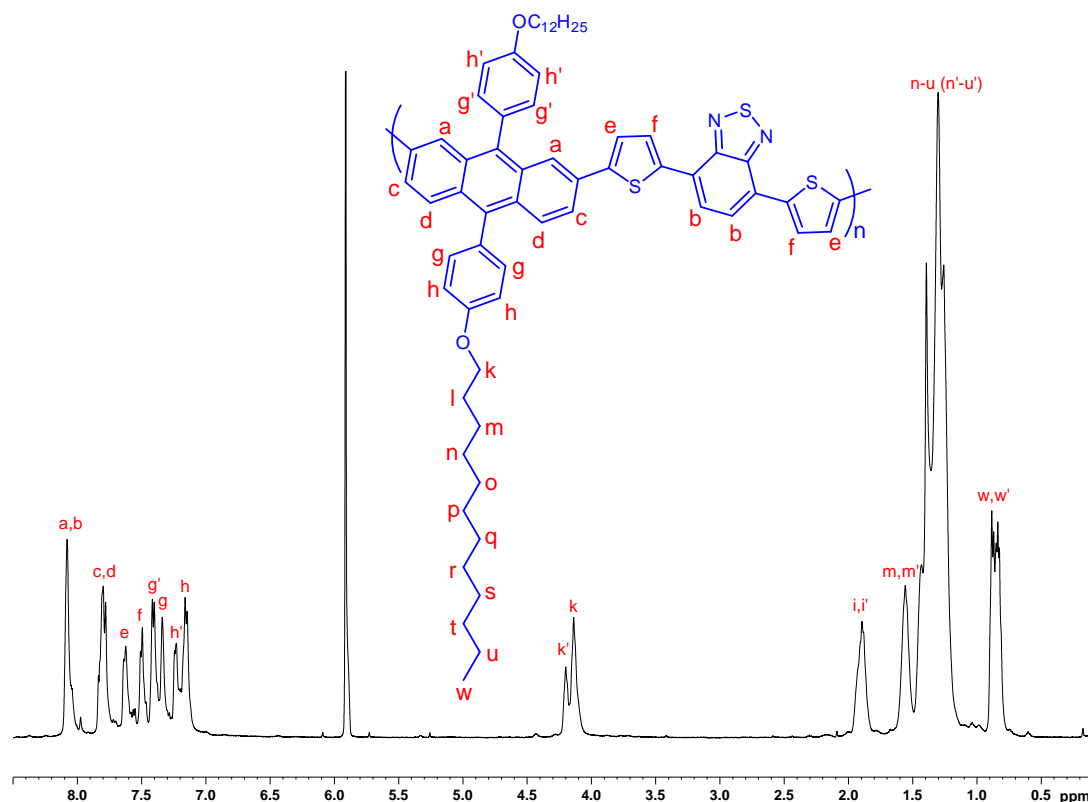


Figure 64. <sup>1</sup>H NMR spectrum of P10 in C<sub>2</sub>D<sub>2</sub>Cl<sub>4</sub> at 100 °C

The structure of **P11** was confirmed using <sup>1</sup>H NMR as shown in Figure 65. It is clear that the singlet peak which is displayed at 8.40 ppm is related to the anthracene protons in the positions (a). The four anthracene protons in the positions (b) and (c) are observed at 8.11 and 7.79 ppm. Also, the spectrum shows two doublet peaks at 7.67 and 7.51 ppm which are related to the thiophene protons in the positions (d) and (e) respectively. The structure of this polymer is not symmetrical and so the attached phenyl groups protons are displayed at different chemical environments. Thus, the spectrum shows doublet peaks at 7.42 and 7.37 ppm which are related to the phenyl group protons in the positions (f') and (f) respectively while the other phenyl group protons in the position (g') and (g) are observed as doublet peaks at 7.21 and 7.16 ppm respectively. The broad singlet

peak at 4.15 ppm corresponds to the protons on the carbon which is bonded directly to the oxygen atom of the phenyl group attached to the anthracene units and to the protons on the carbons which are bonded to the oxygen atom attached to the benzothiadiazole on the positions (h), (h') and (h''). The multiplet peaks 1.97-1.82 and 1.61-1.17 ppm corresponds to the alkyl chain protons that attached to the anthracene (l-u) and (l'-u'). The multiplet peak at 0.91-0.77 ppm can be assigned to the CH<sub>3</sub> group protons at the end of the alkyl chains that attached to the phenyl group in the positions (y) and (y') and the benzothiadiazole position (y'').

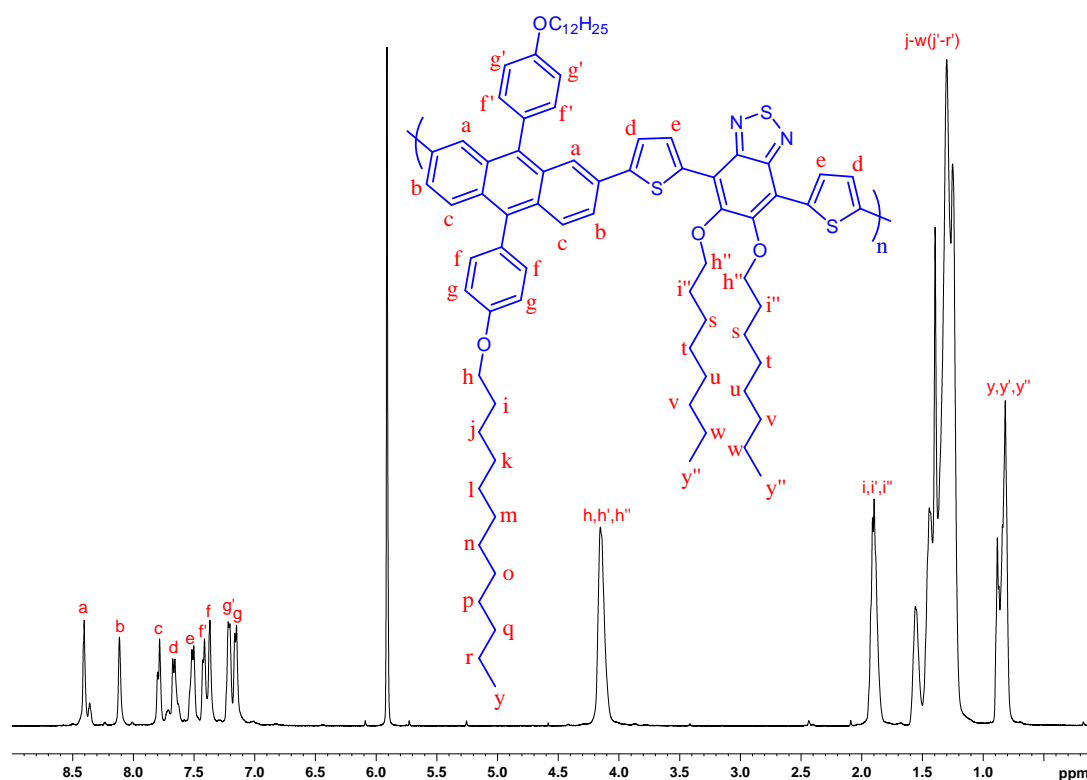


Figure 65. <sup>1</sup>H NMR spectrum of P11 in C<sub>2</sub>D<sub>2</sub>Cl<sub>4</sub> at 100 °C.

The <sup>1</sup>H NMR spectrum of P12 (Figure 66) reveal the protons of the anthracene hydrogen in the aromatic region with doublet peak at 8.73 ppm appointed to the four protons on the positions (a) and (b). The broad singlet peak at 8.06 ppm is related to the anthracene protons in the position (c). The signals at 7.76 and 7.62 ppm can be assigned to the selenophene protons in the positions (d) and (e) respectively. Again, 2,7-anthracene based copolymers do not show a symmetrical structure and so two chemical environments were observed for attached phenyl

groups. Thus, the spectrum shows doublet peaks at 7.48 and 7.41 ppm which are related to the phenyl group protons in the positions (f') and (f) respectively while the other phenyl group protons in the position (g') and (g) are observed as doublet peaks at 7.21 and 7.15 ppm respectively. The broad singlet peak centre around 4.16 ppm corresponds to the protons on the carbons which are bonded directly to the oxygen atoms of the phenyl group and to the protons on the carbons which are bonded to the oxygen atoms attached to the benzothiadiazole units on the positions (h, h') and (h''). The multiplet peaks 2.04-1.80 and 1.61-1.17 ppm corresponds to the alkyl chain protons that attached to the anthracene (l-u) and (l'-u'). The multiplet peak at 0.91-0.78 ppm can be assigned to the CH<sub>3</sub> group protons at the end of the alkyl chain that attached to the phenyl group in the positions (y,y') and the benzothiadiazole position (y'').

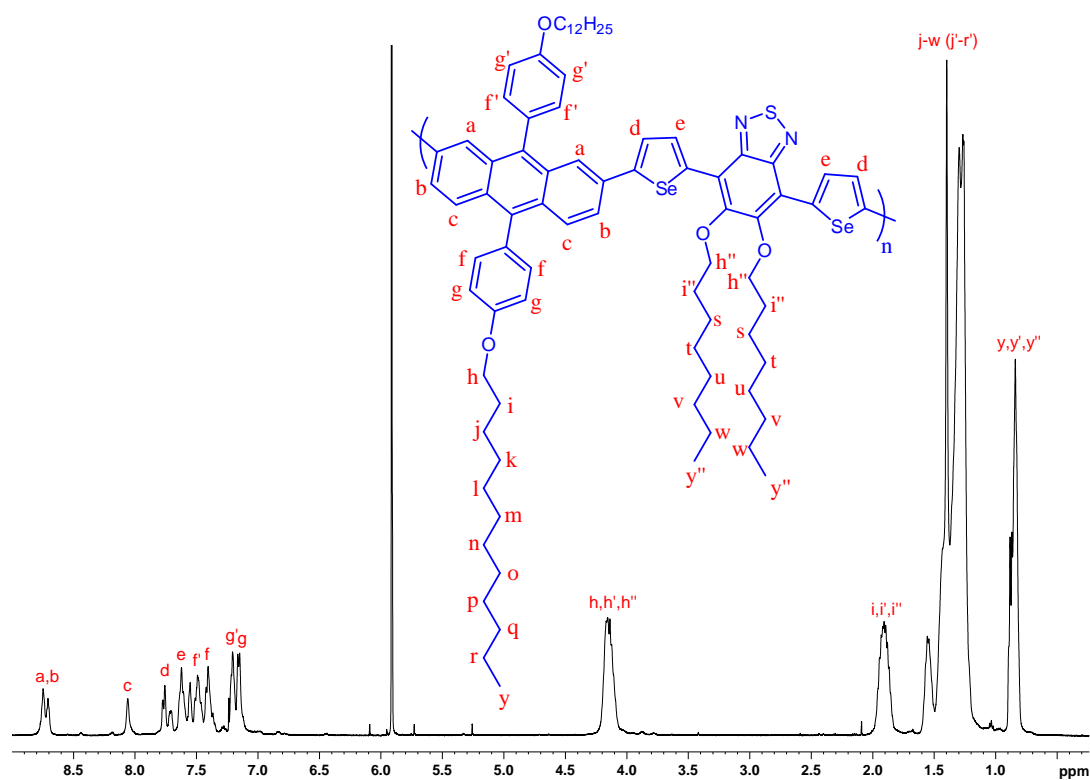


Figure 66. The <sup>1</sup>HNMR for the P12 in C<sub>2</sub>D<sub>2</sub>Cl<sub>4</sub> at 100 °C.

### 5.3.2.3. UV-visible absorption spectroscopy analysis of P10, P11 and P12

UV-Visible absorption studies on **P10** (chloroform fraction), **P11** and **P9** were performed in chloroform solutions and on thin films at room temperature.

Figure 67 shows the UV spectra of **P10**, **P11** and **P12** in chloroform solutions. All three polymers show two absorption bands, the first bands are between 377 and 383 nm while the second bands are between 517 and 533 nm. It is interesting to note that **P12** absorption maxima are red shifted compared to those of **P10** and **P11** as a result of Se-Se interaction<sup>151</sup>. In addition, **P10** and **P11** have comparable absorption maxima (501 nm for **P10** vs 505 nm for **P11** vs 513 nm for **P12**) even with the negative impact of dioctyloxy groups on the accepting properties of the benzothiadiazole.

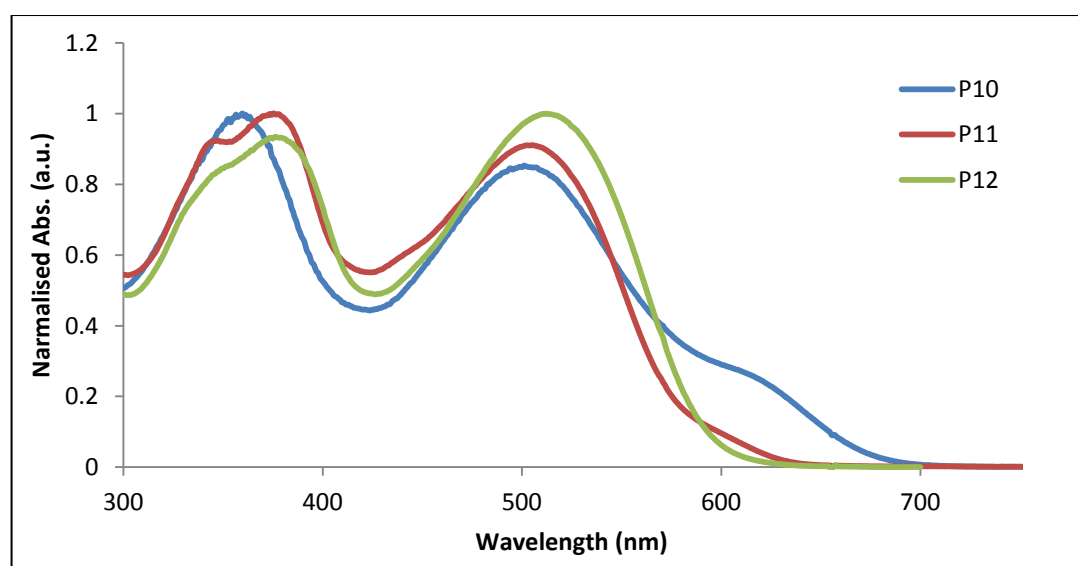
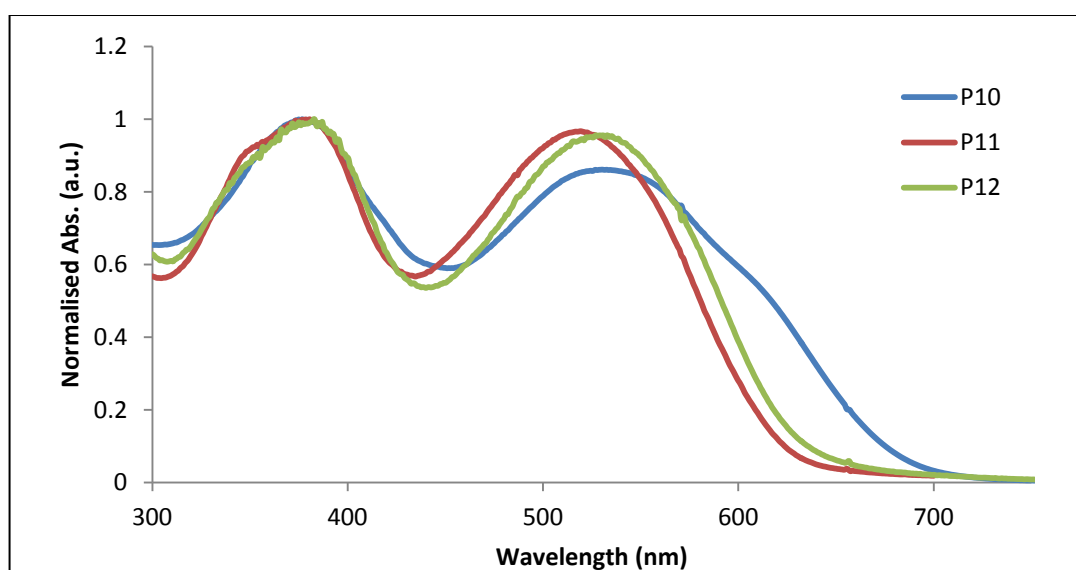


Figure 67. Absorption spectra of P10, P11 and P12 in Chloroform solution.

Figure 68 shows UV-Vis spectra for **P10**, **P11** and **P12** as solid thin film. The polymers show different absorption maxima as a result from having different acceptor units. **P10** and **P11** have benzothiadiazole repeat units but **P11** has octyloxy groups attached to the benzothiadiazole repeat units in order to increase solubility of the polymer (acceptor unit). It can be seen that **P10** has higher absorption maxima compared to **P11** (377 and 525 nm for **P10** vs 381 and 517 nm for **P11**). Also, from the onset of absorption of the polymers in films, the optical

band gap energy for **P10** is narrower than that of **P11** (1.82 eV for **P10** vs 2.02 eV for **P11**) which means that the octyloxy substituents attached to the benzothiadiazole repeat units reduce the electron accepting properties of the repeat unit and as a result provide **P11** with a wider optical band gap energy than **P10**. A comparison of **P11** and **P12** absorption spectra shows the effect of replacing thiophene with selenophene on their conjugation. **P12** has higher absorption maxima than **P11** (381 and 517 nm for **P11** vs 383 and 533 nm for **P12**). The optical band gap energy for **P12** is lower than **P11** (1.82 eV for **P10** vs 2.02 eV for **P11** vs 1.98 eV for **P12**). Thus, replacing thiophene repeat units with selenophene repeat units leads to increasing the intramolecular charge transfer along the polymer backbone as a result of Se-Se interaction along the polymer backbone<sup>151</sup>. A comparison the optical band gap energy of **P10** and **P12** indicates that **P12** has a wider optical band gap energy than **P10** (1.82 eV for **P10** vs 1.98 eV for **P12**) but the absorption maxima of **P12** is red shifted compared to that of **P10** (377 and 525 nm for **P10** vs 383 and 533 nm for **P12**).



**Figure 68. Absorption spectra of P10, P11 and P12 as thin films.**

Figure 69 shows a comparison of **P7** with **P10** as a thin film. The spectra indicates that **P10** is blue shifted compared to that of **P7** (368, 563 nm for **P7** vs 377, 525 nm for **P10**). On the other hand, they have comparable optical band gap energies (1.85 eV for **P7** vs 1.83 eV for **P10**). In addition, the molar absorptivity measurements

illustrated that **P7** has higher molar absorptivity than polymer **P10** ( $35200 \text{ L.mol}^{-1}.\text{cm}^{-1}$  for **P7** vs  $31300 \text{ L.mol}^{-1}.\text{cm}^{-1}$  for **P10**).

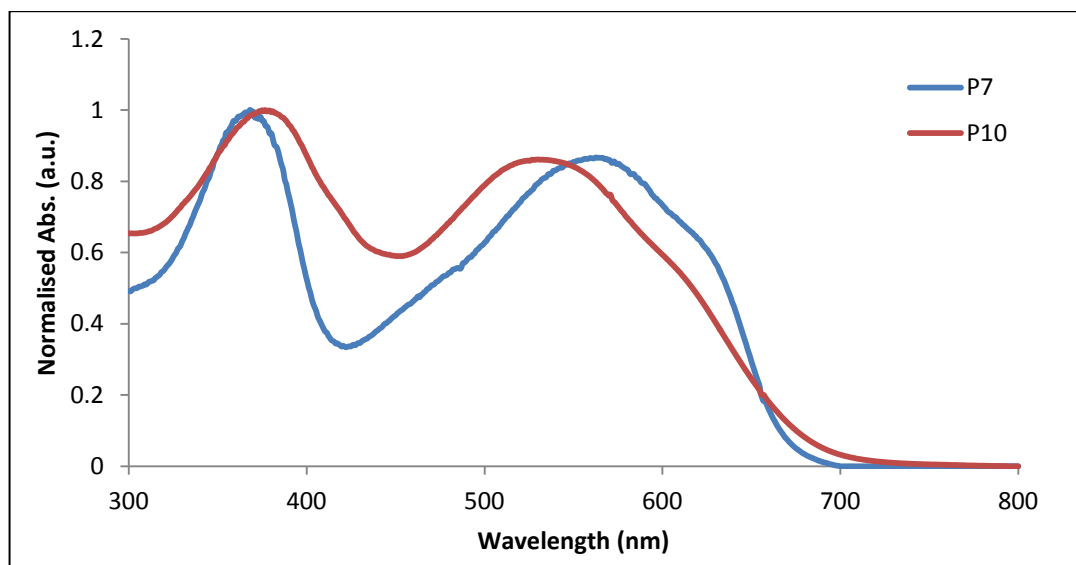


**Figure 69.** Absorption spectra of **P7** and **P10** as thin films.

Figure 70 shows a comparison of **P8** with **P11** as thin films. It is clear that **P8** is blue shifted in the first absorption band at  $\lambda_{\text{max}}$  compared to that of **P11** (365 nm for **P8** vs 376 nm for **P11**) while **P8** is red shifted in the second absorption  $\lambda_{\text{max}}$  compared to **P11** (523 nm for **P8** vs 517 nm for **P11**). It is interesting to note that the optical band gap energy of **P11** as measured from the onset of its absorption in films also indicates a wider value than that of **P8** (1.98 eV for **P8** vs 2.02 eV for **P11**). In addition, the molar absorptivity measurements illustrated that **P8** has a higher molar absorptivity compared to polymer **P11** ( $40000 \text{ L.mol}^{-1}.\text{cm}^{-1}$  for **P8** vs  $36600 \text{ L.mol}^{-1}.\text{cm}^{-1}$  for **P11**). The results indicate that 2,6-linked anthracene polymers have slightly higher electronic conjugation and intramolecular charge transfer along polymer backbones compared to those of 2,7-linked anthracene polymers. The chemical structure of 2,7-linked anthracene polymers might show a slight amount of chain twisting due to steric hindrance which leads to reduce electron delocalisation along the polymer backbone.

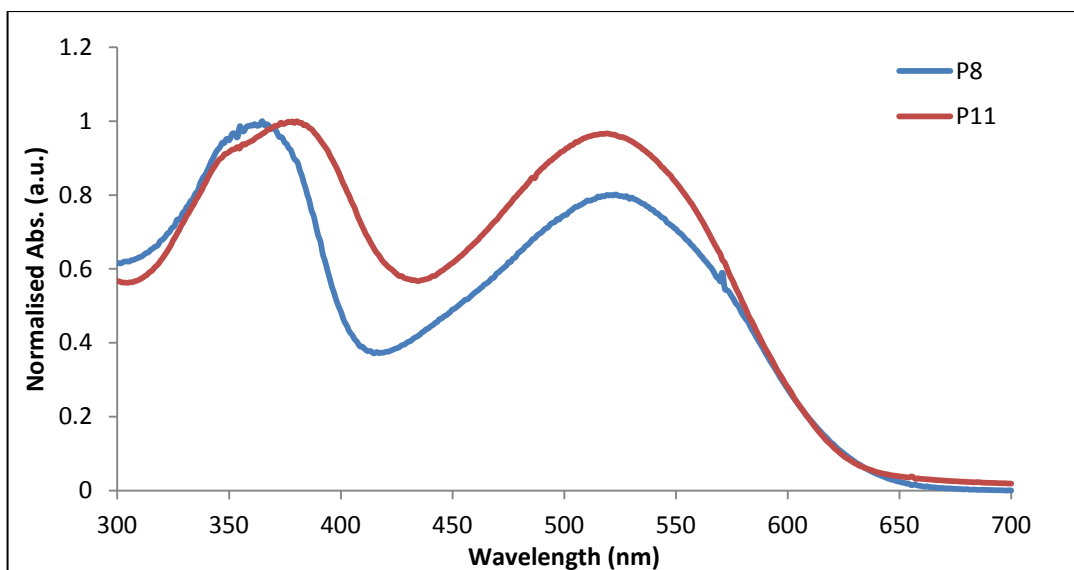


**Figure 70. Absorption spectra of P8 and P11 as thin films.**

A comparison of **P12** with its analogous 2,6-linked anthracene (**P9**) shows that **P9** has higher conjugation compared to that of **P12** as shown in Figure 71. The optical band gap energy difference between **P11** with its analogous 2,6-linked anthracene (**P8**) is 0.06 eV. On the other hand, the optical band gap energy difference between **P12** with its analogous 2,6-linked anthracene (**P9**) is 0.13 eV (1.85 eV for **P9** vs 1.98 eV for **P12**). This is resulting from the high molecular weights of **P9** compared to those of **P12** ( $M_n= 48700$ ,  $M_w= 101400$  for **P9** vs  $M_n= 33300$ ,  $M_w= 52200$  for **P12**). It is clear that **P9** is blue shifted in the first absorption band at  $\lambda_{max}$  compared to that of **P12** (379 nm for **P9** vs 383 nm for **P12**) while **P9** is red shifted in the second absorption  $\lambda_{max}$  compared to that of **P12** (569 nm for **P9** vs 533 nm for **P12**) which is in agreement with the comparison result of **P8** and **P11**. In addition, the molar absorptivity shows a big difference between them. **P9** has a much higher molar absorptivity compared to that of **P12** ( $42000 \text{ L}\cdot\text{mol}^{-1}\cdot\text{cm}^{-1}$  for **P9** vs  $23500 \text{ L}\cdot\text{mol}^{-1}\cdot\text{cm}^{-1}$  for **P12**). Again, the result indicates that 2,6-linked anthracene polymers have higher extended conjugation along polymer backbone compared to that of 2,7-linked anthracene polymers. The chemical structure of 2,7-linked anthracene possibly suffers from a slight amount of chain twisting due to steric hindrance which leads to a reduction in the electron delocalisation along the polymer

backbone. Also, the big molecular weight difference has a very important impact on their conjugation properties.

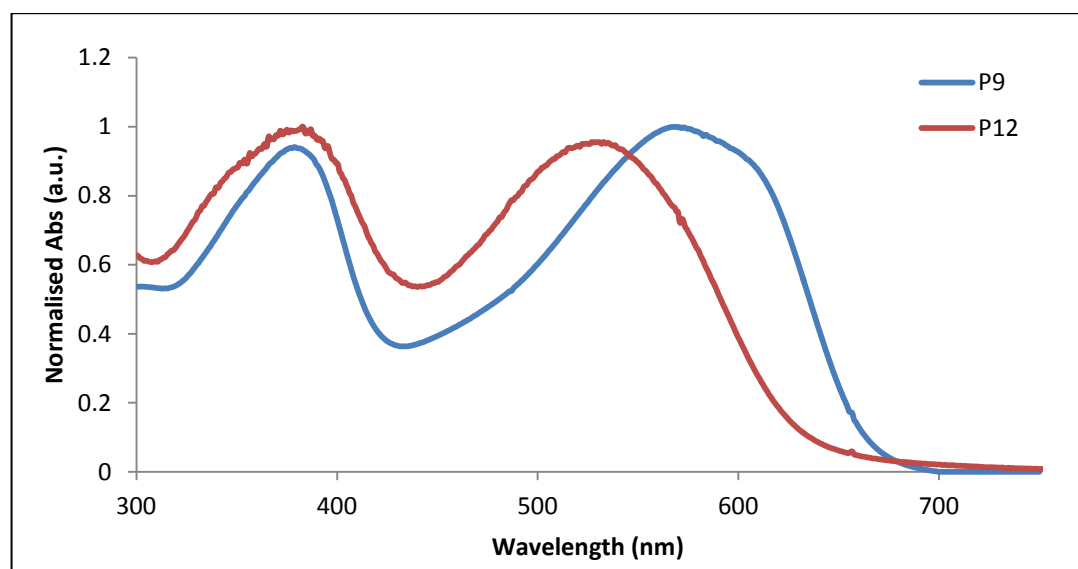


Figure 71. Absorption spectra of P9 and P12 as thin films.

#### 5.3.2.4. Cyclic Voltammetry (CV) analysis of P10, P11 and P12

In order to study the electrochemical properties of the polymers, Cyclic Voltammetry was carried out on drop-cast polymer films in acetonitrile and tetrabutylammonium perchlorate as electrolyte. The onset of oxidation and reduction can be obtained from cyclic voltammetry curves and assess the energy level of HOMO and LUMO (ferrocene has an ionisation potential of - 4.8 eV<sup>149</sup> and the oxidation takes place at 0.083 eV against the Ag/Ag<sup>+</sup> reference couple). In addition, the electrochemical band gap energy can be calculated from the energy difference between HOMO and LUMO.

Figure 72 shows the cyclic voltammetry curves of **P10**, **P11** and **P12**. It can be seen that **P10** has the lowest electrochemical band gap energy compared to **P8** and **P9** (2.28 eV for **P10** vs 2.46 eV for **P11** vs 2.44 eV for **P12**). A comparison of HOMO energy levels of polymers **P10** and **P11** indicates that they have comparable levels (-5.54 eV for **P10** vs -5.57 eV for **P11**) because they have the same donor unit. On the other hand, polymer **P10** shows deeper LUMO energy level to that of polymer

**P11** as a result of the effect of octyloxy substituents attached to the benzothiadiazole repeat units on **P11** (-3.26 eV for **P10** vs -3.14 eV for **P11**). It can be seen that the octyloxy substituent groups attached to the benzothiadiazole has a negative impact to the electronic delocalisation along polymer backbone and reducing the electron accepting ability of the benzothiadiazole on **P11**. A comparison of **P11** and **P12** indicates that they have the same electrochemical band gap energy as a result of having comparable HOMO and LUMO energy levels. It can be seen that replacing thiophene with selenophene has no clear effect on the HOMO and LUMO energy levels of **P11** and **P12**.

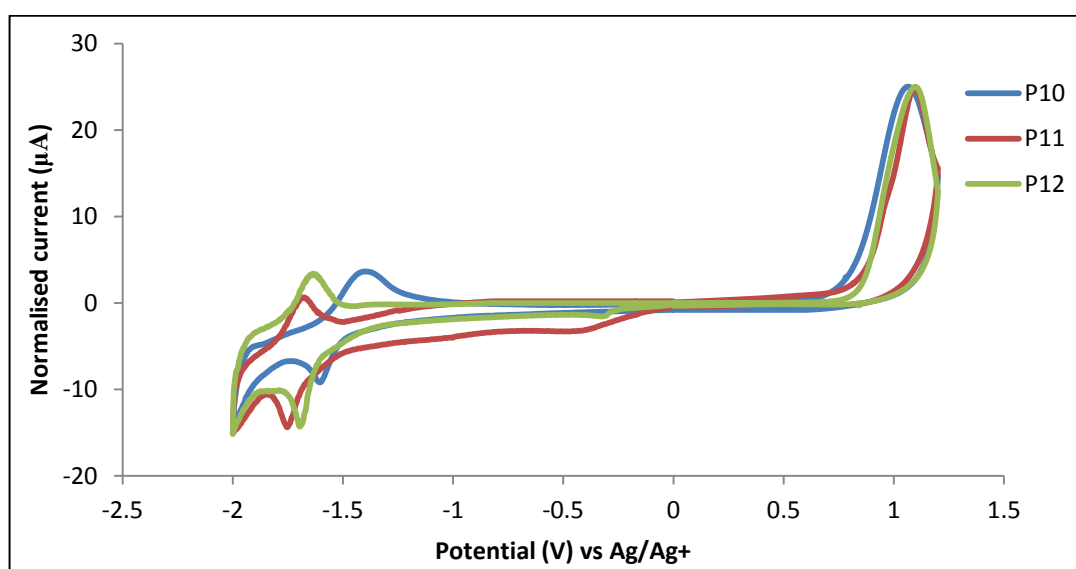


**Figure 72.** Cyclic voltammetry curves of **P10**, **P11** and **P12**.

Comparison of **P10** electrochemical results with its analogous 2,6-linked anthracene copolymer (**P7**) indicates that **P7** has lower electrochemical band gap energy ( $E_{\text{elect}} = 2.20$  eV for **P7** vs  $E_{\text{elect}} = 2.32$  eV for **P10**). In addition, it can be seen that both of **P7** and **P10** have the same LUMO energy levels (-3.24 eV for **P7** vs -3.22 eV for **P10**) because they have the same benzothiadiazole acceptor repeated units. The HOMO energy level of **P10** is slightly deeper than **P7** (-5.44 eV for **P7** vs -5.54 eV for **P10**). A comparison of **P11** electrochemical results with its analogous 2,6-anthracene copolymer **P8** indicates that **P8** has lower electrochemical band gap energy ( $E_{\text{elect}} = 2.34$  eV for **P8** vs  $E_{\text{elect}} = 2.46$  eV for **P11**). They have almost the same LUMO energy level but **P8** has higher HOMO energy

level (- 5.48 eV for **P8** vs - 5.57 eV for **P11**). Moreover, a comparison of **P12** with its analogous 2,6-anthracene copolymer **P9** indicates that **P12** has higher electrochemical band gap energy ( $E_{\text{elect}} = 2.44$  eV for **P12** vs  $E_{\text{elect}} = 2.33$  eV for **P9**). The same as **P8** vs **P11** **P9** and **P12** have the same LUMO energy levels but **P12** has a deeper HOMO energy level energy (- 5.47 eV for **P12** vs - 5.56 eV for **P9**). The higher oxidation potential of 2,7-linked anthracene polymers and its deeper HOMO energy level compared to that of 2,6-linked anthracene analogous polymers is possibly due to steric hindrance which reduce the electron delocalisation and the intramolecular charge transfer along the polymer backbone.

**Table 6. The UV-Vis and CV results of P6 – P12.**

Polymer	$\lambda_{\text{max}}$ (Solution)	$\lambda_{\text{max}}$ (Thin Film)	$E_{\text{op}}$	Molar Abs.	HOMO (eV)	LUMO eV	$E_{\text{elect}}$
<b>P7</b>	360, 532	368, 563	1.84	35200	-5.44	-3.24	2.20
<b>P8</b>	352, 507	365, 523	1.96	40000	-5.48	-3.14	2.34
<b>P9</b>	375, 555	379, 569	1.85	43000	-5.47	-3.14	2.33
<b>P10</b>	360, 501	377, 525	1.82	31300	-5.54	-3.22	2.32
<b>P11</b>	376, 505	381, 516	2.02	36600	-5.57	-3.11	2.46
<b>P12</b>	376, 513	383, 533	1.98	23500	-5.56	-3.12	2.44

### 5.3.3. Thermal analysis of P10, P11, P12

The thermal stability of **P10**, **P11** and **P12** were studied using TGA as shown in Figure 73. It can be seen that **P10** exhibits a high thermal stability up to 400 °C which is similar to the its analogous 2,6-linked anthracene (**P7**). The degradation onset of **P10** occurs at 445 °C which is very close to the degradation onset of **P7**

(438 °C), the total weight loss percentage is 75.2% at 800 °C for **P10**. The TGA curve for **P11** shows two main degradation onsets, the first one occurs at 313 °C and the second one takes place at 453 °C, the total weight loss percentage is 60 % at 800 °C. There are two degradation onsets for **P12**, the first one occurs at 312 °C which is similar to the its analogous 2,6-anthracene (310 °C for **P9**), the second degradation onset takes place at 409 °C, the total weight loss percentage is 53.5 % at 800 °C.

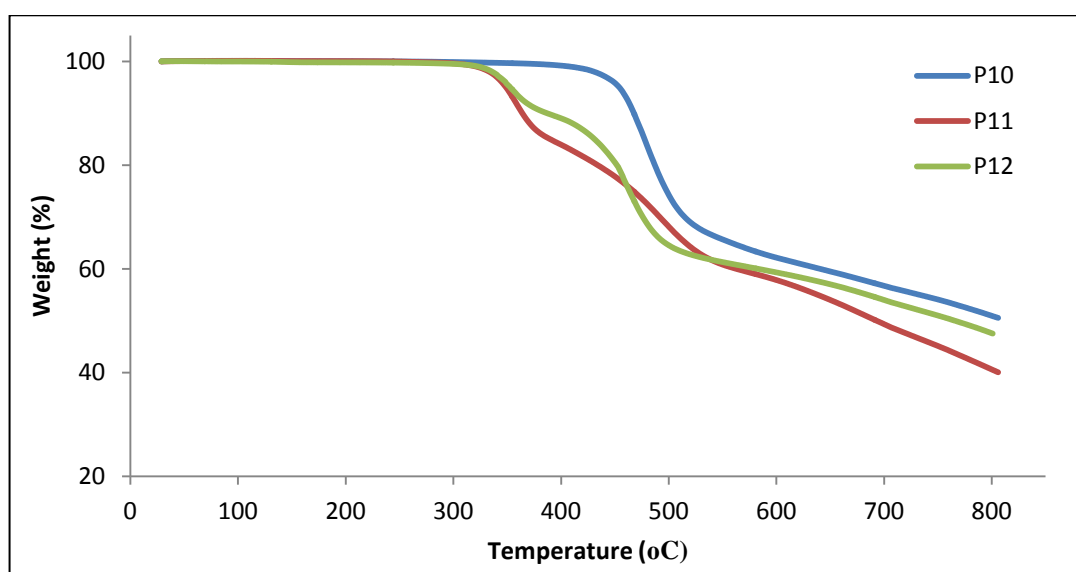


**Figure 73. TGA curves of P10, P11 and P12.**

It can be seen that the degradation of **P11** and **P12** start earlier than for **P10** due to the effect of alkoxy groups attached to the benzothiadiazole repeat units. Thus, the alkoxy groups provide higher solubility but lower thermal stability to the polymers.

#### 5.4. Anthracene based polymers (P13, P14, P15)

In this project a series of 2,6- and 2,7-linked anthracene based polymers were prepared successfully. The investigation has indicated that 2,6-linked anthracene copolymers have higher extended conjugation along polymer backbone than 2,7-linked anthracene copolymers. In order to support this study **P13**, **P14** and **P15** were suggested. They are homopolymer systems as shown in Figure 74. **P13**, **P14** and **P15** were synthesised successfully using Suzuki cross coupling and analysed by  $^1\text{H}$ NMR, elemental analysis and GPC. The thermal stability, the physical and electronic properties were studied using TGA, UV-Vis spectroscopy and CV.

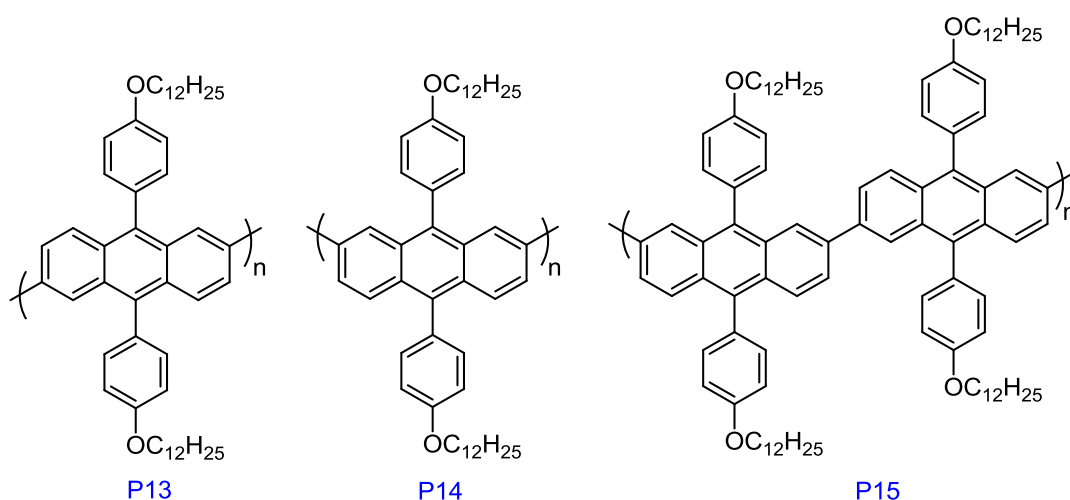
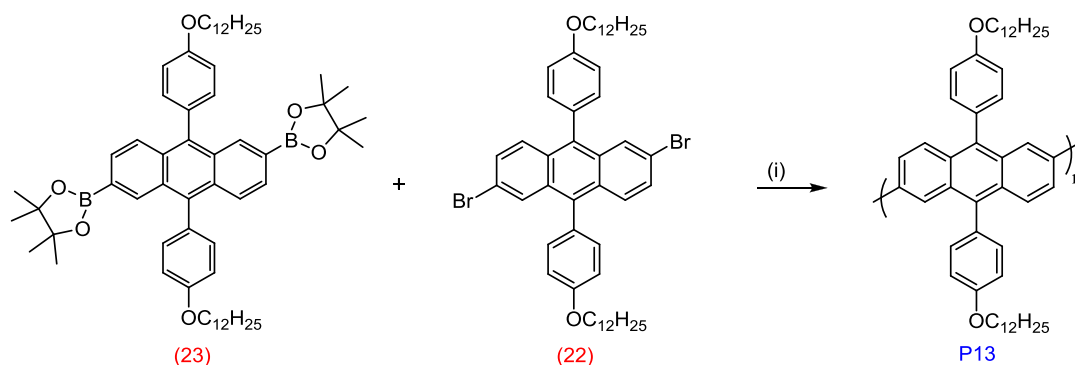


Figure 74. The chemical structure of P13 , P14 , P15.

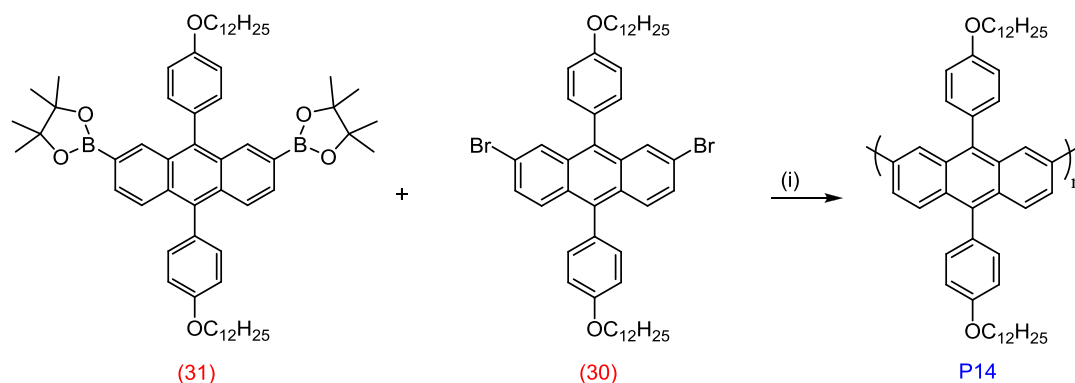
##### 5.4.1. Preparation of P13 , P14 , P15

The preparation of **P13**, **P14** and **P15** were carried out using Suzuki cross coupling polymerization reactions. The mechanism of the reaction is illustrated in Figure 44. The Poly[9,10-bis(4-(dodecyloxy)phenyl)-anthracene-2,6-diyl] (**P13**) was prepared by reacting 2,6-bis-(4,4,5,5-tetramethyl-[1,3,2]dioxaborolan-2-yl)-9,10-bis(4-(dodecyloxy) phenyl)anthracene (**23**) with 2,6-dibromo-9,10-bis(4-(dodecyloxy)phenyl)anthracene. (**22**), as shown in Scheme 69.



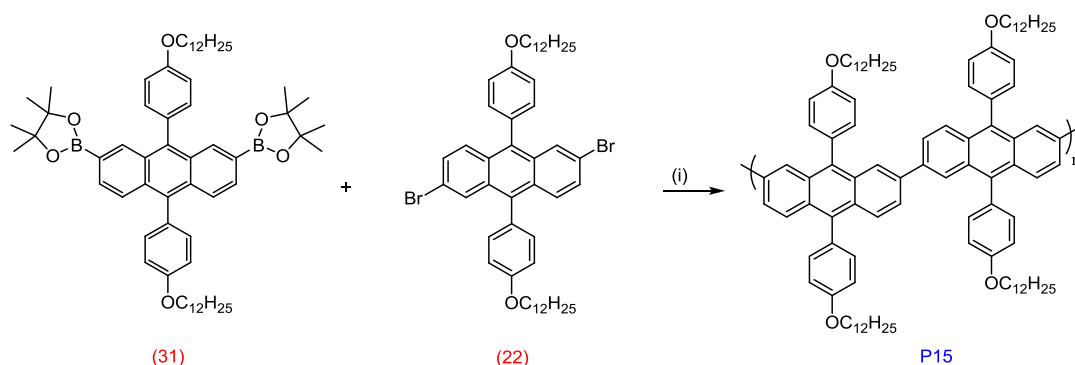
**Scheme 69. Preparation of P13. (i) Pd(AcO)<sub>2</sub>, tri-*o*-tolylphosphine, Toluene, tetraethylammonium hydroxide.**

Poly[9,10-bis(4-(dodecyloxy)phenyl)-anthracene-2,7-diyl] (**P14**) was prepared by reacting 2,7-bis-(4,4,5,5-tetramethyl-[1,3,2]dioxaborolan-2-yl)-9,10-bis(4-(dodecyloxy)phenyl)anthracene (**31**) with 2,7-dibromo-9,10-bis(4-(dodecyloxy)phenyl)anthracene (**30**), as shown in Scheme 70.



**Scheme 70. Preparation of P14. (i) Pd(AcO)<sub>2</sub>, tri-*o*-tolylphosphine, Toluene, tetraethylammonium hydroxide.**

Poly[9,10-bis(4-(dodecyloxy)phenyl)-anthracene-2,6-diyl-alt-9,10-bis(4-(dodecyloxy)phenyl)-anthracene-2,7-diyl] (**P15**) was prepared by reacting 2,7-bis-(4,4,5,5-tetramethyl-[1,3,2]dioxaborolan-2-yl)-9,10-bis(4-(dodecyloxy)phenyl)anthracene (**31**) with 2,6-dibromo-9,10-bis(4-(dodecyloxy)phenyl)anthracene (**22**) as shown in Scheme 71.



**Scheme 71. Preparation of P15. (i) Pd(AcO)<sub>2</sub>, tri-*o*-tolylphosphine, Toluene, tetraethylammonium hydroxide.**

## 5.4.2. Characterization of P13 , P14 , P15

### 5.4.2.1. Gel Permeation Chromatography studies of P13, P14 and P15.

All the GPC result are illustrated in Table 7, with the polydispersity (PD) and the degree of polymerization (DP).

**Table 7. Yields and GPC results for P13 , P14 and P15.**

Polymer	Yield %	Solvent				
		Fraction	M <sub>n</sub>	M <sub>w</sub>	PD	DP
P13	46.5	Toluene	21600	35300	1.60	31
	49.6	Chloroform	50800	74900	1.47	73
P14	78.9	Toluene	21700	35400	1.63	36
P15	85.6	Toluene	33300	52200	1.56	21

### 5.4.2.2. <sup>1</sup>HNMR analysis of P13, P14 and P15

The <sup>1</sup>HNMR analysis of polymers **P13**, **P14** and **P15** were carried out in C<sub>2</sub>D<sub>2</sub>Cl<sub>4</sub> at 100 °C in order to avoid broad signal especially in the down field region around (6 – 9 ppm) as a result of polymer aggregation.

As shown in Figure 75, the  $^1\text{H}$ NMR spectrum of **P13** are similar to the spectrum of (**23**). They show a singlet peak at 7.96 ppm corresponds to the protons on position (a) in the anthracene. Also, the spectrum reveals two doublet peaks at 7.76 and 7.55 ppm which are related to the anthracene protons in the positions (b) and (c) respectively. It can be seen that the doublet peaks at 7.35 and 7.11 ppm can be assigned to the attached phenyl group protons on positions (d) and (e) respectively. The broad singlet peak at 4.14 ppm corresponds to the protons on the carbon which is bonded directly to the oxygen atom of the phenyl group in the position (f). The multiplet peaks at 1.94-1.83, 1.61-1.50 and 1.48-1.20 ppm correspond to the alkyl chain protons. The triplet peak at 0.86 ppm can be assigned to the six protons on the  $\text{CH}_3$  group at the end of the alkyl chain.

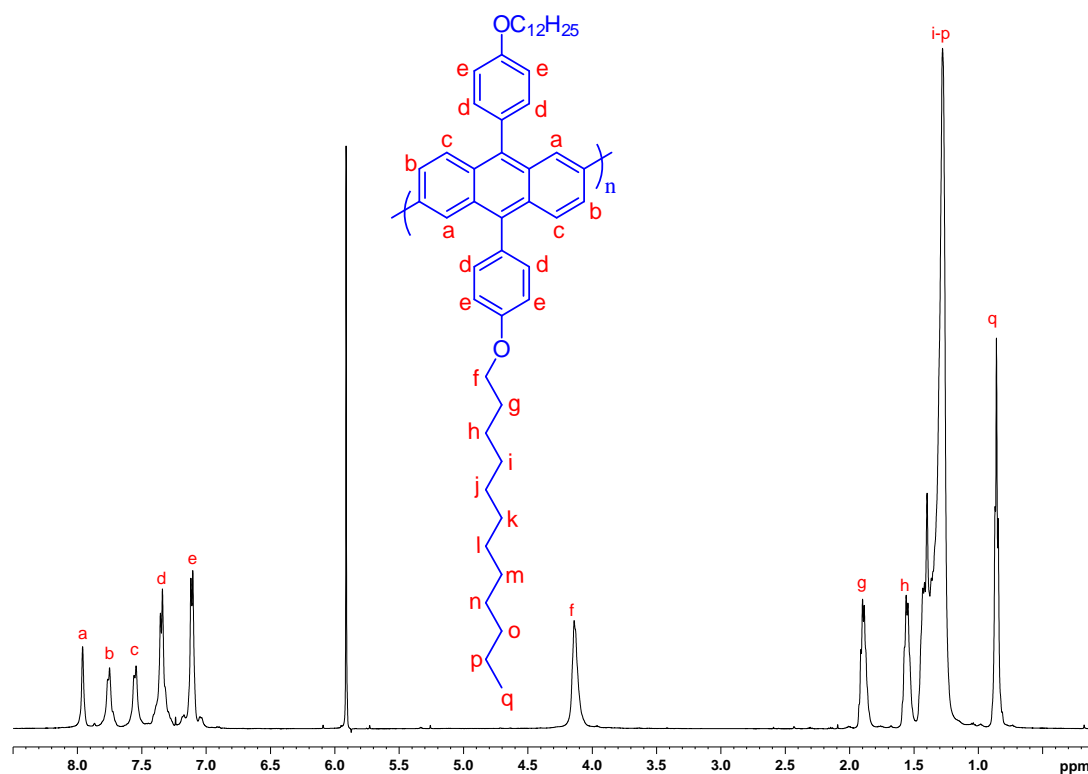
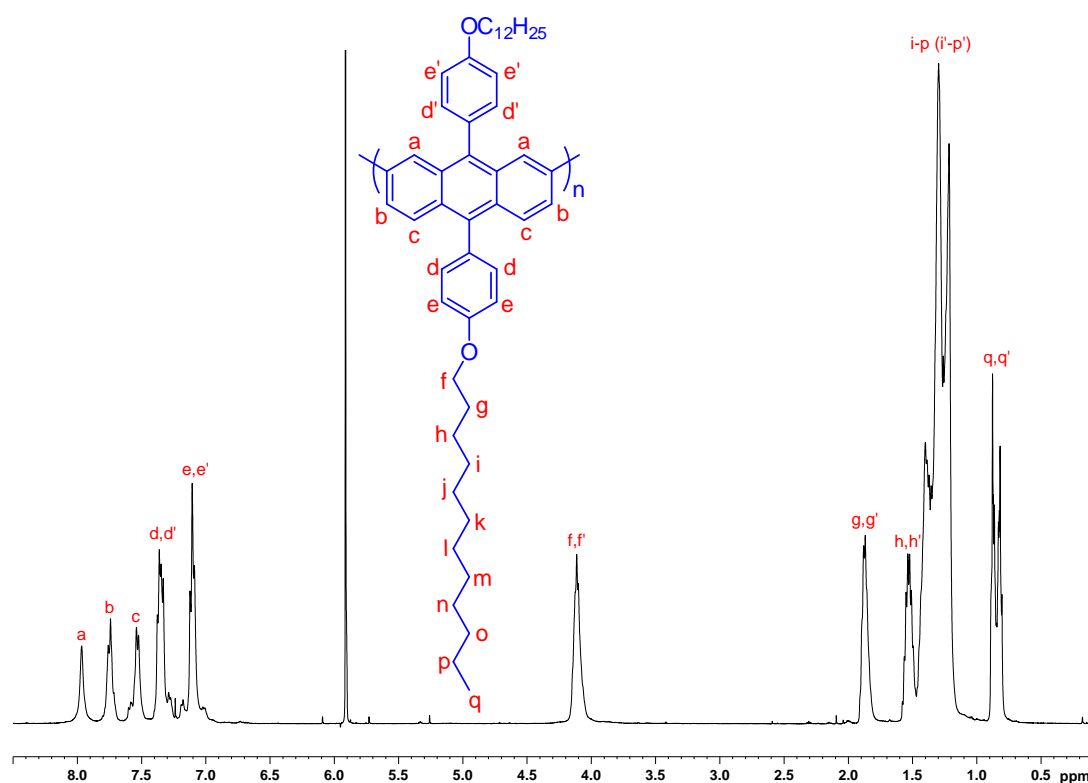


Figure 75.  $^1\text{H}$ NMR spectrum of **P13** in  $\text{C}_2\text{D}_2\text{Cl}_4$  at  $100\text{ }^\circ\text{C}$

The structure of **P14** was confirmed using  $^1\text{H}$ NMR as shown in Figure 76. The spectrum is comparable to the  $^1\text{H}$ NMR of (**30**). It is clear that the singlet peak at 7.96 ppm is related to the anthracene protons in the position (a). The four anthracene protons in the positions (b) and (c) are observed at 7.75 and 7.53 ppm.

The structure of this polymer is not symmetrical; the attached phenyl group protons are displayed at different chemical environments. So, the spectrum shows multiplet peak at 7.35 ppm which is related to the four protons in the attached phenyl groups in the positions (d) and (d'). Also, the multiplet peak at 7.11 ppm is related to the phenyl group protons in the positions (e) and (e'). The remaining peaks at 4.11, 1.92-1.82, 1.60-1.47, 1.47-1.16 and 0.91-0.78 are related to the aliphatic protons of the alkyl chain attached to the phenyl group.



**Figure 76.**  $^1\text{H}$ NMR spectrum of P14 was carried out in  $\text{C}_2\text{D}_2\text{Cl}_4$  at  $100\text{ }^\circ\text{C}$ .

Figure 77 shows the  $^1\text{H}$ NMR spectrum of **P15**. The anthracene protons in position (a) are assigned as a broad singlet peak at 7.94 ppm. It can be seen that the doublet peaks at 7.74 and 7.54 are related to the anthracene protons in the positions (b) and (c). The doublet peak at 7.35 ppm is related to the phenyl group protons in the position (d), while the broad singlet peak at 7.11 ppm corresponds to the other protons in the phenyl group positions (d). The rest of the peaks 4.12, 1.95-1.82, 1.61-1.48, 1.47-1.14 and 0.91-0.78 can be assigned the aliphatic chain hydrogens attached to the phenyl groups.

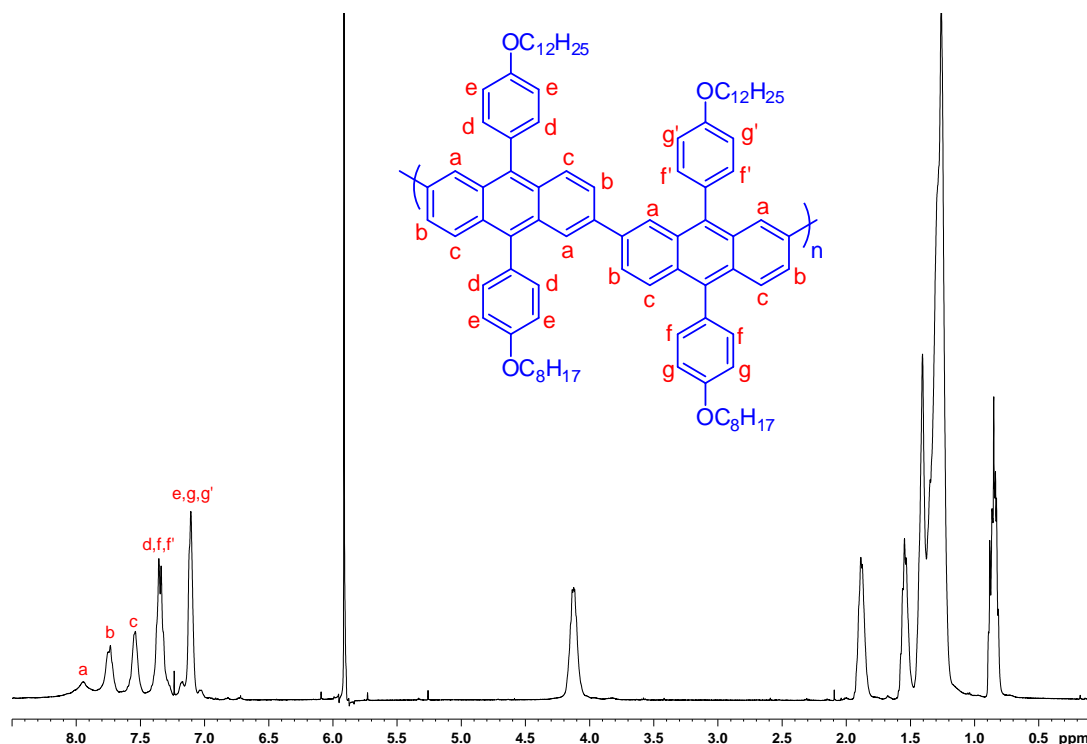
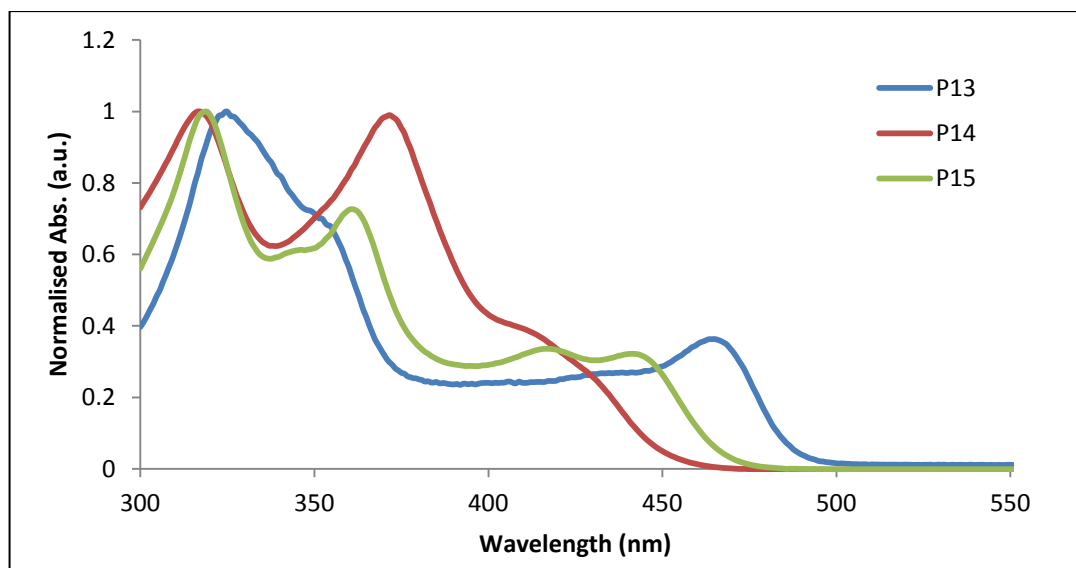


Figure 77.  $^1\text{H}$ NMR spectrum of P15 in  $\text{C}_2\text{D}_2\text{Cl}_4$  at  $100\text{ }^\circ\text{C}$ .

#### 5.4.2.3. UV-visible absorption spectroscopy analysis of P13, P14 and P15

UV-Visible absorption studies of **P13** (toluene fraction), **P14** and **P15** were performed in chloroform solutions and on thin films at room temperature.

The absorption spectra of **P13**, **P14** and **P15** in chloroform solutions are shown in Figure 78. All of these polymers are wide band gap polymers as expected. They show two broad absorption bands, the first bands with maxima between 317 and 325 nm and the second bands between 361 and 465 nm. It is interesting to note that they has strong and clear absorption at low wavelength absorption as a result of the delocalisation  $\pi - \pi^*$  transition in the polymer chains <sup>154</sup>.



**Figure 78. Absorption spectra of P13, P14 and P15 in chloroform solutions.**

Figure 79 shows a comparison of the UV-Vis spectra for **P13**, **P14** and **P15** as thin films. Again, the slight red shift between thin film and solution absorptions are observed due to aggregation thin film allows more planer structures to the polymer backbone than in solution. The freedom of movement of polymers in solution leads to increase polymer chain twisting and reduced electronic conjugation and so leads to lower absorption maxima. A comparison of **P13** and **P14** indicates that **P13** has higher absorption maxima compared to **P14** (326 and 468 nm for **P13** vs 320 and 375 nm for **P14**). In addition, **P14** has a wider optical band gap energy compared to that of **P13** (2.7 eV for **P14** vs 2.5 eV for **P13**). It can be seen that, **P15** has higher absorption maxima than **P14** but lower than **P13** (326 and 468 nm for **P13** vs 320 and 375 nm for **P14** vs 320, 364 and 444 nm for **P15**). The optical band gap energy of **P15** is 2.6 eV which higher than **P13** and lower than **P14**. It is interesting to note that the structure of 2,6-anthracene polymer (**P13**) provides higher electron delocalisation along the polymer backbone compared to the structure of 2,7-anthracene polymer (**P14**) which affects its electron delocalisation due to increase the steric hindrance effects.

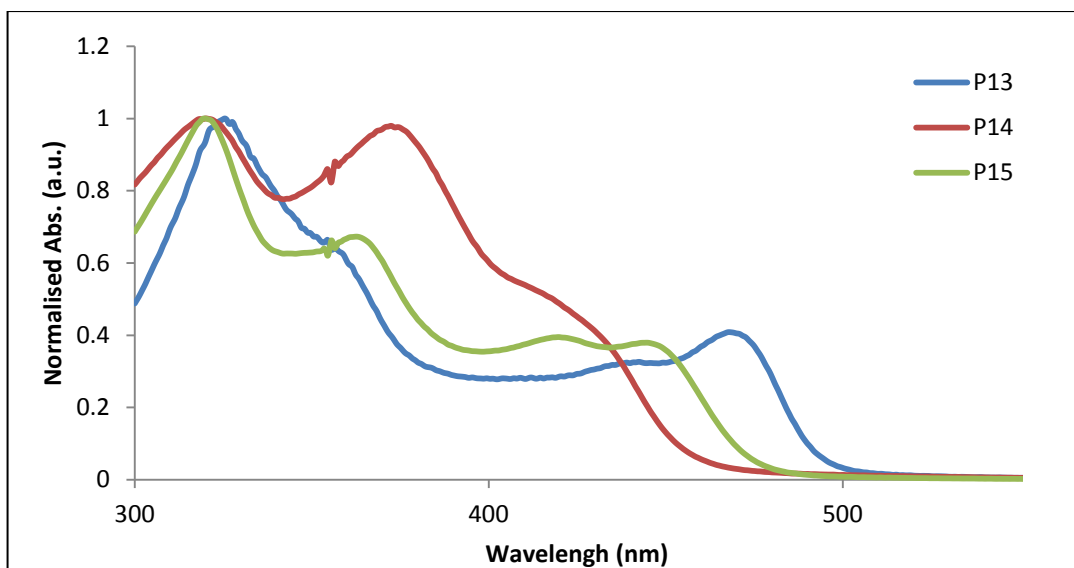


Figure 79. Absorption spectra of P13, P14 and P15 as thin films.

#### 5.4.2.4. Cyclic Voltammetry (CV) analysis of P13, P14 and P15

In order to study the electrochemical properties of the polymers, Cyclic Voltammetry was carried out by drop-cast polymer films in acetonitrile and tetrabutylammonium perchlorate as electrolyte. The onset of oxidation and reduction can be obtained from cyclic voltammetry curves and used to assess the energy level of the HOMO and LUMO levels (ferrocene has an ionisation potential of -4.8 eV vs vacuum level<sup>149</sup> and the oxidation takes place at 0.083 eV against the Ag/Ag<sup>+</sup> reference couple). In addition, the electrochemical band gap energy can be calculated from the energy difference between HOMO and LUMO.

As shown in Figure 80, the redox behaviour of **P13**, **P14** and **P15** indicates that they have the same LUMO energy level at (-2.97 eV for **P13** vs -2.96 eV for **P14** vs -2.96 eV for **P15**). On the other hand, **P14** has the deepest HOMO energy level compared to P13 and **P15** (-5.81 eV for **P13** vs -5.87 eV for **P14** vs -5.84 eV for **P15**). It can be seen that **P13** has the lowest electrochemical band gap energy compared to that of **P14** and **P15** (2.84 eV for **P13** vs 2.91 eV for **P14** vs 2.88 eV for **P15**). The electrochemical band gap energies (2.84-2.91 eV) are higher than the

optical band gap energies (2.5-2.7 eV) due to exciton binding energy which is in the range (0.4-1.00 eV)<sup>150</sup>.

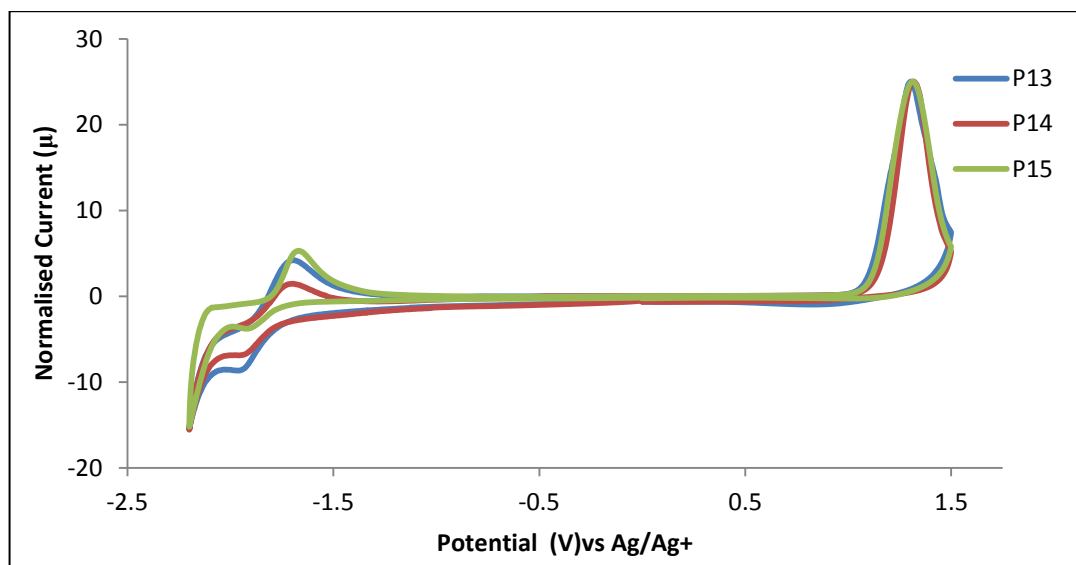


Figure 80. Cyclic voltammetry curves of P13, P14 and P15.

Table 8. Summary of the UV-Vis and CV results of P13-P15

Polymer	$\lambda_{\max}$ (Solution)	$\lambda_{\max}$ (Thin Film)	$E_{op}$	HOMO (eV)	LUMO eV	$E_{elect}$
<b>P13</b>	325, 465	326, 468	2.5	-5.81	-2.97	2.84
<b>P14</b>	317, 372	320, 375	2.7	-5.87	-2.96	2.91
<b>P15</b>	319, 361	320, 363	2.6	-5.84	-2.96	2.88

#### 5.4.3. Thermal analysis of P13, P14, P15

The thermal degradation of polymers **P13**, **P14** and **P15** were investigated using TGA as shown in Figure 81. It can be seen that all of three polymers shows high degree of thermal stability (up to 400 °C). The degradation onset of **P13** occurred at

419 °C and the total weight loss percentage is 21.3 % at 800 °C. In addition, the degradation onset of **P14** occurred at 429 °C and the total weight loss percentage is 23.4 % at 800 °C. Finally, the degradation onset of **P15** occurred at 410 °C and the total weight loss percentage is 27 % at 800 °C. It is clear, they have degradation onsets in the range (429 – 410 °C) which indicates that the degradation can be assigned to the alkyl chain attached to the phenyl groups which are attached to the anthracene repeat units.

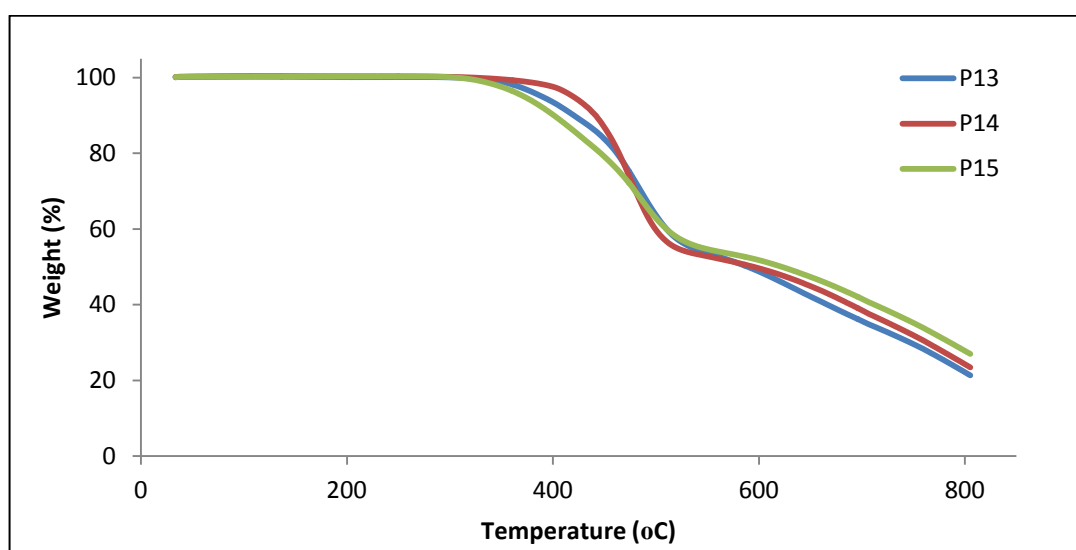


Figure 81. TGA curves of P13, P14 and P15.

### 5.5. Diketopyrrolopyrrole (DPP) based copolymers (P16, P17, P18, P19, P20)

Diketopyrrolopyrrole (DPP) based copolymers are designed according to the concept of weak donor and strong acceptor systems as a result of alternation of donor and acceptor groups along the polymer chain should lead to low band gap copolymers (harvest more photons from the sunlight) with high open circuit voltages. **P16**, **P17**, **P18**, **P19** and **P20** (Figure 82) were synthesised successfully using Suzuki cross coupling and analysed by  $^1\text{H}$ NMR, elemental analysis and GPC. The thermal stability was studied using TGA and the physical and electrical properties of these polymers were studied using UV-Vis and CV.

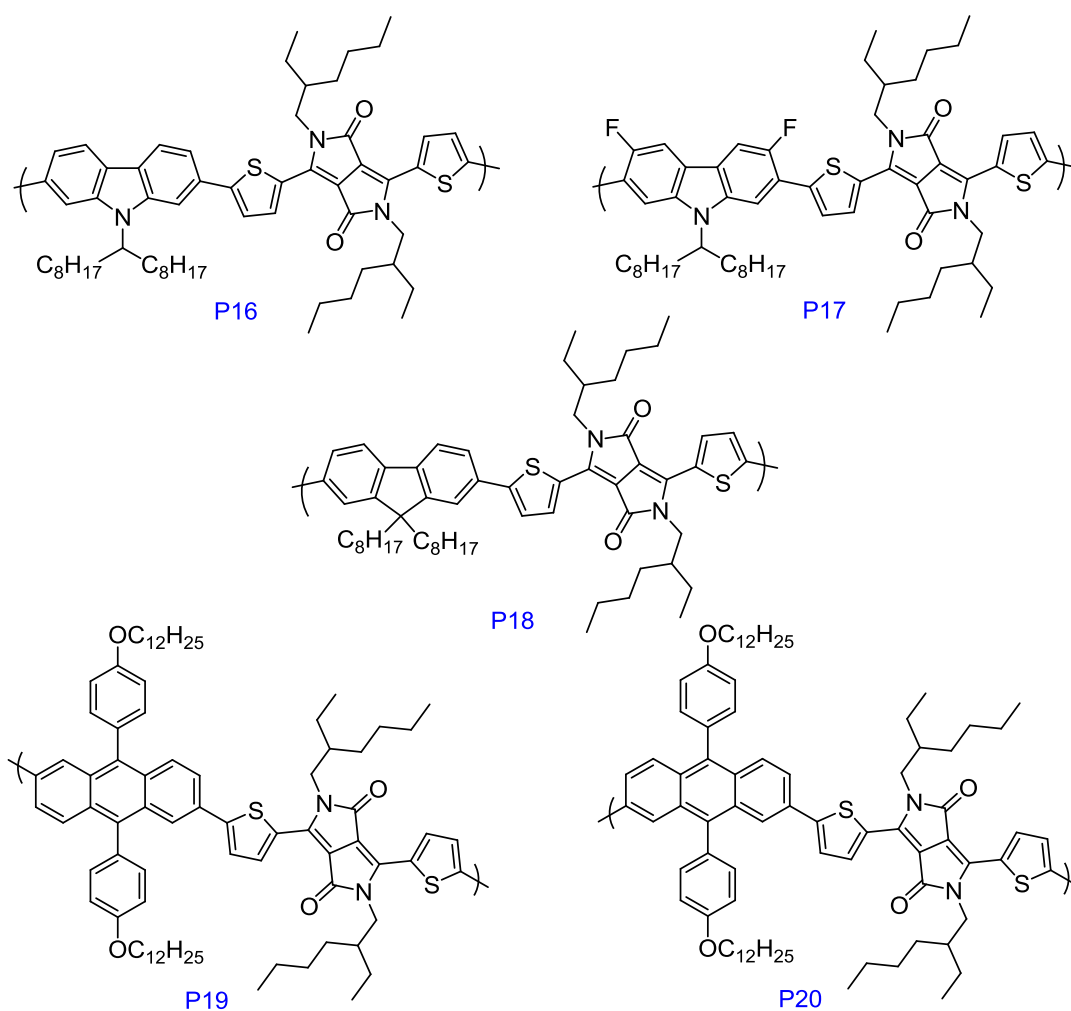
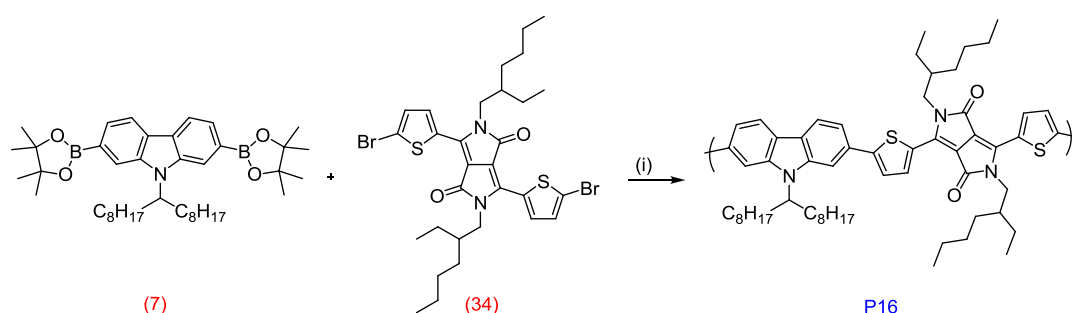


Figure 82. The chemical structures of P16, P17, P18, P19 and P20.

### 5.5.1. Preparation of P16, P17, P18, P19, P20

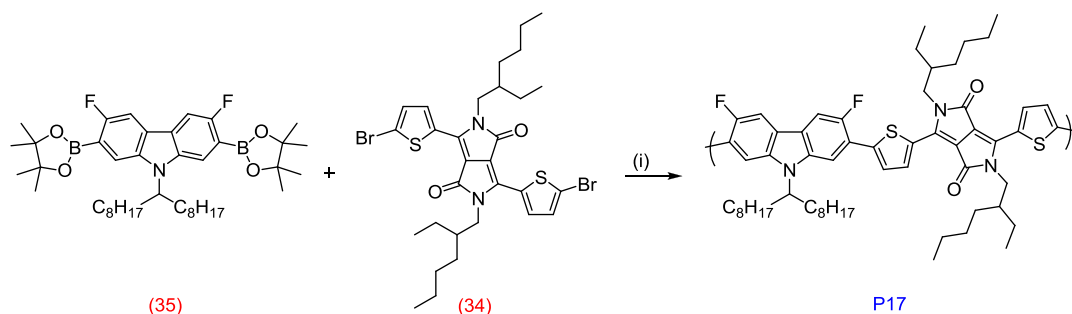
The preparation of **P16** - **P20** was undertaken using Suzuki cross coupling polymerization reactions. The mechanism of the reaction is illustrated in Figure 44.

Poly [9-(1-octyl-nonyl)-9H-carbazole-2,7-diyl-alt-3,6-bis(thiophen-5-yl)-2,5-di(2-ethylhexyl)-pyrrolo[3,4-c]pyrrole-1,4-dione-5',5'-diyl] (**P16**) was prepared by reacting 9-(heptadecan-9-yl)-2,7-bis(4,4,5,5-tetramethyl-1,3,2-dioxaborolan-2-yl)-9H-carbazole (**7**) with 3,6-bis(5-bromothiophen-2-yl)-2,5-bis(2-ethylhexyl)pyrrolo[3,4-c]pyrrole-1,4(2H,5H)-dione (**34**) (Scheme 72).



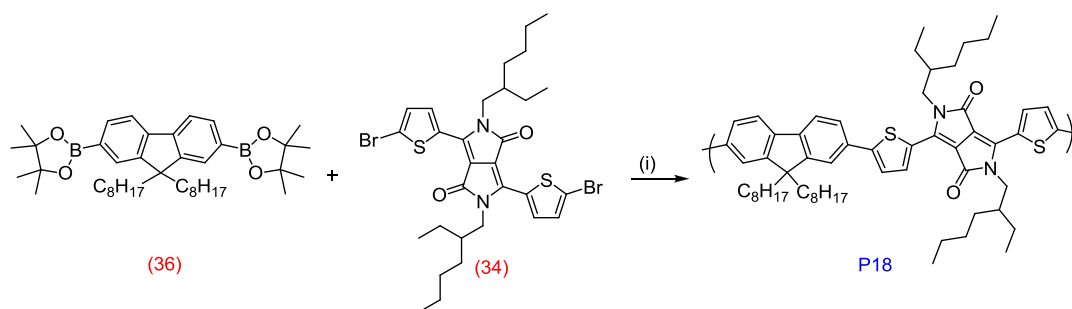
**Scheme 72. Preparation of P16. (i) Pd(AcO)<sub>2</sub>, tri-*o*-tolylphosphine, Toluene, tetraethylammonium hydroxide.**

Poly [3,6-difluoro-9-(1-octyl-nonyl)-9H-carbazole-2,7-diyl-alt-3,6-bis(thiophen-5-yl)-2,5-di(2-ethylhexyl)-pyrrolo[3,4-c]pyrrole-1,4-dione-5',5'-diyl] (**P17**) was prepared by reacting 3,6-difluoro-9-(heptadecan-9-yl)-2,7-bis(4,4,5,5-tetramethyl-1,3,2-dioxaborolan-2-yl)-9H-carbazole (**35**) with 3,6-bis(5-bromothiophen-2-yl)-2,5-bis(2-ethylhexyl)pyrrolo[3,4-c]pyrrole-1,4(2H,5H)-dione (**34**) (Scheme 73).



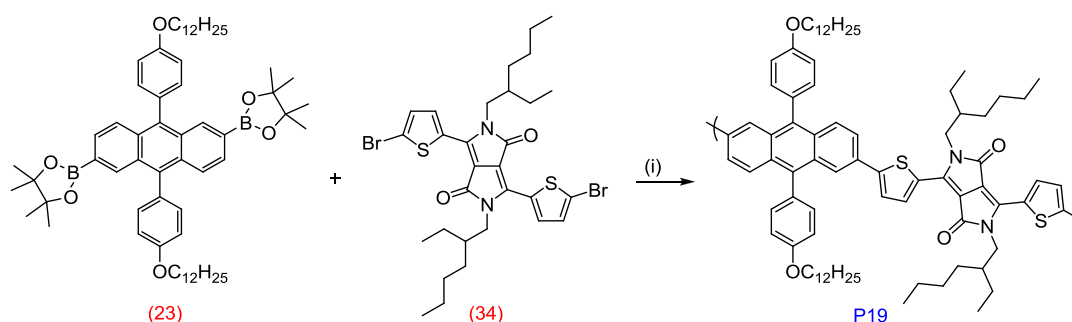
**Scheme 73. Preparation of P17. (i) Pd(AcO)<sub>2</sub>, tri-*o*-tolylphosphine, Toluene, tetraethylammonium hydroxide.**

Poly[9,6-dioctyl-9H-fluorene-2,7-diyl-alt-3,6-bis(thiophen-5-yl)-2,5-di(2-ethylhexyl)-pyrrolo[3,4-c]pyrrole-1,4-dione-5',5'-diyl] (**P18**) was prepared by reacting 9,9-Dioctylfluorene-2,7-diboronic acid bis(1,3-propanediol) ester (**36**) with 3,6-bis(5-bromothiophen-2-yl)-2,5-bis(2-ethylhexyl)pyrrolo[3,4-c]pyrrole-1,4(2H,5H)-dione (**34**) (Scheme 74).



**Scheme 74. Preparation of P18. (i) Pd(AcO)<sub>2</sub>, tri-*o*-tolylphosphine, Toluene, tetraethylammonium hydroxide.**

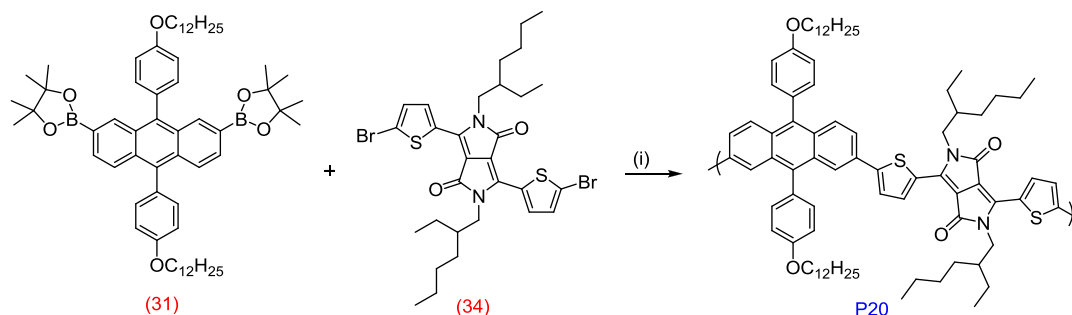
Poly [9,10-bis(4-(dodecyloxy)phenyl)-anthracene-2,6-diyl-alt-3,6-bis(thiophen-5-yl)-2,5-di(2-ethylhexyl)-pyrrolo[3,4-c]pyrrole-1,4-dione-5',5'-diyl] (**P19**) was prepared by reacting 2,6-bis-(4,4,5,5-tetramethyl-[1,3,2]dioxaborolan-2-yl)-9,10-bis(4-(dodecyloxy)phenyl) anthracene (**23**) with 3,6-bis(5-bromothiophen-2-yl)-2,5-bis(2-ethylhexyl)pyrrolo[3,4-c]pyrrole-1,4(2H,5H)-dione (**34**) (Scheme 75).



**Scheme 75. Preparation of P19. (i) Pd(AcO)<sub>2</sub>, tri-*o*-tolylphosphine, Toluene, tetraethylammonium hydroxide.**

Poly[9,10-bis(4-(dodecyloxy)phenyl)-anthracene-2,7-diyl-alt-3,6-bis(thiophen-5-yl)-2,5-di(2-ethylhexyl)-pyrrolo[3,4-c]pyrrole-1,4-dione-5',5'-diyl] (**P20**) was

prepared by reacting 2,7-bis-(4,4,5,5-tetramethyl-[1,3,2]dioxaborolan-2-yl)-9,10-bis(4-(dodecyloxy)phenyl) anthracene (**31**) with 3,6-bis(5-bromothiophen-2-yl)-2,5-bis(2-ethylhexyl)pyrrolo[3,4-c]pyrrole-1,4(2H,5H)-dione (**34**) (Scheme 76).



**Scheme 76. Preparation of P20. (i) Pd(AcO)<sub>2</sub>, tri-*o*-tolylphosphine, Toluene, tetraethylammonium hydroxide.**

## 5.5.2. Characterization of P16, P17, P18, P19, P20

### 5.5.2.1. Gel Permeation Chromatography studies of P16, P17, P18, P19 and P20

All the GPC results are illustrated in Table 9, with the polydispersity (PD) and the degree of polymerization (DP) of polymers **P16 – P20**.

**Table 9. Yields and GPC results for P16, P17, P18, P19 and P20.**

Polymer	Yield %	Solvent				
		Fraction	M <sub>n</sub>	M <sub>w</sub>	PD	DP
<b>P16</b>	67.1	Chloroform	39600	78800	1.99	43
<b>P17</b>	12.4	Toluene	12200	17100	1.4	13
<b>P18</b>	33.7	Chloroform	25400	40100	1.57	28
<b>P19</b>	58.2	Chloroform	9100	12600	1.4	8
<b>P20</b>	76.5	Chloroform	9100	12600	1.4	8

5.5.2.2.  $^1\text{H}$ NMR analysis of P16, P17, P18, P19 and P20

$^1\text{H}$ NMR analysis of polymers **P16**, **P17**, **P18**, **P19** and **P20** were carried out in  $\text{C}_2\text{D}_2\text{Cl}_4$  at 100 °C in order to avoid broad signals especially in the down field region around (6 – 9 ppm) as a result of polymer aggregation.

Figure 83 shows the  $^1\text{H}$ NMR spectrum of **P16**, the singlet and doublet peaks at 8.91 and 8.09 ppm correspond to the thiophene protons on positions (a) and (b) respectively. It is clear that the thiophene protons (positions (a) and (b)) are shifted to the left due to the effect of the lactam part of the DPP repeat units which exhibits a high electron withdrawing effect. The broad singlet peak at 7.77 ppm is related to the carbazole protons in position (c), the broad peak is obtained due to the atropisomerism phenomenon which result from the restricted rotation around a singlet bond at the nitrogen-carbon bond. It can be seen that the singlet peak at 7.55 ppm is assigned to the other carbazole protons on positions (d) and (e). The broad peaks at 4.61 and 4.10 ppm are related to the (N – C - H) protons on the carbazole (position (f)) and the DDP (position (g)).

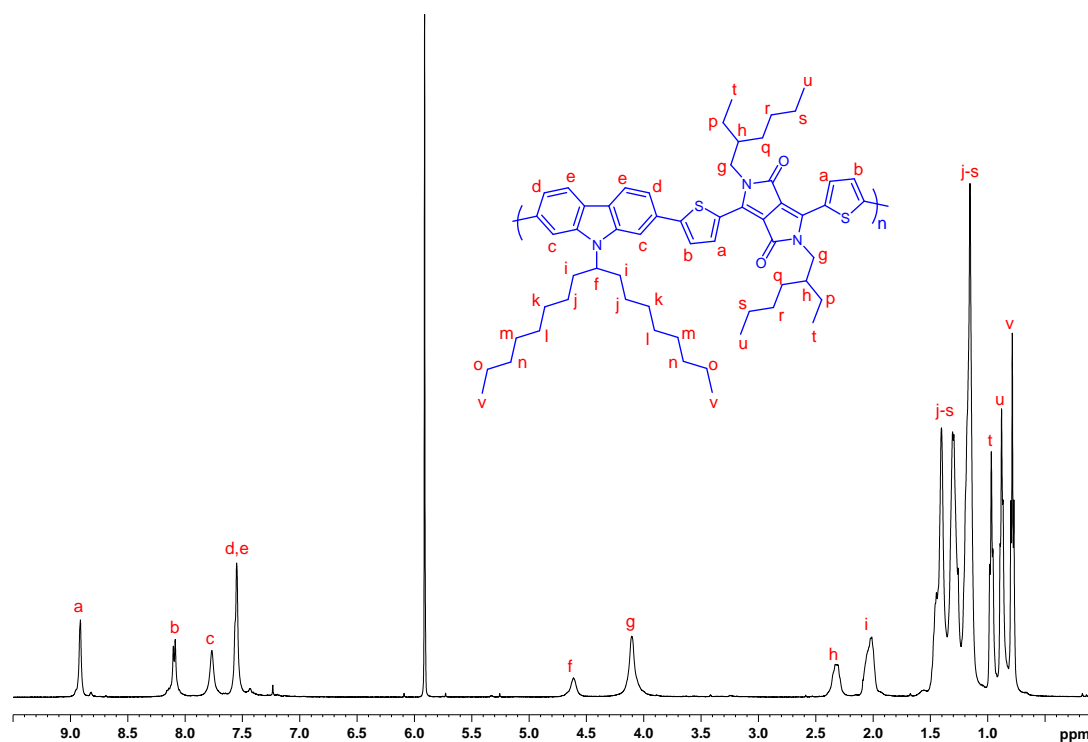
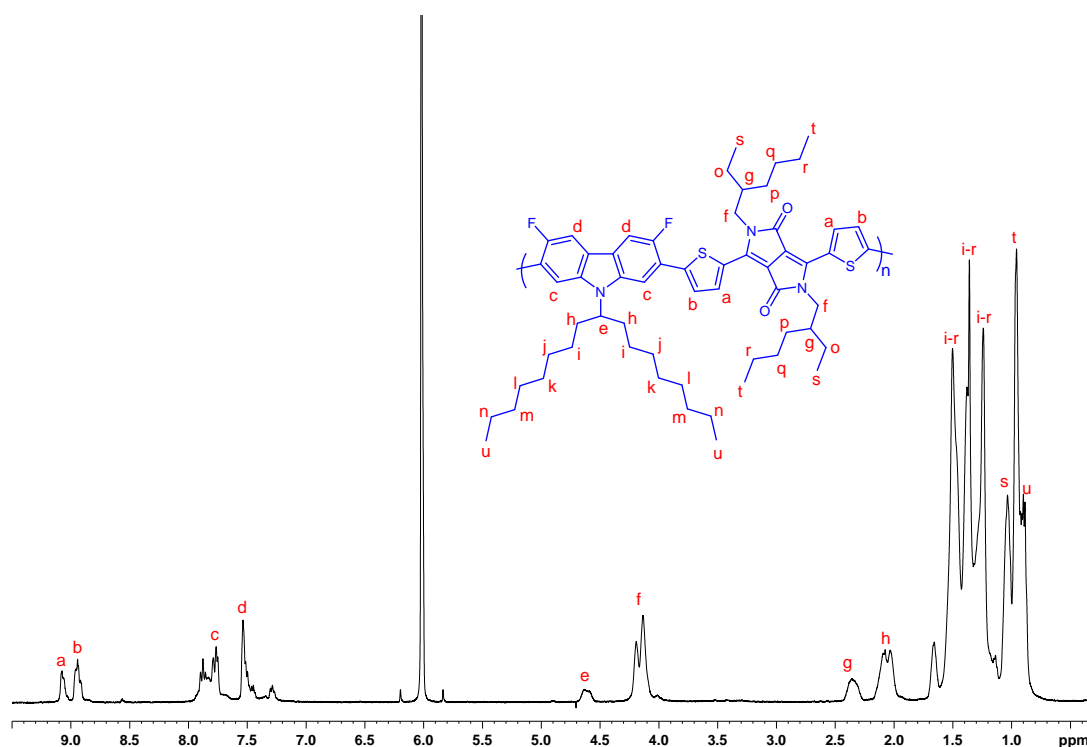


Figure 83.  $^1\text{H}$ NMR spectrum of P16 in  $\text{C}_2\text{D}_2\text{Cl}_4$  at 100 °C.

Figure 84 shows the  $^1\text{H}$ NMR spectrum of **P17**, the singlet and doublet peaks at 9.07 and 8.09 ppm correspond to the thiophene protons on positions (a) and (b) respectively. The multiplet peak at 7.94-7.73 ppm is related to the carbazole protons in the positions (c) while the other carbazole protons in the position (d) are assigned at 7.53 ppm as a singlet peak. The broad peaks at 4.62 and 4.16 ppm are related to the (N – C - H) protons on the carbazole (position (e)) and the DDP (positions (f)) respectively.



**Figure 84.**  $^1\text{H}$ NMR spectrum of **P17** in  $\text{C}_2\text{D}_2\text{Cl}_4$  at  $100\text{ }^\circ\text{C}$ .

The  $^1\text{H}$ NMR spectrum of **P18** (Figure 85) shows four chemical environments for aromatic protons on the fluorene and DPP units. The fluorene protons in positions (c), (d) and (e) are noticed at 7.75 and 7.61 ppm. The DPP aromatic protons at positions (a) and (b) are observed at 8.96 and 7.84 ppm respectively. In addition, the spectrum shows a broad peak at 4.18 ppm which is related to the (N – C - H) protons of the DDP (position (f)).

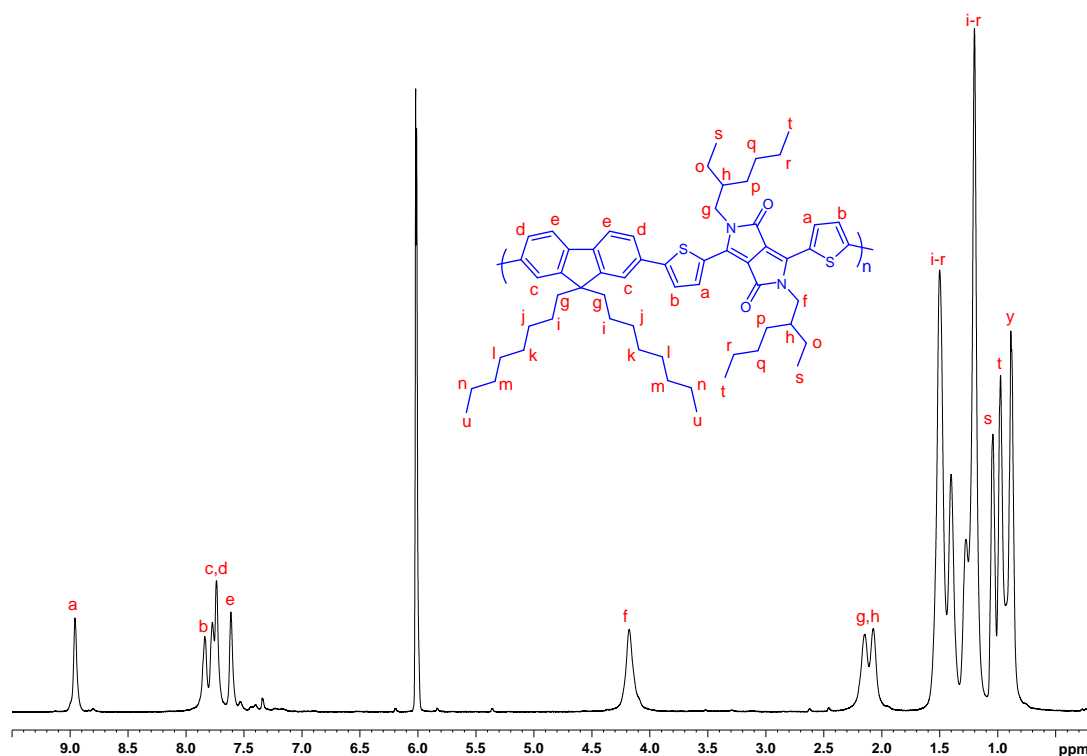


Figure 85. <sup>1</sup>H NMR of P18 in C<sub>2</sub>D<sub>2</sub>Cl<sub>4</sub> at 100 °C.

The spectrum of **P19** (Figure 86) shows six peaks in the aromatic region which are assigned to the anthracene and DPP protons in the positions (a) to (g). The singlet peaks at 8.88 and 8.09 ppm are related to the thiophene protons in the positions (a) and (b) respectively. The anthracene protons at positions (c) and (d) are observed at 7.82 and 7.60 ppm while the anthracene protons in positions (e) combined with the attached phenyl groups protons (position (f)) at 7.41 ppm. The doublet peak at 7.16 ppm is related to the protons in position (g) in the attached phenyl groups. The broad peaks at 4.13 and 3.98 ppm are related to the (O-C-H) and the (N – C - H) protons on the anthracene (position (h)) and the DDP (position (i)). The rest of peaks at 3.98, 1.90, 1.62-1.12 and 0.95-0.73 ppm are assigned to the alkyl chain protons of the anthracene and DDP units.

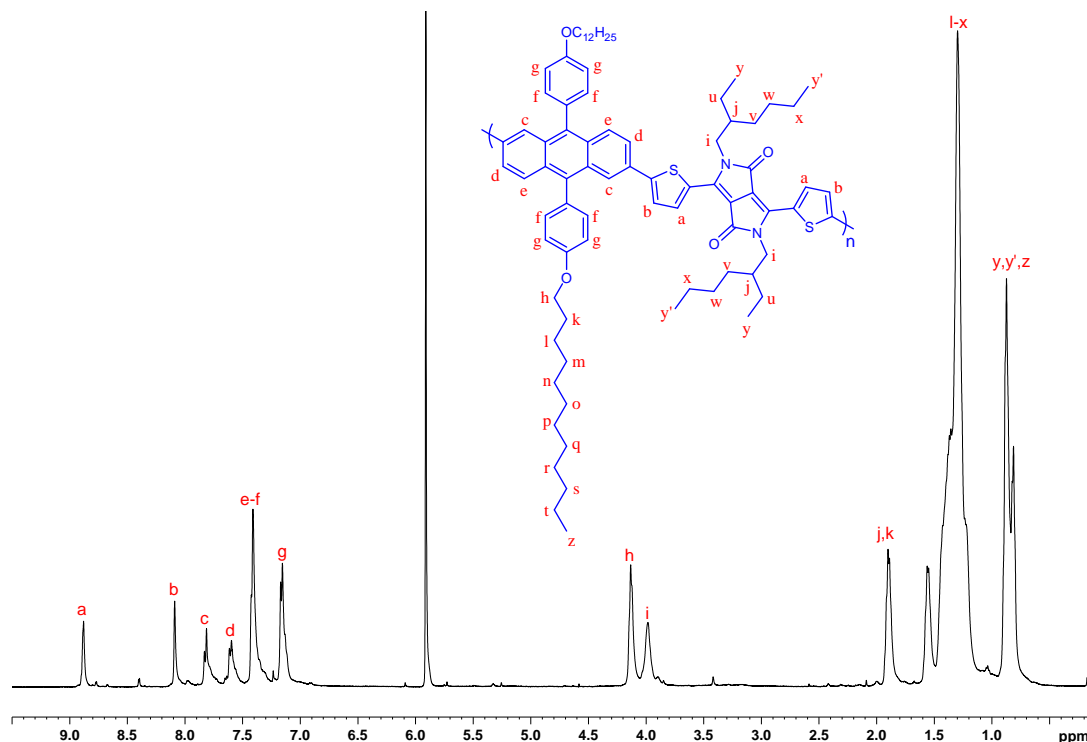


Figure 86.  $^1\text{H}$ NMR spectrum of P19 in  $\text{C}_2\text{D}_2\text{Cl}_4$  at  $100\text{ }^\circ\text{C}$ .

The spectrum of **P20** (Figure 87) shows doublet peaks at 8.98 and 8.20 ppm which are related to the thiophene protons in positions (a) and (b) respectively. The anthracene protons in the positions (c) and (d) are observed at 7.82 and 7.60 ppm as doublet peaks. The broad peak at 7.49 ppm is assigned to the protons in the positions (e) and (f,f'). The broad singlet peak at 7.24 ppm is related to the protons in the position (g) in the attached phenyl groups. The broad peaks at 4.22 and 4.08 ppm are related to the (O-C-H) and the (N - C - H) protons on the anthracene (position (h)) and the DDP (position (i)). The rest of peaks at 1.99, 1.74-1.22 and 1.06-0.84 ppm are assigned to the alkyl chain protons of the anthracene and DDP units.

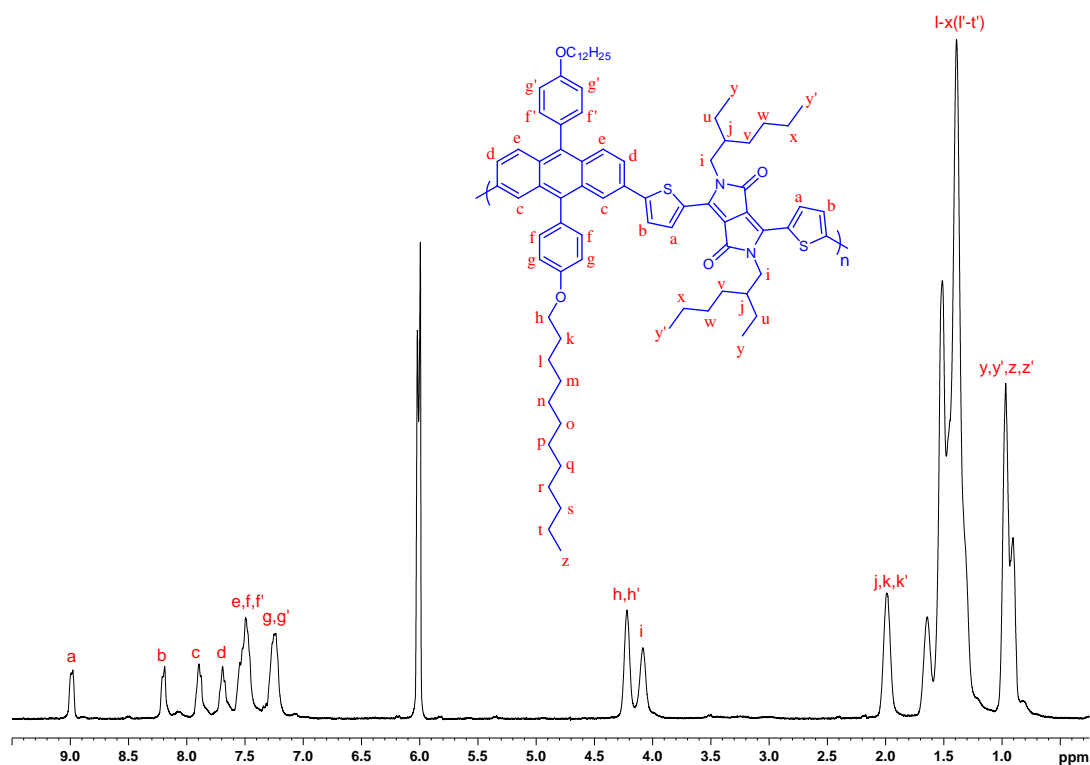


Figure 87.  $^1\text{H}$ NMR spectrum of P20 in  $\text{C}_2\text{D}_2\text{Cl}_4$  at  $100\text{ }^\circ\text{C}$ .

### 5.5.2.3. UV-visible absorption spectroscopy analysis of P16, P17, P18, P19 and P20

UV-Visible absorption studies on **P16**, **P17**, **P18**, **P19** and **P20** were performed in chloroform solutions and on thin films at room temperature.

Figure 88 shows the UV spectra of **P16**, **P17** and **P18** in chloroform solutions. It can be seen that all polymers show two absorption bands with the first band between 359 and 373 nm while the second band is between 653 and 724 nm. The spectra indicate that **P16** has higher absorption maxima than **P18** as a result of the carbazole repeat units having stronger donating ability compared to fluorene repeat units while **P17** is red shifted compared to both **P16** and **P18** due to the electrostatic interaction between fluorine substituents on the carbazole repeat units and hydrogen atoms on the 4-position on the thiophene rings as shown in Figure 91. This interaction leads to an increase in the planarity of the polymer structure and so increase the conjugation which results in having lower optical band gap energy. similar phenomenon was reported by Hursthouse et al<sup>146</sup>.

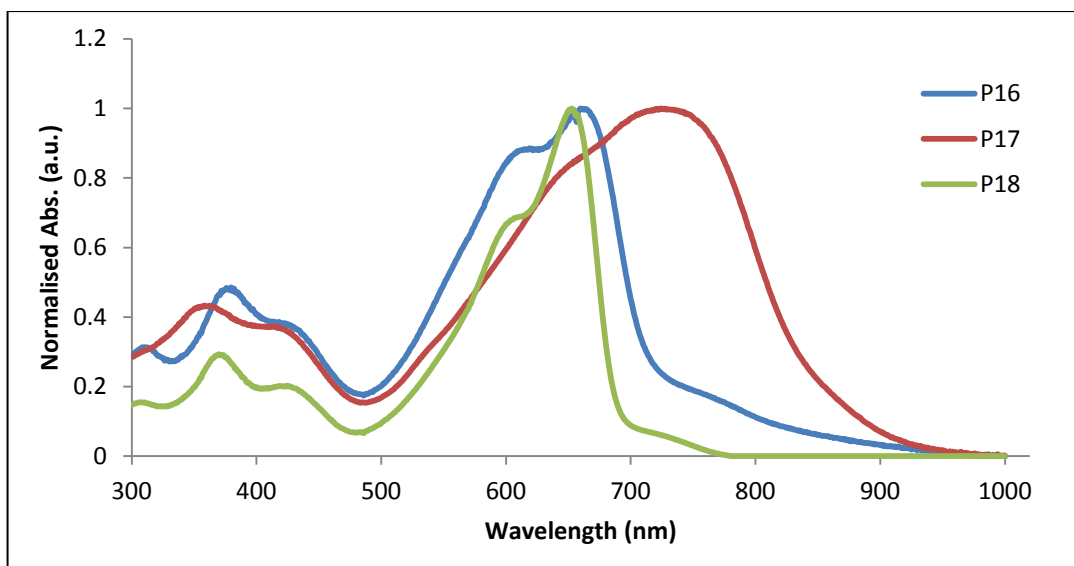


Figure 88. Absorption spectra of P16, P17 and P18 in Chloroform solutions.

Figure 89 shows the UV-Vis spectra of **P19** and **P20** in chloroform solutions. It indicates that **P19** has a red shifted absorption maximum compared to that of **P20** (342, 666 nm for **P19** vs 352, 645 nm for **P20**) which is in agreement with the previous finding, with the 2,6-linked anthracene polymers having higher extended conjugation along the polymer backbone compared to their 2,7-linked anthracene analogues.

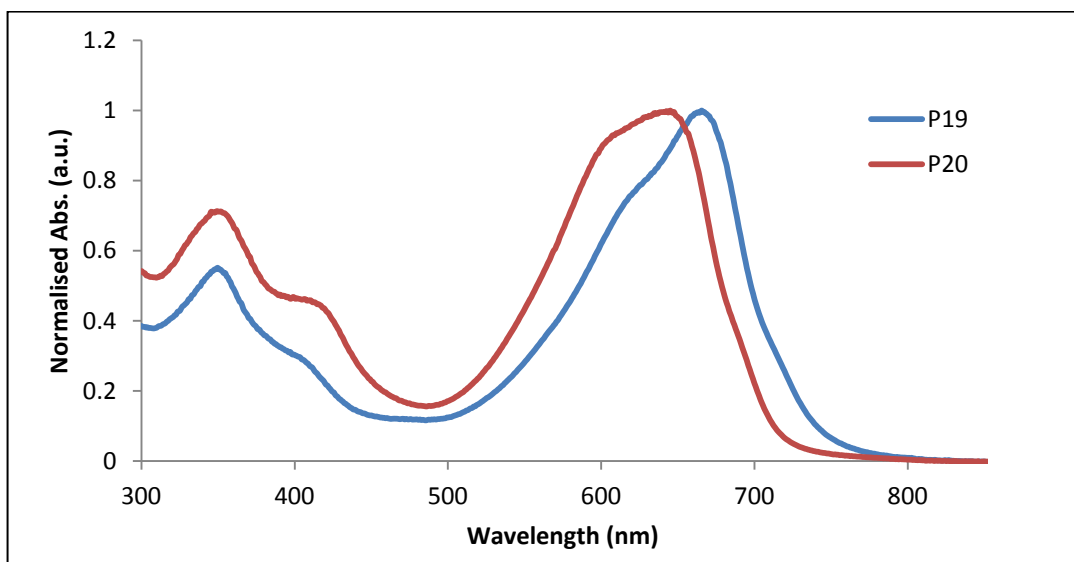
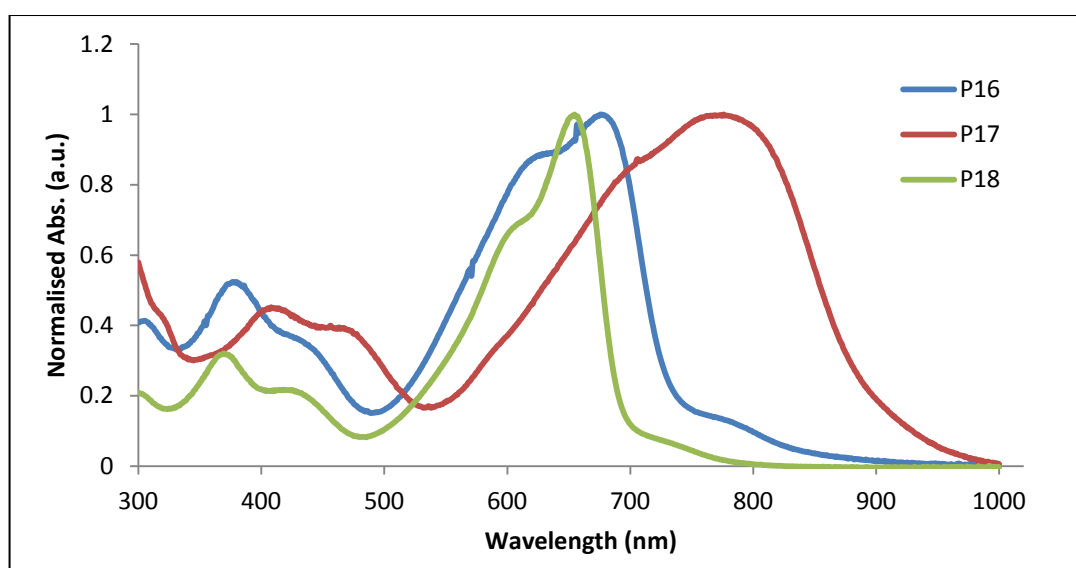


Figure 89. . Absorption spectra of P19 and P20 in Chloroform solutions.

Figure 90 shows the UV-Vis spectra of **P16**, **P17** and **P18** as solid thin films. It is clear that they have different absorption maxima because they have different donor repeat units. It is interesting to note that they have broad and strong absorption within the visible and infrared regions. It can be seen that **P17** has higher absorption maxima compared to that of **P16** and **P18** (380 and 676 nm for **P16** vs 408 and 776 nm for **P17** vs 373 and 655 nm for **P18**) due to the electrostatic interaction between fluorene substituents on the carbazole and hydrogens in the 4-position on the thiophene as shown in Figure 91. This interaction leads to increased planarity of the polymer structure and so increased the conjugation which results in the polymer having lower optical band gap energy. A similar phenomenon was reported by Hursthouse et al<sup>146</sup>. A comparison of **P16** and **P18** indicates that **P16** has higher absorption bands values at  $\lambda_{\max}$  than **P18** which is expected due to fluorene being a weak donor compared to carbazole due to the lone pair on the nitrogen atom on the carbazole which participates on the electron delocalization and so increase the conjugation in the carbazole.



**Figure 90.** Absorption spectra of **P16**, **P17** and **P18** as thin films.

In addition, **P17** has the lowest optical band gap energy compared to **P16** and **P18** due to electrostatic interaction in **P17** (1.67 eV for **P16** vs 1.36 eV for **P17** vs 1.75 eV for **P18**). On the other hand, the optical band gap energy of **P17** is very low

which might lead to the polymer having a low open circuit voltage in devices and so low power conversion efficiency.

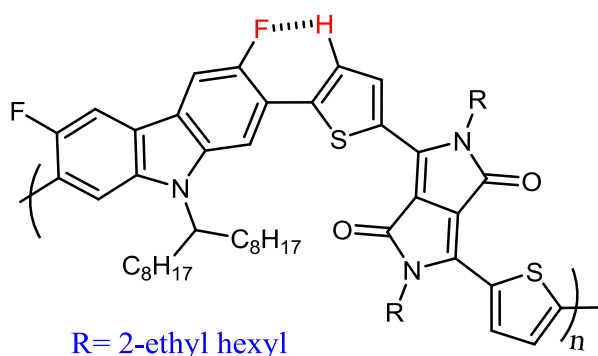


Figure 91. The H-F electrostatic interaction of P17.

Figure 92 shows the UV-Vis spectra of **P19** and **P20** as solid thin films. It can be seen that **P19** has higher absorption maxima than **P20** (357, 657 and 702 nm for **P19** vs 361, 624 and 681 nm for **P20**). In addition, **P19** has lower optical band gap energy compared to that of **P20** (1.61 eV for **P19** vs 1.70 eV for **P20**) which possibly results from steric hindrance effects in the **P20** structure which reduce the donating ability of the repeat units as a result to afford a polymer that has a higher band gap energy and lower absorption maxima than **P19**.

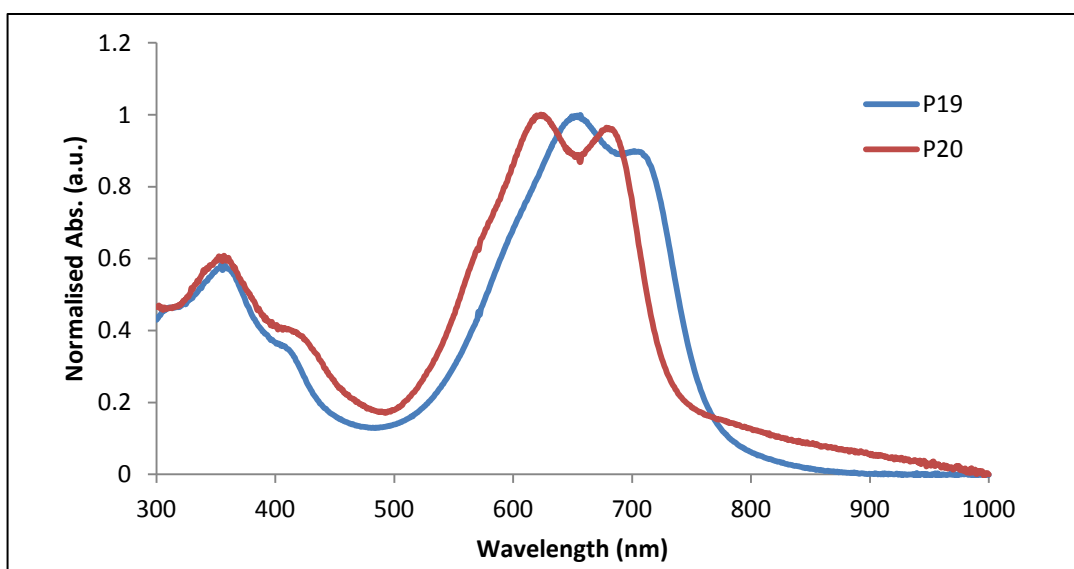


Figure 92. Absorption spectra of P19 and P20 as thin films.

A comparison of **P16** and **P19** indicates that **P19** has a lower optical band gap (1.67 eV for **P16** vs 1.61 eV for **P19**) as a result of anthracene repeat providing more planar polymers compared to carbazole repeat units. It is also interesting to note that **P18** has the highest molar absorptivity compared to that of **P16** and **P17** (76800 L.mol<sup>-1</sup>.cm<sup>-1</sup> for **P16** vs 16500 L.mol<sup>-1</sup>.cm<sup>-1</sup> for **P17** vs 81500 L.mol<sup>-1</sup>.cm<sup>-1</sup> for **P18**). Again, a comparison of the molar absorptivity of **P19** with **P20** indicates that 2,6-anthracene based polymer shows higher molar absorptivity than 2,7-anthracene based polymer (64600 L.mol<sup>-1</sup>.cm<sup>-1</sup> for **P19** vs 50200 L.mol<sup>-1</sup>.cm<sup>-1</sup> for **P20**) which is in agreement with previous result on anthracene polymers (**P7** vs **P10**, **P8** vs **P11**, **P9** vs **P12**). It can be seen that polycarbazole based polymer **P16** and polyflourene based polymer **P18** reveal higher molar absorptivity compared to that of anthracene based polymer **P19** and **P20**.

A comparison of the UV-Vis absorption spectra of **P16** with polybenzothiadiazole equivalent (**PCDTBT**)<sup>11b</sup> (Figure 60) indicates that **P16** has broader and stronger absorption in the visible and near infrared than **PCDTBT** ( $\lambda_{\max}$  380 and 676 nm for **P16** vs  $\lambda_{\max}$  390 and 545nm for **PCDTBT**). In addition, **P16** has a lower optical band gap energy (1.67 eV) compared to that of **PCDTBT** (1.88 eV). In addition, a comparison of **P17** with polybenzothiadiazole equivalent reported by Iraqi *et. al.*<sup>147</sup> (**PFCDTBT**) (Figure 60) indicates a lower band gap for **P17** (1.36 eV for **P17** vs 1.73 eV for **PFCDTBT**). In addition, the **PFCDTBT** revealed absorption bands at  $\lambda_{\max}$  416 and 595 nm which means **PFCDTBT** is blue shifted compared to that of **P17**. Moreover, a comparison of **P18** with polybenzothiadiazole equivalent (**APFO 3**) which was reported by Admassie *et al.*<sup>148</sup> (Figure 60) indicates that **APFO 3** has larger optical band gap energy (1.80 eV for **APFO 3** vs 1.75 eV for **P18**). On the other hand, they have comparable absorption maxima (386 and 554 nm for **APFO 3** vs 373 and 655 for **P18**). It can be seen that DDP repeat units are stronger electron acceptors compared to benzothiadiazole repeat units due to the lactam part makes them exhibit a high electron withdrawing effect and hence it has a high electron affinity which increases their accepting properties and the intramolecular charge transfer along polymer backbones.

---

A comparison of **P19** with its equivalent benzothiadiazole polymer **P7** indicates that **P19** absorption spectra are red shifted compared to those of **P7** (368 and 563 nm for **P7** vs 357, 657 and 702 for **P19**) as shown in Figure 93. Also, **P19** has lower band gap energy compared to that of **P7** (1.84 eV for **P7** vs 1.61 eV for **P19**) which indicates that DPP has higher intramolecular charge transfer along polymer backbone compared to benzothiadiazole. In addition, the molar absorptivity shows a big difference between them **P19** has much higher molar absorptivity compared to that of **P7** ( $64600 \text{ L}\cdot\text{mol}^{-1}\cdot\text{cm}^{-1}$  for **P19** vs  $35200 \text{ L}\cdot\text{mol}^{-1}\cdot\text{cm}^{-1}$  for **P7**). Again, it can be seen that DPP repeat units are stronger acceptors compared to benzothiadiazole repeat units due to lactam part in the DPP which makes them exhibit a high electron withdrawing effect, and hence it has high electron affinity and so **P19** has higher extended electronic conjugation along the polymer backbone.

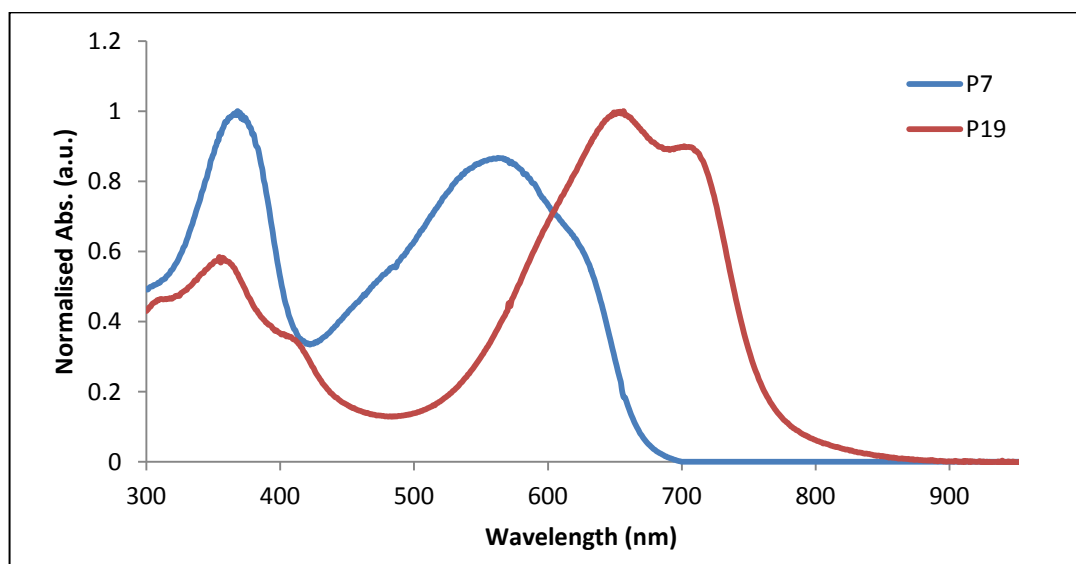
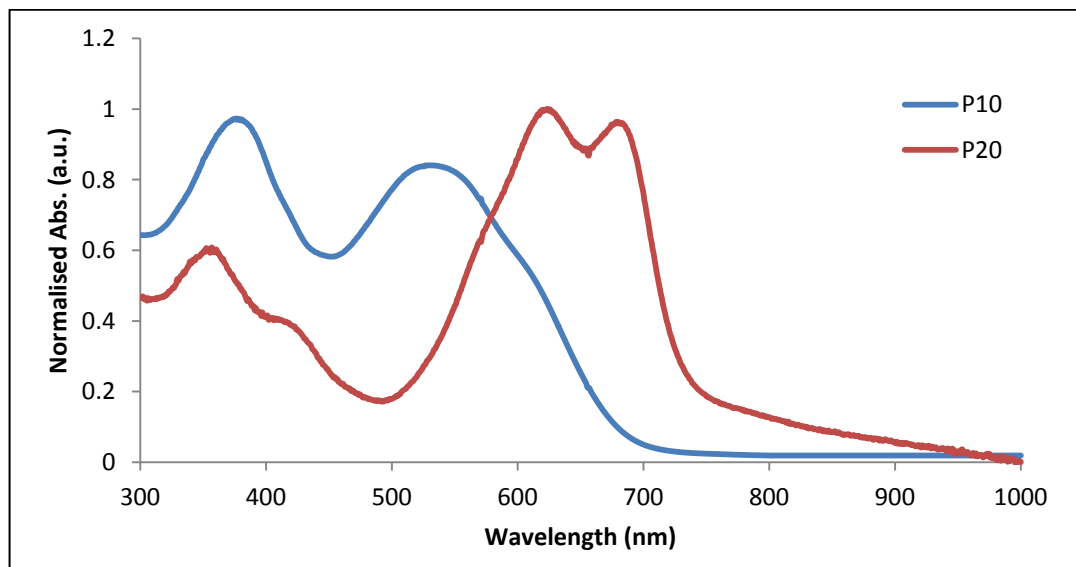


Figure 93. Absorption spectra of P7 and P19 as thin films.

A comparison of **P20** with its equivalent benzothiadiazole polymer (**P10**) shows that **P20** has broader and stronger absorption as a result of a high extended conjugation along polymer backbone as shown in Figure 94. It can be seen that, the spectra indicates that **P20** is blue shifted compared to **P10** (377 and 525 nm for **P10** vs 361, 624 and 681 for **P20**). Also, **P20** has lower band gap energy compared to **P10** (1.82 eV for **P10** vs 1.70 eV for **P20**). In addition, molar absorptivity measurements show a big difference between them as **P20** has a much higher molar

absorptivity compared to **P10** ( $50200 \text{ L}\cdot\text{mol}^{-1}\cdot\text{cm}^{-1}$  for **P20** vs  $31300 \text{ L}\cdot\text{mol}^{-1}\cdot\text{cm}^{-1}$  for **P10**). This confirms again that DDP repeat units are stronger acceptor compared to benzothiadiazole repeat units.



**Figure 94.** Absorption spectra of **P10** and **P20** as thin films.

#### 5.5.2.4. Cyclic Voltammetry (CV) analysis of **P16**, **P17**, **P18**, **P19** and **P20**

In order to study the electrochemical properties of the polymers, Cyclic Voltammetry was carried out on drop-cast polymer films in acetonitrile and tetrabutylammonium perchlorate as electrolyte. The onset of oxidation and reduction can be obtained from cyclic voltammetry curves and used to assess the energy levels of HOMO and LUMO (ferrocene has an ionisation potential of  $-4.8 \text{ eV}$  vs vacuum level<sup>149</sup> and the oxidation takes place at  $0.083 \text{ eV}$  against the  $\text{Ag}/\text{Ag}^+$  reference couple). In addition, the electrochemical band gap energy can be calculated from the energy difference between the HOMO and LUMO levels.

The cyclic voltammetry curves of **P16**, **P17** and **P18** are shown in Figure 95. They indicate that **P17** has the lowest electrical band gap energy due to the electrostatic interaction between fluorine substituents on the carbazole and hydrogens at the 4-position on the thiophene (Figure 91). **P16** has lower electrochemical band gap energy than **P18** as a result of the carbazole being a stronger donor compared to

flourene (1.75 eV for **P16** vs 1.65 eV for **P17** vs 1.80 eV for **P18**). It is clear that they have comparable LUMO energy levels (-3.55 eV for **P16** vs -3.56 eV for **P17** vs -3.51 eV for **P18**) as a result of all the polymers having the same acceptor unit. On the other hand, **P16** and **P18** have deeper HOMO energy levels than **P17** due to the high planarity of its structure which results from electrostatic interaction (Figure 91) (-5.29 eV for **P16** vs -5.21 eV for **P17** vs -5.31 eV for **P18**).

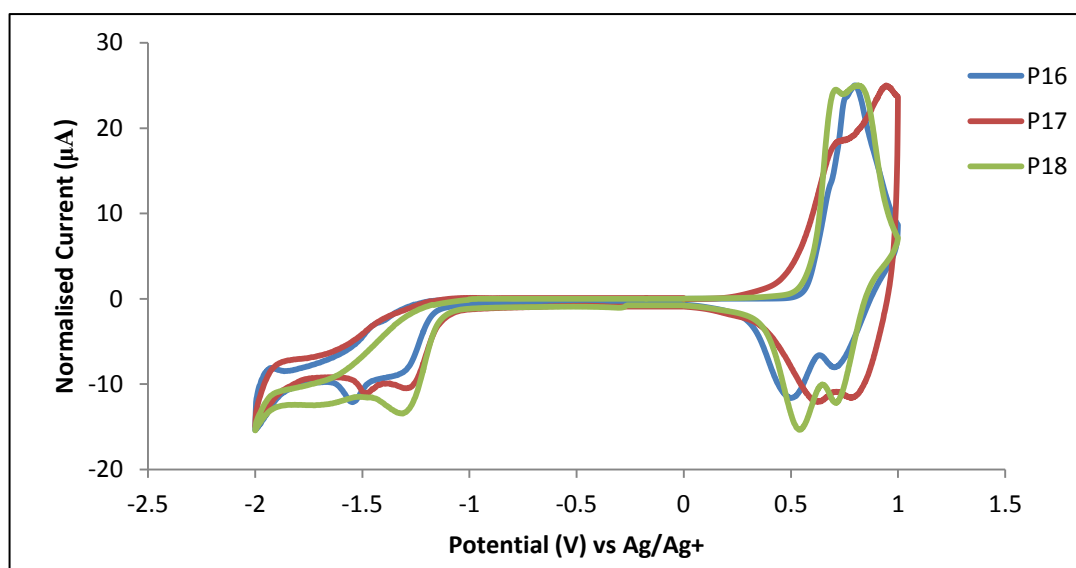


**Figure 95. Cyclic voltammetry curves of P16, P17 and P18.**

As shown in Figure 96, **P19** has a lower electrochemical band gap energy than **P20** (1.69 eV for **P19** vs 1.72 eV for **P20**) due to steric hindrance effects in the structure of **P20**. They (**P19** and **P20**) have comparable HOMO energy levels (-5.23 eV for **P19** vs -5.24 eV for **P20**) and LUMO energy level (-3.53 eV for **P19** vs -3.51 eV for **P20**). A comparison of **P16** and **P19** indicates that **P19** has lower electrochemical band gap (1.75 eV for **P16** vs 1.69 eV for **P19**) as a result of providing more planar polymer chain compared to the carbazole homopolymers. It can be seen that these polymers show promising result for heterojunction devices for solar cell applications.

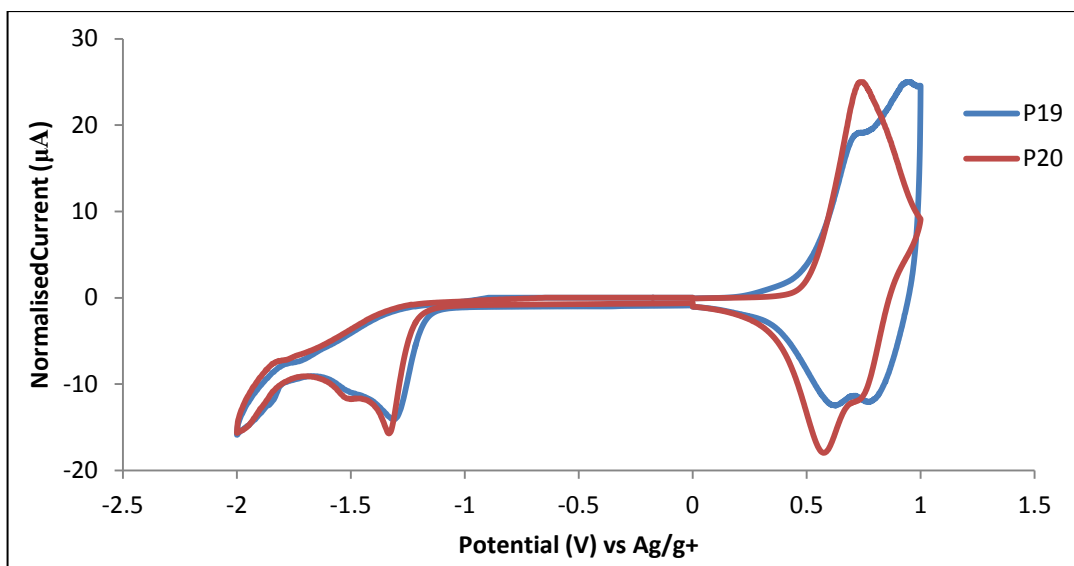


Figure 96. Cyclic voltammetry curves of P19 and P20.

Table 10. UV-Vis and the CV results for P16 – P20.

Polymer	$\lambda_{\max}$ (solution)	$\lambda_{\max}$ (Thin Film)	$E_{op}$	Molar Abs.	HOMO (eV)	LUMO (eV)	$E_{elect}$ (eV)
<b>P16</b>	379, 660	380, 676	1.67	76800	-5.29	-3.55	1.75
<b>P17</b>	359, 724	408, 776	1.36	16500	-5.19	-3.53	1.66
<b>P18</b>	373, 753	373, 655	1.75	81500	-5.31	-3.51	1.80
<b>P19</b>	342, 666	357, 657, 702	1.61	64600	-5.23	-3.53	1.69
<b>P20</b>	376, 505	361, 624, 681	1.70	50200	-5.24	-3.51	1.73

A comparison of the electrochemical results of **P16** with its benzothiadiazole equivalent copolymer **PCDTBT** reported by Leclerc et al.<sup>11b</sup> (Figure 51) indicates that **PCDTBT** has deeper HOMO energy level than **P16** (-5.29 eV for **P16** vs -5.5 eV for **PCDTBT**). In addition, **P16** LUMO energy level is higher than the LUMO

energy level of **PCDTBT** (-3.55 for **P16** vs -3.6 for **PCDTBT**). It is clear from the HOMO and LUMO energy levels that **P16** should have a lower open circuit voltage than **PCDTBT** but it does have lower electrochemical band gap energy than **PCDTBT** which should enable it to harvest more photons from sunlight (1.75 for **P16** vs 1.88 for **PCDTBT**). A comparison of the electrochemical results of **P17** with its equivalent benzothiadiazole copolymer **PFCDTBT** reported by Iraqi et al.<sup>147</sup> (Figure 51) indicates that **P17** has a lower electrochemical band gap energy ( $E_{\text{elect}} = 1.36$  eV for **P17** vs 1.80 eV for **PFCDTBT**). In addition, a comparison of the HOMO and LUMO energy levels shows that they have comparable LUMO energy levels (-3.56 for **P17** vs -3.54 for **PCDTBT**) while **P17** has a higher HOMO energy level than **PFCDTBT** (-5.22 for **P17** vs -5.34 for **PFCDTBT**). It is clear that from HOMO and LUMO energy levels that **P17** should have a lower open circuit voltage than **PFCDTBT** but it does have lower electrochemical band gap energy than **PFCDTBT** which should enable it harvest more photons from sunlight. A comparison of **P18** electrochemical results with its equivalent benzothiadiazole copolymer **APF03** reported by Admassie et al.<sup>148</sup> (Figure 51) indicates that **P18** has a lower electrochemical band gap energy ( $E_{\text{elect}} = 1.80$  eV for **P18** vs  $E_{\text{elect}} = 2.00$  eV for **APF03**). In addition, **P18** shows a deeper LUMO energy level than **APF03** (-3.51 eV for **P18** vs -3.3 eV for **APF03**) but they have the same HOMO energy levels (-5.31 eV for **P18** vs -5.3 eV for **APF03**). Thus, they should theoretically have the same open circuit voltage while **P18** has lower electrochemical band gap energy. In addition, a comparison of **P19** electrochemical results with its benzothiadiazole polymer equivalent **P7** indicates that **P19** has lower electrochemical band gap energy ( $E_{\text{elect}} = 1.69$  eV for **P19** vs  $E_{\text{elect}} = 2.20$  eV for **P7**). In addition, **P19** has a deeper LUMO energy level compared to that of **P7** (-3.53 eV for **P19** vs -3.21 eV for **P7**) while **P7** has a lower HOMO energy level than **P19** (-5.23 eV for **P19** vs -5.44 eV for **P7**). Moreover, a comparison of **P20** electrochemical results with its benzothiadiazole polymer equivalent **P10** indicates that **P20** has lower electrochemical band gap energy ( $E_{\text{elect}} = 1.72$  eV for **P20** vs  $E_{\text{elect}} = 2.44$  eV for **P10**). In addition, **P20** has a deeper LUMO energy level compared to that of **P10** (-3.51 eV for **P20** vs -3.26 eV for **P10**) while **P10** has a deeper HOMO energy level than **P20** (-5.24 eV for **P20** vs -5.54 eV for **P10**). It is

---

clear that DDP based polymers have a high electronic conjugation due to enhanced intramolecular electronic charge transfer along their polymer backbones.

### 5.5.3. Thermal analysis of P16, P17, P18, P19 and P20

The thermal stability of **P16**, **P17** and **P18** were studied using TGA as shown in Figure 97. It can be seen that all three polymers exhibit a high thermal stability up to 400 °C which is high enough for the requirements of solar cell applications. The degradation onset of **P16** occurred at 405 °C and the total weight loss percentage is 45.8% at 800 °C. In addition, the degradation onset of **P17** occurred at 431 °C and the total weight loss percentage is 49.2 % at 800 °C. Finally, the degradation onset of **P18** occurred at 405 °C and the total weight loss percentage is 35.7 % at 800 °C. It is clear, **P16** and **P18** have similar degradation onset which indicates that the degradation can be assigned to the alkyl chains attached to the carbazole and fluorene and DPP.

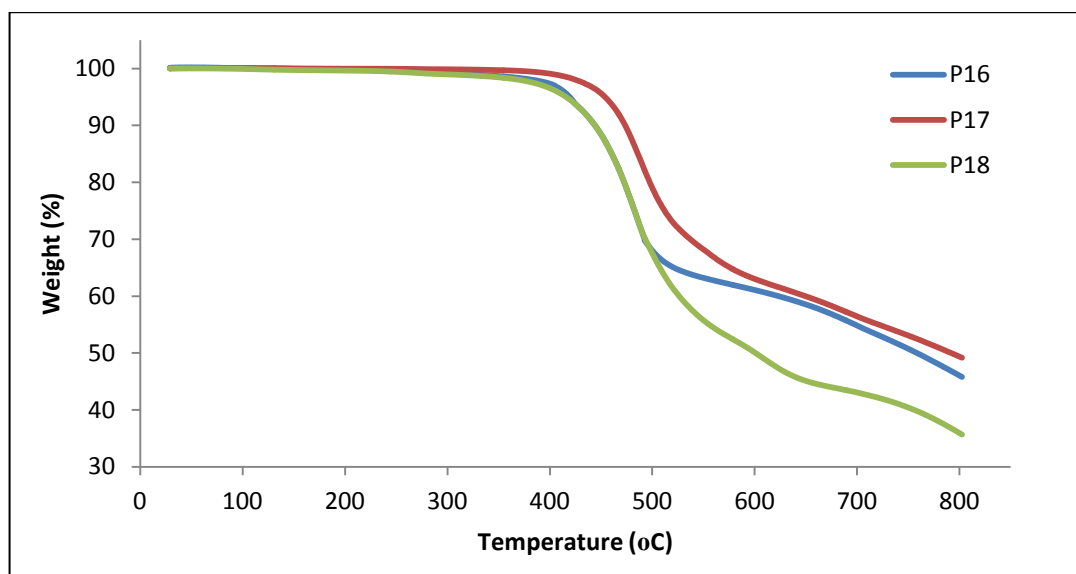


Figure 97. TGA curves of P16, P17 and P18.

**P19** and **P20** have shown a high thermal stability up to 400 °C which is similar to the previous anthracene copolymers as shown in Figure 98. The degradation onset of **P19** occurs at 414 °C which is lower than that for the degradation onset of benzothiadiazole analogous **P7** (438 °C). In addition, **P7** and **P19** have very close

total weight loss percentage at 800 °C (75% for **P9** vs 77.8% for **P19**). The degradation onset of **P20** occurs at 426 °C which is higher than its 2,6-anthracene analogous **P19** (414 °C) but it is lower than its benzothiadiazole polymer equivalent **P10** (445 °C). It can be seen benzothiadiazole polymers exhibit higher thermal stability than DPP polymers.

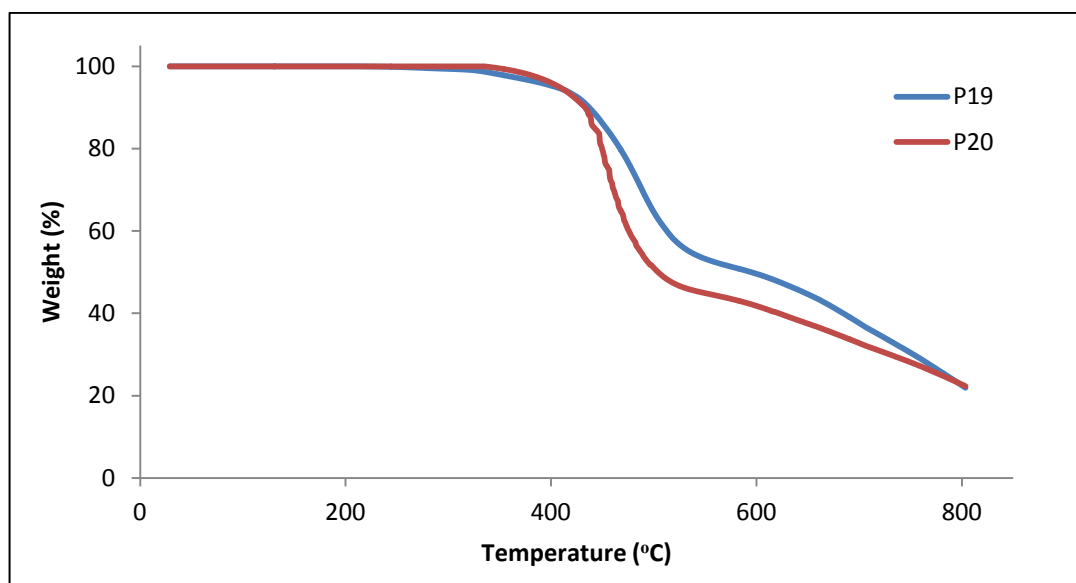


Figure 98. TGA curves of P19 and P20.

## 5.6.1. Photovoltaic studies

Photovoltaic properties of the polymers were studied by the Lidzey group from the department of Physics and Astronomy at The University of Sheffield. All the polymers were blended with Phenyl-C<sub>70</sub>-butyric acid methyl ester (PC<sub>70</sub>BM) as electron acceptor in heterojunction photovoltaic devices with different ratio in order to optimise their performance in devices. The photovoltaic properties of **P7**, **P8**, **P10**, **P11**, **P12**, **P16**, **P18**, **P19** and **P20** are summarised in Table 11, the rest of the polymers studied are still under investigation.

Table 11. Photovoltaic properties of polymers.

Polymer	Polymer:PCBM Weight Ratio	I <sub>sc</sub> (mAcm <sup>-2</sup> )	V <sub>oc</sub> (V)	FF (%)	PCE (%)
<b>P7</b>	1:4	-7.60	0.59	43.43	1.93
<b>P8</b>	1:4	-9.70	0.84	48.20	3.92
<b>P10</b>	1:2	-4.50	0.56	59.47	1.50
<b>P11</b>	1:2	-7.80	0.75	49.09	2.87
<b>P12</b>	1:4	-8.16	0.85	47.66	3.31
<b>P16</b>	1:3	-8.05	0.79	50.2	3.19
<b>P18</b>	1:3	-3.62	0.85	56.4	1.73
<b>P19</b>	1:3	-6.67	0.65	45.5	2.00
<b>P20</b>	1:3	-4.69	0.70	47.5	1.53

The structure of the devices of **P7** and **P8** is (ITO/PEDOT:PSS/Active layer/Ca/Al), while **P10**, **P11** and **P12** were fabricated with a (ITO/MoO<sub>x</sub>/Active layer/Ca/Al) structure. **P16**, **P18**, **P19** and **P20** were fabricated in a (ITO/PEDOT:PSS/Active layer/Ca/Al) structure. Organic solar cell devices were fabricated on pre-prettering indium tin oxide (ITO) glass substrate that bought from Ossila Limited. The substrate was placed in a solution of sodium hydroxide (10%) for five minutes the 120 – 30 nm layer of PEDOT:PSS was spin-coated on the top of the ITO. The result coated substrate was annealed at 125 °C for five minutes in order to remove any trace of moisture. Then, the active layer was spin-coated on the top of the coated substrate using solvents that would not dissolve the PEDOT:PSS layer. A different solvents were used to dissolve a mixture of polymer with PCBM such as dichlorobenzene, chlorobenzene and chloroform. Also, a different concentration ratio of polymer:PCBM (55-75 nm) in the range 1:2 to 1:4 (mass/mass) were used. A layer of Ca (10 nm) was vapour deposited directly on the top of the polymer layer then aluminium layer (100 nm) was vapour deposited on the top of the Ca layer and the device was encapsulated.

From Table 11, it can be seen that anthracene based polymers show power conversion efficiency ranging from 3.93-1.50 %. A comparison of the photovoltaic properties of these different polymers indicates that 2,6-linked anthracene based polymers show better performance in bulk heterojunction devices than 2,7-linked anthracene analogous. As an example, 2,6-linked anthracene based polymer (**P7**) has a power conversion efficiency (PCE) of 1.93 % while 2,7-linked anthracene based polymer (**P10**) has a power conversion efficiency of 1.50 %. Similarly, 2,6-linked anthracene based polymer (**P8**) has a power conversion efficiency of 3.92 % while 2,7-linked anthracene based polymer (**P11**) has a power conversion efficiency of 2.87 %. In addition, 2,6-linked anthracene based polymers show higher short circuit current ( $I_{sc}$ ) and open circuit voltage compared to of 2,7-linked anthracene based polymers. On the other hand, 2,7-linked anthracene based polymers show higher fill factor (FF) compared to 2,6-linked anthracene based polymers. It is interesting to note the dioctyloxy groups that are attached to the benzothiadiazole repeat units in **P8** and **P11** improve the performance of the devices compared to

those made with **P7** and **P10** due to the poor solubility of **P7** and **P10**. Also, replacing thiophene with selenophene improves the performance of polymers in devices with 3.31 % power conversion efficiency recorded for selenophene based polymer (**P12**), while a power conversion efficiency of 2.87% was recorded for thiophene based polymer (**P11**).

Power conversion efficiencies between 3.19-1.53 % were obtained for DDP based polymers and **P16** shows the highest power conversion efficiency (3.19 %) amongst this class of polymers. Again, 2,6-linked anthracene polymers show better performance in devices than 2,7-linked anthracene polymers that **P19** have higher power conversion efficiency (PCE) and short circuit current ( $I_{sc}$ ) than **P20**. However, they (**P19** and **P20**) show comparable fill factor (FF) and open circuit voltage ( $V_{oc}$ ). Finally, it can be seen that a series of polymers for used in organic photovoltaic devices were prepared successfully and their performance in photovoltaic devices were studied. They show promising result for use in organic solar cell devices especially **P8**. Also, further photovoltaic studies and optimisation will be carried out such as changing PCBM:polymer concentration ratio and using new device structure especially the electron and hole transport layers between electrodes and active layer such as  $MoO_x$  and PFN.

## Chapter Six: Conclusion and Future Work

A series of low band gap copolymers for use in bulk heterojunction organic solar cell were prepared successfully using Suzuki cross coupling reaction. The carbazole, fluorene–pyrrole based copolymers (**P1**, **P2**, **P3**) results indicate that they have wider band gap energy compared to those from thiophene analogous copolymers reported in the literature due to the fact that N-methyl pyrrole providing more steric hindrance along polymer chains than thiophene repeat units and as a result leading to less intramolecular charge transfer along copolymer backbones. In addition, **P1** has been prepared twice with two different molecular weights obtained. The result indicates the importance of having a high molecular weight on the photo-physical and electrical properties of conjugated polymers as **P1(2)** has more extended electronic conjugation along its polymer chains compared to **P1(1)**. The photophysical and the electrochemical properties of **P1(1)**, **P2** and **P3** copolymers (similar molecular weights) illustrate that **P2** has the narrowest optical and electrochemical band gap energy as a result of electrostatic interaction between the hydrogen at the 4-position on the N-methylpyrrole repeat units and the fluorine substituent on the carbazole repeat units which increases the planarity of the copolymer. Also, the results show that **P3** has the widest optical and electrochemical band gap energy as a result of the fluorene having a lower electron donating ability compared to that of carbazole and so it has lower donor/acceptor intramolecular charge transfer along polymer chains.

The molecular weights of copolymers **P1**, **P2** and **P3** were low because they preipitate out of solution in the early stages of polymerization as a result of the poor solubility of these copolymers. Due to the short chain length of polymers **P1**, **P2** and **P3** and the link between the extent of electronic delocalisation and chain length, it is necessary to explore a new version of this series of copolymers with higher solubilities. So, attachment of solubilising groups on the benzothiadiazole repeat units was hence pursued in this work. Unfortunately, 4,7-bis(1-methyl-1H-pyrrol-2-yl)-5,6-bis(octyloxy)benzo[c][1,2,5]thiadiazole (**17**) could not be purified via column chromatography and HPLC. Pure products are crucial at this step

because it is followed by a bromination step which requires accurate stoichiometry of brominating reagents in order to avoid over bromination which could provide monomers that are extremely difficult to purify and so 4,7-bis(5-bromo-1-methyl-1H-pyrrol-2-yl)-5,6-bis(octyloxy)benzo[c][1,2,5]thiadiazole (**18**), **P4**, **P5** and **P6** could not be prepared and this section of project was then abandoned.

A series of new donor-acceptor 2,6-anthracene based copolymers were prepared successfully. They show very promising results for use in solar cell applications. They (**P7**, **P8** and **P9**) show low optical band gap energies in the range (1.84 – 1.96 eV) which is lower than their analogous carbazole copolymers. **P7** has the narrowest optical and electrochemical band gap energy while **P8** has the widest. The results indicate that the alkoxy groups attached to the benzothiadiazole units improve the solubility and molecular weight of the polymers obtained. However, these substituents have a negative effect on the conjugation properties of **P8**. The donating properties of the octyloxy substituents attached to the benzothiadiazole repeat units decrease their electron accepting properties and intramolecular charge transfer along the polymer backbone. Also, they possibly affect the planarity of the polymer backbone due to steric hindrance and so lead to wider band gap polymers. In addition, the results show that replacing thiophene with selenophene leads to an increase in the electron donating properties of the donor repeat units as a result of the Se – Se interactions which leads to higher intramolecular charge transfer along the polymer backbone in **P9**. The alkoxy chain substituents reduce the thermal stability of these copolymers when compared to that of **P7** which does not have these substituents on **P8** and **P9** while **P7** has an onset of degradation at ~ 400 °C, **P8** and **P9** have a lower degradation onset (~ 300 °C).

A new version of anthracene copolymers were prepared successfully and fully characterised. They are similar to the previous 2,6-anthracene copolymers but are linked in different positions (2,7-linkage). The effect of octyloxy substituents attached to the benzothiadiazole units and replacement of thiophene with selenophene has been studied in these anthracene polymers. The results indicate that 2,6-linked anthracene copolymers have slightly higher conjugation compared to that of 2,7-linked anthracene copolymers. The chemical structure of 2,7-linked

anthracene polymers might lead to a slight amount of chain twisting due to steric hindrance which leads to reducing the electron delocalisation along the copolymer backbones. In addition, 2,7-linked anthracene copolymers have slightly lower molar absorptivities compared to those of the 2,6-linked anthracene analogous copolymers. These results were confirmed by preparing 2,6- and 2,7- linked homopolymer (**P13** and **P14**) and 2,6 and 2,7 linked copolymer (**P15**). Again, the results these polymers (**P13**, **P14** and **P15**) confirm the previous result that 2,6-linked anthracene polymers have slightly higher extended electronic conjugation along polymer backbones compared to that of 2,7-linked polymers.

A series of diketopyrrolopyrrole (DPP) based copolymers were prepared successfully. They show low optical and electrochemical band gap energies as a result of the strong electron accepting ability of DPP. **P17** has the lowest optical and electrochemical band gap energies with 1.36 and 1.65 eV respectively as a result of electrostatic interaction between the hydrogen at the 4-position on the thiophene repeat units and the fluorine substituents on the carbazole repeat units which increases the planarity of the copolymer while **P18** shows the highest optical and electrochemical band gap energies in the series of polymers with 1.72 and 1.80 eV. Again, the results indicate that 2,6-linked anthracene copolymer **P19** has slightly higher extended conjugation along its polymer backbone compared to the 2,7-linked copolymer **P20**. **P19** has lower optical and electrochemical band gap energies with 1.61 and 1.69 eV respectively than **P20** (1.70 and 1.72 eV). In addition, 2,7- linked anthracene copolymer **P19** shows higher extended conjugation along polymer backbone than the homopolymers carbazole based copolymer **P16** which gives a clear indication that anthracene based polymers provide more planar polymers than carbazole based polymers. All of these polymers show HOMO energy levels in the range (-5.21 to -5.31 eV) which are in the range required for PV applications while the LUMO energy levels are in the range (-3.51 to -3.55 eV) which is slightly higher than the optimal polymers required in this area. Also, all of this series of copolymers exhibit high thermal stabilities up to 400 °C which is high enough for the requirements of solar cell applications.

Future work should include studies on the physical properties of the blends of these copolymers with fullerene derivatives. The anthracene copolymers show promising results for use in organic solar cell devices. Thus, it is worth to investigate new version of anthracene derivatives in order to improve their photophysical and electrochemical properties by using various alkyl chain substituents in the 9- and 10- positions which would influence their efficiency when used in bulk heterojunction photovoltaic devices. Furthermore, studies the photophysical and electrochemical properties of these derivatives with other electron acceptor monomers such as dioxypyrrolothiophene (DOPT) derivatives should also lead to important new classes of donor-acceptor conjugated polymers with a great potential for application in solar cells.

---

## References

- (1) Hatfield, C. B. *Nature* **1997**, 387, 121.
  - (2) Ruehl, C.; Giljum, J. *Energy* **2011**, 2030, 2.
  - (3) *Energy Policy Act 2005, Section 1837 [electronic resource] : national security review of international energy requirements / prepared by the U.S. Department of Energy*; U.S. Dept. of Energy: [Washington, D.C.] :, 2006.
  - (4) (a) Wa, P.; Würfel, P. *Physics of Solar Cells: From Principles to New Concepts*; Wiley-VCH, 2008(b) McGehee, M. D.; Goh, C., 2006; p 119.
  - (5) Hirsch, R. L. *The Atlantic Council of the United States, XVI* **2005**, 3.
  - (6) Dennler, G.; Sariciftci, N. S. *Proceedings of the IEEE* **2005**, 93, 1429.
  - (7) Okamoto, Y.; Gordon, A.; Movsovicius, F.; Hellman, H.; Brenner, W. *Chemistry & Industry* **1961**, 2004.
  - (8) Feast, W.; Tsibouklis, J.; Pouwer, K.; Groenendaal, L.; Meijer, E. *Polymer* **1996**, 37, 5017.
  - (9) (a) Chiang, C.; Fincher Jr, C.; Park, Y.; Heeger, A.; Shirakawa, H.; Louis, E.; Gau, S.; MacDiarmid, A. G. *Physical Review Letters* **1977**, 39, 1098(b) Shirakawa, H.; Louis, E. J.; MacDiarmid, A. G.; Chiang, C. K.; Heeger, A. J. *J. Chem. Soc., Chem. Commun.* **1977**, 578(c) Chiang, C.; Druy, M.; Gau, S.; Heeger, A.; Louis, E.; MacDiarmid, A. G.; Park, Y.; Shirakawa, H. *Journal of the American Chemical Society* **1978**, 100, 1013(d) Shirakawa, H. *Angewandte Chemie International Edition* **2001**, 40, 2574.
  - (10) Heeger, A. J.; MacDiarmid, A.; Shirakawa, H. *The Nobel Foundation* **2000**.
  - (11) (a) Heeger, A. J. *Chem. Soc. Rev.* **2010**, 39, 2354(b) Blouin, N.; Michaud, A.; Leclerc, M. *Adv. Mater.* **2007**, 19, 2295(c) Heeger, A. J. *Synth. Met.* **2001**, 125, 23.
  - (12) (a) Winder, C.; Sariciftci, N. S. *J. Mater. Chem.* **2004**, 14, 1077(b) Peet, J.; Heeger, A. J.; Bazan, G. C. *Accounts of Chemical Research* **2009**, 42, 1700.
  - (13) (a) Burroughes, J. H.; Bradley, D. D. C.; Brown, A. R.; Marks, R. N.; Mackay, K.; Friend, R. H.; Burns, P. L.; Holmes, A. B. *Nature* **1990**, 347, 539(b) Friend, R. H.; Gymer, R. W.; Holmes, A. B.; Burroughes, J. H.; Marks, R. N.; Taliani, C.; Bradley, D. D. C.; Dos Santos, D. A.; Bredas, J. L.; Logdlund, M.; Salaneck, W. R. *Nature* **1999**, 397, 121.
  - (14) (a) Dimitrakopoulos, C. D.; Malenfant, P. R. L. *Adv. Mater.* **2002**, 14, 99(b) Babel, A.; Jenekhe, S. A. *Adv. Mater.* **2002**, 14, 371.
  - (15) (a) Adhikari, B.; Majumdar, S. *Progress in Polymer Science* **2004**, 29, 699(b) McQuade, D. T.; Pullen, A. E.; Swager, T. M. *Chemical reviews* **2000**, 100, 2537.
  - (16) (a) Li, Q. F.; He, R. H.; Jensen, J. O.; Bjerrum, N. J. *Chemistry of Materials* **2003**, 15, 4896(b) Novak, P.; Muller, K.; Santhanam, K. S. V.; Haas, O. *Chemical reviews* **1997**, 97, 207.
  - (17) Gribov, B. G.; Zinov'ev, K. V. *Inorganic Materials* **2003**, 39, 653.
  - (18) Chang, J. F.; Sun, B. Q.; Breiby, D. W.; Nielsen, M. M.; Solling, T. I.; Giles, M.; McCulloch, I.; Sirringhaus, H. *Chemistry of Materials* **2004**, 16, 4772.
-

- 
- (19) Hebner, T. R.; Wu, C. C.; Marcy, D.; Lu, M. H.; Sturm, J. C. *Appl. Phys. Lett.* **1998**, *72*, 519.
- (20) Ling, M. M.; Bao, Z. N. *Chemistry of Materials* **2004**, *16*, 4824.
- (21) Krebs, F. C.; Gevorgyan, S. A.; Alstrup, J. *J. Mater. Chem.* **2009**, *19*, 5442.
- (22) Krebs, F. C. *Solar energy materials and solar cells* **2009**, *93*, 394.
- (23) Kim, S. S.; Na, S. I.; Jo, J.; Tae, G.; Kim, D. Y. *Adv. Mater.* **2007**, *19*, 4410.
- (24) Forrest, S. R. *Nature* **2004**, *428*, 911.
- (25) Pron, A.; Rannou, P. *Progress in Polymer Science* **2002**, *27*, 135.
- (26) (a) Bradford, w. *Electronic and optical properties of conjugated polymers*; Oxford Science Publication: United State, 2005(b) Heeger, A. J.; Sariciftci, N. S.; Namdas, E. B. *Semiconducting and metallic polymers*; Oxford University Press, 2011.
- (27) Friend, R. H. *Pure Appl. Chem.* **2001**, *73*, 425.
- (28) Salaneck, W. R.; Lundström, I.; Rånby, B. G. *Conjugated polymers and related materials: the interconnection of chemical and electronic structure: proceedings of the Eighty-first Nobel Symposium*; Oxford University Press, USA, 1993.
- (29) Ajayaghosh, A. *Chemical Society Reviews* **2003**, *32*, 181.
- (30) (a) Roth, S.; Carroll, D. L. *One-dimensional metals: conjugated polymers, organic crystals, carbon nanotubes*; Vch Verlagsgesellschaft Mbh, 2004(b) Jenekhe, S. A. *Nature* **1986**, *322*, 345(c) Bredas, J. L.; Silbey, R.; Boudreaux, D. S.; Chance, R. R. *Journal of the American Chemical Society* **1983**, *105*, 6555(d) Baughman, R. H.; Bredas, J. L.; Chance, R. R.; Elsenbaumer, R. L.; Shacklette, L. W. *Chemical reviews* **1982**, *82*, 209(e) Wohlgenannt, M.; Jiang, X. M.; Vardeny, Z. V. *Physical Review B* **2004**, *69*.
- (31) De Paoli, M. A.; Gazotti, W. A. *Journal of the Brazilian Chemical Society* **2002**, *13*, 410.
- (32) (a) Bundgaard, E.; Krebs, F. C. *Solar energy materials and solar cells* **2007**, *91*, 954(b) Hadziioannou, G.; VAN HUTTEN, P. F. *Recherche* **2005**, *67*, 02.
- (33) (a) Miyaura, N.; Suzuki, A. *Journal of the Chemical Society-Chemical Communications* **1979**, 866(b) Miyaura, N.; Yamada, K.; Suzuki, A. *Tetrahedron Letters* **1979**, *20*, 3437.
- (34) Suzuki, A. *Proceedings of the Japan Academy, Series B* **2004**, *80*, 359.
- (35) Suzuki, A.; Heck, R. F.; Negishi, E.-i. **2010**.
- (36) Kotha, S.; Lahiri, K.; Kashinath, D. *Tetrahedron* **2002**, *58*, 9633.
- (37) (a) Milstein, D.; Stille, J. *Journal of the American Chemical Society* **1978**, *100*, 3636(b) Milstein, D.; Stille, J. *Journal of the American Chemical Society* **1979**, *101*, 4992.
- (38) Nicolaou, K.; Bulger, P. G.; Sarlah, D. *Angewandte Chemie International Edition* **2005**, *44*, 4442.
- (39) Stille, J. K. *Angewandte Chemie International Edition in English* **1986**, *25*, 508.
- (40) Archer, M. D.; Hill, R. *Clean electricity from photovoltaics (Series on Photoconversion of Solar Energy vol. 1)*; Imperial College Press, London, 2001.
-

- 
- (41) Stine, W. B.; Geyer, M. *Published online at www. powerfromthesun. net* **2001**.
- (42) (a) Tang, C. W. *Appl. Phys. Lett.* **1986**, *48*, 183(b) Tang, C. W.; Google Patents, 1979.
- (43) O'regan, B.; Gratzel, M. *Nature* **1991**, *353*, 737.
- (44) Green, M. A.; Emery, K.; Hishikawa, Y.; Warta, W.; Dunlop, E. D. *Progress in Photovoltaics: Research and Applications* **2012**, *20*, 12.
- (45) Thelakkat, M.; Schmitz, C.; Schmidt, H. W. *Adv. Mater.* **2002**, *14*, 577.
- (46) Sariciftci, N.; Braun, D.; Zhang, C.; Srdanov, V.; Heeger, A.; Stucky, G.; Wudl, F. *Appl. Phys. Lett.* **1993**, *62*, 585.
- (47) Yu, G.; Pakbaz, K.; Heeger, A. *Appl. Phys. Lett.* **1994**, *64*, 3422.
- (48) (a) Yu, G.; Heeger, A. J. *Journal of Applied Physics* **1995**, *78*, 4510(b) Halls, J.; Walsh, C.; Greenham, N.; Marseglia, E.; Friend, R.; Moratti, S.; Holmes, A. **1995**.
- (49) Granström, M.; Petritsch, K.; Arias, A.; Lux, A.; Andersson, M.; Friend, R. *Nature* **1998**, *395*, 257.
- (50) Kim, J. Y.; Lee, K.; Coates, N. E.; Moses, D.; Nguyen, T. Q.; Dante, M.; Heeger, A. J. *Science* **2007**, *317*, 222.
- (51) Kippelen, B.; Brédas, J. L. *Energy Environ. Sci.* **2009**, *2*, 251.
- (52) Nelson, J. *Current Opinion in Solid State and Materials Science* **2002**, *6*, 87.
- (53) (a) Topham, P. D.; Parnell, A. J.; Hiorns, R. C. *Journal of Polymer Science Part B: Polymer Physics* **2011**(b) Lloyd, M. T.; Anthony, J. E.; Malliaras, G. G. *Materials Today* **2007**, *10*, 34(c) Padinger, F.; Rittberger, R. S.; Sariciftci, N. S. *Advanced Functional Materials* **2003**, *13*, 85.
- (54) (a) Arias, A. C.; MacKenzie, J. D.; Stevenson, R.; Halls, J. J. M.; Inbasekaran, M.; Woo, E. P.; Richards, D.; Friend, R. H. *Macromolecules* **2001**, *34*, 6005(b) Stoessel, M.; Wittmann, G.; Staudigel, J.; Steuber, F.; Blassing, J.; Roth, W.; Klausmann, H.; Rogler, W.; Simmerer, J.; Winnacker, A.; Inbasekaran, M.; Woo, E. P. *Journal of Applied Physics* **2000**, *87*, 4467.
- (55) Moses, D.; Dogariu, A.; Heeger, A. J. *Synth. Met.* **2001**, *116*, 19.
- (56) Mihailetschi, V. D.; Koster, L. J. A.; Hummelen, J. C.; Blom, P. W. M. *Physical Review Letters* **2004**, *93*.
- (57) (a) Yang, X. N.; Loos, J.; Veenstra, S. C.; Verhees, W. J. H.; Wienk, M. M.; Kroon, J. M.; Michels, M. A. J.; Janssen, R. A. J. *Nano Letters* **2005**, *5*, 579(b) Gregg, B. A.; Hanna, M. C. *Journal of Applied Physics* **2003**, *93*, 3605.
- (58) (a) Spanggaard, H.; Krebs, F. C. *Solar Energy Materials and Solar Cells* **2004**, *83*, 125(b) Gledhill, S. E.; Scott, B.; Gregg, B. A. *Journal of Materials Research* **2005**, *20*, 3167.
- (59) (a) Sirringhaus, H.; Tessler, N.; Friend, R. H. *Science* **1998**, *280*, 1741(b) Kline, R. J.; McGehee, M. D.; Kadnikova, E. N.; Liu, J. S.; Frechet, J. M. J. *Adv. Mater.* **2003**, *15*, 1519(c) Coakley, K. M.; McGehee, M. D. *Chemistry of Materials* **2004**, *16*, 4533(d) Yang, C.-M.; Liao, H.-H.; Horng, S.-F.; Meng, H.-F.; Tseng, S.-R.; Hsu, C.-S. *Synth. Met.* **2008**, *158*, 25.
- (60) Thompson, B. C.; Fréchet, J. M. J. *Angewandte Chemie International Edition* **2008**, *47*, 58.
-

- 
- (61) (a) Sariciftci, N. S.; Smilowitz, L.; Heeger, A. J.; Wudl, F. *Science* **1992**, 258, 1474(b) Morita, S.; Zakhidov, A. A.; Yoshino, K. *Solid state communications* **1992**, 82, 249.
- (62) (a) Cowan, S. R.; Banerji, N.; Leong, W. L.; Heeger, A. J. *Advanced Functional Materials* **2012**(b) Cowan, S. R.; Street, R.; Cho, S.; Heeger, A. *Physical Review B* **2011**, 83, 035205.
- (63) (a) Saunders, B. R.; Turner, M. L. *Advances in Colloid and Interface Science* **2008**, 138, 1(b) Brabec, C. J.; Sariciftci, N. S.; Hummelen, J. C. *Advanced Functional Materials* **2001**, 11, 15.
- (64) Na, S. I.; Kim, S. S.; Jo, J.; Kim, D. Y. *Adv. Mater.* **2008**, 20, 4061.
- (65) Irwin, M. D.; Buchholz, D. B.; Hains, A. W.; Chang, R. P. H.; Marks, T. J. *Proceedings of the National Academy of Sciences* **2008**, 105, 2783.
- (66) Liu, Z.; Li, J.; Sun, Z. H.; Tai, G.; Lau, S. P.; Yan, F. *ACS nano* **2011**, 6, 810.
- (67) (a) Brabec, C. J.; Shaheen, S. E.; Winder, C.; Sariciftci, N. S.; Denk, P. *Appl. Phys. Lett.* **2002**, 80, 1288(b) Gadisa, A.; Tvingstedt, K.; Admassie, S.; Lindell, L.; Crispin, X.; Andersson, M. R.; Salaneck, W. R.; Inganäs, O. *Synth. Met.* **2006**, 156, 1102.
- (68) Hoppea, H.; Sariciftci, N. S. *J. Mater. Res* **2004**, 19, 1945.
- (69) Coakley, K. M.; Liu, Y.; Goh, C.; McGehee, M. D. *MRS bulletin* **2005**, 30, 37.
- (70) Zhou, H.; Yang, L.; You, W. *Macromolecules* **2012**, 45, 607.
- (71) Yamamoto, T.; Zhou, Z. H.; Kanbara, T.; Shimura, M.; Kizu, K.; Maruyama, T.; Nakamura, Y.; Fukuda, T.; Lee, B. L.; Ooba, N.; Tomaru, S.; Kurihara, T.; Kaino, T.; Kubota, K.; Sasaki, S. *Journal of the American Chemical Society* **1996**, 118, 10389.
- (72) (a) van Mullekom, H. A. M.; Vekemans, J.; Havinga, E. E.; Meijer, E. W. *Materials Science & Engineering R-Reports* **2001**, 32, 1(b) Cheng, Y. J.; Yang, S. H.; Hsu, C. S. *Chemical reviews* **2009**, 109, 5868.
- (73) Mayer, A. C.; Scully, S. R.; Hardin, B. E.; Rowell, M. W.; McGehee, M. D. *Materials Today* **2007**, 10, 28.
- (74) Kirchartz, T.; Taretto, K.; Rau, U. *The Journal of Physical Chemistry C* **2009**, 113, 17958.
- (75) Brabec, C. J.; Dyakonov, V.; Parisi, J.; Sariciftci, N. S. *Organic photovoltaics: concepts and realization*; Springer, 2003.
- (76) (a) Moliton, A.; Nunzi, J. M. *Polymer International* **2006**, 55, 583(b) Lo, M. F.; Ng, T. W.; Liu, T. Z.; Roy, V. A. L.; Lai, S. L.; Fung, M. K.; Lee, C. S.; Lee, S. T. *Appl. Phys. Lett.* **2010**, 96(c) Muhlbacher, D.; Scharber, M.; Morana, M.; Zhu, Z. G.; Waller, D.; Gaudiana, R.; Brabec, C. *Adv. Mater.* **2006**, 18, 2884.
- (77) Zhou, H. X.; Yang, L. Q.; Stoneking, S.; You, W. *Acs Applied Materials & Interfaces* **2010**, 2, 1377.
- (78) (a) Scharber, M. C.; Wuhlbacher, D.; Koppe, M.; Denk, P.; Waldauf, C.; Heeger, A. J.; Brabec, C. L. *Adv. Mater.* **2006**, 18, 789(b) Koster, L. J. A.; Mihailetschi, V. D.; Blom, P. W. M. *Appl. Phys. Lett.* **2006**, 88.
- (79) (a) Pivrikas, A.; Neugebauer, H.; Sariciftci, N. S. *Solar Energy* **2011**, 85, 1226(b) Kline, R. J.; DeLongchamp, D. M.; Fischer, D. A.; Lin, E. K.; Richter, L. J.; Chabinyc, M. L.; Toney, M. F.; Heeney, M.; McCulloch, I.
-

- Macromolecules* **2007**, *40*, 7960(c) Thompson, B. C.; Kim, B. J.; Kavulak, D. F.; Sivula, K.; Mauldin, C.; Frechet, J. M. J. *Macromolecules* **2007**, *40*, 7425(d) Liu, F.; Gu, Y.; Jung, J. W.; Jo, W. H.; Russell, T. P. *Journal of Polymer Science Part B: Polymer Physics* **2012**.
- (80) Kokil, A.; Yang, K.; Kumar, J. *Journal of Polymer Science Part B-Polymer Physics* **2012**, *50*, 1130.
- (81) (a) Zhao, Q.; Liu, S. J.; Huang, W. *Macromolecular Chemistry and Physics* **2009**, *210*, 1580(b) Beaupré, S.; Boudreault, P. L. T.; Leclerc, M. *Adv. Mater.* **2010**, *22*, E6(c) Mikroyannidis, J. A.; Beka, P. M.; Papadopoulos, J. F. *Synth. Met.* **2005**, *149*, 203.
- (82) (a) Abbel, R.; Schenning, A. P. H. J.; Meijer, E. *Journal of Polymer Science Part A: Polymer Chemistry* **2009**, *47*, 4215(b) Koetnuyom, W.; Keawprajak, A.; Piyakulawat, P.; Jiramitmongkon, K.; Nukeaw, J.; Pratontep, S.; Asawapirom, U. *The Canadian Journal of Chemical Engineering* **2012**.
- (83) (a) Inganäs, O.; Zhang, F.; Andersson, M. R. *Accounts of Chemical Research* **2009**, *42*, 1731(b) Leclerc, M. *Journal of Polymer Science Part A: Polymer Chemistry* **2001**, *39*, 2867.
- (84) Slooff, L. H.; Veenstra, S. C.; Kroon, J. M.; Moet, D. J. D.; Sweelssen, J.; Koetse, M. M. *Appl. Phys. Lett.* **2007**, *90*.
- (85) (a) Grazulevicius, J.; Strohriegl, P.; Pielichowski, J.; Pielichowski, K. *Progress in Polymer Science* **2003**, *28*, 1297(b) Li, J.; Grimsdale, A. C. *Chemical Society Reviews* **2010**, *39*, 2399(c) Blouin, N.; Leclerc, M. *Accounts of Chemical Research* **2008**, *41*, 1110.
- (86) Morin, J. F.; Leclerc, M.; Ades, D.; Siove, A. *Macromolecular Rapid Communications* **2005**, *26*, 761.
- (87) (a) Bai, F.; Zheng, M.; Yu, G.; Zhu, D. *Thin Solid Films* **2000**, *363*, 118(b) Sotzing, G. A.; Reddinger, J. L.; Katritzky, A. R.; Soloduchko, J.; Musgrave, R.; Reynolds, J. R.; Steel, P. J. *Chemistry of Materials* **1997**, *9*, 1578.
- (88) Morin, J. F.; Leclerc, M. *Macromolecules* **2001**, *34*, 4680.
- (89) Li, J. L.; Dierschke, F.; Wu, J. S.; Grimsdale, A. C.; Mullen, K. *J. Mater. Chem.* **2006**, *16*, 96.
- (90) Park, S. H.; Roy, A.; Beaupre, S.; Cho, S.; Coates, N.; Moon, J. S.; Moses, D.; Leclerc, M.; Lee, K.; Heeger, A. J. *Nature Photonics* **2009**, *3*, 297.
- (91) (a) Huo, L. J.; Hou, J. H. *Polymer Chemistry* **2011**, *2*, 2453(b) Blouin, N.; Michaud, A.; Gendron, D.; Wakim, S.; Blair, E.; Neagu-Plesu, R.; Belletête, M.; Durocher, G.; Tao, Y.; Leclerc, M. *Journal of the American Chemical Society* **2008**, *130*, 732.
- (92) Zhou, H. X.; Yang, L. Q.; Stuart, A. C.; Price, S. C.; Liu, S. B.; You, W. *Angewandte Chemie-International Edition* **2011**, *50*, 2995.
- (93) (a) Yi, H. N.; Al-Faifi, S.; Iraqi, A.; Watters, D. C.; Kingsley, J.; Lidzey, D. G. *J. Mater. Chem.* **2011**, *21*, 13649(b) Qin, R. P.; Li, W. W.; Li, C. H.; Du, C.; Veit, C.; Schleiermacher, H. F.; Andersson, M.; Bo, Z. S.; Liu, Z. P.; Inganäs, O.; Wuerfel, U.; Zhang, F. L. *Journal of the American Chemical Society* **2009**, *131*, 14612.
- (94) (a) Boudreault, P. L. T.; Najari, A.; Leclerc, M. *Chemistry of Materials* **2011**, *23*, 456(b) Chen, J.; Cao, Y. *Accounts of Chemical Research* **2009**, *42*, 1709.

- 
- (95) McCullough, R. D.; Lowe, R. D. *Journal of the Chemical Society-Chemical Communications* **1992**, 70.
- (96) Glenis, S.; Horowitz, G.; Tourillon, G.; Garnier, F. *Thin Solid Films* **1984**, *111*, 93.
- (97) Ma, W. L.; Yang, C. Y.; Gong, X.; Lee, K.; Heeger, A. J. *Advanced Functional Materials* **2005**, *15*, 1617.
- (98) (a) Clarke, T. M.; Ballantyne, A. M.; Tierney, S.; Heeney, M.; Duffy, W.; McCulloch, I.; Nelson, J.; Durrant, J. R. *Journal of Physical Chemistry C* **2010**, *114*, 8068(b) Heeney, M.; Zhang, W.; Crouch, D. J.; Chabinyc, M. L.; Gordeyev, S.; Hamilton, R.; Higgins, S. J.; McCulloch, I.; Skabara, P. J.; Sparrowe, D.; Tierney, S. *Chem. Commun.* **2007**, 5061.
- (99) Chen, H. Y.; Hou, J. H.; Zhang, S. Q.; Liang, Y. Y.; Yang, G. W.; Yang, Y.; Yu, L. P.; Wu, Y.; Li, G. *Nature Photonics* **2009**, *3*, 649.
- (100) Svensson, M.; Zhang, F.; Inganäs, O.; Andersson, M. R. *Synth. Met.* **2003**, *135*, 137.
- (101) (a) Farnum, D. G.; Mehta, G.; Moore, G. G. I.; Siegal, F. P. *Tetrahedron Letters* **1974**, 2549(b) Gendron, D.; Leclerc, M. *Energy & Environmental Science* **2011**, *4*, 1225.
- (102) Wallquist, O.; Lenz, R. *Macromol. Symp.* **2002**, *187*, 617.
- (103) Cao, D. R.; Liu, Q. L.; Zeng, W. J.; Han, S. H.; Peng, J. B.; Liu, S. P. *Journal of Polymer Science Part a-Polymer Chemistry* **2006**, *44*, 2395.
- (104) (a) Woo, C. H.; Beaujuge, P. M.; Holcombe, T. W.; Lee, O. P.; Frechet, J. M. J. *Journal of the American Chemical Society* **2010**, *132*, 15547(b) Bronstein, H.; Chen, Z. Y.; Ashraf, R. S.; Zhang, W. M.; Du, J. P.; Durrant, J. R.; Tuladhar, P. S.; Song, K.; Watkins, S. E.; Geerts, Y.; Wienk, M. M.; Janssen, R. A. J.; Anthopoulos, T.; Sirringhaus, H.; Heeney, M.; McCulloch, I. *Journal of the American Chemical Society* **2011**, *133*, 3272(c) Bijleveld, J. C.; Zoombelt, A. P.; Mathijssen, S. G. J.; Wienk, M. M.; Turbiez, M.; de Leeuw, D. M.; Janssen, R. A. J. *Journal of the American Chemical Society* **2009**, *131*, 16616(d) Bijleveld, J. C.; Gevaerts, V. S.; Di Nuzzo, D.; Turbiez, M.; Mathijssen, S. G. J.; de Leeuw, D. M.; Wienk, M. M.; Janssen, R. A. J. *Adv. Mater.* **2010**, *22*, E242.
- (105) (a) Teng, C.; Yang, X. C.; Yang, C.; Li, S. F.; Cheng, M.; Hagfeldt, A.; Sun, L. C. *Journal of Physical Chemistry C* **2010**, *114*, 9101(b) Shin, J.; Kang, N. S.; Kim, K. H.; Lee, T. W.; Jin, J. I.; Kim, M.; Lee, K.; Ju, B. K.; Hong, J. M.; Choi, D. H. *Chem. Commun.* **2012**, *48*, 8490.
- (106) (a) Matsuo, Y. *Journal of Synthetic Organic Chemistry Japan* **2012**, *70*, 541(b) Matsuo, Y. *Chemistry Letters* **2012**, *41*, 754(c) Hummelen, J. C.; Knight, B. W.; Lepeq, F.; Wudl, F.; Yao, J.; Wilkins, C. L. *Journal of Organic Chemistry* **1995**, *60*, 532(d) Sonar, P.; Lim, J. P. F.; Chan, K. L. *Energy & Environmental Science* **2011**, *4*, 1558.
- (107) (a) McNeill, C. R.; Abrusci, A.; Zaumseil, J.; Wilson, R.; McKiernan, M. J.; Burroughes, J. H.; Halls, J. J. M.; Greenham, N. C.; Friend, R. H. *Appl. Phys. Lett.* **2007**, *90*(b) Armstrong, N. R.; Wang, W. N.; Alloway, D. M.; Placencia, D.; Ratcliff, E.; Brumbach, M. *Macromolecular rapid communications* **2009**, *30*, 717(c) Westenhoff, S.; Howard, I. A.; Hodgkiss, J. M.; Kirov, K. R.; Bronstein, H. A.; Williams, C. K.; Greenham, N. C.; Friend, R. H. *Journal of the American Chemical Society* **2008**, *130*, 13653.
-

- 
- (108) Dillon, A. C. *Chemical reviews* **2010**, *110*, 6856.
- (109) Liu, Z. F.; Liu, Q.; Huang, Y.; Ma, Y. F.; Yin, S. G.; Zhang, X. Y.; Sun, W.; Chen, Y. S. *Adv. Mater.* **2008**, *20*, 3924.
- (110) Gritzner, G. *Pure Appl. Chem.* **1990**, *62*, 1839.
- (111) Yamato, T.; Hideshima, C.; Suehiro, K.; Tashiro, M.; Prakash, G. K. S.; Olah, G. A. *The Journal of Organic Chemistry* **1991**, *56*, 6248.
- (112) Usta, H.; Lu, G.; Facchetti, A.; Marks, T. J. *Journal of the American Chemical Society* **2006**, *128*, 9034.
- (113) Sonntag, M.; Strohhriegl, P. *Chemistry of materials* **2004**, *16*, 4736.
- (114) Rong, L.; Liu, Q.; Tang, J.; Chi, Z. *ChemInform* **2010**, *41*, no.
- (115) Jo, W. J.; Kim, K. H.; No, H. C.; Shin, D. Y.; Oh, S. J.; Son, J. H.; Kim, Y. H.; Cho, Y. K.; Zhao, Q. H.; Lee, K. H. *Synth. Met.* **2009**, *159*, 1359.
- (116) Zoombelt, A. P.; Fonrodona, M.; Wienk, M. M.; Sieval, A. B.; Hummelen, J. C.; Janssen, R. A. J. *Organic Letters* **2009**, *11*, 903.
- (117) Mancilha, F. S.; DaSilveira Neto, B. A.; Lopes, A. S.; Moreira, P. F.; Quina, F. H.; Gonçalves, R. S.; Dupont, J. *European journal of organic chemistry* **2006**, *2006*, 4924.
- (118) Torun, L.; Liu, S.; Madras, B. K.; Meltzer, P. C. *Tetrahedron letters* **2006**, *47*, 599.
- (119) Kim, J. J.; Choi, H.; Lee, J. W.; Kang, M. S.; Song, K.; Kang, S. O.; Ko, J. *J. Mater. Chem.* **2008**, *18*, 5223.
- (120) Zhang, C.; Google Patents, 2007.
- (121) Helgesen, M.; Gevorgyan, S. A.; Krebs, F. C.; Janssen, R. A. J. *Chemistry of materials* **2009**, *21*, 4669.
- (122) Ding, P.; Chu, C. C.; Liu, B.; Peng, B.; Zou, Y.; He, Y.; Zhou, K.; Hsu, C. S. *Macromolecular Chemistry and Physics* **2010**, *211*, 2555.
- (123) Vila, N.; Zhong, Y. W.; Henderson, J. C.; Abruna, H. D. *Inorganic chemistry* **2009**, *49*, 796.
- (124) Abou-Elkhair, R. A. I.; Dixon, D. W.; Netzel, T. L. *The Journal of Organic Chemistry* **2009**, *74*, 4712.
- (125) Klare, J. E.; Tulevski, G. S.; Sugo, K.; de Picciotto, A.; White, K. A.; Nuckolls, C. *Journal of the American Chemical Society* **2003**, *125*, 6030.
- (126) Cammidge, A. N.; Gopee, H. *Journal of Porphyrins and Phthalocyanines* **2009**, *13*, 235.
- (127) Cui, W.; Wu, Y.; Tian, H.; Geng, Y.; Wang, F. *Chem. Commun.* **2008**, 1017.
- (128) Palamà, I.; Di Maria, F.; Viola, I.; Fabiano, E.; Gigli, G.; Bettini, C.; Barbarella, G. *Journal of the American Chemical Society* **2011**, *133*, 17777.
- (129) Alesi, S.; Di Maria, F.; Melucci, M.; Macquarrie, D. J.; Luque, R.; Barbarella, G. *Green Chem.* **2008**, *10*, 517.
- (130) Kato, S.; Matsumoto, T.; Ishi-i, T.; Thiemann, T.; Shigeiwa, M.; Gorohmaru, H.; Maeda, S.; Yamashita, Y.; Mataka, S. *Chem. Commun.* **2004**, 2342.
- (131) Yang, J.; Dass, A.; Rawashdeh, A. M. M.; Sotiriou-Leventis, C.; Panzner, M. J.; Tyson, D. S.; Kinder, J. D.; Leventis, N. *Chemistry of Materials* **2004**, *16*, 3457.
-

- 
- (132) Perry, P. J.; Reszka, A. P.; Wood, A. A.; Read, M. A.; Gowan, S. M.; Dosanjh, H. S.; Trent, J. O.; Jenkins, T. C.; Kelland, L. R.; Neidle, S. *Journal of medicinal chemistry* **1998**, *41*, 4873.
- (133) Chen, G. Y.; Chiang, C. M.; Kekuda, D.; Lan, S. C.; Chu, C. W.; Wei, K. H. *Journal of Polymer Science Part A: Polymer Chemistry* **2010**, *48*, 1669.
- (134) Bürckstümmer, H.; Weissenstein, A.; Bialas, D.; Würthner, F. *The Journal of Organic Chemistry* **2011**, *76*, 2426.
- (135) Cohen, T.; Cristea, I. *Journal of the American Chemical Society* **1976**, *98*, 748.
- (136) Morrison, R.; Boyd, R.; Englewood Cliffs, NJ: Prentice Hall, 1992.
- (137) (a) Cammidge, A. N.; Crepy, K. V. L. *Journal of Organic Chemistry* **2003**, *68*, 6832(b) Clayden, J. *Tetrahedron* **2004**, *60*, 4335.
- (138) Espinet, P.; Echavarren, A. M. *Angewandte Chemie International Edition* **2004**, *43*, 4704.
- (139) Bui, T. T.; Thiebaut, O.; Grelet, E.; Achard, M. F.; Garreau-de Bonneval, B.; Ching, M. C.; Kathleen, I. *European Journal of Inorganic Chemistry* **2011**, *2011*, 2663.
- (140) Jiang, J. M.; Yang, P. A.; Hsieh, T. H.; Wei, K. H. *Macromolecules* **2011**, *44*, 9155.
- (141) Galli, C. *J. Chem. Soc., Perkin Trans. 2* **1984**, 897.
- (142) Zou, Y.; Gendron, D.; Najari, A.; Tao, Y.; Leclerc, M. *Macromolecules* **2009**, *42*, 2891.
- (143) (a) Kürti, L.; Czakó, B. *Strategic applications of named reactions in organic synthesis: background and detailed mechanisms*; Academic Press, 2005(b) de Meijere, A.; Diederich, F. *Metal-catalyzed cross-coupling reactions*; Wiley-VCH Weinheim, Germany, 2004.
- (144) Krebs, F. C.; Nyberg, R. B.; Jørgensen, M. *Chemistry of materials* **2004**, *16*, 1313.
- (145) Bringmann, G.; Price Mortimer, A. J.; Keller, P. A.; Gresser, M. J.; Garner, J.; Breuning, M. *Angewandte Chemie International Edition* **2005**, *44*, 5384.
- (146) Crouch, D. J.; Skabara, P. J.; Lohr, J. E.; McDouall, J. J. W.; Heeney, M.; McCulloch, I.; Sparrowe, D.; Shkunov, M.; Coles, S. J.; Horton, P. N.; Hursthouse, M. B. *Chemistry of materials* **2005**, *17*, 6567.
- (147) Chauhan, S. S. (2009). Development of conjugated polymers and their application in devices. Sheffield, The University of Sheffield. UK. PhD.
- (148) Admassie, S.; Ingnas, O.; Mammo, W.; Perzon, E.; Andersson, M. R. *Synth. Met.* **2006**, *156*, 614.
- (149) Pommerehne, J.; Vestweber, H.; Guss, W.; Mahrt, R. F.; Bassler, H.; Porsch, M.; Daub, J. *Adv. Mater.* **1995**, *7*, 551.
- (150) Wu, P. T.; Kim, F. S.; Champion, R. D.; Jenekhe, S. A. *Macromolecules* **2008**, *41*, 7021.
- (151) Chen, H.-Y.; Yeh, S.-C.; Chen, C.-T.; Chen, C.-T. *J. Mater. Chem.* **2012**, *22*, 21549.
- (152) Alghamdi, A. A. B.; Watters, D. C.; Yi, H. N.; Al-Faifi, S.; Almeataq, M. S.; Coles, D.; Kingsley, J.; Lidzey, D. G.; Iraqi, A. *J. Mater. Chem. A* **2013**, *1*, 5165.
-

- (153) Camaioni, N.; Tinti, F.; Franco, L.; Fabris, M.; Toffoletti, A.; Ruzzi, M.; Montanari, L.; Bonoldi, L.; Pellegrino, A.; Calabrese, A. *Organic Electronics* **2012**.
- (154) (a) Perzon, E.; Wang, X. J.; Admassie, S.; Inganas, O.; Andersson, M. R. *Polymer* **2006**, *47*, 4261(b) Persson, N. K.; Sun, M.; Kjellberg, P.; Pullerits, T.; Inganäs, O. *The Journal of chemical physics* **2005**, *123*, 204718.